

University of Nottingham
UK | CHINA | MALAYSIA

Remote sensing investigation of tropical peat swamp forest degradation

Chloe Brown

BSc (Joint Hons)

Thesis submitted to the University of Nottingham
for the degree of Doctor of Philosophy

September 2019

Acknowledgements

Firstly, I would like to thank my supervisors, Professor Doreen Boyd and Dr. Sofie Sjögersten for their incredible support and guidance throughout the PhD. Their drive and passion for their work has been a constant source of inspiration for me over the past four years. I know their knowledge, advice and enthusiasm for science will stay with me in future endeavours. I would also like to extend my gratitude to Professor Paul Aplin, Dr. Stephanie Evers, and Dr. Daniel Crawley for their help and advice in the PhD project.

This research would not have been possible without the funding provided by the Natural Environment Research Council (NERC) (NE/L002604/1) through the Envision DTP and support from the University of Nottingham. The funding allowed me to attend essential conferences and training courses which have been crucial in my academic development.

I would like to express my gratitude to NERC's Airborne Research Facility for providing the airborne lidar datasets. I am also grateful to Martin Isenburg for generously granting the research in this thesis with a complimentary full academic LASTools license, under the LASmoons programme. I am very appreciative to the Selangor State Forestry Department for granting access to NSPSF and to the forest rangers who assisted with data collection and happily shared their knowledge and experience working in the reserve. A massive thank you also goes to Dr. Stephanie Evers, Lahiru Wijedasa, Martha Ledger, Dr. Selvakumar Dhandapani, and the staff at GEC for their support and assistance during the three field campaigns in this PhD research.

I am very grateful to all my colleagues at the School of Geography. In particular, I am thankful for the assistance given by the technical staff in the department - Ian Conway, Teresa Needham and Claire Templey – for their patience and infinite wisdom on the practical aspects of research. I must also thank my office pals – Catherine, Phil, Savannah and Simon – who were always there to offer a shoulder to cry, laugh or lean on throughout the PhD - more often than not at the pub.

On a more personal level, I would like to thank my friends and family for supporting me throughout my PhD. A very special thank you goes to Savannah, Darcy and Alex who gave up their time to painstakingly read and comment on sections of my draft thesis. Finally, I owe an enormous thank you to my parents – Nigel and Suzanne. Ultimately, this PhD is a testament to their love and belief in me at every stage of my academic and personal life, and for that I am very thankful.

.

Table of Contents

Acknowledgements ii

List of Figures viii

List of Tables xiii

Abstract 1

Chapter 1: Introduction 5

1.1 Tropical peatland overview 5

1.2 Drivers of tropical peat swamp forest degradation 7

1.3 Tropical peat swamp forest restoration 9

1.4 Research objectives 10

1.5 Thesis structure 12

1.6 Thesis publication 15

Chapter 2: Literature Review 17

2.1 Remote sensing data sources 17

2.1.1 Optical 18

2.1.2 Radar 21

2.1.3 Lidar 22

2.2 Modelling approaches 27

2.3 Application of remote sensing in tropical peat ecosystems 29

2.3.1 Land cover 30

2.3.2 Fire 32

2.3.3 Above Ground Biomass 34

2.3.4 Peat soil 35

2.4 Summary: Research challenges and opportunities 37

Chapter 3: Data 39

3.1 Study site 39

3.2 Remote sensing 44

3.2.1 Airborne lidar data 44
3.2.2 Space-borne optical data 46
3.3 Field data *50*
3.3.1 Forest inventory plot design 54
3.3.2 Forest inventory data 55
3.3.3 Allometric AGB model 56
3.3.4 Peat core data 57
3.4 Software *59*
3.5 Supplementary material *61*
Chapter 4: Tropical peatland vegetation structure and biomass: optimal exploitation of airborne laser scanning 62
4.1 Introduction *62*
4.2 Materials and Methods *67*
4.2.1 Study site 67
4.2.2 Field data 68
4.2.3 Lidar data acquisition 70
4.2.4 DR-derived metrics 71
4.2.5 FW-derived metrics 73
4.2.6 Statistical modelling and analyses 73
4.3 Results *75*
4.4 Discussion *83*
4.5 Conclusions *88*
Chapter 5: Restoration of Malaysia's tropical peat: remote sensing for monitoring restoration management in tropical peat swamp forests 90
5.1 Introduction *90*
5.2 Methods *94*
5.2.1 Study site 94
5.2.2 Workflow 96

5.2.3 Sentinel-2 data and pre-processing 96
5.2.4 Sentinel-2 model input variables 97
5.2.5 Training and validation data 100
5.2.6 Random Forest regression 103
5.2.7 Wall-to-wall AGB for NSPSF 105
5.2.8 2018 AGB validation 106
5.2.9 AGB change analysis 106
5.3 Results 107
5.3.1 Random Forest model performance 107
5.3.2 Predictive performance of Random Forest model 109
5.3.3 Wall-to-Wall AGB maps 110
5.3.4 2018 AGB independent validation 111
5.3.5 Change analysis 113
5.4 Discussion 118
5.5 Conclusion 123
Chapter 6: Detecting tropical peatland degradation: combining Remote Sensing and Organic Geochemistry 125
6.1 Introduction 125
6.2 Methods 128
6.2.1 Study site 128
6.2.2 Field Sampling 131
6.2.3 Sample Processing 132
6.2.4 Remote sensing data 135
6.2.5 Additional geo-spatial data 136
6.2.6 Data analysis 137
6.3 Results 138
6.3.1 Carbon stock 138
6.3.2 Remote Sensing and GIS 139

6.3.3 Rock-Eval indices and parameters 141
6.4 Discussion *147*
6.4.1 Carbon stocks 147
6.4.2 Application of remote sensing in tropical peat soil degradation 148
6.4.3 Tropical peat decomposition trends 150
6.4.4 Limitations of peat sampling strategy 151
6.5 Conclusion *152*
6.6 Supplementary material *154*
Chapter 7: Synthesis 155
7.1 Research chapter summary *156*
7.2 Contribution of research *159*
7.2.1 Methodological contribution 160
7.2.2 Environmental management and policy contribution 162
7.3 Limitations *165*
7.4 Recommendations for further research *168*
7.5 Concluding remarks *170*
References 172
Appendix 1: Tropical peatland vegetation structure and biomass: optimal exploitation of airborne laser scanning 213
Appendix 2: Denial of long-term issues with agriculture on tropical peatlands will have devastating consequences 235

List of Figures

Chapter 1

Figure 1-1 Dominant tropical peat areas (in red) in South-East Asia (from– Page *et al.,* 2004). 5

Figure 1-2 Thesis overview and interaction between the three resaerch chapters (**Chapter 4, 5 and 6**). 14

Chapter 2

Figure 2-1 Difference between passive and active sensors. 18

Figure 2-2 Electromagnetic spectrum (not to scale). Modified from Pettorelli *et al.,* (2018). 19

Figure 2-3 Difference between discrete return (left) and full waveform (right) lidar systems. Modified from Ferraz *et al.,* (2009). 26

Chapter 3

Figure 3-1 The location of the State of Selangor in Peninsular Malaysia 39

Figure 3-2 (a) Map of NSPSF showing the canals network and the Sungai Tenggi River; (b) Map of NSPSF showing the landuse adjacent to forest reserve. 41

Figure 3-3 Example of one of the ARF flightline DR point cloud datasets representing a transition zone from peat swamp forest within the reserve to oil palm plantation adjacent. The point cloud is coloured by elevation 45

Figure 3-4 Comparison of Landsat 7 ETM+, Landsat 8 OLI TIRS and Sentinel-2 MSI band selection and position 48

Figure 3-5 The forest plot and peat core site locations sampled in the three field campaigns. Point locations displayed on a Landsat data scene captured in 2019. 52

Figure 3-6 Forest inventory plot design and field photography. 56

Figure 3-7 Field photography of peat core collection. 58

Chapter 4

Figure 4-1 (a) the location of the North Selangor Peat Swamp Forest in Peninsular Malaysia; (b) magnified study area map at bottom left corner shows forest type (forest height (high, medium, low) and forest density (high, medium, low)), results from a forest management inventory undertaken in 2000 (RCFM and EMS, 2000).. 67

Figure 4-2 Example field inventory plot design 69

Figure 4-3 (a) ARF lidar flighlines; (b) lidar flightline subset; (c) field plot location; d) field plot location..... 71

Figure 4-4 Illustration of FW metrics location on an example pseudo-vertical waveform from the NSPSF FW dataset. Plotted Amplitude (DN)/ Time (ns). 73

Figure 4-5 Field measured AGB modelled by the mean value from the FW mean HOME metric (H_mean). Bands represent the 95% confidence envelope..... 76

Figure 4-6 Centre point (1 m buffer) plot vegetation profiles, each waveform height has been subtracted from lidar derived DTM; graphs are fitted Height (m)/Amplitude (DN). Height scale (y-axis) ranges from 0 to 40 m, and the amplitude (x-axis) from 0 to 120 DN. Graphs are accompanied with forest canopy..... 77

Figure 4-7 Predicted vs fieldmeasured AGB fromthe best performingmodels: (a) DR-model; (b) FW-model; (c) Combination-model. Bands represent the 95% confidence envelope..... 81

Figure 4-8 (a) LiDAR flightline subset; (b) estimation of AGB (Mg/ha) within the NSPSF boundary calculated from the Combination-model, at a 5 m (0.0025 ha) spatial resolution, overlaid on Sentinel-2 multispectral image. 82

Figure 4-9 Frequency distribution for DR-, FW- and Combination-model generated AGB (Mg/ha) across the 30 field plots, presented with model generated plot minimum, maximum, mean and standard deviation AGB..... 82

Chapter 5

Figure 5-1 Workflow of the major tasks carried out in this research chapter ….....96

Figure 5-2 'lidar AGB model' coverage overlaid onto forest type (forest height (high, medium, low) and forest density (high, medium, low)) results from a forest inventory undertaken in 2000 (RCFM, 2000).....101

Figure 5-3 The top 25 ranked variables from the optimised Random Forest model based on the permutation vairtbale importance (Importance). Where: 3V-RE6 = 3x3 Variance Red-Edge band 6; 5V-RE6 = 5x5 Variance Red-Edge band 6; Red = band 4; 7V-RE6 = 7x7 Variance Red-Edge band 6; 9V-RE6 = 9x9 Variance Red-edge 6; 3V-Green = 3x3 Variance Green band 3; 9V-Green = 9x9 Variance Green band 3; 5V-Green = 5x5 Variance Green band 3; 7V-Green = 7x7 Variance Green band 3; 5V-NarrowNIR = 5x5 Variance Narrow NIR band 8a; 3M-Red = 3x3 Mean Red band 4; 9M-RE6 = 9x9 Mean Red-Edge band 6; 7M-RE6 = 7x7 Mean Red-Edge band 6; 3V-NarrowNIR = 3x3 Variance Narrow NIR band 8a; 9M-Green = 9x9 Mean Green band 3; 7M-Green = 7x7 Mean Green band 3; 7V-NarrowNIR = 7x7 Variance Narrow NIR band 8a; 5M-Green = 5x5 Mean Green band 3; 9V-NarrowNIR = 9x9 Variance Narrow NIR band 8a; 5M-RE6 = 5x5 Mean Red-Edge band 6; SR-RE5 = Simple Ration Index band 5; NDVI-RE5 = Normlaised Difference Vegetation Index Red-Edge band 5; SR-RE6 = Simple Ration Index band 6; NDVI-RE6 = Normlaised Difference Vegetation Index Red-Edge band 6; RE6 = Red-Edge band 6. 108

Figure 5-4 Observed vs. predicted AGB using the optimised Random Forest model with an independent validation dataset.. 109

Figure 5-5 2015 AGB (Mg/ha) estimated for NSPSF reserve calculated from the optimised Random Forest model, at a 10 m (0.01 ha) spatial resolution. 110

Figure 5-6 2018 AGB (Mg/ha) estimates for NSPSF reserve calculated from the optimised Random Forest model, at a 10 m (0.01 ha) spatial resolution. 111

Figure 5-7 Observed vs. predicted AGB using the 2018 predicted AGB results and field inventory estimated AGB. 112

Figure 5-8 AGB change between the years 2015 and 2018 for NSPSF reserve. Classified as high gain, low gain, stable, low loss, and high loss.…..113

Figure 5-9 Management zone C2 illustrated with cause and evidence of peat swamp degradation.....116

Figure 5-10 Management zone R1 and E5 illustrated with past restoration interventions.....117

Chapter 6

Figure 6-1 Location for the peat cores sampled under the four different forest condition classes. Areas of high fire risk, location of the Sungai Tenggi River and the canal network are labelled. 131

Figure 6-2 Carbon storage in the vegetation and peat soil for each of the four forest condition classes, mean and SEM shown. 138

Figure 6-3 Remote sensing derived products: (a) Normalised Burn Ratio (NBR) mean; (b) Normalised Burn Ratio (NBR) standard deviation (sd) 140

Figure 6-4 Significant relationships between remote sensing derived products and Rock-Eval analysis parameters: (a) correlation with Normalised Burn Ration Standard deviation (sd) and Carbon Stock held in the top 50 cm; (b) Carbon stock held in top 50 cm mean values and SEM for the four forest condition classes; (c) correlation with Normalised Burn Ration mean and HI for the top 50 cm; (d) HI for the top 50 cm mean values and SEM for the four forest condition classes. 141

Figure 6-5 Rock-Eval indices for Central Forest sites: a) I/R diagram; b) boxplots of R-index values for peat profile layers; c) boxplots of I-index values for peat profile layers 143

Figure 6-6 Rock-Eval indices for disturbed sites: a) I/R diagram; b) boxplots of R-index values for peat profile layers; c) boxplots of I-index values for peat profile layers.....144

Figure 6-7 Van Krevelen pseudo diagrams. (a) Central Forest; (b) disturbed sites. 146

Figure 6-8 I/R diagram for mangrove peat core from Bocas Del Toro Panama (source data from (Upton *et al.*, 2018)). 154

List of Tables

Chapter 1

Table 1-1 Drivers of tropical peatland degradation in South-East Asia. Adapted from Dohong *et al.,* 2017.....8

Table 1-2 The paper title, status of publication and journal (target journal) for research conducted during my PhD.. 16

Chapter 2

Table 2-1 Examples of common optical sensor/platforms, with their spatial and temporal resolutions and band number information 20

Chapter 3

Table 3-1 Landsat mission summary.....47

Table 3-2 Landsat and Sentinel-2 data product levels and description. 49

Table 3-3 2016 field campaign data. 51

Table 3-4 2017 field campaign data. 53

Table 3-5 2018 field campaign data. 54

Table 3-6 Software used in this thesis research. 60

Table 3-7 Summary statistics for model (Feldpuash) and observed (field data)….. 61

Chapter 4

Table 4-1 Plot measured forest parameters. 75

Table 4-2 Results from simple linear regression using DR metrics. Where: Min = minimum height; Max = maximum height; Avg = average height; Std = standard deviation; Skw = skewness; Kur = kurtosis; Qav = average square height; P01, P05, P10, P25, P50, P75, P90, P9, P99 = height percentiles; B10, B20, B30, B40, B50,

B60, B70, B80, B90 = height bincentiles. Values underlined represent metrics of non-significance p > 0.05 78

Table 4-3 Results from simple linear regression using FW metrics. Where: H_mean = mean HOME metric; H_sd = standard deviation HOME metric; W_mean = mean WD metric; W_sd = standard deviation WD metric; R_mean = mean ROUGH metric; R_sd = standard deviation ROUGH metric. Values underlined represent metrics of non-significance p > 0.05 79

Table 4-4 Model equations. Where: P75 = 75th height percentile; Ske = skewness; H_mean = mean HOME metric; W_sd = standard deviation WD metric; B50 = 50th height bincentile. 79

Table 4-5 Results from the best preforming models for predicting AGB. Where: P75 = 75th height percentile; Ske = skewness; H_mean = mean HOME metric; W_sd = standard deviation WD metric; B50 = 50th height bincentile 80

Chapter 5

Table 5-1 Vegetation indices with equation and the Senitnel-2 MSI bands used. 98

Table 5-2 The GLCM-based texture variables formula……..... 99

Table 5-3 Performance of 'lidar AGB model' developed in **Chapter 4** (Brown *et al.*, 2018). Where: H_mean = mean plot height of median energy (HOME); B50 = 50th height bincentiles; R^2 = R square; RMSE = root mean square error; rRMSE = relative root mean square error. 100

Table 5-4 Summary statistics for the 'lidar AGB model' developed in **Chapter 4** (Brown *et al.*, 2018) 102

Table 5-5 Performance of optimised Random Forest model on an independent validation dataset. Where: R^2 = R square; Adj-R^2 = adjusted R square; RMSE = root mean square error; %RMSE = percentage normalised root mean square error……. 109

Table 5-6 Independent validation results from 2018 AGB estimation. Where: R^2 = R square; Adj-R^2 = adjusted R square; RMSE = root mean square error; %RMSE = percentage normalised root mean square error……..112

Table 5-7 Prominent management zones of change in NSPSF and the associated IMP interventions and proposed regeneration strategies……...114

Chapter 6

Table 6-1 Description of forest condition classes. 130

Table 6-2 Median carbon stock (Mg/ha) and interquartile range (IQR) for above ground vegetation and peat soil. 139

Table 6-3 R- and I- index median and interquartile range (IQR) for upper 50 cm section in the peat profile for the four forest condition classes. Significant pairwise Wilcoxon tests with Bonferroni adjustments share the same subscript letter.....145

Table 6-4 R- and I- index median and interquartile range (IQR) for upper 50 cm section in the peat profile for Central Forest and disturbed sites.. 145

Table 6-5 R- and I- index median and interquartile range (IQR) for combined below water table and deeper layers for the four forest condition classes. Significant pairwise Wilcoxon tests with Bonferroni adjustments share the same subscript letter.. 146

Abstract

Tropical peat swamp forest degradation is a major issue in South-East Asia. Covering an estimated 441,025 km^2 (~11% of global peatland resources) tropical peat swamps have been increasingly recognised for their global importance as natural carbon sinks, storing immense carbon deposits (~69 Gt) in their above-ground biomass (AGB) and underlying rich peat soils. However, increased climate variability, amplified by degradation associated with land use change and resource management, have the potential to shift tropical peatlands from a net carbon sink, to a source. Despite the importance of tropical peat swamp forests, there is a severe lack of data and knowledge on tropical peatland ecosystem dynamics and response to degradation, which is vital to guide sustainable management and restoration planning.

This thesis examines the relationship between peat properties, the overlying vegetation and their remote sensing signature. Techniques are developed for estimating tropical peatland AGB, investigating the use of multi-platform remote sensing methods in large-scale tropical peatland mapping, and exploring the strengths and weaknesses of remote sensing in tropical peat soil assessment. Remote sensing data has been coupled with field-based measurements throughout the thesis, combining the accuracy and detail of traditional ecological field assessment with the spatial and temporal coverage afforded by remote sensing. The research focuses on North Selangor Peat Swamp Forest (NSPSF), a large tropical peat swamp forest in Peninsular Malaysia, which experiences varying degrees of growth and degradation, and environmental pressures from multiple sources.

The first research chapter (**Chapter 4**) examines the relationship between tropical peat swamp forest AGB and small-footprint airborne Light Detection and Ranging (lidar) discrete return (DR) and full waveform (FW) metrics, with a view to establishing the optimal use of this technology in this environment, which has different characteristics to other environments readily studied using lidar data (e.g. temperate/boreal forests). Plot-based multiple regression analysis was performed to establish the strongest predictive models of peat swamp forest AGB using DR metrics (only), FW metrics (only), and a combination of both DR and FW metrics. Overall, the results demonstrated that a combination-model, coupling the benefits derived from both DR and FW metrics, had the best performance in modelling AGB for tropical peat swamp forest (R^2 = 0.77, RMSE = 36.4, rRMSE = 10.8%). However, no statistical difference was found between the rRMSE of the combination-model and the best models using only one lidar system. The research concluded that the optimal approach for using airborne lidar in the estimation of peat swamp forest AGB was more dependent on the inclusion of lidar metrics that describe the mid-canopy structures than the type of lidar system.

The second research chapter (**Chapter 5**) demonstrates the use of Sentinel-2 MSI satellite data in delivering accurate, high resolution AGB maps of NSPSF for the years 2015 and 2018. This research adopted the site specific AGB model built in **Chapter 4** as model training and testing data using a Random Forest machine learning approach. The results demonstrated that a Random Forest algorithm is a useful and robust method for estimating AGB with Sentinel-2 MSI derived spectral and textural predictor variables; 2015 (R^2 = 0.80, RMSE = 55.2, rRMSE = 24.6%) and 2018 (R^2 = 0.92, RMSE = 23.4,

rRMSE =8.73%). A change analysis was run on the 2015 and 2018 AGB map outputs. AGB gains and losses between the years 2015 and 2018 are discussed in terms of reserve management and known peat swamp forest disturbance. Areas of AGB gain were found to be focused on central areas of the reserve where natural regeneration has been encouraged through forest protection and drain blocking activities. AGB loss was attributed to frequent fire events hampering recovery efforts or the negative impacts of poorly designed water management. The research concluded by recommending the continued tracking of AGB across NSPSF to build an archive of data which is representative of this on-going active period of conservation and regeneration.

The third research chapter (**Chapter 6**) investigates the use of remote sensing and organic geochemistry methods for assessing the impact of tropical peat swamp forest degradation on the underlying peat soil profile. The research demonstrated the utility of stacked Landsat archive data for landscape scale assessment of degradation in NSPSF over a 30-year time period (1989 - 2019). Peat cores collected from 4 different forest condition classes (Central Forest, Managed Recovery, Disturbed Forest, and Fire Affected) were processed using Rock-Eval 6 pyrolysis, to quantify the carbon stored in the peat and track soil organic matter (SOM) thermal stability throughout the peat profiles. The research found carbon stocks to be significantly different between vegetation (derived from AGB values produced in **Chapter 5**) and peat soil (Wilcoxon test: W= 121, d.f. = 1, p-value = <0.001). Peat profiles collected in Central Forest sites followed a general negative linear relationship between I- and R- index with depth. This reflects the relationship between decay processes and SOM stabilisation, however, the research found that disturbed

sites (Fire Affected, Disturbed Forest, and Managed Recovery) did not follow this uniform pattern. The research concluded that remote sensing derived products cannot predict peat soil carbon stocks and peat properties associated with degradation for the entire peat profile. However, remote sensing derived products do have a relationship with carbon stock (Spearman's rho = -0.66, S = 366, p-value = 0.030) and the Hydrogen Index (Spearman's rho = 0.7, S = 66, p-value = 0.020) for the surface and sub-surface layers in the peat profiles. The research recommended the use of remote sensing as a tool to identify key areas of surface peat degradation, to focus regeneration and restoration activates.

Chapter 1: Introduction

1.1 Tropical peatland overview

Peatlands are immensely important in the global climate system (Scharlemann *et al.,* 2014; Yu, 2012). Current estimates report peatlands to cover 4.23 million km ^{2}, approximately 2.84% of the Earth's land surface (Xu *et al.,* 2018). Despite their relatively small surface area, peatlands hold more than 30% of global soil carbon stocks, of these stores the largest deposits are found in the tropics (Rieley and Page, 2016). Tropical peatlands are found predominantly in South-East Asia, but are also located in Africa, Central and South America and elsewhere around the Pacific Ocean. In total, tropical peatlands cover an estimated 441,025 km^2, spanning more than 180 countries and represent ~11% of global peatland resources. With a total peat carbon pool of 88.5 Gt (range 81.5-91.8 Gt), tropical peatlands represent one of the largest near-surface pools of terrestrial carbon, with the highest share in South-East Asia (77%) (Dargie *et al.,* 2017; Page *et al.,* 2011) (Figure 1-1).

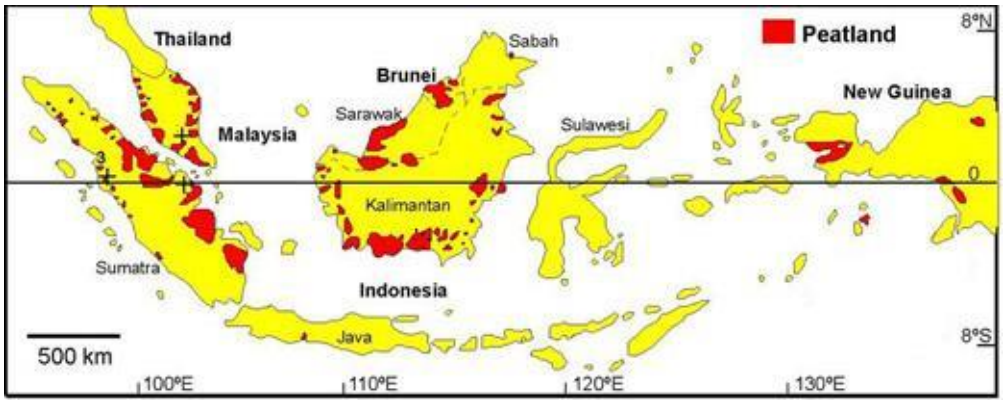


Figure 1-1 Dominant tropical peat areas (in red) in South-East Asia (from– Page *et al.,* 2004).

Tropical peat formation is governed by the high temperature and high precipitation climatic conditions found in these regions. In South-East Asia, peatlands commonly occupy low altitude coastal and sub-coastal environments, but can also extend inland along river valleys and basins (Reiley *et al.,* 2008). As a result of high rainfall, poor drainage, permanent waterlogging and acidic conditions (pH 4 or less), decompositions of organic material in tropical peatlands is slow (Yule, 2010). Thus creating the optimum conditions required for peat accumulation. Tropical peat is comprised of mainly undecomposed woody plant material, and is typically covered by a tropical swamp forest (Page *et al.,* 1999). Often, peatlands in South-East Asia are characterised as having a domed, convex topography. Highly developed peat domes in South-East Asia can accumulate peat depths of up to 20 m (Anderson, 1983).

In addition to carbon sequestration and storage, tropical peatlands provide a range of valuable ecosystem services and goods vital to local livelihoods and international communities (Bonn *et al.,* 2016; Reed *et al.,* 2014). Tropical peatlands support a range of unique habitats, and are home to a number of endemic and endangered species (flora and fauna). These areas represent an important component of global biodiversity (Carroll *et al.,* 2015; Sunarto *et al.,* 2012; Posa *et al.,* 2011). They also play an important role in water resources management, including: water storage, moderation of river flows and flood prevention (Gao *et al.,* 2016; Holden, 2005).

1.2 Drivers of tropical peat swamp forest degradation

Over the last two decades rapid disturbance and conversion by human interventions has transformed tropical peat swamp forest environments and their ecosystem function (Kolka *et al.,* 2016). Tropical peat swamp forests are particularly vulnerable to destruction due to the synergistic nature of these ecosystems, negative impacts to the vegetation, peat or hydrology can easily unbalance the whole system. The connected impact of land use change ((logging and conversation to plantation estates) (Margono *et al.,* 2014a; Koh *et al.,* 2011), drainage (Konecny *et al.,* 2016; Hooijer *et al.,* 2012), and fire (Hoscilo *et al.,* 2011; Langer *et al.,* 2009) have rendered South-East Asia a global hotspot for tropical peatland degradation (Table 1-1).

Between 1990 and 2010, more than 5.4 Mha of peat swamp forests were deforested in South-East Asia alone, with annual deforestation rates of 3.7% (Miettinen *et al.,* 2012a). Tropical peatland degradation has directly increased greenhouse gas emissions, predominantly from the removal of above- and below-ground biomass, peat decomposition and oxidation caused by drainage, and peat combustion caused by fires (Gaveau *et al.,* 2014b; Couwenberg *et al.,* 2013; Jauhianen *et al.,* 2012; Hooijer *et al.,* 2012; Hergoualc'h and Verchot, 2011; *Page et al.,* 2009a). Additionally, peatland degradation has been identified as a major source of air pollution (See *et al.,* 2007; Heil and Goldammer, 2001), reduced biodiversity (Azhar *et al.,* 2011; Pose *et al.,* 2011; Danielsen *et al.,* 2009) and loss of local livelihoods (Chokkalingam *et al.,* 2005).

Table 1-1 Drivers of tropical peatland degradation in South-East Asia. Adapted from Dohong *et al.*, 2017.

Drivers of degradation	Description of degradation	References:
Logging	- removal of commercially profitable species - loss of biodiversity (endemic and endangered species) - creates gaps in the canopy, changing the forest microclimate and increasing the temperature of the peat surface; this encourages peat shrinkage and drying - construction of logging roads and wooden railways to ease access and transportation of felled log further disturbs the peat	Gaveau *et al.*, 2014a; Bryan *et al.*, 2013; Franke *et al.*, 2012; Smith *et al.*, 2012; Miettinen *et al.*, 2011; Miettinen and Liew, 2010; Satrio *et al.*, 2009; Langer *et al.*, 2007; Casson and Obidzinski, 2002; Böhm and Siegert, 2001
Conversion to large-scale plantations	- initial removal of ground vegetation - introduction of fertilisers and liming to increase the pH and boost microbial activity (peat oxidation) - construction of canal systems for drainage and water table management; encourages greater decomposition of organic matter (oxidation), lowers peat surface (subsidence) and releases greenhouse gasses	Schrier-Uijl *et al.*, 2013; Miettinen *et al.*, 2012b; Miettinen *et al.*, 2012c; Koh *et al.*, 2011; Azhar *et al.*, 2011; Reijnders *et al.*, 2008
Fire	- removal of above- and below- carbon stock - release of greenhouse gasses - destruction of on-site seed bank - increases emissions and health effects from regional haze episodes	Saputra *et al.*, 2017; Cattau *et al.*, 2016; Elvidge *et al.*, 2015; Gaveau *et al.*, 2014b; Hoscilo *et al.*, 2011; Page *et al.*, 2009a; Tansey *et al.*, 2008; Wösten *et al.*, 2006; Page *et al.*, 2002; Siegert *et al.*, 2001
Drainage	- lowers the groundwater table and elevates the peatland surface - increases surface water run-off and reduces water storage capacity; this encourages peat oxidation, consolidation and shrinkage, leading to peat subsidence and greenhouse gas emissions	Jauhiainen *et al.*, 2014; Hooijer *et al.*, 2014; Hooijer *et al.*, 2012; Hooijer *et al.*, 2010; Anshari *et al.*, 2010; Langner *et al.*, 2009; Holden *et al.*, 2006; Furukawa *et al.*, 2005

1.3 Tropical peat swamp forest restoration

Recognition of the global consequences of tropical peat swamp forest degradation has led to increased international efforts to reduce tropical peatland deforestation and drainage, along with the associated greenhouse gas emissions. This has encouraged a number of global climate policy and land management initiatives. For example, peatland restoration is recognised as a key focus in reaching carbon emission reduction targets under the Kyoto Protocol (IPCC, 2014; Hiraishi *et al.,* 2013) and as a terrestrial ecosystem management and protection aim under the United Nations (UN) Sustainable Development Goal (SDG) number 15 (SDG Knowledge platform, 2018). Specific to South-East Asia, the Association of Southeast Asia Nations (ASEAN) Peatland Forests Project (APFP) supports the implementation of a number of multi-stakeholder peatland management strategies to restore tropical peatlands and reduce the rate of degradation and risk of fire and haze.

At a more local-scale, a number of tropical peatland restoration initiatives have been trialled (Dohong *et al.,* 2018). These initiatives include: hydrological management (canal/ ditch blocking and infilling) (Ritzema *et al.,* 2014; Page *et al.,* 2009b; Suryadiputra *et al.,* 2005), natural recolonisation (seed germination, seed rain, and seed dispersal systems) (Blackham *et al.,* 2014; Blackham *et al.,* 2013; Gunawan *et al.,* 2012; D'arcy and Graham, 2008), revegetation (seedling nurseries and transplanted seedlings) (Graham and Page, 2014; Graham and Page, 2013), and community fire prevention schemes (Herawati and Santoso, 2011).

Given the increasing awareness of the importance of tropical peat swamp forest ecosystems, there is an urgent need to understand the response of both the above- and below- ground environments to intensive and often multiple degradation activities. The discipline of tropical peatland restoration is in its infancy (Padfield *et al.,* 2014) and information is urgently needed to successfully guide and improve current tropical peatland resource management, and support global climate mitigation programmes. However, there is a severe lack of data at an appropriate scale and frequency to assess the impact of both degradation (anthropogenic and natural) and rehabilitation activities on tropical peatland ecosystems as a whole.

Remote sensing has the unique capability to cover extensive geographical areas in a cost efficient manner, bridging the gap between local small scale measurements' and landscape scale assessment. Advances in sensor technology and data processing have the potential to provide valuable information for sustainable tropical peatland management, allowing for a more complete understanding (via mapping or spatial modelling) of the spatial and temporal complexities of tropical peatland ecosystems and their response to both degradation and regeneration.

1.4 Research objectives

This thesis focuses on North Selangor Peat Swamp Forest (NSPSF), a large tropical peatland in Peninsular Malaysia. In the past, NSPSF has experienced varying degrees of growth and degradation from multiple sources, and is now under an active period of tropical peatland restoration and recovery. The research in this thesis aims to support the sustainable management and

rehabilitation of NSPSF, as well as contribute to the growing field of tropical peatland restoration science. The research investigates the use of remote sensing to provide present-day and historical insights into tropical peat swamp forest dynamics, specifically examining the relationship between peat properties, the overlying vegetation, and their remote sensing signature. This is achieved through developing techniques for estimating tropical peatland above ground biomass (AGB), investigating the use of multi-platform remote sensing methods in large-scale tropical peatland mapping, and exploring the strengths and weaknesses of remote sensing in peat soil assessment. Remote sensing data has been coupled with field-based measurements throughout this thesis, combining the accuracy and detail of traditional ecological field assessment with the spatial and temporal coverage afforded by remote sensing.

Specifically, this research has the following objectives:

1. To investigate the optimal use of occupied airborne Light Detection and Ranging (lidar) technology to quantify tropical peat swamp forest AGB (addressed in **Chapter 4)**.

2. To quantify the AGB stored in NSPSF using space-borne optical data (addressed in **Chapter 5**).

3. To assess the effectiveness of tropical peat restoration activities on AGB dynamics over a focused period of rehabilitation interventions (2015 - 2018) in NSPSF (addressed in **Chapter 5**).

4. To examine the impact of tropical peatland degradation in NSPSF on the underlying peat soil deposits (addressed in **Chapter 6**).

1.5 Thesis structure

This thesis is divided into seven chapters:

- **Chapter 1**, provides an overview on tropical peatlands and threats to their function, setting the scene for the research presented in this thesis.
- **Chapter 2**, synthesises the relevant scientific literature, focusing on the most commonly used remote sensing technologies and methods in investigating tropical peat swamp forests, specifically land cover dynamics, fire events and AGB estimation.
- **Chapter 3**, introduces the study area and the datasets used in this thesis.
- **Chapter 4**, presents the methods and results that have been used to address **objective 1**; the research in this chapter examines the relationship between tropical peat swamp forest AGB and small-footprint occupied airborne lidar discrete return and full waveform derived metrics, with a view to establishing the optimal use of the technology in this environment.
- **Chapter 5**, presents the methods and results that have been used to address **objectives 2 and 3**; the research in this chapter uses the knowledge and data outputs derived from **Chapter 4** to demonstrate the capability of Sentinel-2 satellite data in delivering accurate, high resolution AGB maps of the study site for the years 2015 and 2018 using a Random Forest machine learning method. The research further explores the AGB dynamics between 2015 - 2018 in terms of peat

swamp forest gains and losses in response to reserve management and restoration activities.

- **Chapter 6**, presents the methods and results that have been used to address **objective 4**; the research in this chapter investigates the use of remote sensing and organic geochemistry methods for assessing the impact of tropical peat swamp forest degradation on the underlying peat soil profile. The research demonstrates the utility of Landsat archive data for landscape scale assessment of degradation over a 30 year time period (1989 -2019). Soil cores collected from 4 different forest condition classes (Central Forest, Management Recovery, Disturbed Forest, and Fire Affected) was processed using Rock-Eval 6 pyrolysis, to quantify the carbon stored in the peat and track soil organic matter thermal stability throughout the peat profiles.

- **Chapter 7**, summaries the results obtained from this thesis in relation to each of the four research objectives. The impact of the research is discussed in view of the methodological contributions and the environmental management and policy contributions. Limitations of the research, a future outlook and recommendations for future tropical peat swamp forest mapping and monitoring is also presented.

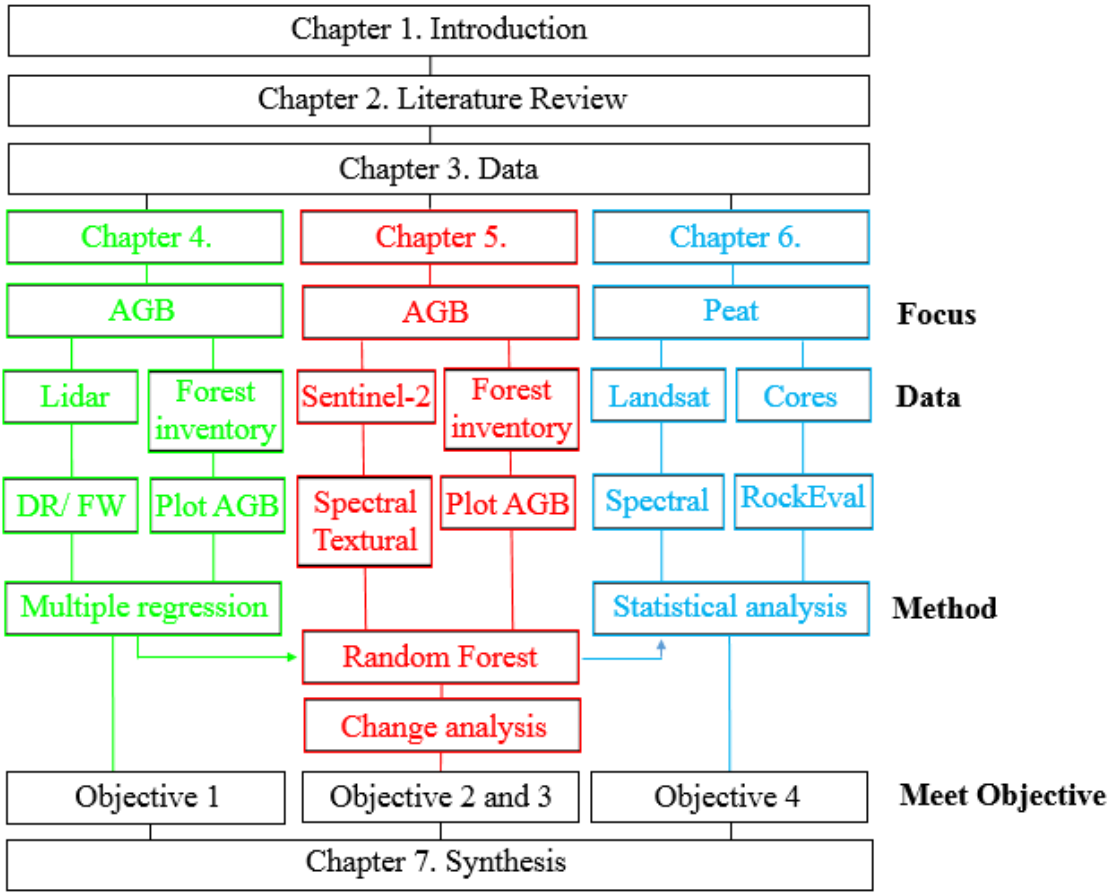


Figure 1-2 Thesis overview and interaction between the three research chapters (**Chapter 4, 5 and 6)**.

Figure 1-2 provides an overview of the thesis chapters, illustrating how chapter outputs are linked and interact to meet the research objectives. **Chapter 4** focuses on AGB, producing an optimal AGB lidar derived model, via multiple regression, meeting **objective 1.** AGB lidar model results are fed into **Chapter 5** as training and validation data for a Random Forest modelling method. **Chapter 5** focuses on AGB, producing AGB maps covering the entire reserve to meet **objective 2**, this output is fed into **Chapter 6** as data for statistical analysis. A change analysis is run on the Random Forest AGB map outputs for the years 2015 and 2018 to characterise AGB gain and loss across the entire NSPSF, meeting **objective 3**. **Chapter 6** focuses on peat, where a

variety of statistical analysis methods are run on datasets derived from remote sensing and organic geochemistry methods to assess the impact of tropical peat swamp forest degradation, meeting **objective 4**. Combined, the research objectives are designed to form a more complete understanding of degradation and rehabilitation in NSPSF. This thesis recognises the synergy between AGB and peat soil in tropical peat swamp forests and the importance of researching the interactions and connections between them.

1.6 Thesis publication

Chapter 4, 5 and 6 are in various stages of the publication process (Table 1-2). For chapters which have been published the published manuscript can be found at the end of the thesis (**Appendix 1**).

Table 1-2 The paper title, status of publication and journal (target journal) for research conducted during my PhD.

Title	Status	Journal (Target Journal)
Tropical peatland vegetation structure and biomass: optimal exploitation of airborne laser scanning **(Appendix 1)**	Published (2018)	*Remote Sensing*
Restoration of Malaysia's tropical peat: remote sensing for monitoring restoration management in tropical peat swamp forests	In prep	*(Journal of Environmental Management)*
Detecting tropical peatland degradation: combining remote sensing and organic geochemistry	In prep	*(PloS one)*
Denial of long-term issues with agriculture on tropical peatlands will have devastating consequences **(Appendix 2)**	Published (2017)	*Global Change Biology*

Throughout the course of my PhD I have been involved in a number of different projects related to tropical peat swamp forest research that have not been included as research chapters in this thesis. **Appendix 2** presents the article 'Denial of long-term issues with agriculture on tropical peatlands will have devastating consequences' published by *Global Change Biology* in 2017, on which I am a co-author.

Chapter 2: Literature Review

This chapter provides an overview of the main sensors and modelling methods used in tropical peatland assessment. It also highlights some of the challenges inherent in to the applications of remote sensing data for tropical peatland assessment.

2.1 Remote sensing data sources

Remote sensing, the science of obtaining information via noncontact recording, has become an indispensable tool in the mapping and monitoring of tropical peatland environments. Three broad types of remote sensing sensors will be discussed: optical (passive), radar (active), and lidar (active). Passive sensors register energy that is either reflected by or emitted from an object, whereas active sensors produce their own energy source and record the return signal (Figure 2-1). Remote sensing can provide the opportunity to produce repeatable Earth observation datasets from local to global scales. Each broad sensor type has its own particular sensitives and capabilities. Users need to be aware of these benefits and limitations of the sensors when selecting an appropriate data source. Remote sensing data selection is largely determined by: the project objective, cost of data, climatic conditions (especially cloud cover) and the technical complexity of data processing and interpretation.

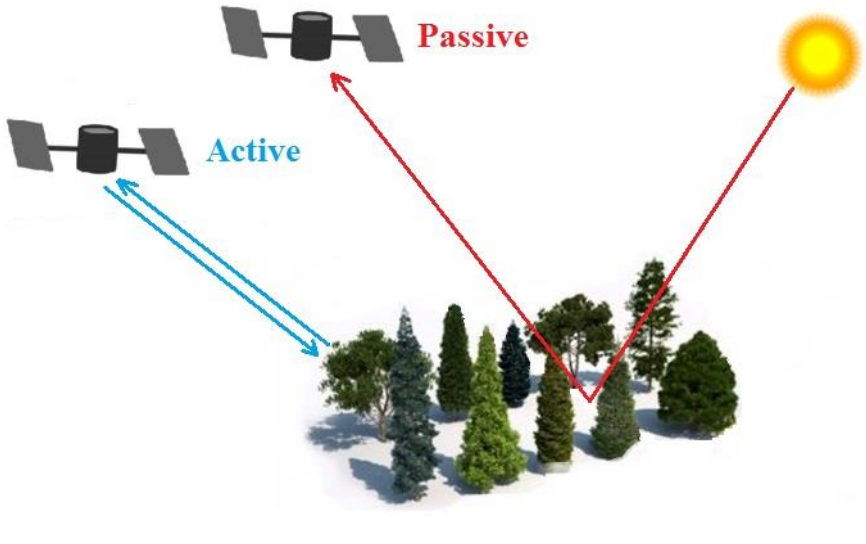


Figure 2-1 Difference between passive and active sensors.

2.1.1 Optical

Optical sensors detect and record energy (radiation) that is emitted or reflected by an object, typically in the visible, near-infrared, and short-wave infrared areas of the electromagnetic spectrum (approx. 0.4 – 2.5 μm) (Figure 2-2). Different materials reflect, absorb and transmit the Sun's energy at different wavelengths, this unique response is known as an object or surface's spectral reflectance signature. Optical sensors record areas of the electromagnetic spectrum as 'bands'. The number, position and width of these bands are specific to the optical sensor system and largely driven by the desired application for the data output. Dependent on these band specifications, optical sensors can be categorised as multispectral or hyperspectral. Hyperspectral sensors use hundreds to thousands of narrow bands (10 - 20 nm band width) to record the Earth's surface. Typically, hyperspectral data is recorded from an imaging spectrometer, with the ability to build highly detailed spectral reflectance signatures for objects/targets. This provides data not purely for object or surface detection, but also for improved classification of the material

and chemical composition. Multispectral, or broadband, sensors typically use 3 to 15 broadly defined spectral bands, (Campbell and Wynne, 2011) to image the Earth's surface.

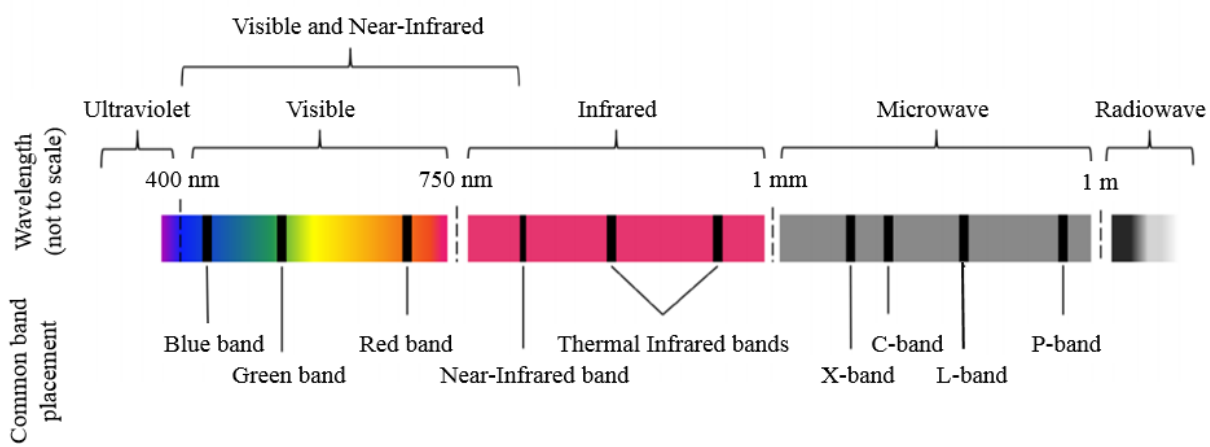


Figure 2-2 Electromagnetic spectrum (not to scale). Modified from Pettorelli *et al.*, (2018).

Spectral indices are an algebraic combination of spectral bands (two or more) calculated to enhance the features of interest in optical data. A large variety of spectral indices have been established (Cundill *et al.*, 2015), vegetation indices are the most common example, as well as indices related to fire damage, water, man-made structures, and geologic features. Since the early development of vegetation indices in the late 1960's (Jordan, 1969), hundreds of indices have been investigated to improve the assessment and characterisation of vegetation. Vegetation indices are often generated to capture vegetation productivity, reduce the effects of extraneous influences (such as soil background or atmosphere), or to focus on other chemical or structural components.

Table 2-1 Examples of common optical sensor/platforms, with their spatial and temporal resolutions and band number information.

Sensor/ Platform	Spatial resolution (pan)	Spatial resolution (multi)	Spatial resolution (thermal)	Revisit time	Band number
AVHRR/NOAA		1 km	1 km	daily	5 bands
MODIS/ Terra		250 – 1000 m	1000 m	1-2 days	36 bands
ASTER/Terrs		15 – 30 m	90 m	16 days	14 bands
ETM+/ Landsat-7	15 m	30 m	60 m	18 days	8 bands
OLI and TIRS/ Landsat-8	15 m	30 m	100 m	16 days	11 bands
MSI/ Sentinel-2		10 – 60 m		5 days	12 bands
RapidEye		5 m		5.5 days	5 bands
SPOT- 6 & 7	1.5 m	6 m		daily	5 bands
Ikonos	82 cm	3.2 m		1-3 days	5 bands
Doves		3 m		daily	4 bands
Quickbird-2	61 cm	2.4 m		1-3 days	5 bands
WorldView-2	50 cm	1.85 m		1-4 days	9 bands
WorldView-3	31 cm	1.24 – 3.7 m		1-4 days	29 bands
Geo-Eye-1	46 cm	1.84 m		2.1 days	5 bands

There are a large number of multispectral sensors on board satellites currently in orbit which differ in their spectral, temporal, and spatial resolutions. For multispectral space-borne sensors, the data produced is largely determined by the trade-off between spatial and temporal resolution (Table 2-1).

The capacity for large coverage, easy access, and low cost (often free at lower spatial resolutions 10 m – 1 km), from multispectral space-borne sensors offers a practical and economical means to study the Earth's surface. Additionally, long standing satellite series, such as the Landsat mission, have created rich archives of global optical data for over 45 years. However, clouds

and their shadows can block or reduce an optical sensors view of the Earth's surface. This impacts the spectral information captured, reducing the accuracy of the target data and interpretation (Zhu *et al.*, 2015). Moreover, optical sensors are also restricted to daylight hours, thus reducing the number of potential imaging hours in comparison to active sensors.

2.1.2 Radar

Radar (RAdio Detection And Ranging) data was not used in this thesis research, so is only mentioned briefly here for completeness. Radars are active sensors which produce their own source of microwave radiation (wavelengths ranging from around 1 m – 0.001 m (300 MHz - 300 GHz)). The basic principle is high energy pulses are emitted, and the returning echoes are recorded by the same antenna. Unlike optical sensors, radar is not limited to daylight hours or by atmospheric conditions, for example haze, clouds and light rain, making them ideal for use over the tropics where persistent haze and cloud cover limits the effectiveness of optical data. However, the application of radar data has been restricted by the complexity of data processing and analysis in comparison to optical sensors.

Synthetic Aperture Radar (SAR) is the most common type of imaging radar system for mapping and monitoring the Earth's surface. SAR (airborne or space-borne) is a side-looking radar system. It uses relative motion between the antenna and the target to derive long-term coherent signal variations which are used to generate imagery. SAR data has been used to investigate properties such as: slope, roughness, humidity, textural in-homogeneities, and dielectric constant. Interferometric SAR (InSAR) combines multiple SAR images over the same area to detect change (Evans and Schulz, 2018).

SAR satellites operate at a designated radar frequency, with increased wavelength size categorised as X-, C-, S-, L- and P-band sensors. The longer the wavelength, the deeper the radar pulse can penetrate through dense vegetation structures. For example, the X-band will reflect back from the canopy layer whereas the longer L- and P-bands have the potential to penetrate through the canopy and retrieve soil surface information (Englhart *et al.,* 2011; Goetz *et al.,* 2009). Several SAR satellites are currently in orbit, including the Copernicus sensors Sentinel-1A and 1B (C-band) and Advanced Land Observing Satellite PALSAR (L-band). Products such as ERS-1/2, JERS-1, ENVISAT ASAR, and RADARSAT-1/ 2 are available at a 10 m or finer spatial resolution at a high temporal frequency.

2.1.3 Lidar

Lidar (Light Detection And Ranging) is an active sensor technology. These systems work under similar principles to radar but use light energy from a laser pulse to derive distance, or range, measurements between the sensor and the target surface, using the algorithm:

$$R=ct/2$$

Where: R = distance between the lidar instrument and the target, t = time between transmission and reception of the pulse, and *c* = the speed of light.

Lasers used for terrestrial applications typically operate in the near-infrared region of the spectrum, in the range of 900 - 1064 nm, where reflectance of green vegetation is high. This ensures a high energy return back to the sensor. However, a disadvantage of recording in this region is the absorption of near-

infrared wavelengths by clouds; this restricts the use of these instruments in cloudy conditions (Mather and Koch, 2011).

A laser alone cannot determine the coordinates of the ground targets, it must be teamed with a positioning system to determine precisely these points in space. This includes a Global Positioning System (GPS) to measure the exact position of the sensor platform in space (x, y, z), an Inertial Navigation System (INS) - also referred to as inertial measurement units (IMU) - to measure the altitude (roll, pitch and yaw) of the sensor, and angle encoders for the orientation of scanning mirrors (for scanning systems). Combining the information obtained from these technologies with accurate time referencing yields the absolute positioning of the reflected target surface or surfaces. Advances in these technologies have driven the rapidly increasing number of applications for lidar technology (Wuldner *et al.*, 2012a).

Lidar systems can be classified according to:

- platform: ground based, airborne and space-borne
- footprint size: small footprint and large footprint
- return signal: discrete return and full waveform

Platform -

There are three main types of lidar sensor platform: ground based, airborne and space-borne. The choice of sensor platform is ultimately based on the data's purpose (Popescu *et al.*, 2011). The three platforms vary in the size of the area to be captured, the range of measurement desired, and the cost of equipment. Ground based platforms, or terrestrial lidar systems, can produce

very high-resolution sampling densities (potential sub-centimetre resolution), however, the data is limited to local scales. Ground based systems are typically mounted on stationary tripods or on moving vehicle. Airborne lidar platforms are further classified as occupied (systems mounted on helicopters and airplanes) or unoccupied (systems mounted on Unmanned Aerial Vehicles (UAVs)). Airborne lidar provides the best measurement accuracy for terrain elevation and vegetation heights, producing very high resolution datasets. However, these systems are associated with the highest operational costs limiting the extent and frequency of spatial and temporal sampling (Zhao *et al.,* 2009). Space-borne lidar systems are mounted on satellites that orbit the Earth. Space-borne lidar, such as the Advanced Topographic Laser Altimeter System aboard the Ice Cloud and Land Elevation Satellite 2 (ICESat-2), can sample at continental to global scales at a low sampling density (relative to airborne or ground based platforms).

Footprint size -

A lidar sensor's footprint is the horizontal sampling area, typically circular or elliptical in shape, with the size of the footprint increasing with distance from target surface to the system (Popescu *et al.,* 2011). Small footprint systems are classified as having a footprint with a diameter of 0.2 - 3 m, depending on the flight height and beam divergence (Mallet and Bretar, 2009). These systems provide a high point density and an accurate surface representation (Wulder *et al.,* 2012a), and as a result have been routinely employed in detailed local topographic applications. The main disadvantage associated with small footprint systems is that their small beam size means mapping large areas require extensive surveys at a high cost. Additionally, for forestry

applications, small footprint systems can be restricted by the spacing between the points at which the lidar pulse hits a target. Small footprint systems frequently oversample the crown shoulder and can miss the tops of trees, which means that true canopy topography must be reconstructed statistically.

Large footprint systems are classified as having a footprint with a diameter of 10 - 70 m (Mallet and Bretar, 2009). This increase in beam size combats the biases of small footprint systems in forestry applications, since the beam is greater than the average crown diameter of a canopy-forming tree (10 - 25 m). This means the probability of the laser energy consistently hitting both the ground and the canopy top is increased. Additionally, large foot-print systems have a wide image swath, therefore when mapping extensive areas the expense and survey time is reduced.

Return signals -

A lidar sensors return signal can be categorised as discrete return (DR) or full waveform (FW) (Figure 2-3). DR systems record single or multiple returns from an emitted laser pulse. A filter is employed so that as the laser pulse is reflected back to the sensor the largest peaks (the brightest returns) are interpreted to be discrete objects in the path of the laser beam. These peaks are recorded as discrete points. Alternatively, FW systems record the entire reflected energy from a laser return. A waveform is constructed, plotting amplitude against time, thus representing the complete vertical profile of the area of interception.

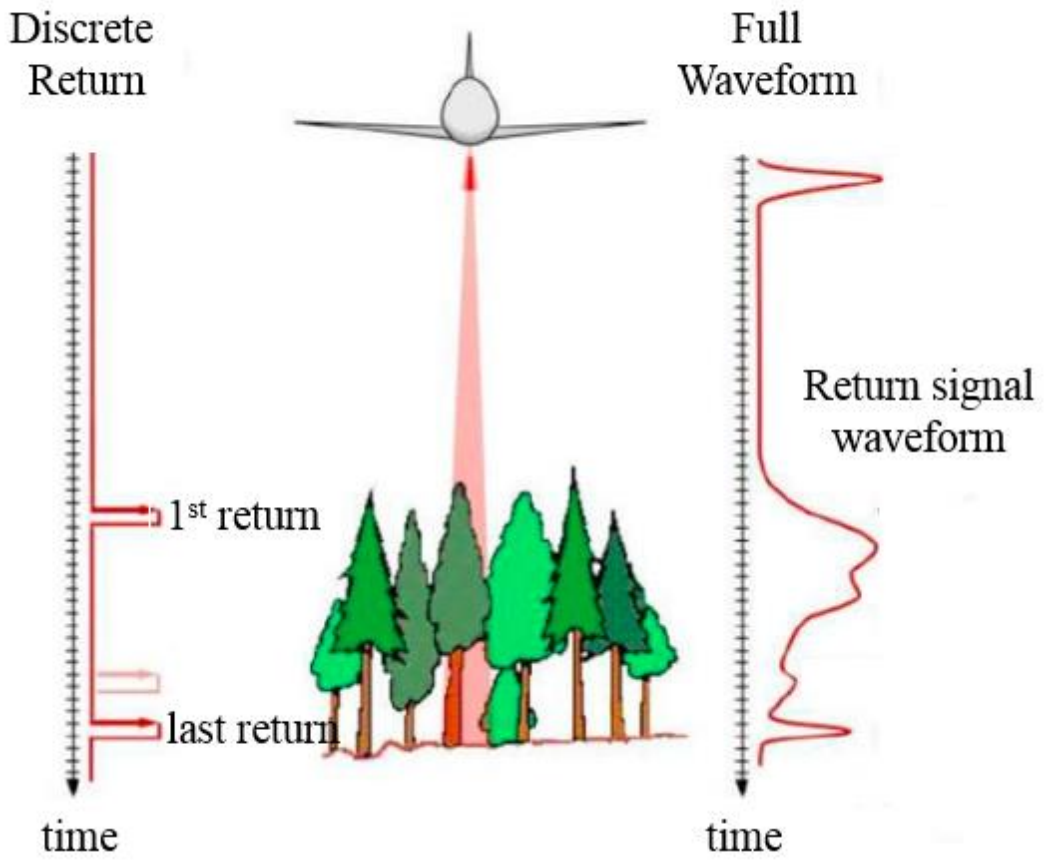


Figure 2-3 Difference between discrete return (left) and full waveform (right) lidar systems. Modified from Ferraz *et al.*, (2009).

Both DR and FW systems have advantages and disadvantages. DR systems are known to produce high ground point density datasets (Wulder *et al.*, 2008; Naesset, 2004). These datasets have enabled high resolution representation of complex surfaces in the horizontal plane (Ussyshkin and Theriault, 2011), making DR the preferred data choice in detailed topographic mapping. However, the coarser resolution of measurements in the vertical plane (1 to 5) has restricted the use of DR data for some three-dimensional mapping applications (Lim *et al.*, 2003). For example, the analysis of dense forest canopies is often limited by DR systems, as the full vertical profile of the canopy structure is not recorded. Instead only a proportion of the canopy layer

and ground surface is represented. In contrast, FW systems produce a more complete data representation of dense canopy profiles (Magruder *et al.,* 2010; Reitberger *et al.,* 2008; Wagner *et al.,* 2008), in particular for the mid– and lower- levels of the canopy structure often not recorded by DR data. Additionally, by recording the complete backscattered waveform during acquisition, FW data provides the user with more flexibility and control in the data processing and interpretation steps (Chauve *et al.,* 2009). However, the handling and interpretation of FW datasets is a more complex and skilled task in comparison to DR point cloud data, with Ussyshkin and Theriault (2011) suggesting that this has limited the commercial use of FW datasets. The rich content of FW datasets has also limited its application in topographic mapping, as the overwhelming volume of data recorded by FW systems is redundant when only a few discrete points are required to create a digital elevation map (DEM).

2.2 Modelling approaches

A wide range of modelling approaches, developed in the field of computational statistics and machine learning, has been applied to airborne and space-borne remotely sensed datasets. Standard linear modelling has long been employed in the field of remote sensing (Yu *et al.,* 2014), identifying local relationships between remote sensing predictors and reference measurements. However, the enormous increase in remote sensing data - at large extents and at high dimensions (spectral, temporal and spatial) - and computational resources has recently encouraged the use of machine leaning methods (Thanh and Kappas, 2018).

Machine learning is an empirical approach for regression and/ or classification in nonlinear systems. The approach employs algorithms to analyse information, recognize patterns, and improve prediction accuracy through automated, repeated learning and model development. Machine learning has proven to be an extremely powerful tool in a wide variety of Earth system applications (Madadi *et al.,* 2015; Azamathulla *et al.,* 2012; Lary *et al.,* 2009; Brown *et al.,* 2008). Common examples of machine learning algorithms include: Artificial Neural Networks, Support Vector Machines, decision trees and ensemble methods such as Random Forests. A number of recent reviews have investigated the use of machine leaning methodologies (Maxwell *et al.,* 2018; Zhu *et al.,* 2017; Belgiu *et al.,* 2016; Lary *et al.,* 2016). The strengths of machine learning in the field of remote sensing has been attributed to their ability to model complex class signatures and process a large variety and number of input predictors, without making assumptions about the data distribution (i.e. non-parametric).

The main concern with the application of remote sensing data in complex models is the issue surrounding model overfitting. Overfitting occurs when the noise or random fluctuations in training data is learned by the model. This negatively impacts the accuracy or performance of the model on new datasets. Research adopting high dimensional remote sensing training data are often associated with a large number of redundant variables (often highly correlated with each other) which may lead to high variance on parameter estimates and inaccurate predictions (Hawkins, 2004). Several approaches have been developed to avoid overfitting, for example the Akaike Information Criterion is based on fixed penalties for model complexity (Sakamoto *et al.,* 1986).

Alternatively, training data can be split in two, one half for model calibration and the other half for evaluating the model predictive error. Leave-one-out cross validation and k-fold cross-validation follow this approach (Wong *et al.*, 2015). Resampling methods, from jackknife or bootstrapping, can additionally be employed to produce estimates on mean and standard deviation of non-parametric models (Efron, 1981). Machine learning algorithms such as Random Forest or Support Vector Machine typically split the data into training and validation sets.

2.3 Application of remote sensing in tropical peat ecosystems

In order to conserve the remaining tropical peat ecosystems and locate sites for potential peatland restoration efforts, it is essential to have up-to-date data on the extent, health, and dynamics of these valuable ecosystems. Tropical peatland environments can be identified by a unique set of characteristics such as vegetation type, topography (dome structure), and high water table levels (Lawson *et al.*, 2015). Remote sensing has been increasingly used to deliver datasets and products suitable for identifying these characterises as well as analysing tropical peatland area and dynamics at temporal and spatial scales appropriate for large-scale tropical peat swamp forest assessment (Minasny *et al.*, 2019).

Optical data from broadband space-borne sensors are the primary data source for tropical peatland mapping and monitoring. For example, Landsat (Miettinen *et al.*, 2016; Franke *et al.*, 2012; Jaenicke *et al.*, 2010), MODIS (Moderate Imaging Spectrometer) (Wijedasa *et al.*, 2012; Langer *et al.*, 2007), and SPOT (Systeme Pour l'Observation de la Terre) (Miettinen *et al.*, 2010;

Segah *et al.*, 2010). However, high cloud cover and increasing haze/smog episodes often limits the data available from these sensors in the tropics. To overcome this issue, data captured by space-borne sensors with higher revisit rates are often adopted (Table 2-1), which increases the chance of usable data. The trade-off here often being spatial resolution; a potential issue in heterogeneous peat swamp forests and small-scale landscape feature detection (for example logging roads, drainage canals, etc.).

Active sensors which can penetrate cloud cover, such as radar and lidar, have been used to characterise tropical peatland vegetation (Englhart *et al.*, 2013; Boehm *et al.*, 2013) and provide accurate topographic data (Minasny *et al.*, 2018; Ballhornn *et al.*, 2011). Data fusion techniques are emerging as a powerful way to integrate information from multiple sensors in tropical peatland applications (Torbick *et al.*, 2016; Margono *et al.*, 2014b; Wijaya *et al.*, 2010). This combines the benefits offered by different systems and reduces the limitations associated with individual sensors.

Remote sensing data has been notably used in tropical peatlands for land cover and land cover change analysis (forest cover, land conversion, etc.), investigation of fire events, AGB estimation, and analyses of the underlying peat soil.

2.3.1 Land cover

Assessing the location, extent and frequency of land cover, as well as identifying the spatial and temporal patterns of land cover change, provides key information for tropical peatland management and indicate drivers of peatland degradation. Remote sensing approaches for land cover and land

cover change can inform tropical peatland management at a higher accuracy and lower cost compared to ground measurements (Gomez *et al.,* 2016). Long-standing spectral time-series analysis from Landsat and SPOT data found by 2007 forest cover in the tropical peatlands of Peninsular Malaysia, Sumatra and Borneo had decreased to 42% (Miettinen and Liew, 2010), 36 % by 2010 (Miettinen *et al.,* 2012a), and decreased even further to 29% in 2015 (Miettinen *et al.,* 2016). Expansion analyses from land cover maps of industrial plantations for the years 1990, 2000, 2007 and 2010 reported an increased growth of palm oil areas on peatland in Peninsular Malaysia, Sumatra and Borneo of 0.27 Mha in 1990, 1.03 Mha in 2000 and 3.20 Mha in 2010. Annual growth rates of industrial plantations on peatland, based on visual interpretation of space-borne optical data, decreased from 14.44% for 1990 - 2000 to 11.85% for 2000 - 2010 (Miettinen *et al.,* 2012b). Wijedada *et al.,* (2012) demonstrated a new alternative post-classification composting approach for Landsat data in order to deal with the issue of data gaps related to sensor error (SLC-Off) (Wulder *et al.,* 2011) and cloud cover. The study overcame the missing data issues by layering multiple images of the same scene for the years 2000, 2005, and 2010 to produce land cover maps for peatlands in Peninsular Malaysia, Sumatra and Borneo. The study produced an overall classification accuracy of 77% for 2000, 85% for 2005, and 86% for 2010. Torbick *et al.,* (2016), adopted a sensor fusion approach to tackle the issues of similar spectral characteristics between natural forests and forest plantations (for example rubber, acacia and oil palm). The study demonstrated, through a Classification and Regression Tree (CART) framework using Random Forest, the fusion of Sentinel-1 C-band and PALSAR-2 L-band

backscatter metrics, with Landsat-8 OLI reflectance and textural indices, to be useful for separating oil palm and rubber plantations from other land cover classes. As data archives from space-borne sensors grow, land cover methods and products can continue to advance and provide valuable information on tropical peatland dynamics at increasing spatial and temporal resolution.

2.3.2 Fire

Fire is one of the major drivers of tropical peatland degradation, remote sensing has been increasingly adopted to map the extent, severity and frequency of large scale fire events. Space-borne optical archive data has been used to monitor repeated mega-fire events in South-East Asia and quantify millions of hectares of degraded peatland as a result (Hoscilo *et al.*, 2011; Segah *et al.*, 2010; Langer *et al.*, 2009). Cattau *et al.*, (2016) utilised the Active Fire product from NASA's MODIS to investigate the source of human introduced fire in a peat swamp forest area in Central Kalimantan, Indonesia. The MODIS Active Fire product detects fires (1 km spatial resolution) that are burning at the time of sensor overpass using a contextual algorithm (http://modis-fire.umd.edu/). The study refuted the claim that most tropical peat swamp forest fires originate in oil palm concessions in the study area, with 2% of fires detected in the forest originating from oil palm agriculture and 2% as a result of close proximity to settlements. The study found most fires originated in non-forest. Saputra *et al.*, (2017) successfully used the Normalized Burning Ratio (NBR) index, calculated from Landsat data, to evaluate the severity level and total area of burnscar after large-scale fires in 2015 in the Merang-Kepahyang peat forest. The NBR index uses the shortwave-infrared and near-infrared portions of the electromagnetic spectrum

to identify burned areas (Garcia and Caselles, 1991). Elvidge *et al.,* (2015) used a novel approach to investigate smouldering peat fires used short-wave infrared and long-wave infrared nighttime Landsat 8 data to track distinct combustion phases (high temperature flaming and low temperature smoldering). Results could detect smoldering peat fires in Landsat 8 nighttime data in the 40 – 90 m^2 range.

Lidar data has been increasingly used to develop pre- and post-fire peat DEMs, enabling the spatial quantification of burned area extent and depth, calculated as the surface elevation difference between adjacent unburned and burned peat (Ballhorn *et al.,* 2009). Ballhorn *et al.,* (2009) used lidar to determine depth of burn for single fire events in peat swamp forests in Central Kalimantan. On average a mean burned area depth of -0.33 ± 0.18 m was observed. Konecny *et al.,* (2016) investigated fire driven tropical peat loss and the relationships between burned area depth, fire frequency and distance to drainage canals using a lidar peat surface modelling methodology. The study reported burned area depth to decrease after multiple fire events and that increased proximity to drainage canals increased both burned area depth and probability of recurrent fires. Studies, such as those mentioned above, are vital in providing accurate data and gaining new understanding of tropical peat fires to guide and revise tropical peat carbon storage and emission accounting. Despite the success of lidar technology in tropical peat fire assessment, research is often restricted by the high cost of repeated large-scale lidar surveys. Simpson *et al.,* (2016) sought to address this limitation by using structure from motion (SfM) photogrammetry, supplemented with lidar data, to investigate tropical peatland depth of burn. Data was collected using a low-

cost, low-altitude unmanned aerial vehicle for a tropical peatland in Jambi Province on Sumatra, Indonesia. Pre-and post-fire digital terrain models were created with an accuracy of 0.04 m and 0.05 m to calculate burn depths across the study area. On average depth of burn was reported as 0.23 ± 0.19 m.

2.3.3 Above Ground Biomass

Remote sensing technology is routinely used to estimate and assess the spatial distribution of AGB, providing a key insight into forest structure and productivity (Hansen *et al.,* 2016a). AGB governs the potential carbon stock held by vegetation, as a result AGB maps and products have become an important resource in climate change mitigation and restoration initiatives (UNFCCC, 2009). New approaches for assessing large-scale AGB are rapidly developing in South-East Asian peatlands, using space-borne lidar and radar (Berninger *et al.,* 2018; Ballhorn *et al.,* 2011) and occupied airborne lidar datasets (Manuri *et al.,* 2017; Wan-Mohd-Jaafar *et al.,* 2017; Boehm *et al.,* 2013). Jubanski *et al.,* (2013) and Kronseder *et al.,* (2012) both examined the use of lidar point cloud data for AGB estimation in degraded peat swamp forests in Central Kalimantan, Indonesia. The studies concluded that a combined approach of extensive field sampling and lidar point cloud analysis produced the most accurate results for AGB estimation, a result commonly shared in the literature (Fassnacht *et al.,* 2014). However, as previously mentioned lidar data is often limited by its ground coverage. Commonly, lidar campaigns in large forest reserves will capture only a subsection of the forest. Remote sensing studies have sought to tackle this issue of missing data with a sensor fusion approach (Tsui *et al.,* 2013; Lu *et al.,* 2012). Asner *et al.,* (2018) combined lidar transect data with Landsat-8 OIL and TIRS data to generating

a wall-to-wall map of above carbon density (derived from AGB) throughout the State of Sabah, Borneo. The study successfully used a deep learning modelling approach to upscale the above carbon density statistical model, generated from lidar transect data, to wall-to-wall coverage across the entire study area. Advances in AGB methods and sensor fusion have enhanced our understanding of large-scale forest function, as well as opening up the possibility of retrospective estimation of AGB from data archives (Landsat programme) to establish historical baselines and track degradation (Pflugmacher *et al.,* 2014). This information is vital in guiding carbon stock decision-making and sustainable management of tropical peat swamp forests.

2.3.4 Peat soil

Peat soil has a distinctive spectral signature, with a notable lower reflectance in the near-infrared and shortwave-infrared regions of the electromagnetic spectrum (Krankina *et al.,* 2008). However, as previously discussed, tropical peatlands are typically covered by thick, dense swamp forests, which optical sensors cannot penetrate through to detect and measure peat soil in isolation. To overcome this obstacle, past research has investigated the relationships between peat soil (depth and subsidence) and surface features that can be detected and measured by remote sensing methods.

The topography of tropical peatlands can create unique environmental gradients related to peat dome structures, for example, changes in the forest canopy structure. Towards the centre of peat domes (deepest peat deposits) the forest canopy has been documented to be shorter, and more densely packed together as a result of reduced nutrient availability in the peat soil (Page *et al.,* 1999; Bruenig and Droste, 1995; Anderson, 1961). Nguyen *et al.,* (2016) and

Wedeux and Coomes (2015) both investigated the relationship between canopy structure (height and gap density) and peat thickness using occupied airborne lidar data. This approach should be restricted to only natural, undisturbed peat domes as canopy gaps and the absence of tall trees may be a result of selective logging practises common in South-East Asian peatlands. Additionally, local variations in peat depth may also be more dependent on small scale, often complex, variations in the underlying topography (Kettridge *et al.,* 2008).

Alternatively, Rubiyanto *et al.,* (2016) and Rudiyanto *et al.,* (2018) proposed an open digital soil mapping methodology, which utilises open data in an open-source computing environment, as a cost-effective approach to mapping tropical peat thickness. The digital mapping method predicts field observation with a range of factors that are known to influence peat thickness distribution. Multiple remote sensing derived variables used in these studies, including topography, slope, aspect, wetness index, distance to river and vegetation metrics. Rudiyanto *et al.,* (2018) found elevation, wetness (derived from radar data), valley bottom flatness and distance to the nearest river to be the main controls on tropical peat thickness. Results showed that the open digital soil mapping methods can accurately predict peat thickness, explaining up to 98% of the variation of the data with a median relative error of 5% (average error of 0.3 m). This is a significant improvement for peat thickness mapping accuracy and spatial resolution in comparison to previous research (Jaenicke *et al.,* 2008). However, these models assume a direct relationship between peat depths and present accumulation rates controlled by the model variables (such as topography, elevation, slope, aspect and wetness). This may cause an issue

for degraded tropical forest peatlands or converted peatlands where complex peat degradation processes (both artificial and natural) may weaken these relationships.

Recently, developments in SAR data processing, notably the Intermittent Small Baseline Subset (ISBAS) DInSAR algorithm (Sowter *et al.*, 2016; Sowter *et al.*, 2013), has expanded our ability to remotely detect and track peat soil surface movement. The ISBAS DInSAR algorithm has been successfully applied to Senitinel-1 C-band data to detect tropical peat subsidence, peat breathing, and other ground motion changes (Marshall *et al.*, 2018; Sowter *et al.*, 2018; Cigna and Sowter, 2017). Visualising and quantifying peat surface movement from time-series InSAR data offers a practical approach for peat surface monitoring. The regional coverage and high temporal frequency available from space-borne sensors are key advantages in comparison to field-based observations from individual monitoring stations.

2.4 Summary: Research challenges and opportunities

In summary, this chapter presented the main remote sensing data sources (optical, radar and lidar) and advances in modelling approaches, in particular the strengths of machine learning algorithms with complex datasets. The advantages and challenges inherent to each sensor were identified and prominent tropical peatland applications discussed.

From the literature presented, a key division in tropical peat swamp forest research exists between the two disciples of peatland ecology and forest ecology. Research exploring both forests and the underlying peat is rare (Page et al., 1999), thus there is an opportunity to expand our knowledge and

understanding on the connections and interactions between forest and peat in tropical peat swamp forest research.

The reviewed literature demonstrated the recent use of remote sensing data in tropical peatland assessment, which highlighted lidar as an accurate data source to characterise tropical peat swamp forest vegetation and topographic mapping. However, past research in tropical peat swamp forests has been limited to DR lidar only with limited spatial coverage across tropical peatland catchments. An important challenge has emerged in the literature in the optimal use of lidar data in tropical peat swamp forests, alongside developing strategies to overcome limitations in spatial coverage.

This literature review described the various forms of tropical peatland deforestation and degradation in detail alongside the current methods of largescale tropical peatland assessment (from land cover, fire and AGB). To date, a number of tropical peat restoration interventions have been attempted to restore degraded peatlands, yet there remains limited rigorous reflection on the effectiveness of these interventions. A major knowledge gap exists in coherent large-scale assessments of restoration and management efforts. This information is vital to guide and adapt future restoration strategies and sustainable management.

The research in this thesis seeks to address the challenges and opportunities uncovered by the literature review. Research in all of these areas will contribute to the growing field of tropical peat swamp forest ecology, investigating methods to better map and monitor these unique and vulnerable ecosystems.

Chapter 3: Data

3.1 Study site

The research in this thesis focuses on NSPSF, a large tropical peatland located on a flat coastal plain on the north-west sector of Selangor, Peninsular Malaysia (Figure 3-1). NSPSF comprises of four forest reserves - Raja Musa Forest Reserve, Sungai Karang Forest Reserve, Bukit Belata Extension Forest Reserve (partial) and Sungai Dusun Forest Reserve. With a combined total of 81,304 ha (Parish *et al.*, 2014), NSPSF is one of the largest remaining peat

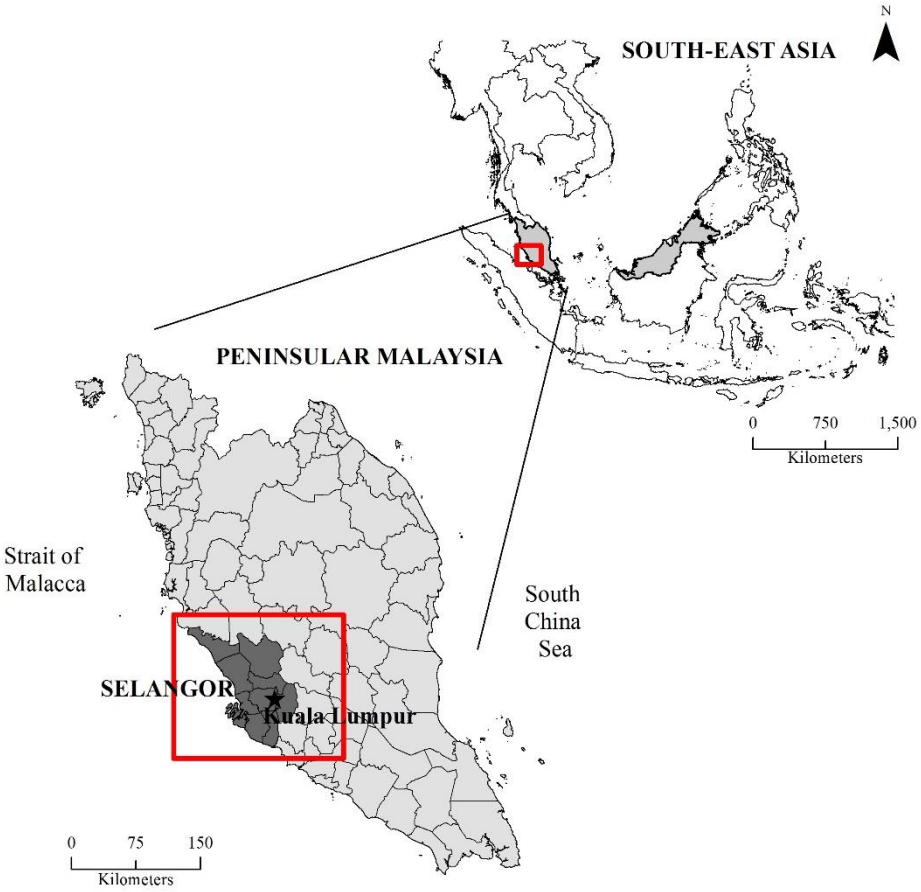


Figure 3-1 The location of the State of Selangor in Peninsular Malaysia.

swamp forests in peninsular Malaysia (Ahmad, 2014). The reserve itself makes up a third of the total area of forest cover in Selangor. As a result, NSPSF has been increasingly recognised for its global importance as a terrestrial carbon store (Davies, 2011; Prentice, 2011; ASEAN Secretariat and Global Environment Centre, 2011).

NSPSF was designated as a permanent reserve forest in 1990. Prior to this status, the forest was classified as state land and was subject to logging activates (without strict controls) (Parish *et al.,* 2014). After more than 30 years of selective timber harvesting large areas of the forest have been left severely degraded. The majority of the reserve is now covered by medium and low density swamp forest, with 5% now covered by grass/ scrub land. The extraction of timber from the reserve led to the construction of a 500 km network of drainage canals throughout NSPSF (Figure 3-2), degrading the forest and accelerating the drainage of the peat soil.

In acknowledgement of the intensity of forest degradation, the Selangor State Government introduced a moratorium on logging for 25 years in forest reserves. All logging activates in NSPSF ceased in 2007 (Parish *et al.,* 2014). No new timber harvesting licenses have been issued for operations within forest reserves in the State of Selangor (Parish *et al.,* 2014). Additionally, a large proportion of potential production forest land in Selangor has been reclassified as heritage parks, where logging is also prohibited.

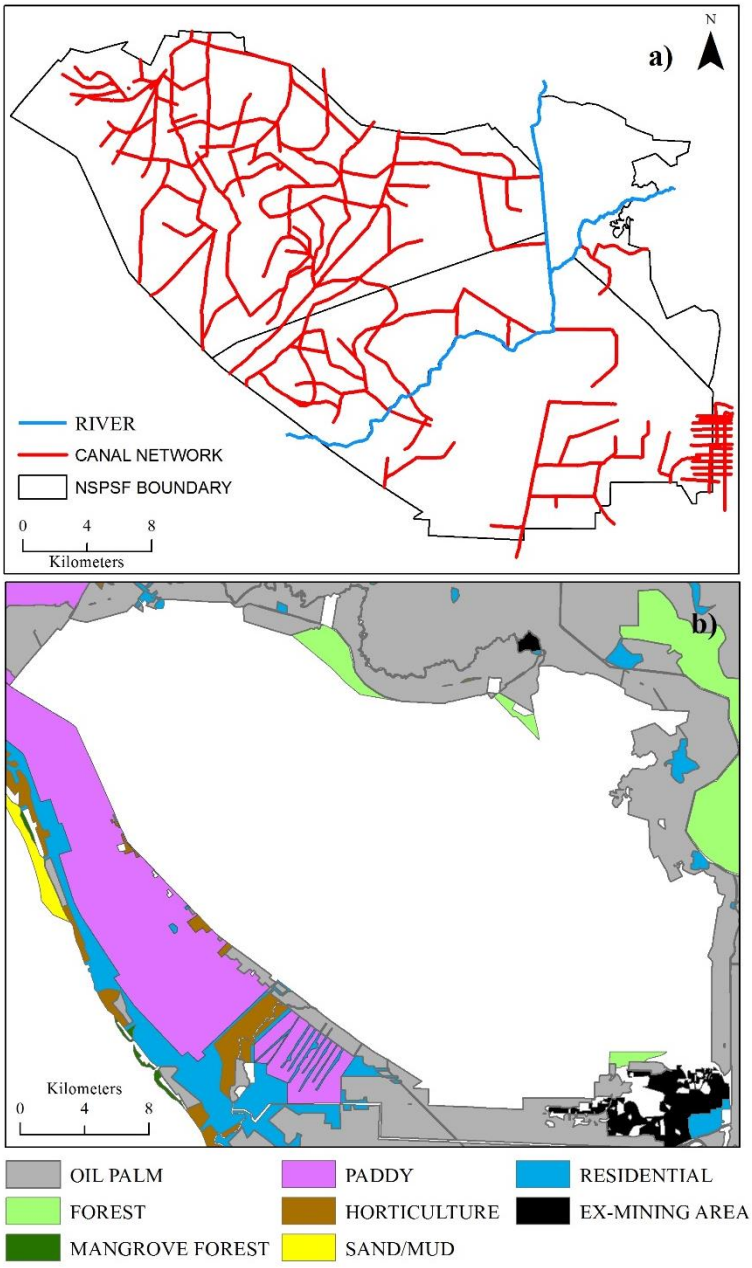


Figure 3-2 (a) Map of NSPSF showing the canals network and the Sungai Tenggi River; (b) Map of NSPSF showing the land use adjacent to forest reserve.

In keeping with the typical dome-shaped morphology of South-East Asian peat swamps, NSPSF is thought to comprise of two peat domes naturally divided by the Sungai Tenggi River. In 2013, a peat depth survey was conducted by the Selangor State Forestry Department throughout the reserve. The survey recorded a maximum peat depth of 10.15 m in the Sungai Karang

Forest Reserve, with an average peat depth of 3.6 m for the entire NSPSF, based on 83 peat depth points (Parish *et al.,* 2014).

NSPSF's tropical climate is characterised by heavy rainfall, high temperatures, and high humidity. The area receives a mean annual rainfall in the range of 1,500 mm to over 2,500 mm (Yule and Gomez, 2009), with distinct peaks from March to April and October to November indicating the monsoon season. The dry season occurs in the months of January to February and May to September. NSPSF has an average recorded shaded air temperature of 28.5^{o}C, with an average monthly relative humidity of 77.2% (Hahn-Schilling, 1994).

NSPSF is of high biodiversity importance. The reserve provides a habitat for some rare species of blackwater fish such as the genus *Encheloclarias* (Ng *et al.,* 1994), the near threatened Black Panther *Panthera pardus* and the vulnerable Malayan Sun Bear *Helarctos malayanus* (Prentice and Aikanathan, 1989). It is also home to several endemic tree species (Appanah *et al.,* 1999). Outside of the reserve boundary, NSPSF is an important water resource for irrigating the paddy fields from the Tanjung Karang Irrigation Scheme and for domestic use (Tanjung Karang and Sekinchan). Water is diverted from the peat swamp via two large drains. These water resources are vital in supporting some of the most productive rice paddy fields in Peninsular Malaysia, with the area earning the title 'the rice bowl of Selangor' (Ahmad, 2014). The land use surrounding NSPSF is dominated by oil palm agriculture (Figure 3-2). The first commercial oil palm cultivation in Peninsular Malaysia (1917) was established directly south of NSPSF in Tennamaram. Since the success of this highly profitable crop, there has been wide spread land conversion to private

oil palm plantations in the State of Selangor. Land conversion to industrial oil palm plantations has occurred in areas towards the north, north-west and south of NSPSF, including land following the Batang Berjuntai-Tanjung Karang road in the south. With the encroachment of plantations towards the reserves boundaries, oil palm poses a serious threat to the protection and integrity of NSPSF.

The recovery and protection of NSPSF has become a key focus for a number of local non-government organisation (NGOs) and community-based initiatives, such as Malaysian Nature Society, Global Environment Centre (GEC) and The Friends of North Selangor Peat Swamp Forest. These groups encourage the sustainable management of NSPSF through tropical peat rehabilitation activities, for example drain and canal blocking, replanting programs, the setup of nurseries among local villages for the supply of saplings, promotion of good agricultural practises among smallholder farmers, and the education of villagers on fire prevention (Parnish et al., 2014).

Previous scientific research in NSPSF has concentrated on: biodiversity (Sasidhran *et al.,* 2016; Irvine *et al.,* 2012; Yule, 2010; Voglmayr and Yule, 2006; Beamish *et al.,* 2003; Bexuijen *et al.,* 2001), microbial communities (Jackson *et al.,* 2009), the impacts of tropical peatland degradation (logging, oil palm conversion and fire damage) (Charters *et al.,* 2019; Cooper *et al.,* 2019; Tonks *et al.,* 2017; Adila *et al.,* 2017; Azhar *et al.,* 2011; Ainuddin *et al.,* 2010) and local livelihoods (Abdulkarim *et al.,* 2017).

3.2 Remote sensing

3.2.1 Airborne lidar data

Airborne lidar data for NSPSF was provided by the Natural Environment Research Council (NERC) Airborne Research Facility (ARF)‘s 2014 Malaysia Campaign. Lidar data was captured by the Leica ALS50-II lidar system, on board a Dornier 228 research aircraft. The campaign recorded 22 flightlines on the 13th November, flying at an average altitude of 2181 m and an average speed of 132 knots, and 7 flightlines on the 14th November, at an average altitude of 2145 m and an average speed of 136 knots.

The Leica ALS50-II lidar system is a small footprint lidar sensor with the capacity to record both DR and FW lidar datasets simultaneously. The system measures the distance between the aircraft and the target surface by emitting a laser pulse (4 or 9ns) and recording the round trip time for the light pulse to return. The footprint of the pulse on the ground is approximately 22 cm when fired from 1000 m altitude (ARF, 2011). The aircraft's position during flight is recorded using a differential GPS, with positional information being relayed from a base station of known position. For NSPSF, the data was supplied with the horizontal and vertical datum WGS84 and projected in UTM47N. Additionally, the orientation (roll, pitch, and bearing) of the aircraft is recorded through the IMU.

The DR data was delivered as LAS 1.2 point cloud and ASCII file format, including the time, Easting, Northing, elevation, intensity, classification, return number, number of returns for a given pulse, and scan angle rank.

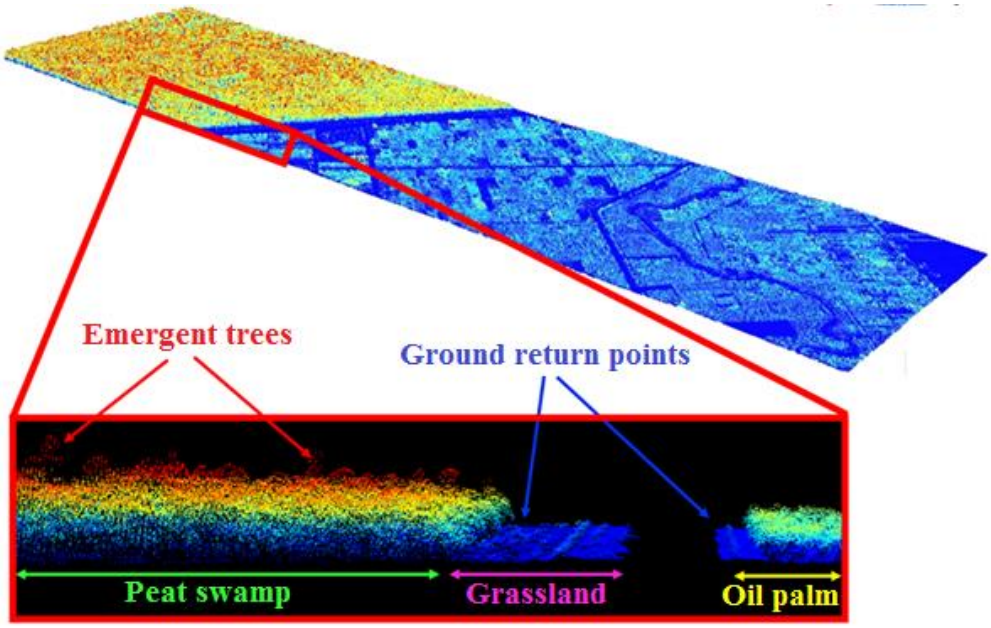


Figure 3-3 Example of one of the ARF flightline DR point cloud datasets representing a transition zone from peat swamp forest within the reserve to oil palm plantation adjacent. The point cloud is coloured by elevation.

For every laser pulse emitted up to 4 returns were recorded, where the 4th is the last return (Figure 3-3). ARF preformed a basic point classification on the datasets to identify potential noisy points, following the American Society of Photogrammetry and Remote Sensing (ASPRS) standard lidar point classes.

The FW data was delivered as LAS 1.3 files, including IMU, GPS, and returned as laser pulse waveform data. The Leica ALS50-II lidar system digitises and records the full return waveform with a digitisation sampling period of 1 nanosecond (ns) or 2 ns. The FW was recorded at 256 samples at 8 bits (or 256 ns). No post-processing by ARF was performed on the FW data.

3.2.2 Space-borne optical data

Space-borne optical data were required in this project to provide the large spatial coverage that the airborne ARF lidar data cannot afford. The project utilised freely available optical data from the longstanding Landsat archive (30 m resolution) and the Sentinel-2 series (10, 20, 60 m resolution) to map the reserve at landscape scales.

3.2.2.1 Landsat archive

The Landsat program (managed by NASA) has acquired, archived, and distributed the longest continuous optical data series, capturing 47 years of global land conditions and dynamics (Markham and Helder, 2012). Since the launch of Landsat-1 in 1972, there has been seven missions in this historic fleet, providing long-term, well-calibrated global coverage (Loveland and Dwyer, 2012) (Table 3-1). The satellites are placed in an orbit with an altitude of 705 km, with 16/18 days repeat overpass mode, on a polar, sun-synchronous orbit.

Table 3-1 Landsat mission summary.

Mission	Launch	End of imaging	Sensors		Repeat cycle
Landsat 1	23rd Jul 1972	6th Jan 1978	MSS (4 band)	RBV (3 band)	18 days
Landsat 2	22nd Jan 1975	25th Feb 1982	MSS (4 band)	RBV (3 band)	18 days
Landsat 3	5th Mar 1978	31st Mar 1983	MSS (5 band)	RBV (pan only)	18 days
Landsat 4	16th Jul 1982	14th Dec 1993	TM (7 band)	MSS (4 band)	16 days
Landsat 5	1st Mar 1984	5th Jun 2013	TM (7 band)	MSS (4 band)	16 days
Landsat 6	5th Oct 1993	Failure to reach orbit	ETM (8 band)		16 days
Landsat 7	15th Apr 1999	Ongoing	ETM+ (8 band)		16 days
Landsat 8	11th Feb 2013	Ongoing	OLI (9 band)	TIRS (2 band)	16 days

The Landsat archive is a free, open access data source supplying optical data either in its raw format or processed as a Level-1 and Level-2 product (Table 3-2). The Earth Explorer (https://earthexplorer.usgs.gov/) and Global Visualization Viewer (http://glovis.usgs.gov/) tools were used to search the Landsat archives for scenes that covered the entire NSPSF over a 30 year time period. Scenes captured by the Landsat Thematic Mapper (TM), Enhanced Thematic Mapper Plus (ETM+) and Operational Land Imager (OLI) were used to carry out analyses on above ground vegetation cover dynamics for NSPSF (See **Chapter 6** for further details).

3.2.2.2 Sentinel-2 mission

Sentinel-2 is a constellation of twin satellites, Sentinel-2A and Sentinel-2B. It is part of the European Space Agency's (ESA) Copernicus programme; a series of satellites under the family name Sentinel with a policy of free and open-access space-borne data. The twin polar, sun-synchronous orbiting satellites (phased at 180° to each other) provide systematic global coverage of land surfaces between latitudes 56° South (southern Americas) and 83° North (northern Greenland). Launched in June 2015, Sentinel-2A offers global coverage with a revisit time of 10 days, combined with Sentinel-2B in March 2017 the pair produce a higher revisit time of 5 days. The two satellites are identical and carry on board the Multispectral Imager (MSI), sampling across thirteen spectral bands at a spatial resolution ranging from 10 - 60 m (Figure 3-4). The MSI sensor's unique band combination importantly includes three vegetation-focussed bands positioned in the red-edge zone (across 705 - 865

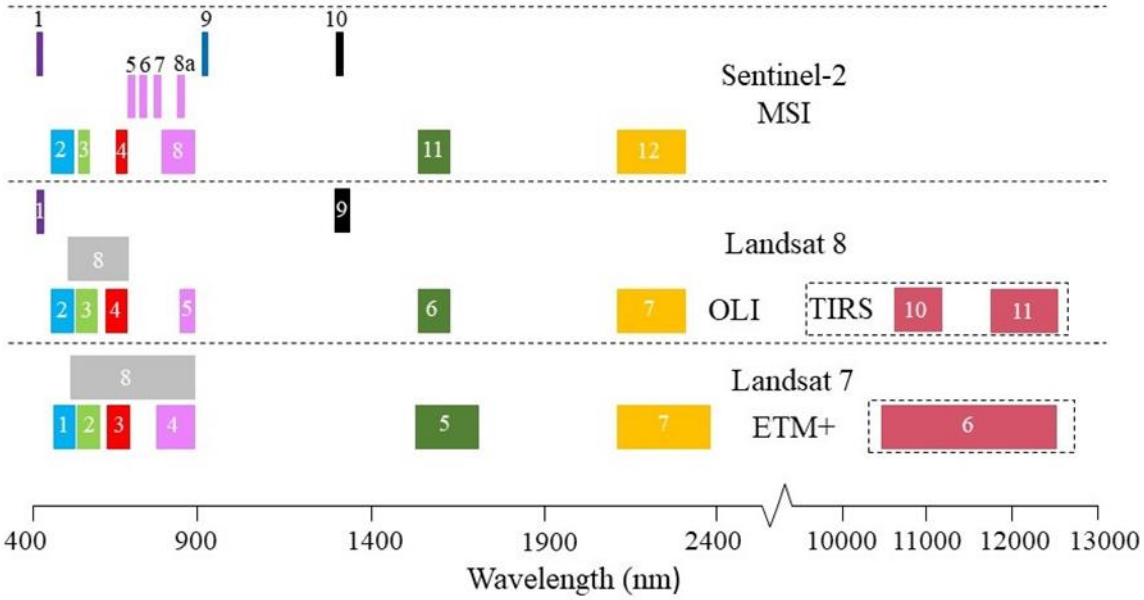


Figure 3-4 Comparison of Landsat 7 ETM+, Landsat 8 OLI TIRS and Sentinel-2 MSI band selection and position.

nm, at a 20 m spatial resolution). Band coverage of the red edge zone provides key information on the state of vegetation, Sentinel-2 is the first civil optical Earth observation mission to include multiple bands in this area.

Sentinel-2 MSI data is supplied as a Level-1B or Level-1C product (Table 3-2). The Copernicus Open Access Data Hub is the official website for ESA (https://scihub.copernicus.eu/). Additionally, data is available to download from Earth Explorer (https://earthexplorer.usgs.gov/). Scenes captured by Sentinel-2 MSI were used to carry out AGB estimation across the entire NSPSF for the years 2015 and 2018 (See **Chapter 5** for further details).

Table 3-2 Landsat and Sentinel-2 data product levels and description.

Landsat TM, ETM+ and OLI/TIRS		**Sentinel-2**	
Product level	**Description**	**Product level**	**Description**
Landsat 4-5 TM C1 Level-1	- top of atmosphere radiance (reflectance rescaling coefficient in metadata) - radiometrically and geometrically corrected; orthorectification	Level-1B	- top of atmosphere radiance - radiometrically and geometrically corrected
Landsat 4-5 TM C1 Level-2	- surface reflectance (Landsat Ecosystem Disturbance Adaptive Processing System algorithm) - radiometrically and geometrically corrected; orthorectification	Level-1C	- top of atmosphere reflectance - radiometrically and geometrically corrected; orthorectification - resampled with a constant Ground Sampling Distance (10, 20 and 60 m)
Landsat 7 ETM+ C1 Level-1	- top of atmosphere radiance (reflectance rescaling coefficient in metadata) - radiometrically and geometrically corrected; orthorectification	Level-2A	- surface reflectance (User generated from Level-1C using the Sentinel-2 Toolbox or the standalone version of the Sen2Cor processor)

Landsat 7 ETM+ C1 Level-2	- surface reflectance (Landsat Ecosystem Disturbance Adaptive Processing System algorithm) - radiometrically and geometrically corrected; orthorectification	
Landsat 8 OLI/TIRS C1 Level-1	- top of atmosphere radiance reflectance (reflectance rescaling coefficient in metadata) - radiometrically and geometrically corrected; orthorectification - Quality Assurance band	
Landsat 8 OLI/TIRS C1 Level-2	- surface reflectance (Landsat Surface Reflectance Code) - radiometrically and geometrically corrected; orthorectification - Quality Assurance band	

3.3 Field data

From a remote sensing perspective, this research used data collected in the field for model calibration and validation. Additionally, field observations and secondary resources where used to guide and support the interpretation of remote sensing derived outputs. From a field ecology perspective, this research used field data to build a comprehensive dataset of NSPSF's below ground peat deposit (description, depth, bulk density, carbon store, stability).

Three field campaigns were carried out for this thesis research:

- 2016 field campaign

A pilot study was undertaken in August – September 2016. The aim was to gain experience in the field and build relationships with the Selangor State Forestry Department. Preliminary data was collected to base the second and third field campaign strategies and plot design on. A total of 24 circular forest inventory plots (radius of 8 m) (Table 3-3) were sampled along 3 transects in the north-west and north-east of the reserve (Figure 3-5). Peat depth was measured in 15 of the forest inventory plots at the central point. Depth ranged from 2.75 m to 8.42 m across transects. Throughout sampling, observations were noted and field photography captured for different land cover types, forest condition and evidence of degradation (fire damage, drainage ditches, oil palm encroachment, etc.).

Table 3-3 2016 field campaign data.

Forest Plot Measurements	**Mean**
	Min/ Max
Tree number	22.54
	12/ 34
Diameter at Breast Height (cm)	14.7
	5.41/ 78.03

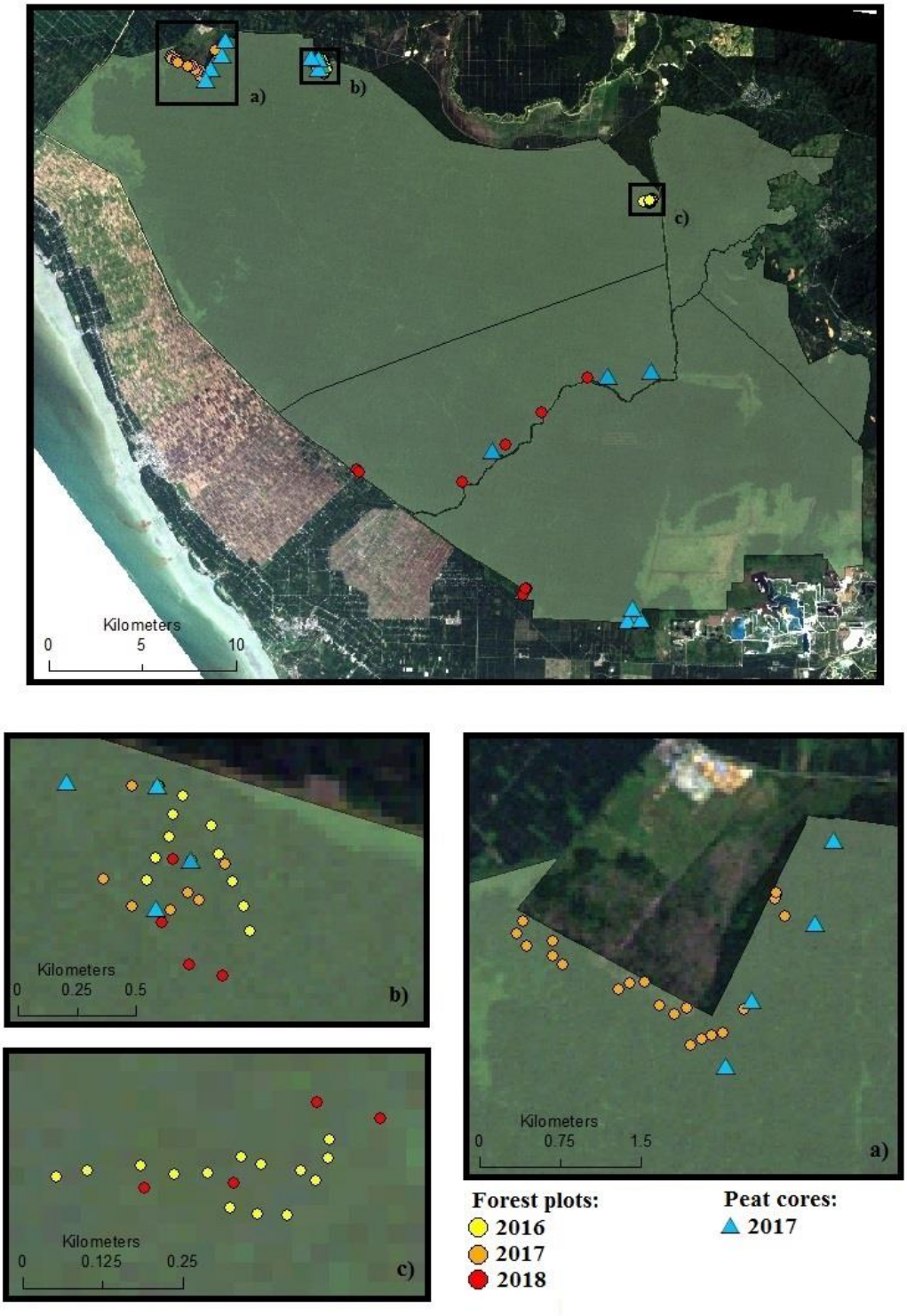


Figure 3-5 The forest plot and peat core site locations sampled in the three field campaigns. Point locations displayed on a Landsat data scene captured in 2019.

- 2017 field campaign

The second field campaign was undertaken in July – August 2017. The aim was to collect forest inventory data to produce accurate AGB estimates at the plot scale for AGB model calibration and validation **(Chapter 4 and 5**) and to sample the below ground peat deposits under different peat swamp forest condition classes (**Chapter 6**). A total of 30 circular forest inventory plots (radius of 15 m) (Table 3-4) were sampled, concentrated in areas covered by the ARF flightlines with relatively little cloud contamination (Figure 3-5). Peat depth and cores were collected throughout the reserve, not constrained to areas covered by ARF flightlines. A total of 14 peat cores were collected under a variety of peat swamp forest condition classes (Figure 3-5) - Central Forest, Managed Recovery, Disturbed Forest, and Fire Affected. For the 14 cores, depth ranged from 0.4 m to 3.08 m.

Table 3-4 2017 field campaign data.

Forest Plot Measurements	**Mean**
	Min/ Max
Tree number	89.33
	39/ 128
Diameter at Breast Height (cm)	14.77
	5/ 119.43
Height (m)	15.16
	4.1/ 34.8

- 2018 field campaign

The third field campaign was undertaken in July – August 2018. The aim was to collect forest inventory data to produce accurate AGB estimates at the plot scale to validation model methods and AGB map outputs (**Chapter 5**). A total of 17 circular forest inventory plots (radius of 15 m) (Table 3-5) were sampled

throughout NSPSF, with a keen effort to sample areas under a variety of different forest type, degradation and reserve management (Figure 3-5).

Table 3-5 2018 field campaign data.

Forest Plot Measurements	Mean Min/ Max
Tree number	83.71 36/ 145
Diameter at Breast Height (cm)	14.73 5.09/ 81.53
Height (m)	15.11 5.6/ 35.2

3.3.1 Forest inventory plot design

Forest inventory plot design (shape and size) has a significant impact on the quality and accuracy of estimating forest attributes and the final prediction models. A circular plot shape was adopted in this research. With only one dimension to define plot boundary (i.e. the radius) and a single plot coordinate (i.e. centre point) required, circular plots were easier to establish in the field compared to square or rectangular plots (Mauya *et al.*, 2015). Using circular plots also reduced potential plot boundary effect as the shape has a smaller circumference to area ratio compared to square or rectangular plots.

Past research has demonstrated the importance and effect of plot size on model fit and precision of forest attribute estimates (Hernández-Stefanoni *et al.*, 2018; Mauya, *et al.*, 2015; Ruiz *et al.*, 2014). Plot size is a key design parameter to set in forest inventory as it has the potential to impact plot edge effects and introduce co-registration error (Frazer *et al.*, 2011). The choice of an 'optimal' forest plot size in this research was determined through a balance between maximising the accuracy of forest attribute estimates and reducing

cost (time and labour in the field). Guided by the outcomes of the 2016 pilot campaign, a radius of 15 m for a 706.9 m^2 plot size was established to estimate forest plot AGB. This plot size is in line with recommendations (Egberth *et al.*, 2017; Ruiz *et al.*, 2014) and within range of commonly adopted plot sizes in tropical forest inventories (Næsset *et al.*, 2016).

Furthermore, forest plots were positioned to cover the wide range of forest structure and density found in NSPSF. Forest plot representation (in terms of height and density) for this research was based on an existing forestry management plan (Parish *et al.*, 2014), multispectral optical data and expert knowledge from NSPSF Rangers. Plot location was depending on the field campaign aim, see **section 3.3**.

3.3.2 Forest inventory data

Forest inventory plots were established throughout the reserve to derive plot level AGB (Figure 3-5). For this research, AGB refers to the dry mass (mega grams) of living above ground vegetation (leaves, branches, and trunks) per hectare. Litter and dead wood are excluded from the definition of AGB in this research.

At each plot the location of the central tree, and thus the centre point of the plot, was recorded by a field GPS (Garmin GPSMAP 64). To maintain consistency and reduce positional error (noise) the plot centre point coordinates were computed over a 10-minute averaging period (Sharif *et al.*, 2004). The positions of all further trees within the plots were noted relative to the central tree (distance and angle) (Figure 3-6). At each plot, all live trees

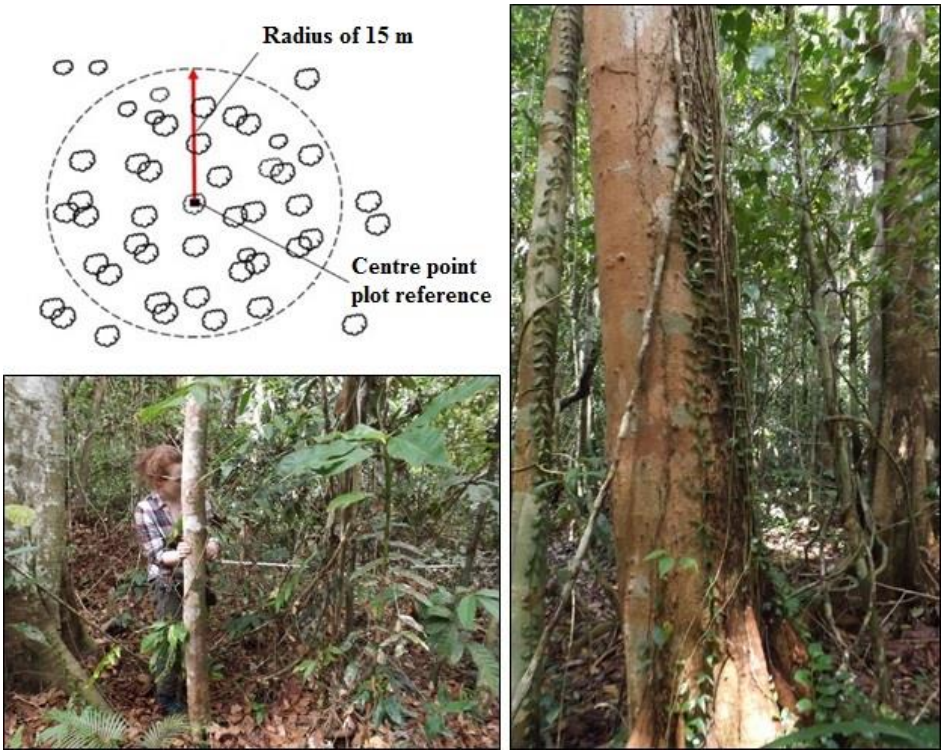


Figure 3-6 Forest inventory plot design and field photography.

with a diameter at breast height (DBH) of >5 cm were measured and tree species (if confidently identified) recorded. Additionally, dependent on the top of tree visibility, selected trees of varying height classes were measured by a laser height meter for each plot.

Photographs were taken of the plot centre and facing outward of the plot centre to capture a record for the forest cover both within the plots and in the surrounding areas.

3.3.3 Allometric AGB model

AGB values for the forest inventory plots were calculated based on the general pan-tropical allometric equation developed by Chave *et al.*, (2014). Inputs included: field-measured DBH, species (to estimate wood density) and tree height when available (missing height data was retrieved from a Feldpuash *et al.*, (2012) averaged model, region set to South-Eastern Asia).

Wood density was estimated for the trees based on their taxonomy using the global wood density database (GWD) (Chave *et al.,* 2009; Zanne *et al.,* 2009), unidentified trees or trees with a missing genus in the GWD were assigned a mean plot-level wood density value. The AGB allometric equation was computed as:

$$AGB = 0.0673 \times (\rho D2H)^{0.976}$$

where ρ = wood density (g/cm^3), D = DBH (cm) and H = height (m).

AGB values calculated for each tree in a plot were summed together to provide plot AGB in mega grams per hectare (Mg/ha).

Based on previous work (Sullivan *et al.,* 2018), the tree height sample size was too small to train an accurate local height-diameter model to estimate missing tree heights. Instead, missing height data was retrieved from a Feldpuash *et al.,* (2012) averaged model, the region set to South-Eastern Asia. See supplementary material for further information.

3.3.4 Peat core data

Peat cores were collected throughout the reserve in order to investigate NSPSF's below ground peat deposits (Figure 3-7). At each peat core collection site GPS coordinates were recorded (Garmin GPSMAP 64). The peat cores were extracted using a side-filling Russian Peat Corer (Van Walt, UK), with a 0.5 m long sampling chamber. Entire peat profiles were sampled in 0.5 m increments, from the ground surface to the underlying mineral material (clay layer). Immediately following extraction the peat cores were photographed and split into 10 cm segments which were bagged and sealed in

the field to avoid moisture loss. Surface leaf litter material was collected and bagged separately at peat core sites.



Figure 3-7 Field photography of peat core collection.

All peat and litter samples were transported to laboratories at the University of Nottingham Malaysia Campus for initial processing. The peat sub-samples (10 cm sections) were weighed for wet weight, oven-dried at 40°C for 48 hours, and then re-weighed for dry weight. The lower oven drying temperature was set to prevent possible charring, oxidation, and/or vaporization of substances other than pore water which may have negatively impacted the results of further organic geochemistry tests and analysis. Tests of this method on samples from the NSPSF site have demonstrated that this drying time is suffice to reach a constant dry weight after 48 hrs (Cooper *et al.*, 2019).The samples were then transported to the University of Nottingham UK Campus for further processing (**Chapter 6**).

3.4 Software

A number of proprietary and open-source software has been developed to meet the growing demands for efficient, high performance geospatial data processing. Table 3-6 outlines a number of key software examples used in this thesis research to process and analysis remote sensing data, as well as implement modelling activities and support statistical analyses.

Table 3-6 Software used in this thesis research.

Software		Description	Open-access?
ArcGIS		GIS environment for visualisation and mapping	No
ENVI		image analysis software, primarily used in this thesis for atmospheric correction (FLAASH)	No
LASTools (LASmoons License		tool for processing lidar point cloud data	No
SPDLib		tool for processing lidar data, designed around storing lidar pulses with digitised waveforms and associated points	Yes
R	**'BIOMASS' package**	estimating aboveground biomass/carbon and its uncertainty in tropical forests	Yes
	'MuMIn' package	performing model selection and model averaging (AICc and alike)	Yes
	'glcm' package	calculating textures from grey-level co-occurrence matrices	Yes
	'ranger' package	implementation of Random Forest (suited to high dimensional data)	Yes
	'raster' package	reading, writing, manipulating, analysing and modelling of gridded spatial data	Yes
	'rgdal' package	geospatial data abstraction library, for reading, writing and converting between spatial formats	Yes
	'sp' package	classes and methods for spatial data	Yes
	'rcompanion' package	summary and analysis statistics	Yes
	'ggplot2' package	data plotting and visualisation	Yes

3.5 Supplementary material

Measuring tree height is time and labour intensive, especially for tropical peat swamp forests. Forest inventory data collection was restricted in this research due to time, access and cost. As a result, tree height data collection was not a priority. For the 2017 field campaign, 3.62% of trees sampled had a tree height measurement, on average 3 tree heights were recorded per field plot (number of trees per plot ranged from 38 – 127).

This sample size was determined to be too small to develop an accurate local height-diameter model. For reference, Sullivan *et al.*, (2018) recommends, *"aiming for a conservative threshold of sampling 50 trees per location for height measurement, and including the ten trees with the largest diameter in this sample",* for accurate height-diameter models (based on ≥150 trees per plot).

Due to the limited sample size, height data for trees not measured was generated from a Feldpuash *et al.,* (2012) averaged model, region set to South-Eastern Asia, as a function within the 'BIOMASS' R package. Accuracy of the model (Feldpuash) and observed (field data) reported: RMSE =2.97 m and BIAS = -1.65. Table 3-7 presents summary statistics for the model generated and observed tree height values for the 2017 field campaign.

Table 3-7 Summary statistics for model (Feldpuash) and observed (field data).

	Model	**Observed**
Minimum	6.5	4.1
Maximum	35.2	34.9
Mean	17.2	15.6
Standard deviation	8.1	8.6

Chapter 4: Tropical peatland vegetation structure and biomass: optimal exploitation of airborne laser scanning

Stage of publication - Accepted in Remote Sensing (24 April 2018). Thesis edit presented.

4.1 Introduction

Tropical peat swamp forests are unique ecosystems; their health and functionality are dependent on the interactions between forest, peat and hydrology. Any unbalance in this sensitive environment from change in one can amplify across the ecosystem and impact the multitude of services they provide, creating positive feedback loops (Wijedasa *et al.,* 2017; Page *et al.,* 1999). Tropical peat swamp forests are thus particularly vulnerable to human disturbances (as well as natural change). This is especially the case in South-East Asia where there has been a long history of tropical peatland degradation (Miettinen *et al.,* 2016; 2012a). At an estimated 88.6 Gt, tropical peatlands are one of the largest pools of terrestrial carbon (Page *et al.,* 2011; IPCC, 2007), however, high volumes of deforestation and land conversion rates have transformed South-East Asian peat swamp forets into one of the largest emitters of carbon globally (Hooijer *et al.,* 2010; Ballhorn *et al.,* 2009; Page *et al.,* 2002). Forest clearance and conversion not only decreases carbon stores directly due to reduction in AGB, but also indirectly increases carbon emissions as a result of peat exposure (Page *et al.,* 2007; Jauhiainen *et al.,* 2005). Fire susceptibility in the landscape also increases (Gaveau *et al.,*

2014b; Van der Werf *et al.,* 2008; Langer *et al.,* 2007), further compounding carbon losses. This, coupled with the need to understand the variability and dynamics of tropical ecosystems in general with respect to their role in the global carbon cycle (Page *et al.,* 2011; Murdiyarso *et al.,* 2010), means there is an urgent need to track change in tropical peat swamp forest via estimation of AGB over space and time. Not only will this afford understanding of carbon losses, this will also help guide tropical peatland restoration and sustainable management activities (Asner *et al.,* 2018; Sullivan *et al.,* 2017a).

The structurally complex nature of tropical peat swamp forests, supporting high (50–70 m) to low (15–25 m) dense canopy forest vegetation, typically with buttresses and thick root mat floors (Yule *et al.,* 2009), presents a challenging landscape for monitoring purposes. This is further complicated by degraded (and/or recovering) peat swamp forest generating even greater variation in forest structure, in response to disturbance events and changes in peat characteristics. Traditionally, forest AGB estimates have been based on field plot inventories, where plot measurements are used to infer AGB estimates through allometric equations (Chave *et al.,* 2014). This manual approach provides the most accurate AGB estimates (Asner *et al.,* 2015), however it is labour intensive, time consuming and expensive (Aplin *et al.,* 2005). Additionally, the extent and inaccessibility of tropical peat swamp forests, coupled with the difficult logistics of fieldwork posed by often waterlogged, swampy conditions, has restricted forest inventory data collection.

Development in remote sensing technology over the last two decades, specifically in lidar (Lim *et al.,* 2003; Dubayah *et al.,* 2000), has

revolutionised the retrieval and accuracy of forest structural attributes, including AGB, across landscapes scales (Wulder *et al.,* 2012b). Lidar data has been widely adopted in forest structural applications, both at the stand and individual tree level (Coomes *et al.,* 2017), due to its ability to characterise both vertical and horizontal structures. A common theme for many studies is the development of lidar-derived metrics related to height distribution, density, and intensity of returns (Thapa *et al.,* 2015; Ni-Meister *et al.,* 2010; Dubayah *et al.,* 2010). Typically, in lidar AGB studies, models are developed from the relationships between field plot estimated AGB, calculated from tree allometry, and lidar-derived metrics (Sullivan *et al.,* 2017b; Ni-Meister *et al.,* 2016; He *et al.,* 2013). Establishing these relationships between metrics and forest attributes are complex, in particular for dense, multi-layered forest canopies associated with the tropics. The majority of work conducted in this area has employed DR lidar derived metrics (Palace *et al.,* 2015), with focus on the utility of DR data for carbon accounting and environmental modelling (Saatchi *et al.,* 2011; Asner *et al.,* 2010). Asner *et al.,* (2012) examined the effectiveness of DR lidar derived mean canopy height to estimate AGB in four tropical regions (Panama, Peru, Madagascar, and Hawaii). The results highlighted the value of DR lidar in generating high-resolution carbon maps across the tropics. However, the application of DR lidar is restricted by the number of returns which can penetrate through dense canopies down to the forest floor, and by the limited point measurements from the canopy and the understory vertical structure (Wang *et al.,* 2009; Hopkinson *et al.,* 2005).

FW lidar data has the potential to provide a more detailed and comprehensive 3D view of forest canopy structure in comparison to DR sensors (Hancock *et*

al., 2015; Wu *et al.,* 2009). Consequently, a growing body of research has focused on developing FW metrics for forest assessment. Drake *et al.,* (2003; 2002) are early examples of the development of FW metrics, using large-footprint FW data (laser vegetation imaging sensor) to generate a list of metrics for AGB estimations. Height of medium energy (HOME) was demonstrated to correlate strongly with mean stem diameter, basal area and AGB. For small-footprint FW lidar, Wu *et al.,* (2009) explored the potential of a list of structural and statistics-based AGB predictor metrics. The results produced a high correlation between FW-derived metrics with individual tree height, foliar and biomass for a savanna environment. Pirotti *et al.,* (2014) also explored the potential for estimating AGB from small-footprint FW data, finding the median height of echo count (HOMTC) performed best at estimating AGB at plot level for a complex tropical forest.

Recently, several studies have evaluated the fusion of DR and FW metrics in forest AGB estimation (Nie *et al.,* 2017; Sumnall *et al.,* 2016; Lindberg *et al.,* 2012; Neuenschwander *et al.,* 2009). Cao *et al.,* (2014a; 2014b) assessed the potential of DR and FW metrics, individually and in combination, as predictors of total living biomass and its components (AGB, root, foliage, branch and trunk) for sub-tropical forests. The study found metrics related to canopy height to be the strongest predictors for AGB; additionally, the combination of DR and FW metrics, by multivariate linear regression, improved AGB estimation.

The benefits of lidar data for monitoring tropical environments has been well established, however with the structural complexity and unique interactions between forest and peat swamp, general tropical forest models may not be

transferable. In particular, non-uniform under and mid-story forest layers in tropical peat swamp forests undergoing restoration pose a challenge in forest attribute assessment. Limited research has been published on the application of lidar in tropical peat swamp forests and has been limited to DR lidar datasets (Manuri *et al.,* 2017; Wan-Mohd-Jaafar *et al.,* 2017). Jubanski *et al.,* (2013) and Kronseder *et al.,* (2012) examined the use of lidar point cloud data in AGB estimation for varied levels of degraded lowland dipterocarp forests in Central Kalimantan, Indonesia. Both studies concluded that AGB could be estimated successfully, though with varying levels of accuracy.

The potential of FW lidar data to provide richer spatial information on the complex canopy characteristics of tropical peat swamp forest in three dimensions remains untested. According to our knowledge, no previous research has examined the use of both DR and FW metrics or the fusion of DR and FW metrics in AGB estimation for tropical peat swamp forest. The research in this chapter will examine the relationship between the AGB of a tropical peat swamp forest in North Selangor, Peninsular Malaysia, and small-footprint airborne lidar (DR and FW) derived metrics. This forest is of particular importance since it is one of the few large areas of peat swamp forest remaining in peninsular Malaysia (Ahmad, 2014). Three lidar-based approaches are investigated for modelling AGB: (1) DR derived metrics (only); (2) FW derived metrics (only); (3) and a combination of DR and FW derived metrics. The accuracy of the models is evaluated by comparing lidar-based AGB estimates with field (in situ plots) measured AGB, with a view to establishing the optimal model for estimating AGB of the NSPSF.

4.2 Materials and Methods

4.2.1 Study site

NSPSF is located on the flat coastal plains of north-west Selangor, Peninsular Malaysia (Figure 4-1). With a combined total of 81,304 ha, NSPSF is one of the largest remaining peat swamp forest in the region; however, over 30 years of intensive timber harvesting has left the once pristine NSPSF degraded and vulnerable to further environmental threat (Yule *et al.*, 2009; Prentice *et al.*, 1989). Repeated cycles of logging activities have created a complex, multi-layered canopy structure, indicated by mixed stand density and height (Figure 4-1). Additionally, the extraction of timber from the forest has led to the formation of a 500 km network of canals (Parish *et al.*, 2014), scarring the forest and accelerating the drainage and erosion of valuable peat soil stores (and the carbon they hold) (Ahmad, 2014).

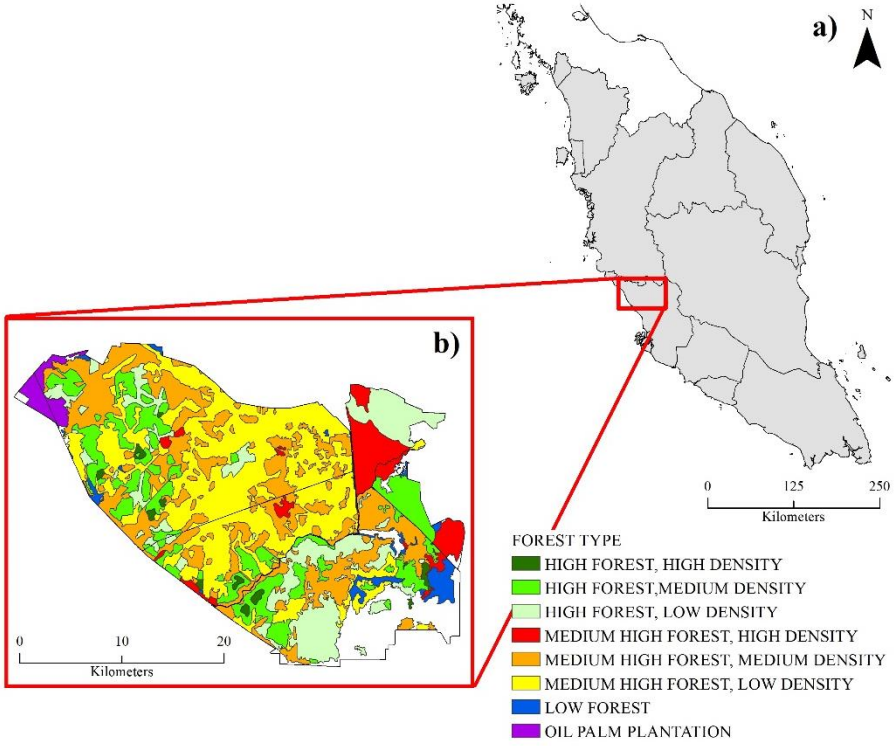


Figure 4-1 (a) the location of the North Selangor Peat Swamp Forest in Peninsular Malaysia**;** (b) magnified study area map at bottom left corner shows forest type (forest height (high, medium, low) and forest density (high, medium, low)), results from a forest management inventory undertaken in 2000 (RCFM and EMS, 2000).

In response to the damaging impact of past logging activities on tropical peatland ecosystem health and the services they provide, the Selangor State Government agreed on a 25-year moratorium on timber harvesting for the State of Selangor, with all logging activities ceased in 2007 (Parish *et al.,* 2014). Despite this halt in logging activities, the reserve remains exposed to disturbance from the surrounding land uses, in particular accelerated drainage from Tanjong Karang Irrigation Scheme and land conversion to oil palm agriculture (Tonks *et al.*, 2017).

4.2.2 Field data

To obtain field estimates of AGB, 30 circular field plots with a radius of 15 m were established within the reserve during 2017. This relatively small sample size, albeit statistically relevant, was determined by the challenging logistics of tropical peat swamp forest fieldwork, as previously mentioned. The forests plots were established to be representative of a secondary peat swamp forest ecosystem, where no obvious structural disturbances were observed since the lidar survey (2014)—for example major tree fall, logging activities or fire events—based on an existing forestry management plan (Parish *et al.*, 2014), multispectral optical data and expert knowledge from NSPSF Rangers. The location of the central tree, and thus the centre point of the plot, was recorded by a field GPS (Garmin GPSMAP 64). The positions of all further trees within the plot were noted relative to the centre (distance and angle) (Figure 4-2). For each plot, all live trees with a DBH of >5 cm were measured and tree species recorded. Additionally, dependent on the top of tree visibility, selected trees of varying height classes were measured by a laser height meter.

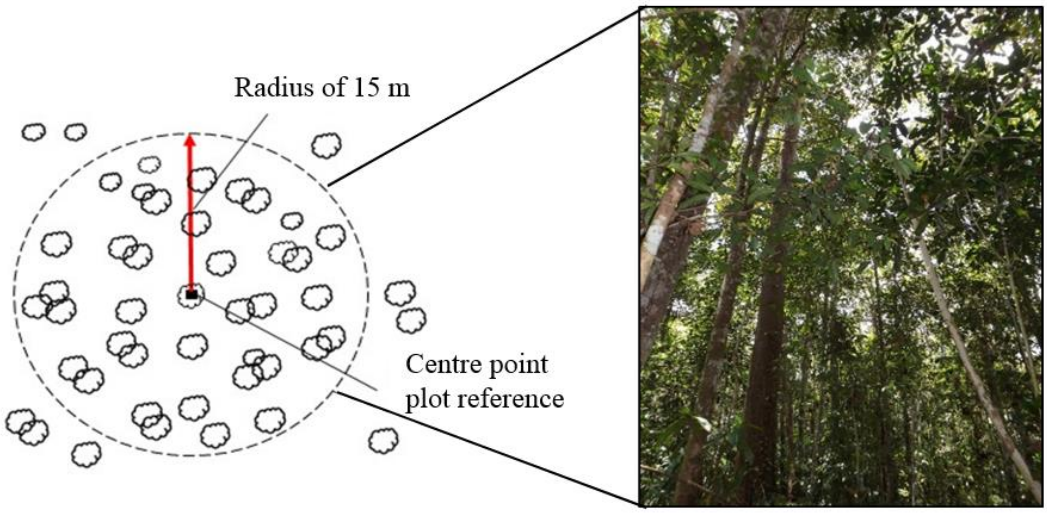


Figure 4-2 Example field inventory plot design.

Plot AGB values were calculated based on the general pan-tropical allometric equation developed by Chave *et al.*, (2014). Inputs included: field-measured DBH, species (to estimate wood density) and tree height when available (missing height data was retrieved from a Feldpuash *et al.*, (2012) averaged model, region set to South-Eastern Asia). Wood density was estimated for the trees based on their taxonomy using the global wood density database (GWD) (Chave *et al.*, 2009; Zanne *et al.*,. 2009), unidentified trees or trees with a missing genus in the GWD were assigned a mean plot-level wood density value. The AGB allometric equation was computed as:

$$AGB = 0.0673 \times (\rho D2H)^{0.976}$$

where ρ = wood density (g/cm^3), D = DBH (cm) and H = height (m).

The 'BIOMASS' package in R software (version 2.10.0) (Rejou-Mechain *et al.*, 2017) was used to run AGB estimation. AGB values were calculated for individual trees within each 15 m radius field plot, and then summed to obtain a total AGB value for each plot.

4.2.3 Lidar data acquisition

Airborne lidar data was collected by the NERC ARF as part of its 2014 Malaysia Campaign. It is important to note the three-year time delay between the airborne lidar data collection (2014) and field plot inventory collection (2017). This may introduce error into the AGB models, however as previously mentioned, all field plots were established to be free from logging and fire, with no obvious disturbance within the three-year period. The data was captured in November 2014 from a Leica ALS50-II lidar system, a small footprint lidar sensor with the capacity to record both DR and FW lidar simultaneously. The Leica ALS50-II lidar system was on board a Dornier 228-201, flying at 132–136 knots at an altitude of 2145–2181 m. The sensor emits the laser beam at 1064 nm, additionally providing an intensity digital image from the return signal intensity data. The accuracy report that accompanied the lidar data estimated the vertical accuracy to be 0.023 m RMSE, where lidar elevation was assessed against ground control points. In total 29 flightlines were flown, surveying an area covering 690 km^2 of the reserve and surrounding area. However, given the constraints of fieldwork and to ensure representation, a subset of the lidar flightlines (161.73 km^2), focused on the north-west of the NSPSF reserve (Figure 4-3), was extracted for optimal lidar-derived AGB model development and assessment. The dataset has an average point density of 2.03 points m^2 and a point spacing of 0.70 m. The lidar data, DR and FW, was pre-processed by NERC's Data Analysis Node and delivered in LAS 1.2 and 1.3 format.

4.2.4 DR-derived metrics

A number of descriptive structural plot-level metrics were calculated from a DR height normalised point cloud. All data processing was carried out in LAStools software (LASTools, 2017) —a complimentary full academic LAStools licence was generously supplied through the LASmoons programme. The geo-located lidar point cloud was supplied with the horizontal and vertical datum WGS84 and projected in the UTM47N reference system. Outliers, or noisy data, were first eliminated and the data filtered to identify laser ground and non-ground (unclassified) hits. The normalised above ground heights were calculated by subtracting the ground points, interpolated into a surface using the adaptive triangulated irregular network (TIN) filtering algorithm, from the non-ground (unclassified) points. To check the quality of the computed ground classification a visual inspection of a hillshaded DTM created from the ground returns was made.

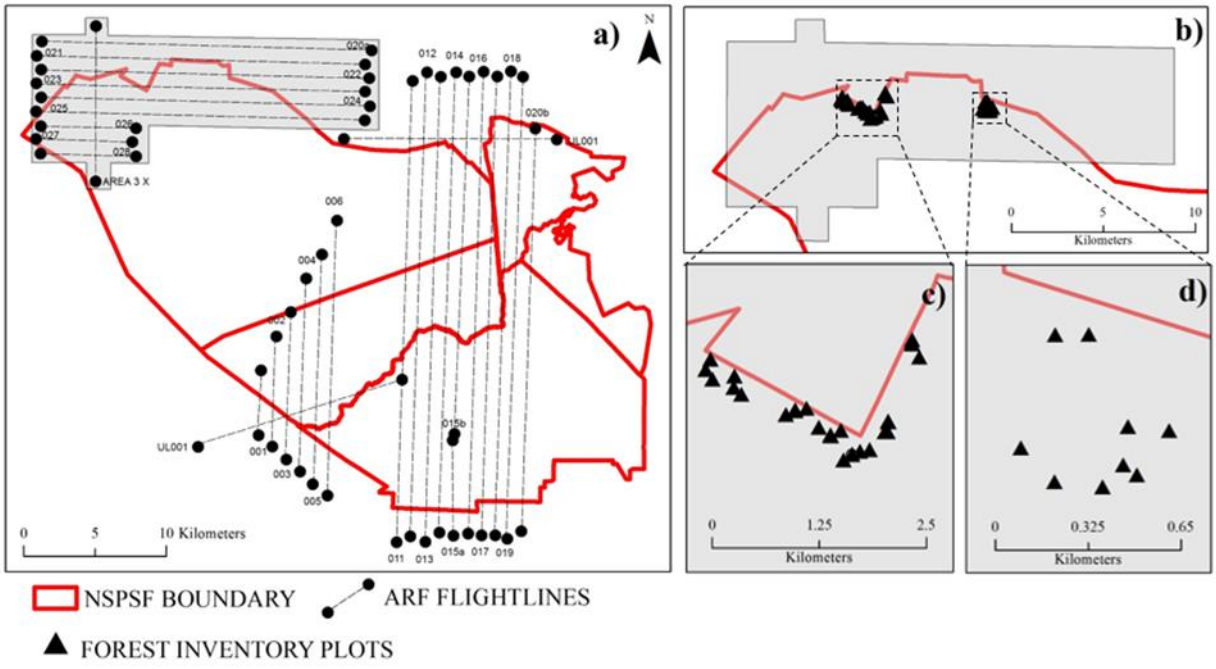


Figure 4-3 (a) ARF lidar flighlines; (b) lidar flightline subset; (c) field plot location; (d) field plot location.

GPS forest inventory plot centre coordinates were imported into the same projection system and buffered to create 15 m radius circular polygons. These polygons were used to clip and export the height normalised lidar points falling inside each of the forest inventory plots. It is noted that the accuracy of estimating AGB is directly influenced by the accuracy of the co-registration of lidar data and field plots. Any error in the absolute position of forest inventory plots will reduce the accuracy of the overall AGB estimation. The Garmin GPSMAP 64 field GPS used in this research has a reported error in the range of 5-10 m (Mika and Siejka, 2016). This GPS error will inevitably introduce positional inaccuracy, however, with a plot size of 706.86 m^2, the overlap between forest inventory plot and lidar data will reduce the potential error associated by inaccurate GPS locations (Hernández-Stefanoni *et al.,* 2018; Frazer *et al.,* 2011).

A suite of descriptive above ground height DR metrics were calculated. DR metrics were selected to provide information on the internal structure of the peat swamp forest, determined by the height distribution of the lidar point returns. DR metrics were computed from all returns higher than 0.5 m, with this threshold set to remove the effect of ground features (Maltamo *et al.,* 2006). DR plot metrics included: minimum height (min), maximum height (max), average height (avg), standard deviation (std), skewness (skw), kurtosis (kur), average square height (qav), height percentile (p01, p05, p10, p25, p50, p75, p90, P9, P99), height bincentiles (b10, b20, b30, b40, b50, b60, b70, b80, b90).

4.2.5 FW-derived metrics

Informed from the success in previous studies-based in the sub-tropics (Cao *et al.*, 2014a; 2014b), three plot-level FW metrics were derived from the recorded waveform. All data processing was carried out in the Sorted Pulse Software Library (SPDlib) (Bunting *et al.*, 2013), benefiting from the recent additions made to the metric library. Gaussian decomposition (Wagner *et al.*, 2004) was applied to each waveform to derive point information (x, y, z). Points were classified into ground or non-ground using a combination of progressive morphology filtering (Zhang *et al.*, 2003) and maximum curvature classification (MCC) (Evans *et al.*, 2007) algorithms to produce a Digital Terrain Model (DTM), to which heights were normalised. The FW plot metrics included: height of median energy (HOME), waveform distance (WD) and roughness of the outermost canopy (ROUGH) (Figure 4-4). FW metrics were summarized as the mean and standard deviation for each plot.

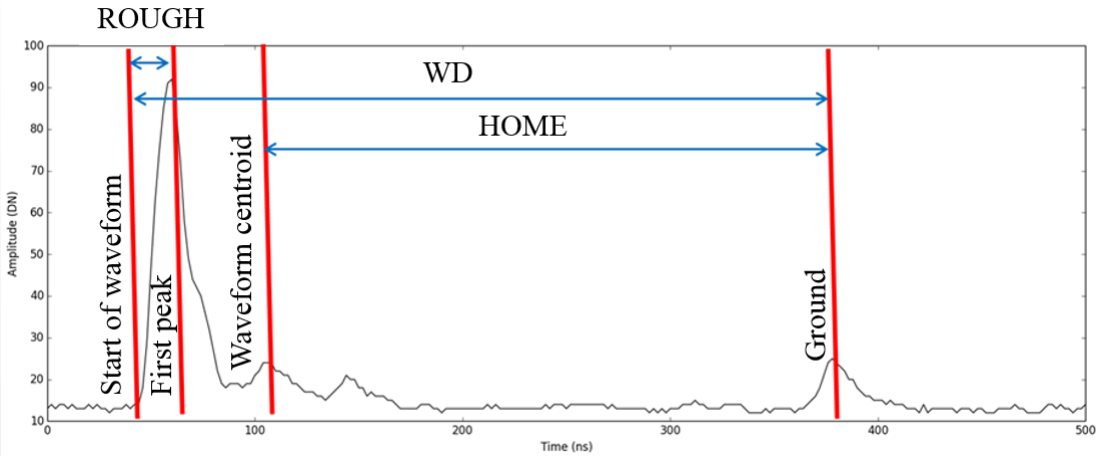


Figure 4-4 Illustration of FW metrics location on an example pseudo-vertical waveform from the NSPSF FW dataset. Plotted Amplitude (DN)/ Time (ns).

4.2.6 Statistical modelling and analyses

Simple linear regression analysis on field measured plot AGB values against lidar derived DR and FW metrics was conducted. Multiple linear regression

models were developed independently from the DR metrics, FW metrics and DR and FW metrics in combination for estimating AGB. To ensure model variables were not highly correlated, a 'data mining' approach, outlined by Langton *et al.,* (2010), was first adopted to identify the key predictor variables for multiple regression analyses. This stage was required to avoid model over-fitting given the relatively small sample size (n = 30) and potential high collinearity of a number of lidar metrics with one another. The 'MuMIn' package for R software (version 1.9.5) (Barton, 2017) was used to run a modified Akaike Information Criterion (AIC), termed AICc (Burnham and Anderson, 2003), this comparing the quality of predictive multiple regression model inputs. An automated stepwise AICc was performed to select input variables for the final models. The delta-AIC value was assessed for each candidate model, a threshold value for delta-AIC was set to <2, models which met this requirement were determined to be within range of plausible models that best fit the observed values (Burnham and Anderson, 2003). The top ranked AICc regression models were assessed based on a number of diagnostics tests (ANOVA, students t-test and variance inflation factor (≤1)) to produce final predictive models for DR metrics (only), FW metrics (only), and a combination of DR and FW metrics. The final predictive modes—DR-model, FW-model, and Combination-model—were fitted and assessed based on a combination of: R-square (R^2), adjusted R-square (Adj-R^2), Root Mean Square Error (RMSE), and the relative Root Mean Square Error (rRMSE).

Additional forest inventory plot data was not collected to test the reliability of the models, thus a leave-one-out-cross validation (LOOCV) was performed.

The LOOCV is an effective method for assessing estimation models where independent validation data are not available (Duncanson *et al.,* 2015; Brovelli *et al.,* 2008), particularly, for models with a small sample size (Peduzzi *et al.,* 2012). With a relatively small sample number (30) it is possible that not every forest type gets adequate statistical coverage. Model validation is limited by this, however as previously mentioned, the forest plots were established to be representative of a secondary peat swamp forest ecosystem and covered a wide range of forest heights, forest densities and AGB values. The Root Mean Square Error from the cross validation analysis (RMSEcv) and bias (BIAScv) was calculated and presented as indicators of the three models' predictive power. Finally, to investigate the significance of the addition of FW metrics in peat swamp forest AGB estimation, the Kruskal-Wallis H test (or one-way ANOVA on ranks) was used to determine if there were statistically significant differences between the three final models' AGB plot predictions.

4.3 Results

Plot-based AGB values were calculated from field measured DBH, species and height data (when available). For the 30 plots, AGB ranged from 126.96 Mg/ha to 443.27 Mg/ha, with a mean value of 319.52 Mg/ha, with a standard deviation of 76.34 Mg/ha (Table 4-1).

Table 4 -1 Plot measured forest parameters.

Plot Measurements	Values: Mean (Std Dev) Min/ Max
Tree number	89.33 (21.09) 39/ 128
Diameter at Breast Height (cm)	14.77 (11.82) 5/ 119.43
AGB (Mg/ha)	319.52 (76.34) 126.96/ 443.27

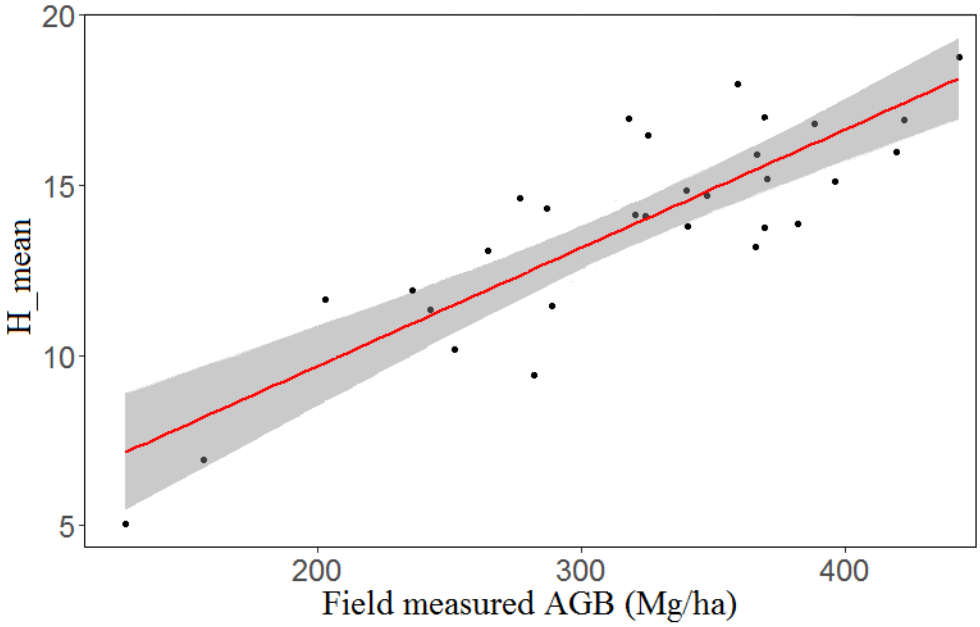


Figure 4-5 Field measured AGB modelled by the mean value from the FW mean HOME metric (H_mean). Bands represent the 95% confidence envelope.

The results from simple linear regression analysis between field-based AGB estimates and 31 lidar derived DR and FW metrics are presented in Tables 4-2 and 4-3. For DR metrics, the 50th height percentile ('p50') showed the highest correlation with field-based AGB (R^2 = 0.68, RMSE = 42.1), followed by average height ('avg') (R^2 = 0.64, RMSE = 45.2). Both minimum height ('min') and standard deviation ('std') displayed no significant relationship or sensitivity to field based AGB. For FW metrics, the mean HOME ('H_mean') provided the highest correlation with field-based AGB (R^2 = 0.72, RMSE = 39.4) (Figure 4-5). The mean input variables calculated for all FW metrics displayed a moderate correlation and significant relationship with field-based AGB, however, the standard deviation input variables calculated for all FW metrics showed very low correlation, with standard deviation HOME ('H_sd') and standard deviation ROUGH ('R_sd') presenting no significant relationship to field-based AGB estimates. It is evident from the linear regression results that metrics representing mid-canopy levels, for example 'p50' and 'H_mean', are important predictors for AGB estimation in tropical peat swamp forests.

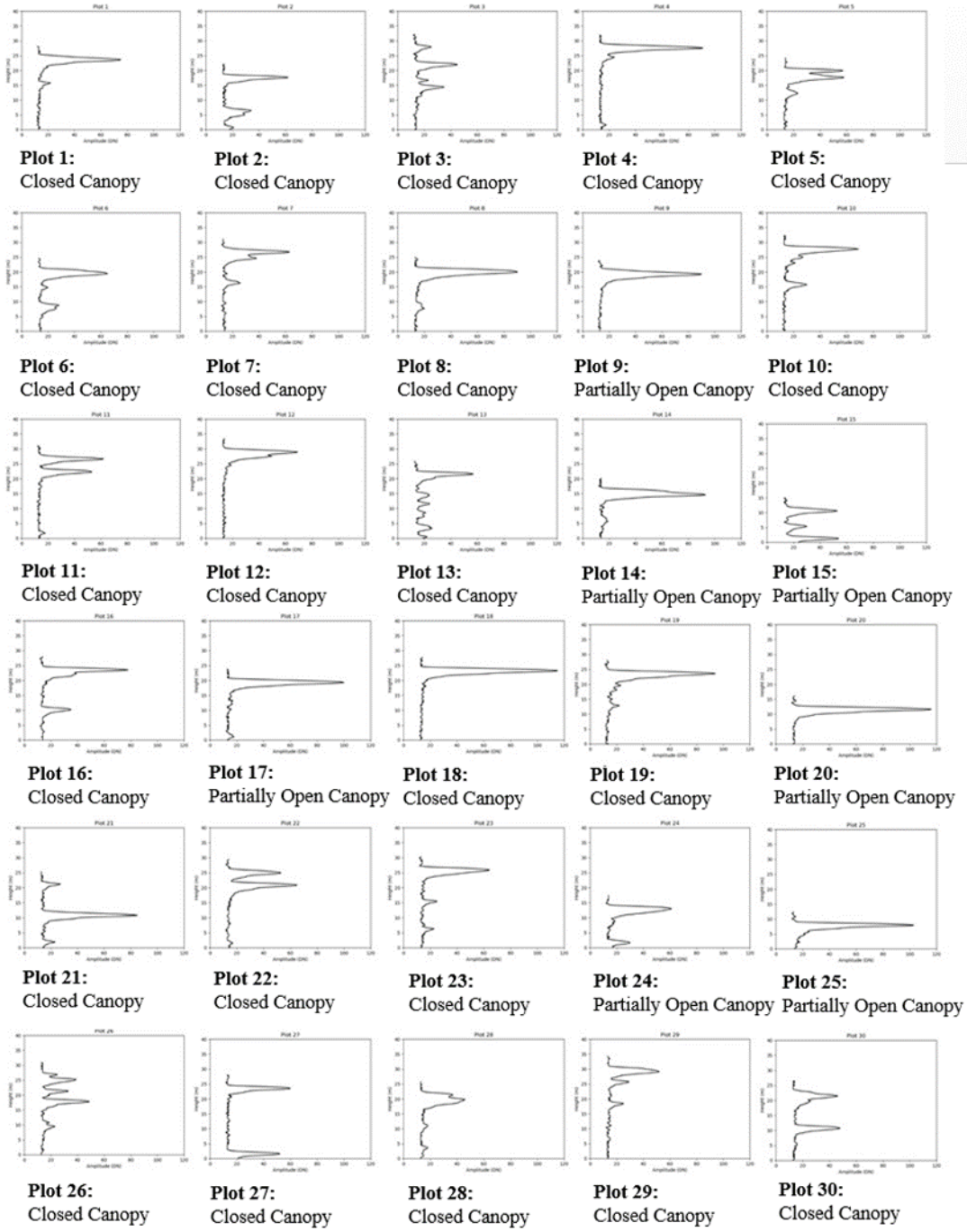


Figure 4-6 Centre point (1 m buffer) plot vegetation profiles, each waveform height has been subtracted from lidar derived DTM; graphs are fitted Height (m)/Amplitude (DN). Height scale (y-axis) ranges from 0 to 40 m, and the amplitude (x-axis) from 0 to 120 DN. Graphs are accompanied with forest canopy structure description.

The variation in mid-canopy structure captured by these metrics can be seen in Figure 4-6. where a waveform has been extracted from the centre point (1 m buffer) for each of the 30 plots.

Table 4-2 Results from simple linear regression using DR metrics. Where: Min = minimum height; Max = maximum height; Avg = average height; Std = standard deviation; Skw = skewness; Kur = kurtosis; Qav = average square height; P01, P05, P10, P25, P50, P75, P90, P9, P99 = height percentiles; B10, B20, B30, B40, B50, B60, B70, B80, B90 = height bincentiles. Values underlined represent metrics of non-significance $p > 0.05$.

DR-metric	R^2	Adj-R^2	RMSE (Mg/ha)	rRMSE (%)
Min	0.04	0.01	73.4	23
Max	0.21	0.18	66.6	20.8
Avg	0.64	0.62	45.2	14.2
Qav	0.59	0.58	48	15
Std	0.1	0.07	71.2	22.3
Ske	0.61	0.6	46.7	14.6
Kur	0.23	0.21	65.7	20.6
P01	0.29	0.26	63.4	19.8
P05	0.29	0.26	63.4	19.8
P10	0.30	0.28	62.7	19.6
P25	0.58	0.57	48.5	15.2
P50	0.68	0.67	42.1	13.2
P75	0.58	0.56	48.9	15.3
P90	0.39	0.36	58.8	18.4
P95	0.30	0.28	62.7	19.6
P99	0.25	0.22	65	20.3
B10	0.25	0.22	65	20.3
B20	0.35	0.33	60.6	19
B30	0.49	0.48	53.4	16.7
B40	0.59	0.57	48.1	15.1
B50	0.62	0.61	46.3	14.5
B60	0.52	0.51	51.8	16.2
B70	0.39	0.37	58.6	18.4
B80	0.25	0.23	64.9	20.3
B90	0.16	0.13	68.9	21.5

Table 4-3. Results from simple linear regression using FW metrics. Where: H_mean = mean HOME metric; H_sd = standard deviation HOME metric; W_mean = mean WD metric; W_sd = standard deviation WD metric; R_mean = mean ROUGH metric; R_sd = standard deviation ROUGH metric. Values underlined represent metrics of non-significance $p > 0.05$.

FW-metric	R^2	Adj-R^2	RMSE (Mg/ha)	rRMSE (%)
H_mean	0.72	0.71	39.4	12.3
H_sd	0.00	-0.03	75	23.5
W_mean	0.57	0.55	49.3	15.4
W_sd	0.17	0.14	68.5	21.4
R_mean	0.61	0.59	47.1	14.7
R_sd	0.00	-0.04	75.1	23.5

The results of the best models for predicting tropical peat swamp forest AGB (DR, FW and Combination) (Table 4-4) are summarised in Table 4-5 and visualized in Figure 4-7. The Combination-model, H_mean/B50, displayed the best agreement with field-based AGB values ($R^2 = 0.77$; RMSE = 36.4; rRMSE = 10.8%). Figure 4-8 displays an example of AGB (Mg/ha) estimates calculated from the Combination-model for a subset of the lidar flightlines in the north-west of the NSPSF reserve at a 5 m (0.0025 ha) spatial resolution.

Table 4-4 Model equations. Where: P75 = 75th height percentile; Ske = skewness; H_mean = mean HOME metric ; W_sd = standard deviation WD metric; B50 = 50th height bincentile.

	Model Equations
DR	=81.786 + 8.940 x P75 - 78.063 x Ske
FW	=101.457 + 19.579 x H_mean - 12.555 x W_sd
Combination	=171.3731 + 14.7802 x H_mean - 1.5752 x B50

Table 4-5 Results from the best preforming models for predicting AGB. Where: P75 = 75th height percentile; Ske = skewness; H_mean = mean HOME metric; W_sd = standard deviation WD metric; B50 = 50th height bincentile.

	Model Variables	**R^2**	**Adj-R^2**	**RMSE (Mg/ha)**	**$RMSE_{cv}$ (Mg/ha)**	**$BIAS_{cv}$**	**rRMSE (%)**
DR	P75 Ske	0.73	0.71	39.2	42.9	-0.83	12.3
FW	H_mean W_sd	0.76	0.74	36.9	40.9	-0.17	11.6
Combination	H_mean B50	0.77	0.75	36.4	39.8	0.38	10.8

However, all three predictive models displayed a strong positive correlation and a significant relationship to field-based AGB estimates (DR-model—R^2 = 0.73; RMSE = 39.2; rRMSE = 12.3%) and (FW-model—R^2 =0.76; RMSE = 36.9; rRMSE = 11.6%). Figure 4-9 displays the frequency distribution for model generated AGB (Mg/ha) values for the 30 plots, presented with model AGB (Mg/ha) summary statistics. The Kruskal-Wallis test showed that there was no statistically significant difference between the three models for tropical peat swamp forest AGB prediction ($H(2) = 0.0038095$; $p = 0.99$). In summary, the synergistic use of DR and FW derived metrics displayed a stronger correlation with field-based AGB estimates in comparison to individual and multiple DR- and FW- models, however, there was no significant difference in tropical peatland AGB prediction between the three best multiple regression models (DR, FW and Combination).

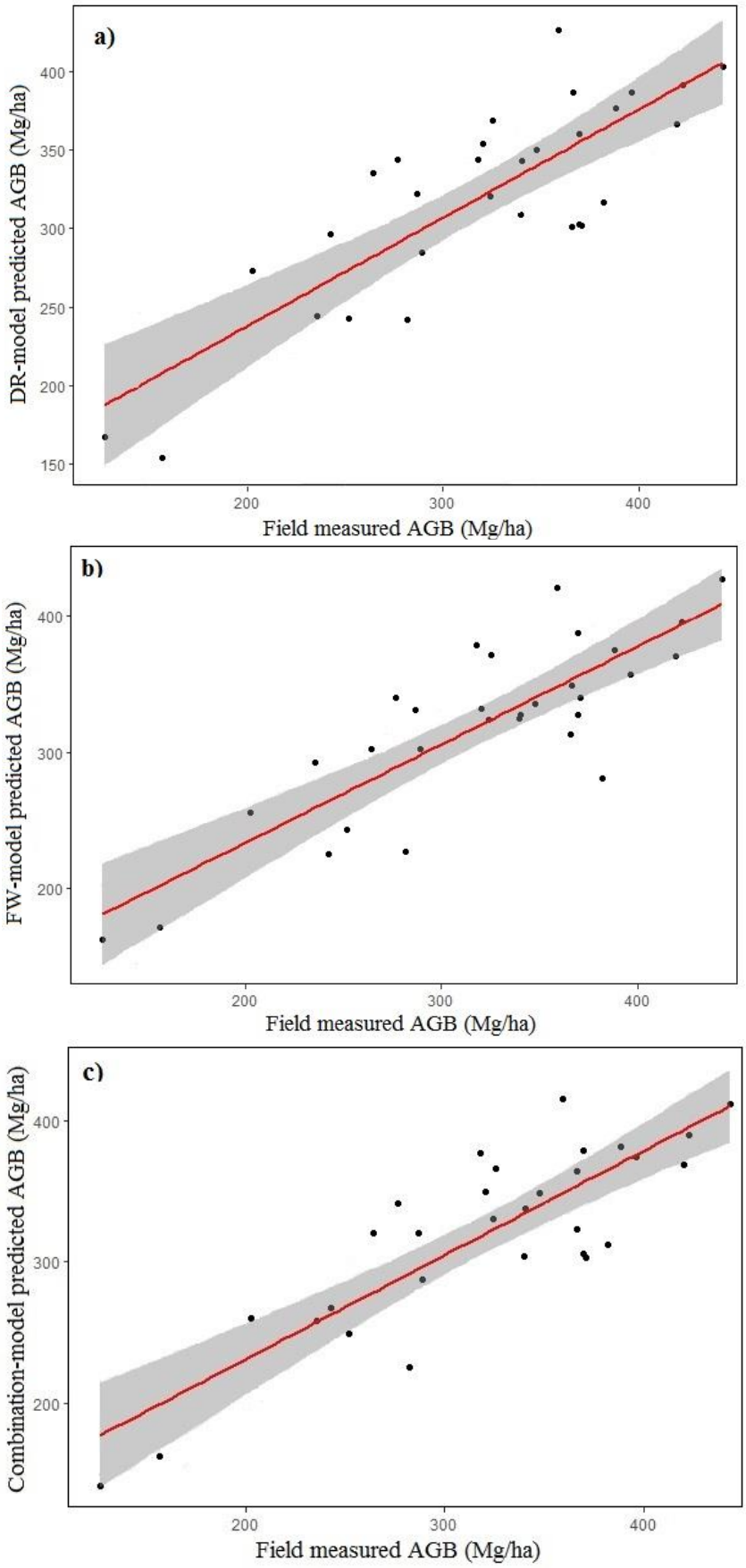


Figure 4-7 Predicted vs fieldmeasured AGB from the best performing models: (a) DR-model; (b) FW-model; (c) Combination-model. Bands represent the 95% confidence envelope.

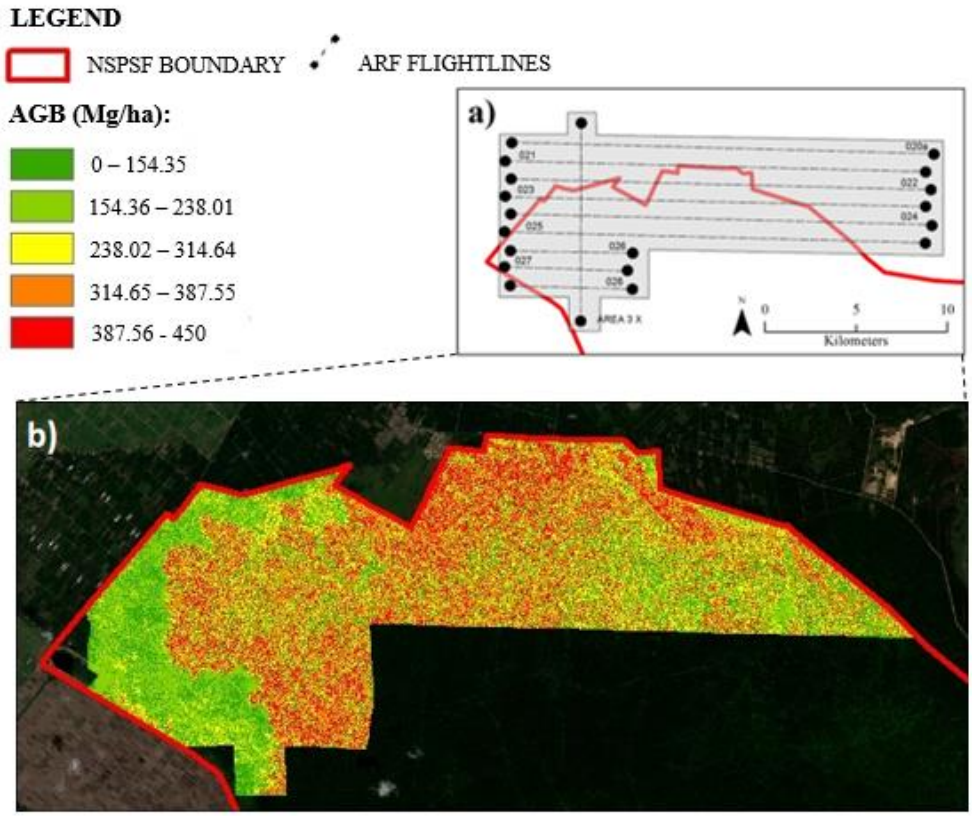


Figure 4-8 (a) lidar flightline subset; (b) estimation of AGB (Mg/ha) within the NSPSF boundary calculated from the Combination-model, at a 5 m (0.0025 ha) spatial resolution, overlaid on Sentinel-2 multispectral image.

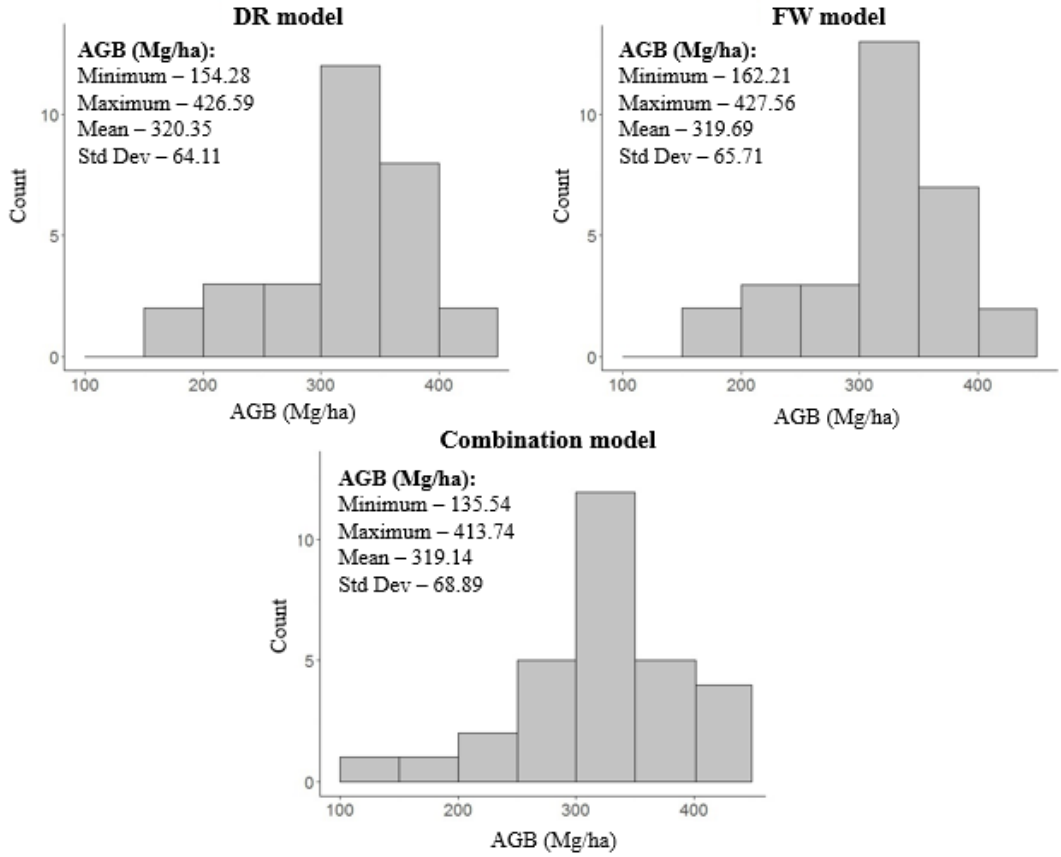


Figure 4-9 Frequency distribution for DR-, FW- and Combination-model generated AGB (Mg/ha) across the 30 field plots, presented with model generated plot minimum, maximum, mean and standard deviation AGB.

4.4 Discussion

Quantification of tropical peat swamp forest AGB cover is required to better understand and safeguard tropical peatlands' ecosystem function and resilience to disturbance, both natural and anthropogenic (Lawson *et al.,* 2015). AGB products provide accurate baseline estimates to support international climate change policies and programs such as the UN REDD+ (United Nations Reducing Emissions from Deforestation and Forest Degradation), as well as the development of sustainable management strategies for local stakeholders. Additionally, knowledge gained from the precise assessment of tropical peatland AGB distribution will assist in Malaysia's work towards meeting their SDGs, specifically relating to SDG-13 'Climate action' and SDG-15 'Life on land'. Using a remote sensing approach to acquiring AGB estimates is attractive in that large spatial extents are covered and monitoring can be frequent, particularly once a calibrated model has been established between forest inventory and remotely sensed data. In this case, the lidar campaign covered 53% of the NSPSF reserve. This is the first time such data had been captured for NSPSF and used in this way. The research demonstrates the utility of both DR and FW lidar data for tropical peat swamp forest AGB estimation and thus illustrates the real potential for a monitoring approach underpinned by laser scanning technologies.

The AGB range presented in the in-situ plots was 126.96–443.27 Mg/ha. AGB plot values are consistent with tropical peat swamp forest estimates from the literature (Kronseder *et al.,* 2012) and therefore considered reliable and reflective of a secondary tropical peat swamp forest, with a diverse structure and density (Figure 4-1). The investigation is limited by the relatively small

sample size (n = 30) used for model development and validation (Zhao *et al.*, 2009). However, the training plots were identified as being representative of the forest conditions found in NSPSF. Forest plot representation (in terms of height and density) for this research was based on an existing forestry management plan (Parish et al., 2014) and expert knowledge from NSPSF Rangers. All field plots had good correspondence with lidar data providing detailed information on both forest canopy and ground (mean ground-classified hits = 8.3% per plot) relative to a densely closed and partially open canopy structure (Figure 4-6). This research recognises that a larger sample size is advisable in future work for model validation. Nevertheless, the plots sampled in this thesis research cover a wide range of forest types found across NSPSF, with plots positioned in high, medium, and low forest height stands with varying densities (Figure 4-1).

From the numerous DR and FW lidar metrics tested against this range in AGB measured in the in situ plots, three AGB prediction models were determined to have a high accuracy with an rRMSE <15%: one model using DR data only (DR-model = 12.3%), one model using FW data only (FW-model = 11.6%) and one model using a combination of DR and FW data (Combination-model = 10.8%). Overall, the Combination-model was best for explaining AGB, with an R^2 of 0.77 (RMSE = 36.4, rRMSE = 10.8%). There was no statistically significant difference between these three best models for tropical peat swamp forest AGB prediction. It is important to note this finding as FW lidar data is highly complex and is associated with high computational and data handling costs. Therefore, DR lidar can be considered a more appropriate and

accessible data source for tropical peat swamp forest management and conservation activities.

Simple linear regression revealed lidar-derived metrics relating to mid-story canopy levels—for example average height, 50th height percentile, 50th height bincentile and HOME—to be the strongest predictors of AGB in tropical peat swamp forest. In this research, models which included FW metrics were dominated by the strong predictive capabilities of the mean HOME metric. Waveform derived HOME is the distance from the waveform centroid to the 'ground' (i.e., the ground position of the pseudo-waveform). The HOME metric considers the shape of the waveform and therefore the canopy structure it represents, for instance it will be higher for a forest with no understory compared to one which has the same height but no understory component. It therefore provides information on mid-canopy structure. HOME has previously been found to be sensitive to canopy openness (including tree density) and the vertical arrangement of a forest stand (Drake et al., 2002; 2003). This suggests that for complex tropical peat swamp forests the often unobserved structural and compositional diversity in the lower portions of the forest canopy is crucial for accurate AGB model prediction. This observation is crucial for understanding how lidar technologies should be employed for optimal AGB estimation in these environments.

Focusing on the FW lidar data it can be seen that the mean values of all FW metrics displayed moderate to high correlations and significant relationships with in situ plot AGB values. These findings are consistent with past research in the use of FW lidar in forestry applications (Hermosilla *et al.*, 2014; Richardson *et al.*, 2011). Reitberger *et al.*, (2009) found FW metrics to

improve the detection of under and mid-story trees compared to first/last DR lidar by 10–15%, though the research was unable to detect 65% of mid-story trees, and 74% of understory trees in leaf on conditions. Indeed, FW lidar is still limited by the lack of significant transmission through dense forest leaves and stems, however its potential to improve our knowledge and understanding of multi-layered forest structures has been widely recognised by the remote sensing community (Bye *et al.,* 2017). Although in this research we found no statically significant enhancement (at 95% level of confidence) with the addition of FW metrics in the predictive models for AGB estimation, the waveforms per plot do show discernible differences. The focus here was on the use of FW lidar metrics common in related literature (Cao *et al.,* 2014; Pirotti *et al.,* 2014; Drake *et al.,* 2002). There may exist alternative FW metrics not tested here which could be implemented in future research. This could improve the already strong predictive AGB models, and also describe other structural variables in the forest. These include crown bulk density, canopy fuel weight and for larger dominant trees, crown width (Alexander *et al.,* 2018; Unger *et al.,* 2014). Thus, the continued development and application of FW lidar in future tropical peat swamp forest AGB research is recommended, with a focus on capturing and describing FW. Recent initiatives, such as the Global Ecosystems Dynamics Investigation (GEDI) lidar due to be deployed on the International Space Station, respond to the recognised need for vertical structure measurements of the Earth's surface, as put forward by the host country's (USA) National Academy of Sciences and NASA's Science Mission Directorate (Science Beta, 2016). The GEDI is just one example of the progress and development in lidar systems and platforms

that should encourage the continued application of lidar data in future tropical peatland applications. Other examples include advancements in small-scale sensor technology which has permitted the use of UAV's as a lidar sensor platform (Wallace *et al.,* 2014; Shang *et al.,* 2014) thus profiting from potentially higher resolution data capture at a considerably lower surveying cost at local scales. Integration with hyperspectral systems could also be advantageous (Pang et al., 2016).

Of those alternative metrics which should be implemented in future tropical peat swamp forest AGB research, those relating to lidar intensity (Kim *et al.,* 2009; Reitberger *et al.,* 2008; Moffiet *et al.,* 2005) are worth considering. Small footprint lidar intensity data (amount of energy reflected back to the sensor) has been increasingly adopted in forestry applications (Sumnall *et al.,* 2017; Kim *et al.,* 2009). Top of canopy intensity metrics, in combination with lidar derived height values, have been proven to contribute significantly to improved forest AGB estimations (Li *et al.,* 2014) and have been linked with tree species number at mid-story canopy level (Brandtberg *et al.,* 2003). For this particular research, lidar intensity metrics were not included in AGB forest estimation because of uneven atmospheric conditions during the flight, therefore the resulting intensity data could not be reliably corrected for or compared between flightlines. This represents a challenge to be tackled in the future.

The results demonstrate the advantage of using both DR and FW lidar data in tropical peat swamp forest AGB inventory programmes, which in turn provide a more detailed and accurate account of peat swamp forest structural cover and above ground carbon allocation across landscape scales. Apart from discerning

the role for lidar in estimating AGB of these tropical peat swamp forests, this research has also provided in situ plot AGB data for the NSPSF, providing new tropical peat swamp forest AGB plot data for an ecosystem underrepresented by global forest inventory databases (Yuen *et al.*, 2016; Manuri *et al.*, 2014). This is important for subsequent research on how these forests function. As stated earlier the airborne lidar data does not fully cover the whole of the NSPSF reserve, in such cases space-borne data (i.e., Sentinel-2 or very high-resolution systems) may be used to scale up AGB estimates across larger landscape scales (Wilkes *et al.*, 2015; Mora *et al.*, 2013). Indeed, given how well the lidar estimates AGB in this environment, forward monitoring could be based on optical space-borne systems with lidar technologies used in a sampling capacity to provide calibration and validation data (Wulder *et al.*, 2012b).

4.5 Conclusions

This research examined the relationship between tropical peat swamp forest AGB and small-footprint airborne lidar DR and FW derived metrics with a view to establishing the optimal use of this technology in this environment. Plot-based multiple regression analysis was performed to establish the best predictive models of tropical peat swamp forest AGB using DR metrics (only), FW metrics (only), and a combination of DR and FW metrics. All three final models presented a high correlation with AGB estimates, with an $R^2 \geq 0.73$ and no statistical difference between the rRMSE of these models.

Overall, the results demonstrate that a Combination-model, coupling the benefits derived from both DR and FW metrics, had the best performance in

modelling AGB for tropical peat swamp forest (R^2 = 0.77, RMSE = 36.4, rRMSE = 10.8%). The research found that perhaps of greater importance is metric selection, as opposed to lidar data type (DR, FW, Combination) for assessing AGB prediction. In particular, the top ranked metrics in the best performing models related to mid-canopy order height metrics, this indicating the importance of suppressed tree crowns and forest structural diversity in the mid-level portions of tropical peat swamp forests for reliable AGB assessment.

Overall, the utility of lidar for tropical peatland AGB mapping and monitoring is enormous. The ever-increasing role of lidar in supporting forestry applications is encouraged by the recent development and expansion in sensor technology and platforms, with lidar data more accessible and at a lower cost than ever before. Published studies on tropical peat swamp forest AGB are few, in particular for Peninsular Malaysia, thus as a result this research contributes significantly to tropical peatland ecology. The research in this thesis underpins AGB estimation across the NSPSF reserve going forward and has direct applications for sustainable tropical peatland management, supporting decision and policy makers in the preservation and protection of South-East Asia's vulnerable tropical peatlands.

Chapter 5: Restoration of Malaysia's tropical peat: remote sensing for monitoring restoration management in tropical peat swamp forests

Stage of publication – In prep (target Journal of Environmental Management).

5.1 Introduction

Human encroachment and intensified agricultural activities have threatened the function, and even existence, of tropical peat swamp forests in South-East Asia (Evers *et al.,* 2017; Page and Hooijer, 2016; Miettinen *et al.,* 2012a). The restoration of these degraded tropical peat swamp ecosystems pose an enormous global challenge for both scientists and policymakers alike (Murdiyarso *et al.,* 2019; Evers *et al.,* 2017; Wijedasa *et al.,* 2017; Padfiled *et al.,* 2014). Tropical peatland restoration is supported by a number of both national and international goals relating to ecosystem management, climate change mitigation and sustainable development. For example, peatland restoration is recognised as a key focus in reaching carbon emission reduction targets under the Kyoto Protocol (IPCC, 2014; Hiraishi *et al.,* 2013) and as a terrestrial ecosystem management and protection aim under the UN SDG number 15 (SDG Knowledge platform, 2018). Therefore, there is an urgent need for the development of landscape-scale measures for verifying and quantifying restoration procedures in order to achieve the goals and commitments related to tropical peat swamp forest recovery.

Mapping AGB dynamics and assessing their changes in response to anthropogenic activities is critical to understand and monitor the current status

of tropical peatlands, as well as the performance of restoration practices (Asner *et al.,* 2018; Brown *et al.,* 2018). Capture of AGB data has traditionally been based on forest inventory plots (Pan *et al.,* 2011). However, despite generating accurate results (Lu, 2006), these ground-based methods have been deemed expensive, time consuming and often limited by their sample size and spatial distribution over landscape-scales (Asner *et al.,* 2012; ESA, 2012). Advances in remote sensing technology and improved computing and image processing techniques have made it possible to estimate large-scale forest AGB in a robust, cost effective manner (Corona, 2016; Verkerk *et al.,* 2014; Gibbs *et al.,* 2007). In particular, space-borne sensors have generated a vast archive of data at a spatial and temporal scale appropriate to support ecosystem restoration and monitoring programs (Huang, 2018; White *et al.,* 2016). For example, the ESA Sentinel-2 constellation which carries the MSI sensor with improved spatial and temporal resolution over existing optical space-borne sensors (e.g. the Landsat series) and unique spectral band selection promises to benefit global forest AGB monitoring efforts (Pandit *et al.,* 2018; Majasalmi *et al.,* 2016). Optical sensors, such as those aboard Sentinel-2, are often limited to recording the reflectance in the topmost part of a forest canopy. The restrictions of optical data in delivering detailed vertical information on forest stand structure has directly impacted the accuracy of forest AGB assessment (Lu *et al.,* 2016). Despite this shortcoming, spaceborne optical imagery remains a popular data option in large-scale forestry applications due to the wide availability of data sources, access to archival datasets, and low cost (at times with no acquisition cost).

Aside from optical remote sensors, AGB information has been derived from active sensors such as SAR and lidar, on space-borne and airborne platforms respectively. Indeed, lidar has become one of the most prominent remote sensing technologies in forest assessment (Urbazaev *et al.*, 2018; Coomes *et al.*, 2017; Ni-Meister and Lee, 2016; Thapa *et al.*, 2014). Lidar metrics, from both DR and FW, have been shown to obtain highly accurate forest AGB and above carbon density (ACD) estimates, with no saturation issues associated with areas of high AGB (Zhao *et al.*, 2009; Naesset and Gobakken, 2008); this is a key benefit associated with the use of lidar data in tropical forest ecosystems. The results in research **Chapter 4** demonstrate the importance of lidar structural information, in particular for lidar metrics related to the mid-canopy forest structure, in tropical peat swamp forest AGB estimation.

Despite these successes (Fasnacht *et al.*, 2014), lidar surveys over landscape-scales are expensive and problematic, where their temporal resolutions can be restrictive. Lidar systems are also often limited by their spatial coverage (airborne acquisition), thus producing results best suited to providing sample transect datasets rather than the wall-to-wall coverage often called for in regional forestry applications, particularly when the demand is for high spatial resolutions (Mitchard *et al.*, 2012; Boudreau *et al.*, 2008). To combat these limitations, many studies have adopted a data fusion approach with lidar and space-borne optical data for landscape-scale forestry application (Garcia *et al.*, 2018; Bolton *et al.*, 2018; Jin *et al.*, 2018; Zald *et al.*, 2016). Here, lidar derived forest attributes or models are commonly adopted as surrogate ground truth data. The large amount of training samples generated from lidar data can significantly improve the performance and accuracy in predicting forest

attributes using machine learning algorithms (Shao *et al.,* 2017; Wulder *et al.,* 2012b), thus overcoming the restrictions posed by traditional field sampling methods.

This research focuses on NSPSF, a large tropical peat swamp forest in Peninsular Malaysia under varying degrees of both growth and degradation from multiple sources. In view of the growing international interest toward tropical peatland conservation and restoration, NSPSF is now under State protection with an established site-specific Integrated Management Plan (IMP) (Parish *et al.,* 2014) set out in 2014 to support and implement tropical peat swamp restoration. The IMP specifically targets key areas of rehabilitation, fire prevention, and buffer zone management. To date, several IMP interventions have been implemented in NSPSF with varying degrees of success, including drain blocking and forest replanting programmes. The years 2015-2018 mark a period of significant effort in the initial trial and installation of several peat swamp management and restoration activities set out by the IMP. Evidence of the impacts (both positive and negative) of these actives on the restoration of NSPSF is required to aid local stakeholders in prioritising and formulating future management strategies. The research in this chapter aims to test and demonstrate the use of Sentinel-2 satellite data in delivering accurate, high resolution AGB maps of NSPSF for the years 2015 and 2018 using a Random Forest machine learning method. Despite the proven accuracy of lidar data in tropical peat swamp forest AGB estimation (demonstrated **Chapter 4**) and the limitations associated with forest stand structural representation, Sentinel-2 data was selected as the practical data option for this research based on data cost, coverage, and cloud contamination.

A reference dataset, derived from the lidar AGB model results in **Chapter 4**, was used as training and validation data in the Random Forest model. Resulting AGB map products will be used to assess the AGB dynamics in NSPSF between 2015 and 2018 in terms of peat swamp forest gains and losses, as such affording an evaluation of the associated peat swamp management activities in NSPSF.

5.2 Methods

5.2.1 Study site

NSPSF is located on the flat coastal plains of north-west Selangor, Peninsular Malaysia (3º33'31 N, 101º18'21 E). Comprised of four forest reserves - Raja Musa Forest Reserve, Sungai Karang Forest Reserve, Bukit Belata Extension Forest Reserve (partial), and Sungai Dusun Forest Reserve – NSPSF is one of the largest remaining peat swamp forests in Peninsular Malaysia (Ahmad *et al.,* 2014) covering a total area of 81,304 ha. NSPSF provides a wealth of ecosystem services - such as habitat biodiversity, carbon sequestration, regulation of fresh water flow and flood mitigation, and climate regulation – which are all essential to the local livelihood of neighbouring human communities (Parish *et al.,* 2014). However, decades of peat swamp forest degradation and encroachment has restricted NSPSF ecosystem function and the services it can provide (Tonks *et al.,* 2018; Azhar *et al.,* 2011; Yule, 2010).

The forest is a recovering secondary mixed swamp forest in which multiple cycles of selective logging has created a complex, multi-layered canopy structure, criss-crossed by a 500 km network of canals (Parish *et al.,* 2014; Pretice and Aikanathan, 1989). The construction of the canals has scarred the

forest, accelerating the drainage of the peat soil and consequently increased fire risk for the reserve and surrounding area. The land use adjacent to the reserve is dominated by large-scale oil palm plantations. Conversion to industrial oil palm has transformed the landscape in North Selangor (Charters *et al.,* 2019), with reserve encroachment and hydrological consequences of plantation drainage posing a serious threat to the protection and ecosystem function of NSPSF. The reserve also notably boarders the Tanjung Karang Irrigation Scheme to the west which predominantly serves the Sekinchan rice paddy fields and mine/ ex-mining activities to the south-east.

As a result of destructive human activities and the degradation of tropical peat swamp forests, the Selangor State Government agreed on a 25-year moratorium on timber extraction across the State from 2007 (Parish *et al.*, 2014). Following this step towards peatland restoration and rehabilitation, the IMP was set out in 2014, prepared by the Global Environment Centre (GEC). This plan is an updated version of a previous IMP for NSPSF incorporating up-to-date research findings from within the reserve and best management practices for peat swamp conservation. The IMP specifically targets key areas in rehabilitation, fire prevention, and buffer zone management across NSPSF, adopting a zonal approach where focused activates of restoration and conservation can be strategically directed to the areas/zones most at risk of degradation. To date, several IMP interventions have been implemented in NSPSF with varying degrees of success, including drain blocking, introduction of strict no burning legislation, and forest replanting programmes.

5.2.2 Workflow

Figure 5-1 illustrates the workflow for estimating tropical peat swamp forest AGB across the entire NSPSF and assessing the impact of natural and anthropogenic change on the site between 2015 and 2018. This includes the extraction of Sentinel-2 model input variables (spectral and textural), the development of a predictive model for tropical peat swamp forest AGB, and change analysis of 2015 and 2018 AGB map outputs.

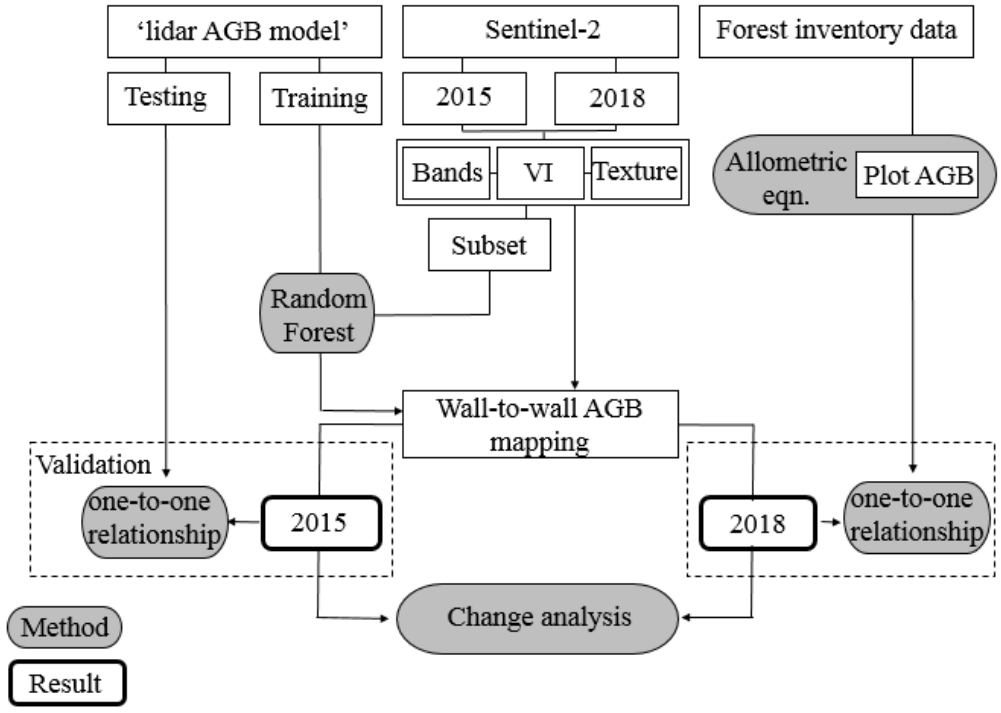


Figure 5-1 Workflow of the major tasks carried out in this research chapter.

5.2.3 Sentinel-2 data and pre-processing

Sentinel-2 is an Earth observation system part of ESA's Copernicus programme - a series of satellites under the family name Sentinel with a policy of free and open-access space-borne data. Sentinel-2 is a constellation of twin satellites, Sentinel-2A and Sentinel-2B. The pair aims to provide enhanced multispectral data with a high revisit time of 5-days (Drusch *et al.*, 2012). The Sentinel-2 satellites carry the MSI sensor that samples across thirteen spectral

bands at a spatial resolution ranging from 10 - 60 m. The MSI sensor's unique band combination importantly incudes three vegetation-focussed bands positioned in the red-edge zone (across 705-865 nm, at a 20 m spatial resolution).

Sentinel-2 MSI scenes were acquired for the 31st December 2015 and 13th February 2018 (both dates fall in the region's dry season), supplied as Level 1C geocoded formatting. As Sentinel-2 Level 1C data is top of atmosphere reflectance, the ENVI FLAASH algorithm was applied to convert this to surface reflectance (bottom of atmosphere). MSI spectral bands with a 20 m spatial resolution (b5, b6, b7, b8a, b11, and b12) were resampled to 10 m applying the nearest-neighbour interpolation algorithm. Both Sentinel-2 MSI scenes were projected to WGS 1984 UTM Zone 47N (the same projection as **Chapter 4** NERC ARF lidar data), key structures in the landscape (GPS data collected in the field), such as clear road junctions and a bridge crossing the canal, were used in a simple visual assessment to check the inter-calibration of the two scenes.

5.2.4 Sentinel-2 model input variables

A suite of spectral and textural variables were calculated to estimate the AGB of NSPSF for the two dates of interest. Spectral variables include the pre-processed Sentinel-2 MSI bands and a selection of vegetation indices (Table 5-1). Selection of vegetation indices was based on their performance in past research (Galidaki *et al.,* 2017; Timothy *et al.,* 2016); these indices were selected to represent the strong contrast in reflectance in the near-infrared (NIR) by plant matter with the strong absorption by chlorophyll in the red part of the electromagnetic spectrum, essentially measuring vegetation

Table 5-1 Vegetation indices with equation and the Senitnel-2 MSI bands used.

Vegetation Index	Equation	Sentinel-2 MSI bands used
Normalised Difference Vegetation Index (NDVI)	= (NIR – R)/(NIR+R)	= (band 8 – band 4)/(band 8+band 4)
Normalised Difference Vegetation Index Red-Edge band 5 (NDVI-RE5)	= (NIR – RE1)/(NIR+RE1)	= (band 8 – band 5)/(band 8+band 5)
Normalised Difference Vegetation Index Red-Edge band 6 (NDVI-RE6)	= (NIR – RE2)/(NIR+RE2)	= (band 8 – band 6)/(band 8+band 6)
Normalised Difference Vegetation Index Red-Edge band 7 (NDVI-RE7)	= (NIR – RE3)/(NIR+RE3)	= (band 8 – band 7)/(band 8+band 7)
Simple Ratio (SR)	= NIR/R	= band 8/band 4
Simple Ratio Red-Edge band 5 (SR-RE5)	= NIR/RE1	= band 8/band 5
Simple Ratio Red-Edge band 6 (SR-RE6)	= NIR/RE2	= band 8/band 6
Simple Ratio Red-Edge band 7 (SR-RE7)	= NIR/RE3	= band 8/band 7
Inverted Red-Edge Chlorophyll Index (IRECI)	= (NIR − R)/(RE1/RE2)	= (band 8 – band 4)/(band 5/band 6)
Sentinel-2 Red-Edge Position (S2REP)	= 705 + 35 * ((((NIR + R)/2) − RE1)/(RE2 − RE1))	= 705 + 35 * ((((band 8 + band 4)/2) – band 5)/(band 6 – band 5))

greenness. Additionally, vegetation indices incorporating or adapted to utilise the red-edge zone are included to take full advantage of the multiple bands covering this sensitive spectral region (Fernández-Manso *et al.,* 2016; Frampton *et al.,* 2013). Vegetation indices were calculated in R software (version 3.5.2) using the '*Raster*' package (Hijmans, 2018)

Texture variables based on the grey-level co-occurrence matrix (GLCM) approach (Haralick *et al.,* 1973) have been adopted here to enhance the spatial discrimination of features in the data scenes, such as tree density and linear structures in the landscape (i.e. canals). Three GLCM metrics - homogeneity, mean and variance (Table 5-2) – have been applied to individual raw Sentinel-2 MSI bands under different windows sizes (3x3, 5x5, 7x7, and 9x9 pixels) at an offset distance of 1 and averaged in all directions. Textural variables were generated in R software (version 3.5.2) using the '*glcm*' package (Zvoleff, 2016).

Table 5-2 The GLCM-based texture variables formula.

$\text{Homogenity} = \sum_{i,j=0}^{N-1} \frac{P_{i,j}}{1+(i-j)^2}$
$\text{Mean} = \sum_{i,j=0}^{N-1} i\left(P_{i,j}\right)$
$\text{Variance} = \sum_{i,j=0}^{N-1} P_{i,j}(i-Mean)^2$

Note: $P_{i,j} = {V_{i,j}}\Big/{\sum_{i,j=0}^{N-1} V_{i,j}}$, where $V_{i,j}$ is the value in the cell *(i, j)* (row *i* and column *j*) of the moving window and *N* is the number of rows or columns.

5.2.5 Training and validation data

5.2.5.1 'lidar AGB model'

In order to overcome the many barriers to obtaining field inventory plot data for AGB estimation, past studies have adopted lidar transects as surrogate plot data (Garcia *et al.*, 2018; Bolton *et al.*, 2018; Jin *et al*., 2018; Zald *et al.*, 2016). In a similar vein, this research adopts the site specific model developed in the research presented in **Chapter 4** (Brown *et al.*, 2018) as model training and testing data for predicting AGB for NSPSF. The predictive model and statistics presented are listed in Table 5-3. Based on this model, a thematic map of tropical peat swamp forest AGB was generated for a subset of lidar flightlines recorded by the NERC ARF team in the 2014 Malaysia campaign, gridded at 10x10 m spatial resolution (scale matching the Sentinel-2 MSI 10 m spatial resolution bands). It is important to note here the three-year time delay between the collection of the airborne lidar data (2014) and field plot inventory data (2017) used in developing this model. This may introduce error into the AGB model, however all field plots were established to be free from logging and fire, with no obvious disturbance within the three-year period.

Table 5-3 Performance of 'lidar AGB model' developed in **Chapter 4** (Brown *et al.*, 2018). Where: H_mean = mean plot height of median energy (HOME); B50 = 50^{th} height bincentiles; R^2 = R square; RMSE = root mean square error; rRMSE = relative root mean square error.

Predictive Model	R^2	RMSE (Mg/ha)	rRMSE (%)
= 171.3732 + 14.7802 x H_mean- 1.5752 x B50	0.77	39.8	10.8

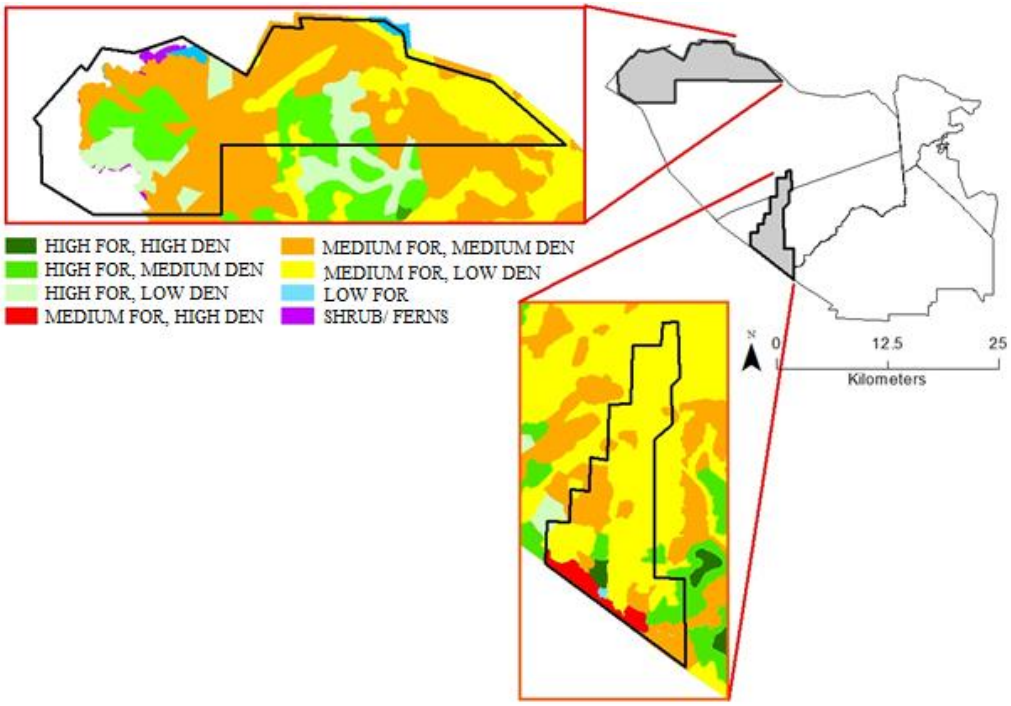


Figure 5-2 'lidar AGB model' area coverage overlaid onto forest type (forest height (high, medium, low) and forest density (high, medium, low)) results from a forest inventory undertaken in 2000 (RCFM, 2000).

The AGB map generated from the model presented in **Chapter 4** (Brown *et al.*, 2018), and here by known as 'lidar AGB model', represents with high accuracy an area of 9,457.08 ha, covering just over 10% of NSPSF (Figure 5-2). These sections of the reserve have faced little reported large-scale forest cover change since the updated IMP implementation in 2014. The areas of the reserve covered by the 'lidar AGB model' supports forest with a range of structural characteristics (i.e., height and density), and thus deemed appropriate and representative as training and testing data for mapping AGB across the whole of the NSPSF (Figure 5-2). A simple visual check on the spatial positioning of datasets was made. Sourcing appropriate structures in the landscape as reference points was restricted due to the forest structure and data resolution (10 m), reference points were limited to clear reserve boundary

lines. The spatial correspondence of datasets in this research may introduce error into the final wall-to-wall AGB estimations for NSPSF.

The 'lidar AGB model' totalled 949,119 pixels (10 m spatial resolution), of which 70% (664,383) were randomly sampled to use as training data, and the remaining 30% (284,736) reserved for testing (Table 5-4).

Table 5-4 Summary statistics for the 'lidar AGB model' developed in **Chapter 4** (Brown *et al.*, 2018).

Sample Number	Mean	Median	SD	Minimum	Maximum
949119	224.53	221.79	122.6242	24.02	600.00

5.2.5.2 Field inventory data

Forest inventory ground truth data was collected in 2018 to be used as model validation data for the 2018 AGB map. To estimate field AGB, 17 circular field plots with a radius of 15 m were established throughout the NSPSF reserve, with a keen effort to cover areas of different locations, forest type, degradation, and management in NSPSF.

For each plot, all live trees with a DBH of >5 cm were measured and recognised tree species recorded. Additionally, dependent on the top of tree visibility, selected trees of varying height classes were measured by laser height meter. Plot AGB values were calculated based on the general pan-tropical allometric equation developed by Chave *et al.*, (2014). Inputs included: field-measured DBH, species (to estimate wood density) and tree height when available (missing height data was retrieved from a Feldpuash *et al.*, (2012) averaged model, region set to South-Eastern Asia). Wood density

was estimated for the trees based on their taxonomy using the global wood density database (GWD) (Chave *et al.,* 2009; Zanne *et al.,* 2009), unidentified trees or trees with a missing genus in the GWD were assigned a mean plot-level wood density value. The AGB allometric equation was computed as:

$$AGB = 0.0673 \times (\rho D2H)^{0.976}$$

where ρ = wood density (g/cm^3), D = DBH (cm) and H = height (m).

The '*BIOMASS*' package in R software (version 3.5.2) (Rejou-Mechain *et al.,* 2017) was used to run AGB estimation. AGB values were calculated for individual trees within each 15 m radius field plot, and then summed to obtain total AGB plot values.

5.2.6 Random Forest regression

The Sentinel-2 2015 spectral and textural variables and the training data (70% of the 'lidar AGB model') were used as inputs for a non-parametric data fusion machine learning algorithm, Random Forests (Brieman, 2001). As previously mentioned, the 'lidar AGB model' is developed from a lidar dataset captured in 2014 and forest inventory plot data collected in 2017, the temporal time difference between 'lidar AGB model' and the Senitnel-2 scenes may introduce error into the Random Forest regression, however, the areas of the reserve covered were established to be free from logging and fire in this time period, with no obvious structural disturbance.

The Random Forest algorithm is widely used in the remote sensing community (Jin *et al.,* 2018; Zald *et al.,* 2016; Karlson *et al.,* 2015; Main-Knorn *et al.,* 2011) due to its capacity to handle potentially noisy and highly correlated variables often associated with remotely sensed datasets (Breiman,

2001; Curran, 1986). Previous research (Shao *et al.*, 2017; Fassnacht *et al.*, 2014), found the Random Forest method to produce superior results in comparison to other approaches such as Support Vector Machine, k-nearest neighbour, and Gaussian processes.

Random Forest is an ensemble learning method based on classification and regression trees, this research follows the latter, implemented in the '*Ranger*' package (Wright and Ziegler, 2015) within R environment software (version 3.5.2). Random Forest regression operates by constructing a large number of trees, i.e. a forest, by randomly selecting the predictor variables from the input dataset and then calculating a mean prediction from all individual trees grown. One-third of the input data, termed the out-of-bag (OOB) sample, is left out of the bootstrap sample and is used to calculate an unbiased estimate for the retrieval error (OOB error). Within the Random Forest regression three parameters need to be optimised: 1) *ntree*, the number of trees grown; 2) *mtry*, the number of different predictors sampled at each node; 3) *nodesize*, the minimal size of the terminal nodes of the trees.

In addition to prediction, Random Forest estimates variable importance measures to rank variables by their predictive importance. The '*Ranger*' package computes permutation importance of a variable, calculated as the difference of prediction performance before and after permuting the values of the variable averaged over all trees built by the Random Forest. In each tree OOB data are included in the variable importance calculation. Importance values are ranked and used to determine the predictor strength and influence on the Random Forest model performance. This information can then be used

to tailor predictor selection by eliminating low ranking predictor variables to produce the best predictive power and help interpret the final model.

An independent validation was performed with the remaining test data (30% of the 'lidar AGB model') unseen by the model. The following statistical parameters were considered for the independent validation: R square (R^2), adjusted R square (Adj-R^2), Root Mean Square Error (RMSE), Normalised Root Mean Square Error (NRMSE) that results in a percentage (%RMSE), and Bias.

5.2.7 Wall-to-wall AGB for NSPSF

Wall-to-wall peat swamp forest AGB maps over the entire NSPSF were generated using the Random Forest model and the Sentinel-2 variables for both 2015 and 2018 scenes. Applying existing models to predict forest inventory attributes is a key benefits for both extending the area of model coverage and updating forest inventories over time. The transferability of existing AGB models spatially (Foody *et al.*, 2003) and temporally (Fekety *et al.*, 2015) maximises the investment in model development (including data acquisition and processing's costs). Re-use of the Random Forest model built from the subset Sentinel-2 2015 variables and 'lidar AGB model' across the entire site for the 2018 scene was deemed appropriate as the training areas covered a good representation of the study site, but importantly covers a large area of all vegetation types. Thematic AGB maps for NSPSF were created at a 10 m spatial resolution (0.01 ha) for 2015 and 2018.

5.2.8 2018 AGB validation

The predictive ability and transferability of the Random Forest model for estimating AGB across the entire reserve for 2018 was assessed using an independent validation dataset of field inventory plot data collected in 2018. A one-to-one relationship between measured and predicted AGB values was fitted. Common statistical parameters were computed – R square (R^2), adjusted R square (Adj-R^2), Root Mean Square Error (RMSE), Normalised Root Mean Square Error (NRMSE) that results in a percentage (%RMSE), and Bias.

5.2.9 AGB change analysis

The NSPSF AGB maps generated for 2015 and 2018 (10x10 m pixel resolution) were used to calculate an AGB change map by subtracting the 2018 AGB map from the 2015 AGB map. The resulting AGB change map was visually analysed and interpreted with reference data acquired from the Selangor State Forestry Department and local NGO's and conservation groups.

The following information was provided:

- Dates and locations of drain blocking activities
- Dates and locations of replanting programs
- Dates and locations of large-scale fire events
- Locations of human hydrological interventions, e.g. clay bungs/ wall installation
- Recent changes in land adjacent to NSPSF, e.g. road upgrades

Interpretation of NSPSF AGB dynamics between 2015 and 2018 was also supported by the IMP documentation and personal knowledge of the reserve obtained from frequent field campaigns in NSPSF.

5.3 Results

5.3.1 Random Forest model performance

The variable importance rankings, based on the permutation variable importance approach, were used to improve the predictive performance of the Random Forest models through a progressive backwards feature elimination (i.e. removing the lowest ranked variable until the model was optimised). The full set of predictor variables generated from the 2015 subset Sentinel-2 data (n = 142) was reduced (n = 62) to yield the highest predictive performance in the final Random Forest model for estimating tropical peat swamp forest AGB in NSPSF. The variables which ranked highest in the final optimised Random Forest model (Figure 5-3) were predominantly based around the variance and mean texture variables, at a variety of window sizes, applied to Sentinel-2 MSI bands positioned in key features of green vegetation spectral response (b3 = Green, b4 = Red, b5 = Red-Edge, b6 = Red-Edge, and b8a = Narrow-NIR). Additionally, vegetation indices incorporating the Sentinel-2 Red-Edge bands also ranked highly in model importance, for example NDVI-RE5, NDVI-RE6, SR-RE5, and SR-RE6.

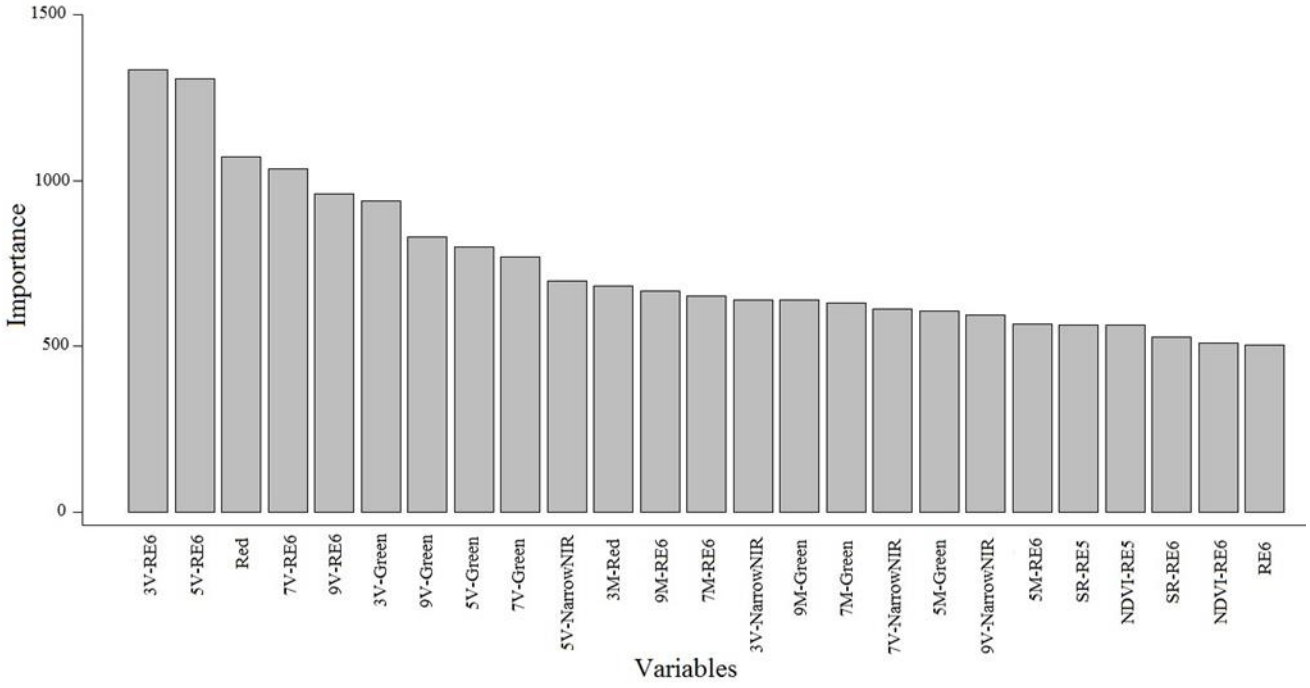


Figure 5-3 The top 25 ranked variables from the optimised Random Forest model based on the permutation vairtbale importance (Importance). Where: 3V-RE6 = 3x3 Variance Red-Edge band 6; 5V-RE6 = 5x5 Variance Red-Edge band 6; Red = band 4; 7V-RE6 = 7x7 Variance Red-Edge band 6; 9V-RE6 = 9x9 Variance Red-edge 6; 3V-Green = 3x3 Variance Green band 3; 9V-Green = 9x9 Variance Green band 3; 5V-Green = 5x5 Variance Green band 3; 7V-Green = 7x7 Variance Green band 3; 5V-NarrowNIR = 5x5 Variance Narrow NIR band 8a; 3M-Red = 3x3 Mean Red band 4; 9M-RE6 = 9x9 Mean Red-Edge band 6; 7M-RE6 = 7x7 Mean Red-Edge band 6; 3V-NarrowNIR = 3x3 Variance Narrow NIR band 8a; 9M-Green = 9x9 Mean Green band 3; 7M-Green = 7x7 Mean Green band 3; 7V-NarrowNIR = 7x7 Variance Narrow NIR band 8a; 5M-Green = 5x5 Mean Green band 3; 9V-NarrowNIR = 9x9 Variance Narrow NIR band 8a; 5M-RE6 = 5x5 Mean Red-Edge band 6; SR-RE5 = Simple Ration Index band 5; NDVI-RE5 = Normlaised Difference Vegetation Index Red-Edge band 5; SR-RE6 = Simple Ration Index band 6; NDVI-RE6 = Normlaised Difference Vegetation Index Red-Edge band 6; RE6 = Red-Edge band 6 .

The Radom Forest algorithm parameters, *ntrees* and *mtyr*, were also adjusted to optimise the model. The Random Forest model was set to *ntrees* – 1800 and *mtry* – 21.

5.3.2 Predictive performance of Random Forest model

The Random Forest model with optimised input variables (n= 62) and parameter adjustments produced a good plausible result (R^2 = 0.8; RMSE = 55.2 Mg/ha) (Table 5-5). The relationship between observed AGB ('lidar AGB model' testing data) and predicted AGB is presented in Figure 5-4. Figure 5-4 clearly displays issues around the lowest observed AGB values overestimating AGB and the highest observed AGB values underestimating AGB, however these represent a low proportion of the 284,736 validation points. These issues could be an effect of the limited sensitivity of satellite sensors to variations in canopy height and structure.

Table 5-5 Performance of optimised Random Forest model on an independent validation dataset. Where: R^2 = R square; Adj-R^2 = adjusted R square; RMSE = root mean square error; %RMSE = percentage normalised root mean square error.

Number of validation points	R^2	Adj-R^2	RMSE (Mg/ha)	%RMSE	Bias
284736	0.80	0.80	55.2	24.6 %	-0.15

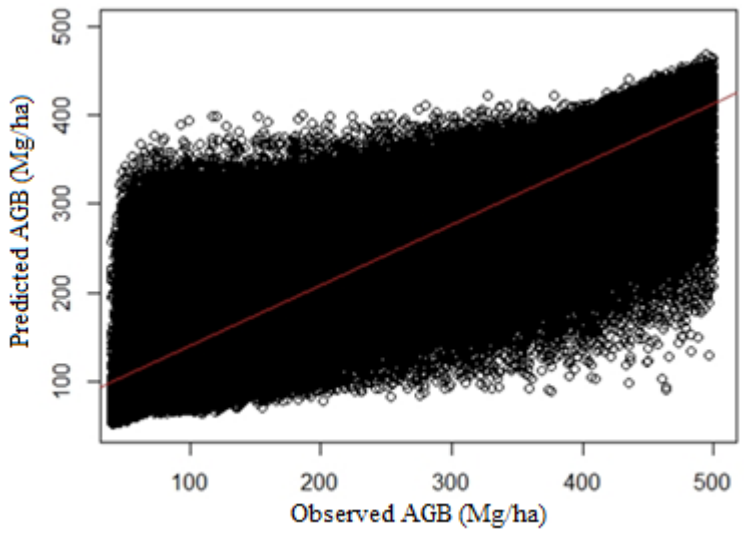


Figure 5-4 Observed vs. predicted AGB using the optimised Random Forest model with an independent validation dataset.

5.3.3 Wall-to-Wall AGB maps

The wall-to-wall AGB map for the entire NSPSF reserve produced for the year 2015 using the final optimised Random Forest model can be seen in Figure 5-5. The Sentinel-2 spectral and textural input variables for producing tropical peat swamp forest AGB estimations were chosen based on the fact that the optimised Random Forest model produced good, plausible results according to the independent validation (Table 5-5). Figure 5-5 displays the distinct AGB spatial distribution within NSPSF reserve in 2015, depicting areas of different tropical peat swamp forest type and density, as well as highlighting areas of potential disturbance or degradation. The mean predicted tropical peat swamp forest AGB estimate was 246 Mg/ha, with a range of 24.95 - 599.12 Mg/ha.

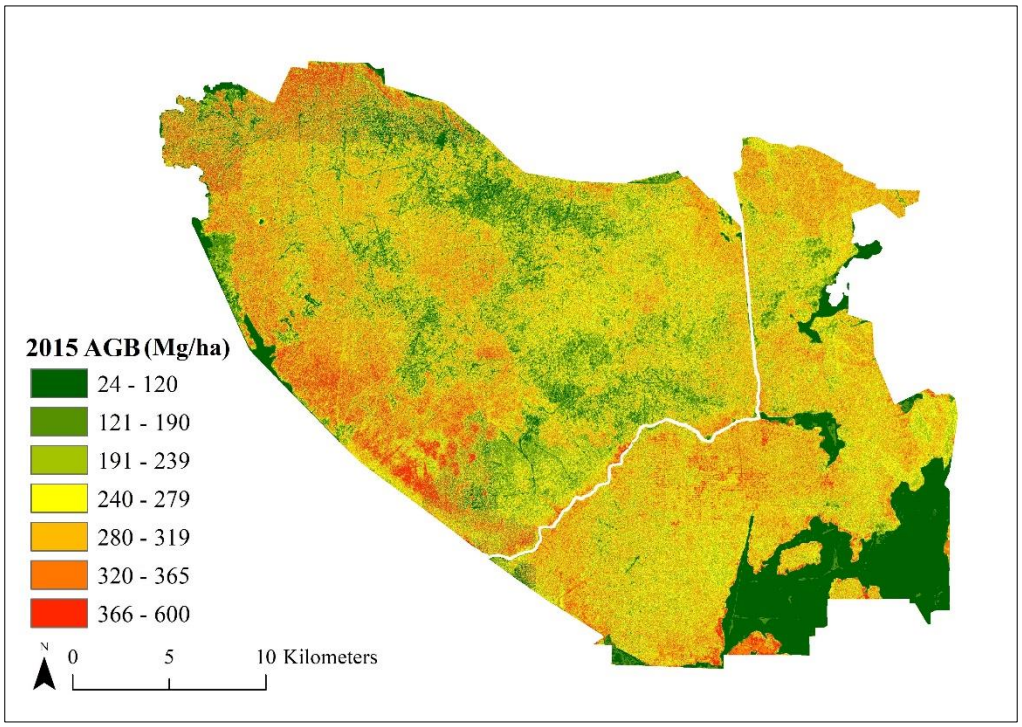


Figure 5-5 2015 AGB (Mg/ha) estimated for NSPSF reserve calculated from the optimised Random Forest model, at a 10 m (0.01 ha) spatial resolution.

The wall-to-wall AGB map for the entire NSPSF reserve produced for the year 2018 re-using the final optimised Random Forest model built from the 2015

subset Sentinel-2 variables and 'lidar AGB model' data can be seen in Figure 5-6. This presents the AGB spatial distribution across the NSPSF reserve for 2018, where visual analysis of the map highlights the variety of tropical peat swamp forest vegetation cover. The mean predicted tropical peat swamp forest AGB estimate was 252.64 Mg/ha, with a range of 25.29 - 584.43 Mg/ha.

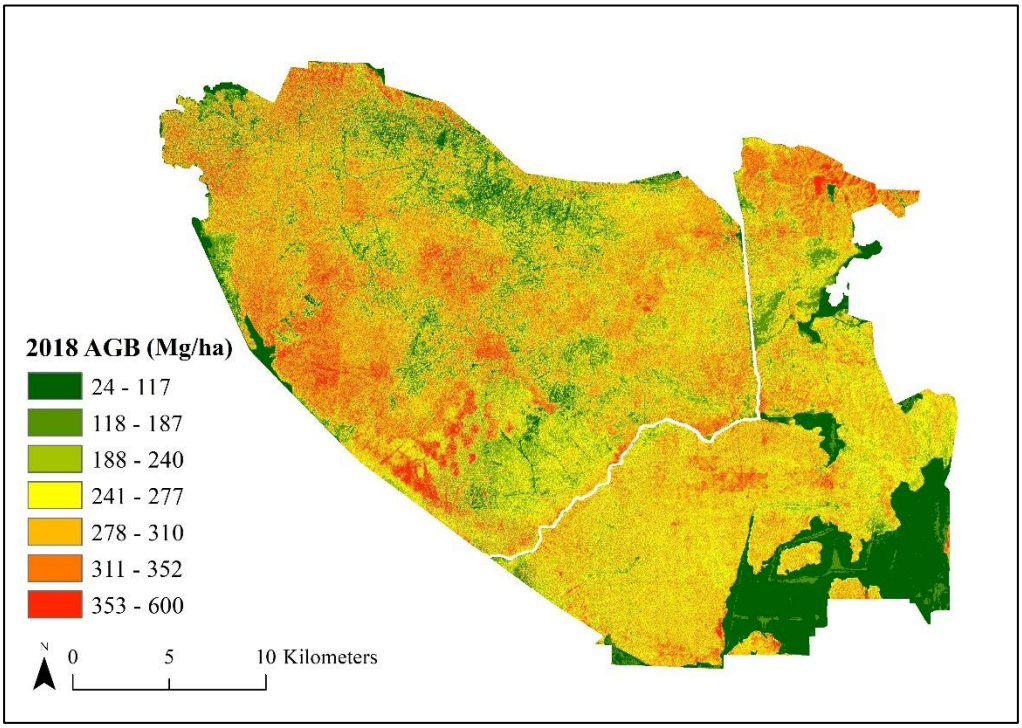


Figure 5-6 2018 AGB (Mg/ha) estimates for NSPSF reserve calculated from the optimised Random Forest model, at a 10 m (0.01 ha) spatial resolution.

5.3.4 2018 AGB independent validation

The validation results from the one-to-one relationship between predicted AGB and observed AGB (field plots) presented a strong agreement (R^2 = 0.92; RMSE = 23.4 Mg/ha) (Table 5-6). The relationship between observed AGB (field data) and predicted AGB for 2018 is presented in Figure 5-7. Overall, the optimised Random Forest model accurately mapped AGB across NSPSF using Sentinel-2 spectral and textural variables for 2018. This result seems

counterintuitive to the findings in **Chapter 4** ('AGB lidar model' reported R^2 = 0.77 (Table 5-3)) and past research reporting lidar as the most accurate data source for AGB estimation (Fassnacht *et al.*, 2014). However, this reported high R^2 may be a result of the small sample size for the test set (17 field plots), which can lead to unstable results. A larger dataset covering a wider and move varied range of AGB values, in particular for lower AGB (<150 Mg/ha) and high AGB (>400 Mg/ha), may expose a less accurate AGB estimation for 2018.

Table 5-6 Independent validation results from 2018 AGB estimation. Where: R^2 = R square; Adj-R^2 = adjusted R square; RMSE = root mean square error; %RMSE = percentage normalised root mean square error.

Number of validation points	R^2	Adj-R^2	RMSE (Mg/ha)	%RMSE	Bias
17	0.92	0.92	23.4	8.73%	-5.4381

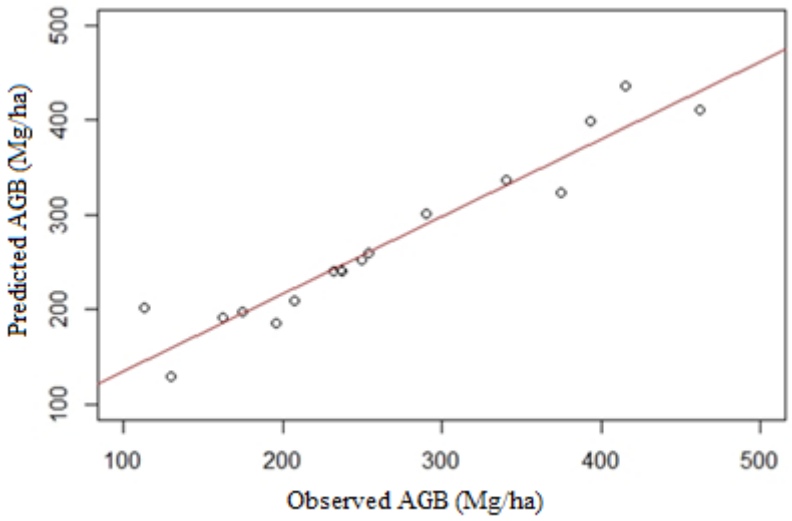


Figure 5-7 Observed vs. predicted AGB using the 2018 predicted AGB results and field inventory estimated AGB.

5.3.5 Change analysis

Change in AGB distribution and abundance is presented in Figure 5-8. The interpretation and analyses of the AGB change map using reference datasets and expert knowledge of the site revealed a number of key areas of change in NSPSF. Table 5-7 identifies the key areas of change, in both AGB gain and loss, alongside a review of the land management activities and disturbance which have impacted these areas.

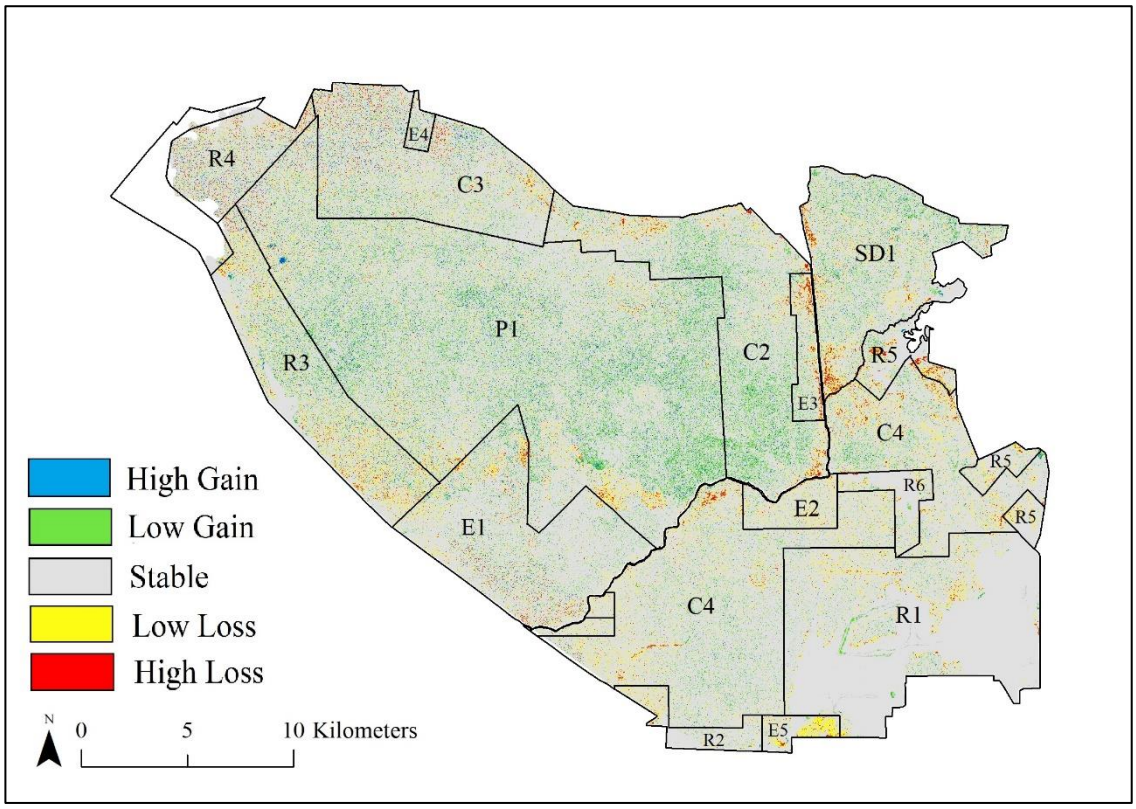


Figure 5-8 AGB change between the years 2015 and 2018 for NSPSF reserve. Classified as high gain, low gain, stable, low loss, and high loss.

Table 5-7 Prominent management zones of change in NSPSF and the associated IMP interventions and proposed regeneration strategies.

AGB Gain	**P1**	This large central section of NSPSF has been marked by the IMP as potential production/ water catchment forest. P1 covers the deepest areas of peat soil and potential peat domes, this area plays a vital role in water storage and the regulation function of NSPSF. Between the years 2015-2018 the key goals of the management designation was forest protection and blocking of the main drainage channels to encourage natural regeneration. The AGB gains provide evidence of the successful regeneration of P1, and present a good example of sustainable management of tropical peat swamp forest.
	C2	This section of NSPSF covers both central areas of the forest (neighbouring P1) and areas of forest on the reserve boundary. These areas have been marked by the IMP as a conservation zone. In the past this area was heavily degraded by intensive logging activities and associated drainage, however the forest is now recovering well, supported by AGB gain values (Figure 5-8). Although the majority of C2 shows AGB gain, there is a focused area of AGB loss at the northern boundary (Figure 5-9). This is thought to be in association with peat drainage and potential peat subsidence due to its close proximity to the Tanjong Malim – Sg Besar road (road upgrade, high drains, and culverts) and oil palm plantations.
AGB Loss	**E5**	This section of NSPSF covers a relatively small area, marked by the IMP as an education and ecotourism zone. However, it is adjacent to zones R2 and R1, which are areas of severely degraded peat swamp annually effected by large scale fire events. E5 and the neighbouring R2 and R1 zones underwent major management interventions between 2015-2018, including large-scale drain blocking campaigns and replanting schemes (Figure 5-10), however, frequent fire events have hampered recovery efforts, seen by the AGB loss in E5.

R3	This section covers the western boundary of the reserve directly adjacent to the main irrigation canal of the IADA Rice Scheme. It is marked by the IMP as a rehabilitation zone. The area was negatively impacted by the construction of a peat/clay bung in 2010 which prevented water flow from the forest to the main irrigation canal. The artificially high water flow levels led to significant tree death and impacted the integrity of the peat soil structure. In 2011 culverts were installed in an effort to restore the natural hydrology of the area, however these were again too high and flooded the forest leading to further water management adjustments in 2012. Although efforts of regeneration and water table recovery have been made in this section, it is evident that these areas bordering the reserve still face significant forest loss.

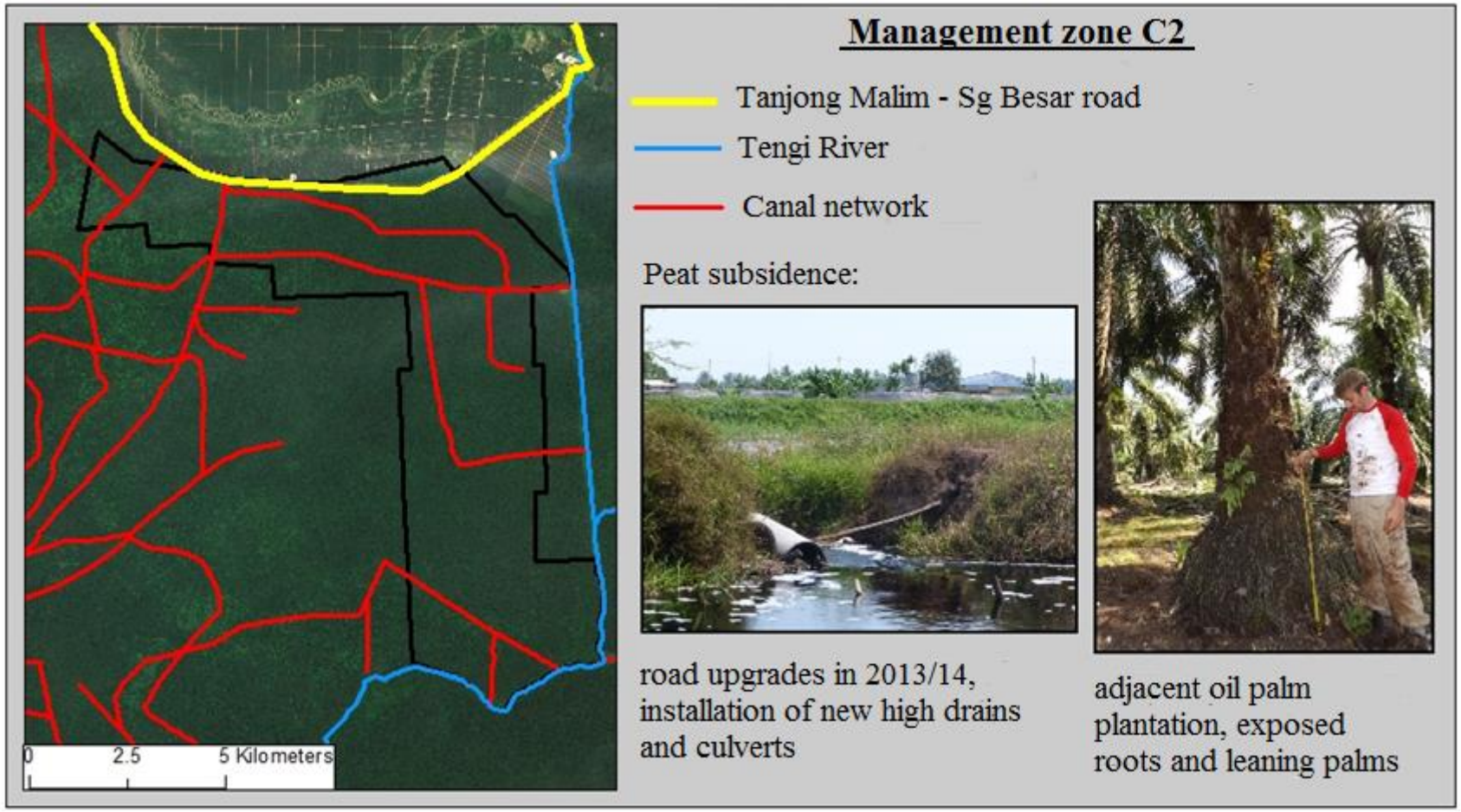


Figure 5-9 Management zone C2 illustrated with cause and evidence of peat swamp degradation.

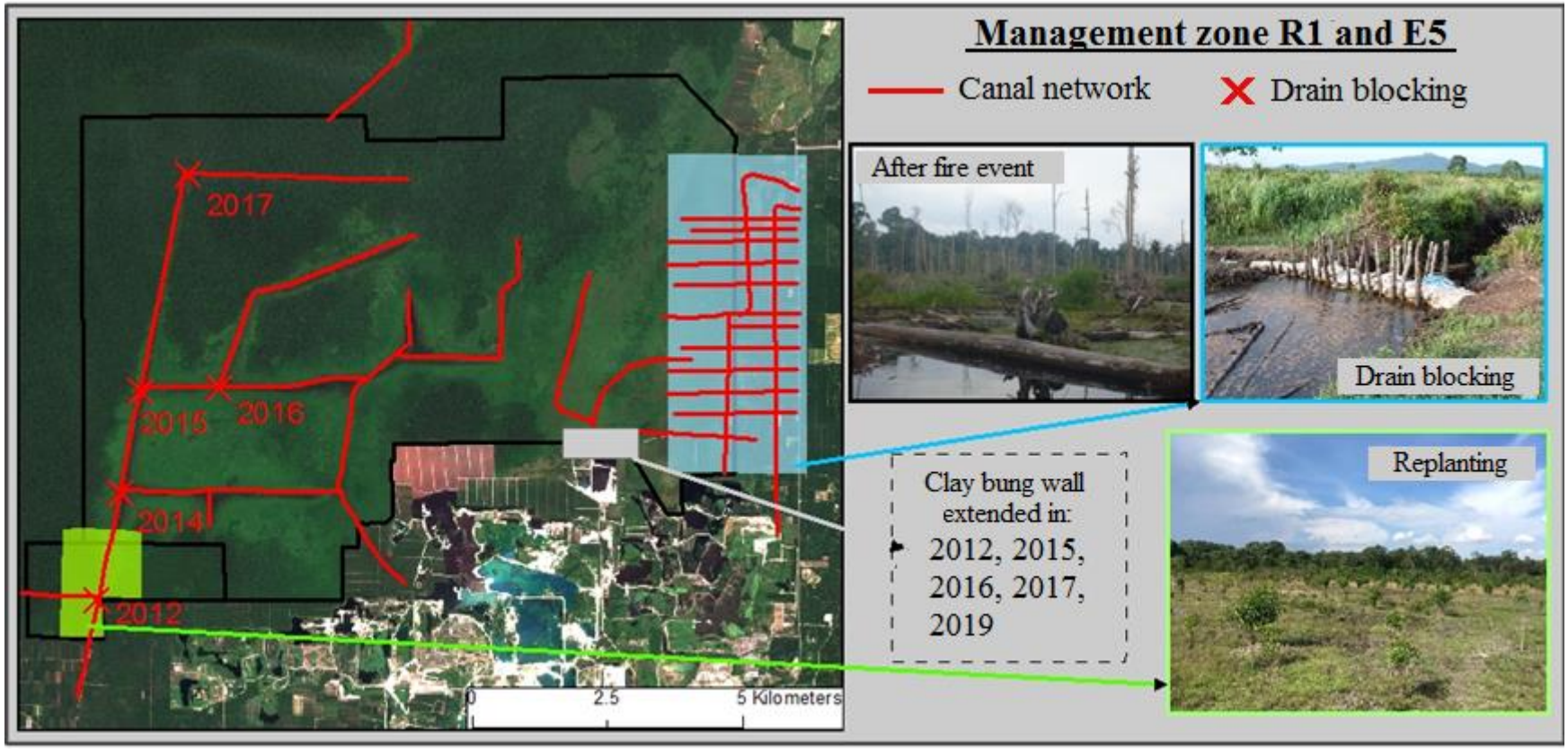


Figure 5-10 Management zone R1 and E5 illustrated with past restoration intervent.

5.4 Discussion

Planning and management to restore and conserve tropical peat ecosystems require spatially explicit and timely estimates of AGB, in particular for tracking the impacts of any restoration interventions (Padfield *et al.*, 2014). As one of the largest remaining tropical peat swamp forests in Peninsular Malaysia, NSPSF has been recognised for its global significance as a carbon store (Davies, 2011; Prentice, 2011; ASEAN Secretariat and Global Environment Centre, 2011). As a result, its ecosystem health and security is of immense importance. The predictive Random Forest model and AGB maps presented in this research provide a quantitative tool for peat swamp forest management in NSPSF reserve, where the local forestry department, NGOs and conservation groups can access a detailed view on the peatlands recovery and begin to build an archive of data on peat swamp forest dynamics. Additionally, it affords the ability to isolate key areas of degradation (both anthropogenic and natural), which can aid in prioritising and formulating sustainable management strategies.

The time period under investigation in this research (2015 - 2018) marks a focused period of restoration and regeneration efforts in the NSPSF reserve. The results from the AGB change analysis demonstrate an overall increase in tropical peat swamp AGB during these years, where the total amount of estimated AGB stored in NSPSF increased from 19.3 Tg in 2015 to an estimated 19.8 Tg in 2018, totals comparable with other AGB estimates conducted in tropical forests of similar size and density in South-East Asia (Asner *et al.*, 2018). Despite this positive result, areas of concern remain within the reserve where continued AGB losses occur, in particular towards

the south-east corner of the reserve. The major factors implicating tropical peat swamp forest recovery and regeneration for NSPSF are drainage (both within the reserve and as a result of land-use adjacent to the reserve) and large-scale fire events. Drainage from the estimated 500 km network of canals within the reserve, as well as a result of adjacent oil palm plantation development and ex-mining activities, continues to stress this vulnerable ecosystem (Tonks *et al.,* 2018). Altering the natural balance of the water table, in combination with frequent large-scale fire events (Cattau *et al.,* 2016), can drive a negative feedback loop in tropical peatland ecosystems, affecting their function and resilience to further degradation (Evers *et al.,* 2017; Page *et al.,* 2009b). The current canal blocking activities and water table management efforts (Dahalan *et al.,* 2016; Rengasamy *et al.,* 2016; Ahmad 2014) must be monitored and extended throughout the entire reserve. Only by rewetting the peat can hydrological functions be restored, peat oxidation decreased and fire risk reduced in NSPSF. It is important to note that recovery can be a slow process, particularly when analysing AGB trends and dynamics at this scale, as large-scale fire events will have a short but dramatic impact, which can form a dominant marker in time series analysis when compared to long term forest regeneration. It is therefore important to have more long-term (+5 years) studies on tropical peat swamp restoration to analyse which methods are the most successful in tropical peat recovery (Page *et al.,* 2009b; Wösten *et al.,* 2008). This is an area of future work in which remote sensing technology could be usefully integrated.

The Random Forest based method used in this research shows great potential to upscale AGB estimates, derived from ‘lidar AGB model’, to larger

landscape-scale areas with Sentinel-2 spectral and textural variables. The variable importance rankings were used to assess the influence of Sentinel-2 spectral and textural inputs on the predictive performance of the Random Forest model. This research found a tailored variable selection approach improved predictions of AGB, this is in line with previous research applying the Random Forest algorithm to remotely sensed data (Adam *et al.,* 2014; Lawrence *et al.,* 2006). The inclusion of textural variables had the greatest importance for modelling of AGB in tropical peat swamp forests using optical satellite data (Figure 5-3). Texture values in an image allow the spatial heterogeneity to be evaluated, this can provide information on the distinct structure and development stages of forest stands (Kelsey and Neff *et al.,* 2014; Wood *et al.,* 2012). In particular, textural variables applied to Sentinel-2 bands positioned in known green vegetation spectral features, for example the red-edge (bands 5,6, and 7) and narrow near-infrared bands (band 8a), improved AGB estimation. The advantage of Sentinel-2 bands covering the red-edge zone has been noted in a number of forestry studies (Chrysafis *et al.,* 2017; Majasalmi and Rautiainen, 2016; Fernández-Manso *et al.,* 2016). Additionally, vegetation indices incorporating red-edge bands proved to be important for modelling AGB, Laurin *et al.,* (2016) suggested that the use of vegetation indices incorporating the red-edge bands may help mitigate the saturation issues associated with the use of traditional vegetation indices in the tropics. A potential opportunity to improve AGB modelling in future work could be the inclusion of textural variables applied to vegetation indices incorporating red-edge bands, combing the benefits of both approaches. Past research has successfully explored the use of combining both spectral and

spatial techniques, namely texture measurement and image ratio (Sarker and Nichol, 2011) and NDVI output texture analysis (Ning *et al.*, 2011; Chen *et al.*, 2001).

It is well documented that the spatial distribution and sample size of training data has considerable influence on the accuracy of model predictions (Cracknell and Reading, 2014; Fassnacht *et al.*, 2014; Ham *et al.*, 2005). Here, the research adopted the results from a model developed in **Chapter 4** (Brown *et al.*, 2018) as training and validation data in replacement of traditional field inventory plots. Errors introduced in the model development in **Chapter 4** will inevitably influence the overall performance of the Random Forest model and AGB map outputs produced in this research. Although, it must be stressed that the 'lidar AGB model' sample size and heterogeneity is considerably larger and better distributed than could be attained from a field-based program covering the same spatial and temporal scope. It is also important to note that both the 'lidar AGB model' dataset and the forest inventory plot estimated AGB values are reference datasets and do not represent actual measurement of AGB, only destructive sampling techniques can afford this. As previously discussed, potential errors may also have been introduced into the AGB models through temporal discrepancies between the 'AGB lidar model' and the S2 2015 scene, and additionally by geo-correlation issues between datasets. Combined, significant deviations from 'true' AGB values may occur.

Remote sensing has played a vital role in practical conservation management (Pettorelli *et al.*, 2014; Nagendra *et al.*, 2013; Panta *et al.*, 2008), establishing baselines for the extent and characteristics of ecosystems and their services, as well as quantifying degradation and subsequent recovery associated with both

natural and anthropogenic events or processes. There are a number of trade-offs associated with the use of different remote sensing technologies and sources (such as data acquisition cost, coverage, and platform considerations), along with their associated level of data complexity and processing expertise. Although alternative remote sensing technology such as lidar has been proven to be superior in AGB estimation in previous research (Fassnacht et al., 2014), optical spaceborne data remains a practical option for conservation management research applications (Timothy et al., 2016; Kennedy et al., 2009).

Space-borne optical data such as the Landsat series has long served as a major data source for ecosystem assessment and management (Willis, 2015; Kennedy *et al.,* 2014). The remote sensing community is now entering a golden age of space-borne sensor technology, in particular for ecosystem structural mapping and biomass prediction (Duncanson *et al.,* 2019; Rodríguez-Veiga *et al.,* 2017). With the next generation of space-borne optical sensors (e.g. ESA's Sentinel-2), lidar profilers (NASA's ICESat-2, NASA's GEDI and JAXA's MOLI) and SAR sensors (e.g. ESA's BIOMASS, NASA/ISRO's NISAR and ESA's Sentinel-1) set to provide a diverse range of datasets specifically designed for AGB assessment at a level of detail and temporal frequency never recorded before. Additionally, new opportunities in high/very high spatial resolution satellite data has emerged from constellations of microsats (Butler, 2014; Sandau *et al.,* 2010). These novel sensors operate at a low orbit and a comparatively low cost, and thus can be deployed in large numbers. The performance of microsats is rapidly evolving (Hand, 2015; Gill *et al.,* 2013), for example Planet Labs have deployed a constellation of 100+

Doves microsats (Safyan, 2019). With a daily 3-5 m data resolution, the Planet Labs constellation has been flagged as an important data resource for assessing AGB, carbon stocks and emissions at a high spatial and temporal frequency (O'Shea, 2019). The field of remote sensing continues to evolve and revolutionise the way we view the Earth's surface leading to countless advances at ground level in both scientific knowledge and practical application. To this end, supporting the data needs required to tackle global issues such as sustainable land recovery and conservation (SDG 15).

5.5 Conclusion

The research in this chapter assessed the potential of Sentinel-2 data for estimating AGB and analysing AGB change for a secondary tropical peat swamp forest undergoing extensive restoration and regeneration management activities. Our results demonstrate that the Random Forest algorithm is a useful and robust method for estimating AGB with Sentinel-2 derived spectral and textural predictor variables and a large, heterogeneous training dataset. The approach set out in this research provides a good opportunity to assess the success and unexpected consequences of different restoration activities (for example drainage and replanting programmes) on AGB dynamics in NSPSF (2015 – 2018). To further conservation efforts, sustainable management and restoration of degraded tropical peatlands must be informed and grounded by up-to-date spatially explicit ecological data, for example AGB cover and trends. I therefore recommend the continued tracking of AGB across NSPSF, building an archive of data which is representative of this on-going active period of conservation and regeneration to better understand the complex

processes of a recovering peatland ecosystem, and aid in the development of best practice peatland management.

Chapter 6: Detecting tropical peatland degradation: combining Remote Sensing and Organic Geochemistry

Stage of publication – In prep (target PloS one).

6.1 Introduction

Tropical peat swamp forests are increasingly recognised for their global importance as carbon sequestering and storing ecosystems, and their role for climate change mitigation. Under stable conditions, lowland tropical peatlands have the potential to form one of the most efficient carbon capture environments, with peat accumulation rates up to ten times faster in the tropics compared with other peatlands (temperate, subarctic, boreal) (Sjögersten *et al.,* 2014; Dommain *et al.* 2011; Chimner and Ewel 2005; Gorham *et al.* 2003). However, increased climate variability, amplified by degradation (associated with land use change and resource management) has the potential to shift tropical peatlands from a net carbon sink to a source (Hooijer *et al.,* 2010; 2006; Jauhiainen *et al.,* 2008; Page *et al.,* 2002). South-East Asia has experienced the most rapid and destructive large-scale peatland degradation. Since the 1980's, widespread degradation through deforestation (Charters *et al.,* 2019; Miettinen *et al.,* 2016; Langner *et al.,* 2007), drainage (Hooijer *et al.,* 2010; 2006) and frequent, intense fire events (Page *et al.,* 2009a; Langner and Siegert, 2009; Langner *et al.,* 2007), have dramatically increased the pressure on peat swamp forests in South-East Asia.

Ombrotrophic tropical peat swamp forests are rainwater-fed ecosystems with environmental and topographic conditions favouring poor drainage, oversaturation and substrate acidification. The peat deposits are formed and

maintained by the continuous input of organic matter from evergreen swamp forest species under waterlogged conditions (Yule *et al.,* 2009; Page et al., 1999). The surplus of water on the peatland floor creates an intermittent lack of oxygen, thus restricting microbial decomposition creating optimum conditions for peat accumulation, in particular during waterlogged conditions (Hoyos-Santillan *et al.,* 2016). The microtopography of tropical peatlands creates an irregular forest floor, with elevated surfaces, hummocks and hollows (Shimamura and Momose 2005; Shepherd *et al,.* 1997). When the organic matter inputs in the peat soil undergo microbial mediated aerobic and anaerobic decomposition greenhouse gasses (carbon dioxide (CO_2), methane (CH_4) and nitrous oxide (N_2O)) can be released into the atmosphere (Wright *et al.*, 2013; Jauhiainen *et al.,* 2005). Tropical peatland degradation accelerates these processes releasing high levels of greenhouse gas emissions into the atmosphere through vegetation removal, peat oxidation and combustion (Hoyos-Santillan *et al.,* 2019; Cooper *et al.,* 2019; Hooijer *et al.,* 2010; Van der Werf *et al.*, 2008; Page *et al.,* 2002).

Remote sensing has become one of the primary data sources for large-scale tropical peat swamp forest assessment (Minasny *et al.*, 2019). This provides a rapid and economical approach to supplement traditional direct field-based methods such as coring and probing (Rudiyanto *et al.*, 2018; Dargie *et al.,* 2017). Typically, field based measurements (with laboratory analyses) are used to determine peat properties (for example - peat thickness, bulk density, carbon content), with remote sensing data used to derive information on the area extent, land use change, fire events and vegetation cover (Konecny *et al.,* 2016; Reddy *et al.,* 2015; Miettinen *et al.,* 2012a). Remote sensing data can be

collected via a number of platforms such as planes, UAV's and kites; in this research chapter we focus on data captured by satellites. Space-borne data offers a low cost (often freely available) data solution, with regular resampling intervals and large area coverage. Additionally, some satellite series offer archival data, for example Landsat series dates from 1972. Due to the sheer extent and inaccessibility often associated with tropical peat swamp forests, remote sensing has been flagged as a key technology in tropical peatland mapping and assessment, particularly for repeated monitoring programs.

Biological, physical and geochemical analyses of *in situ*-samples remains the foundation of peatland soil research. Field measurements are required to develop an accurate, quantitative view on the impact of present-day surface disturbance and land management practises on the underlying peat soil profile formed centuries to millennium ago. Rock-Eval 6 pyrolysis has been identified as a low-cost organic geo-chemistry method for quantifying soil carbon and tracking soil organic matter (SOM) thermal stability in soil horizons (Sebag *et al.,* 2016; Biester *et al.,* 2014; Delarue *et al.,* 2013; Disnar *et al.,* 2003). This method has been previously used to investigate carbon dynamics in a wide range of environments - recently on tropical peats (Cooper *et al.,* 2019; Girkin *et al.,* 2019; Upton *et al.,* 2018), freshwater and saltmarsh peats (Kemp *et al.,* 2017; Newell *et al.,* 2016; Engelhart et al., 2013b) and marine sediments (Hare *et al.,* 2014). A better understanding of tropical peat organic geochemistry dynamics and reactions to disturbance (natural and anthropogenic) is vital for targeting resources and regeneration activities in sustainable peatland ecosystem management.

The aim of the research in this chapter is to explore the use of remote sensing and organic geochemistry for investigating the impact of tropical peat swamp forest degradation on the underlying peat soil profile. In view of this, the research addressed the following questions: (1) What are the relative contributions of above ground vegetation and peat soil to carbon stocks under different peat swamp forest condition classes? (2) Can remote sensing and GIS derived products predict peat soil carbon stocks and properties associated with degradation? and (3) Can the impacts of natural disturbance and past land management be detected throughout a peat profile? The research addressed these questions by combining remote sensing and GIS data with field peat cores collected across multiple sites under different land management in NSPSF, Malaysia

6.2 Methods

6.2.1 Study site

NSPSF (3º33’31 N, 101º18’21 E) is one of the largest remaining tropical ombrotrophic peat swamps in Peninsular Malaysia (Ahmad *et al.*, 2014). Comprised of four forest reserves - Raja Musa Forest Reserve, Sungai Karang Forest Reserve, Sungai Dusun Wildlife Reserve and part of Bukit Belata Forest Reserve Extension – NSPSF covers a total area of 81,304 ha. The reserve is predominantly covered by secondary mixed swamp forest; the majority of the area has been selectively logged from the 19th century up until the 1980’s and as a result forest condition varies throughout the reserve. Additionally, the extraction of timber led to the formation of a 500 km network of drainage canals (Parish *et al.*, 2014), altering the forest structure and accelerating the drainage and erosion of valuable peat soil stores (and the

carbon they hold) (Ahmad *et al.*, 2014). In response to past peat swamp forest degradation key areas of the reserve are under restoration and regeneration programmes, such as the updated IMP (Parish *et al.*, 2014) prepared by the GEC.

A significant area of the northern edge of the reserve has already undergone oil palm conversion (Cooper *et al.*, 2019). Reserve encroachment and the hydrological consequences of oil palm plantation drainage pose a serious threat to the protection and ecosystem function of NSPSF. NSPSF also boarders the Tanjung Karang Irrigation Scheme to the west which predominantly serves the Sekinchan rice paddy fields and mine/ ex-mining activities to the south-east.

During the early Holocene, NSPSF would have been colonized by mangrove species later to be replaced with fresh water peat swamp forest vegetation after the last Holocene interglacial marine incursion. This has resulted in the deposit of acidic peat overlaying grey marine clay (Yule and Gomez, 2009). Past studies have recorded an average peat depth of 3.6 m across the reserve (Parish *et al.*, 2014), with the deepest peat depth recorded in Sungai Karang Forest Reserve at 10.15 m. Typical to tropical peat swamp forest, the peat soil in NSPSF is rich in woody materials, including tree trunks, branches and roots, especially in the upper 50 cm section of the peat profile. The forest floor is covered by large intertwined tree root mats, with a 2-3 cm thick loose layer of fallen leaf litter.

NSPSF's tropical climate is characterised by heavy rainfall, high temperatures, and high humidity. The area receives an average annual rainfall of over 2,000

mm (Yule and Gomez, 2009), with distinct peaks from March to April and October to November. NSPSF has an average recorded shaded air temperature of 28.5 ^{o}C, with a average monthly relative humidity of 77.2% (Hahn-Schilling, 1994).

To investigate the impact of tropical peatland degradation on the underlying peat soil profile, four different peat swamp forest condition classes were identified to reflect the different forms and degrees of degradation (both natural and anthropogenic) (Table 6-1).

Table 6-1 Description of forest condition classes.

Central Forest	**Managed Recovery**
- tall dense forest, closed canopy - close proximity to river - subject to past selective logging activities, no targeted logging in approx. 40 years - limited human disturbance - low fire risk	- tall/medium forest, closed canopy - close proximity to forest boundary - targeted forest regeneration management - subject to past selective logging activities - ecotourism zone - low fire risk
Disturbed Forest	**Fire Affected**
- medium forest, open canopy - close proximity to forest boundary and encroachment of oil palm (active area of forest conversion) - adjacent to targeted drainage for oil palm agriculture - subject to past selective logging activities - medium fire risk	- low forest and scrub vegetation - frequent large scale intense fire events - targeted forest regeneration management - peat subsidence

6.2.2 Field Sampling

Within each of the peat swamp forest condition classes peat cores were collected for the entire peat profile during a field campaign in August 2017 (dry season): Central Forest = 3 cores, Managed Recovery = 2 cores, Disturbed Forest = 4 cores, and Fire Affected = 2 cores (Figure 6-1). It should be noted that the number of peat cores collected under each of the peat swamp forest condition classes are unbalanced, this is a result of poor peat core recovery impacting the number of entire cores collected. The small peat core sample size should be acknowledged, however this sample size is consistent with past research investigating organic geochemistry methods in tropical peatlands (Girkin et al., 2019; Upton et al., 2018). The complexity and non-uniform nature of tropical peat, for example variations in forest floor structure and depth, means that the peat samples should not be spatially extrapolated to represent large areas of the reserve, instead they are purely a representation of the peat and the processes that impact it for the defined sample area.

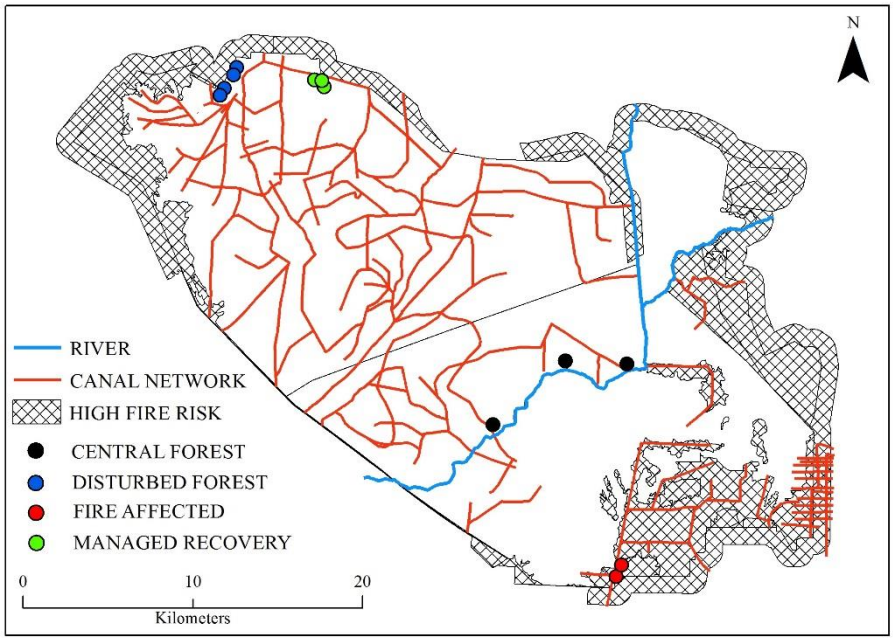


Figure 6-1 Location for the peat cores sampled under the four different forest condition classes. Areas of high fire risk, location of the Sungai Tenggi River and the canal network are labelled.

The peat cores were extracted using a side-filling Russian Peat Corer (Van Walt, UK), with a 0.5 m long sampling chamber. The peat profile was sampled in 0.5 m increments, from the ground surface to the underlying mineral material (clay layer). Immediately following extraction the peat cores were split into 10 cm segments which were bagged and sealed in the field. Surface leaf litter material was collected and bagged separately at each of the sites. All peat and litter samples were transported to laboratories at the University of Nottingham Malaysia Campus for initial processing.

6.2.3 Sample Processing

6.2.3.1 Bulk density and carbon storage

To determine bulk density, all sub-samples from the peat profiles collected were weighed for wet weight, oven-dried at 40°C for 48 hours, and then re-weighed for dry weight. Bulk density was calculated as: oven dried mass (g cm^{-3}) / volume (cm^3)). In this case each 10 cm section = 98.17 cm^3 (Tonks *et al.*, 2017).

The carbon density for the peat sub-samples (g cm^{-2}) were first calculated from the bulk density multiplied by the total organic carbon (TOC) (generated from Rock-Eval analysis), then multiplied by the depth per layer (10 cm). The carbon stock (Mg/cm^2) for each peat core was then calculated as the sum of each 10 cm layer throughout the peat core. Mg/cm^2 was then scaled to Mg/ha.

6.2.3.2 Rock-Eval 6 pyrolysis

Rock–Eval 6 pyrolysis, is a well-established screening tool in petroleum geochemistry (Behar *et al.*, 2001). It has increasingly been used to track bulk changes in organic matter composition and the degree of decomposition

(Newell *et al.,* 2016; Disnar *et al*, 2003), most recently in tropical peatlands (Girkin *et al.,* 2019; Cooper *et al.,* 2019; Upton *et al.,* 2018).

The peat core sub-samples and leaf litter collected were analysed using Rock-Eval 6 pyrolysis. Samples for analyses were selected before and after obvious changes in texture and/or colour in the peat profile stratigraphy. Freeze-dried powdered peat and litter samples (~60 mg) were heated at 200 °C for three minutes before an increase in temperature to 650 °C at a rate of 25 °C per minute in an inert N_2 atmosphere. Residual carbon was subsequently oxidized from 300 °C to 850 °C at a rate of 20 °C per minute. The amount of hydrocarbons released during the two-stage pyrolysis process was detected using a flame ionisation detector, CO and CO_2 were measured using infrared detectors during the thermal cracking of the organic matter. Rock-Eval analysis generated a range of standard parameters, for this research we assessed the organic geochemistry of the peat cores using the following parameters:

- **S1** - a measure of free hydrocarbons released on heating to 200 °C
- **S2**- hydrocarbons released on the thermal cracking of organic matter for temperatures up to 650 °C
- **TOC** (wt %) - calculated from the sum of the carbon moieties (HC, CO, and CO_2)
- **TpkS2** - the temperature associated with the highest yield of bound hydrocarbons
- **S3 CO** and **S3 CO_2** - the CO and CO_2 yielded from the breakdown of kerogen

- **Tmax** (°C) – corresponds to the temperature when the maximum amount of hydrocarbons were released during pyrolysis
- **HI** (mg HC g^{-1} TOC) – the amount of bound hydrocarbons released relative to the TOC
- **OI** (mg O2 g^{-1} TOC) - corresponds to the quantity of oxygen released as CO and CO_2 relative to TOC

The intrinsic organic matter (OM) stability of each peat sample was analysed through the calculation of the refractory OM index (R-index) and immature OM index (I-index) proposed by Sebag *et al.*, (2016). These indices are calculated from the deconvolution of S2 pyrograms using the temperature nodes at 200-340°C (A1), 340-400°C (A2) and 400-460°C (A3) and >460°C (A4). Nodes A1 and A2 are taken to broadly correspond to labile fresh plant mater and lignin and cellulose respectively. The more thermally stable A3 and A4 nodes correspond to highly humified macromolecule and mature recalcitrant soil organic matter, or charcoal respectively (Newell *et al.*, 2016; Saenger *et al.*, 2013).

The R-index is calculated using the higher temperature areas representing more thermally refractory OM compounds:

$$\text{R-index} = (A3+A4/100)$$

The I-index is calculated using the lower temperature areas representing thermally more labile OM compounds:

$$\text{I-index} = \text{Log}_{10}((A1+A2)/A3)$$

6.2.4 Remote sensing data

A satellite time-series, captured by Landsat Thematic Mapper (TM) and Operational Land Imager (OLI), was utilised in this research to investigate forest condition and disturbance in NSPSF over the time period 1989 - 2019. Data selection for this time period (dry season) sought to find data scenes with a relatively cloud free view across the entire study area. Landsat data was acquired for the years 1989, 1995, 2001, 2010 and 2019.

For each Landsat scene, Surface Reflectance (SR) of six spectral bands (blue, green, red, near infrared (NIR) and 2x shortwave infrared (SWIR-1 and SWIR-2)) were downloaded at a spatial resolution of 30 m. The SR products were provided by USGS Earth Resources Observation and Science (EROS) Center Science Processing Architecture (ESPA) (https://espa.cr.usgs.gov); Landsat 5 data was generated by the Landsat Ecosystem Disturbance Adaptive Processing System (LEDAPS) (Masek *et al.*, 2006) and Landsat 8 data was generated by the Landsat Surface Reflectance Code (LaSRC) (Vermote *et al.*, 2016).

The Normalised Burn Ratio (NBR) was calculated for each of the Landsat scenes from the normalised reflectance of NIR and SWIR bands: NBR = (NIR – SWIR-2)/(NIR+SWIR-2). NBR spectral index ranges between 1 and − 1, with low values indicating low or no vegetation present and high values representative of dense healthy vegetation. In the past NBR has been successfully used to measure burn severity of fires (French *et al.*, 2008), detect and classify forest disturbances (Wulder *et al.*, 2009), and assess forest attributes (Frazier *et al.*, 2014; Pflugmacher *et al.*, 2012). Fornacca *et al.*, (2018) and Hislop *et al.*, (2018) found indices that included combinations of

NIR and SWIR Landsat bands where more sensitive to forest moisture and structure for detecting burn area, disturbance and recovery compared with indices that did not. The NBR results for each year were stacked and simple descriptive statistics calculated for the time-series. A raster layer of average NBR was calculated from the NBR time-series stack to guage a recent (relative to the peat profile) view of vegetation cover and condition in NSPSF. The standard deviation (sd) for the pixels in the NBR time-series stack was calculated; the data was proven to have a normal distribution (Shapiro–Wilk test) therefore the resulting standard deviation raster layer can be used as a measure of pixel variability over time. Low variability is expected in areas with low disturbance (natural and anthropogenic). Conversely high variability is expected in areas routinely impacted by repeated disturbance such as: large-scale fire events, repeated drainage, and forest encroachment. All processing was generated in R software (version 3.5.2) using the 'Raster' package (Hijmans, 2018).

6.2.5 Additional geo-spatial data

In addition, the proximity to the river (Sungai Tengi) running though the reserve and the proximity to drainage canals (Figure 6-1) were assessed to help determine the impact of human management and the hydrology on the peat soil profiles. Shapefiles for the river and canal network were provided by the GEC IMP report (Parish *et al.,* 2014). Distance measurements (m) were calculated in ArcGIS 10.2.2. Estimates for carbon stored in the AGB (Mg/ha) for NSPSF was calculated by applying a carbon content conversion factor of 0.47 (Martin and Thomas, 2011) to the AGB estimates generated in the research presented in **Chapter 5**. To reduce positional error from the field

GPS a 3x3 pixel window was applied to the peat core locations (centre point of window) on the AGB carbon raster output, an average value of the 9 pixels was calculated to produce AGB carbon estimates for the peat cores (García-Martín *et al.*, 2012).

6.2.6 Data analysis

All statistical analysis was conducted in R software (version 3.5.2). A variety of non-parametric statistical tests were employed in this research. Spearman's rank correlation coefficient was employed to test for correlation between Rock-Eval parameters and indices with remote sensing and GIS derived products. Wilcoxon test was used to determine if there were statistically significant differences between the carbon stocks (Mg/ha) held in the above ground vegetation and the peat soil. The Kruskal-Wallis test and Pairwise Wilcoxon test (with Bonferroni adjustment to correct for familywise error in the Kruskal-Wallis test) were used to determine if there were statistically significant differences between Rock-Eval parameters and indices between forest condition classes and peat depth layers (surface peat layer, peat just below the water table, and the deepest peat layers within each core which was above the underlying clay layer). The relationships between Rock-Eval parameters (HI and OI) and indices (R-index and I-index) were plotted for visually assessment of degradation patterns linked to these parameters.

6.3 Results

6.3.1 Carbon stock

Carbon stocks were found to be significantly different between above ground vegetation and peat soil (W= 121, d.f. = 1, p-value = <0.001), with 12.2 times more carbon stock held in peat than found in the vegetation (Figure 6-2, Table 6-2). The peat carbon stock did not differ significantly between the four different forest condition classes. Peat carbon stocks are linked to peat depth, which ranged from 0.5 – 3.5 m in the peat cores sampled. The lack of a significant difference in peat carbon stock between forest condition classes can be attributed to similarities in depth.

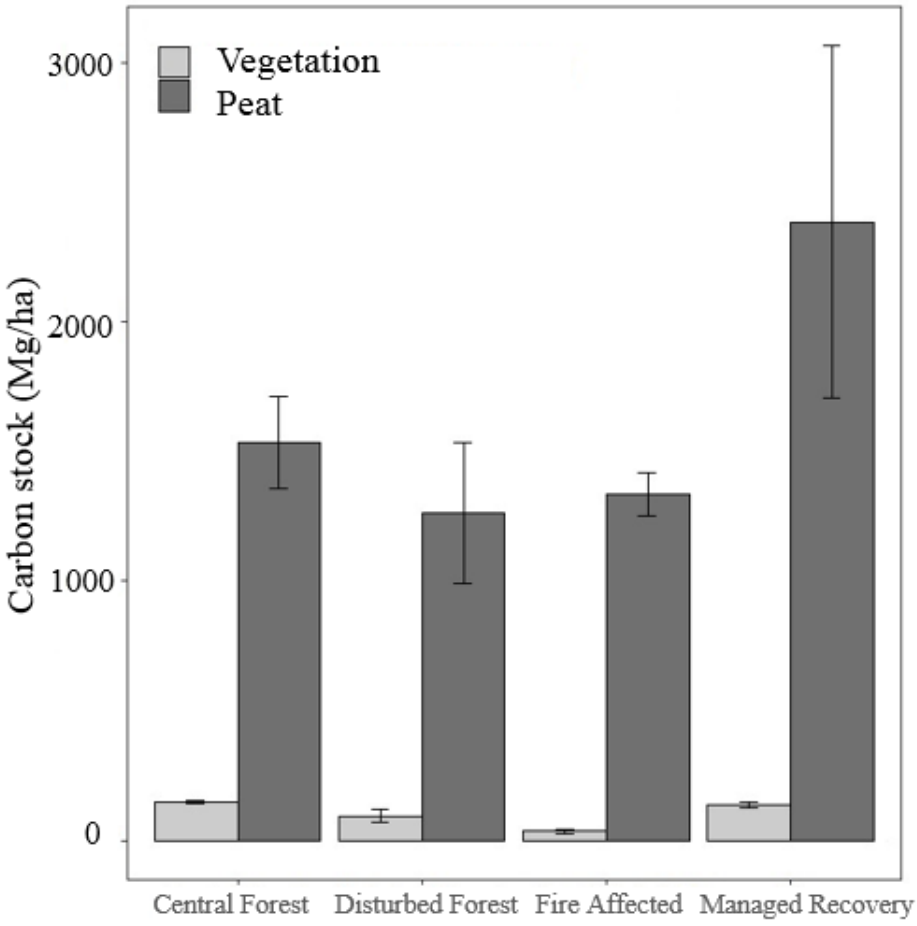


Figure 6-2 Carbon storage in the vegetation and peat soil for each of the four forest condition classes, mean and SEM shown.

Table 6-2 Median carbon stock (Mg/ha)
and interquartile range (IQR) for above ground vegetation and peat soil.

	N	Median	IQR
Vegetation	11	114.70	70.48
Peat	11	1401.51	336.76

6.3.2 Remote Sensing and GIS

The Landsat derived raster layers of average NBR and the standard deviation (sd) for the pixels in the NBR time-series stack (representative of the years 1989, 1995, 2001, 2010 and 2019) can be seen in Figure 6-3. Figure 6-3a. provides a recent (relative to the peat profile) view of vegetation cover and condition in NSPSF. Figure 6-3b. represents a measure of pixel variability over time, this marking change in both peat swamp forest disturbance and recovery.

Peat carbon stock and the parameters generated from Rock-Eval analyses representative of the total peat profile were found to have no significant correlation with remote sensing and GIS derived products. However, in the top 50 cm section of the peat profile, carbon stocks were found to have a significant negative correlation with NBR sd (Spearman's rho = -0.664, S = 366, p-value = <0.05) (Figure 6-4a). HI (the amount of hydrogen relative to the amount of organic carbon) and NBR mean were also found to have a significant positive correlation in the top 50 cm section of the peat profile (Spearman's rho = 0.7, S = 66, p-value = <0.05) (Figure 6-4c).

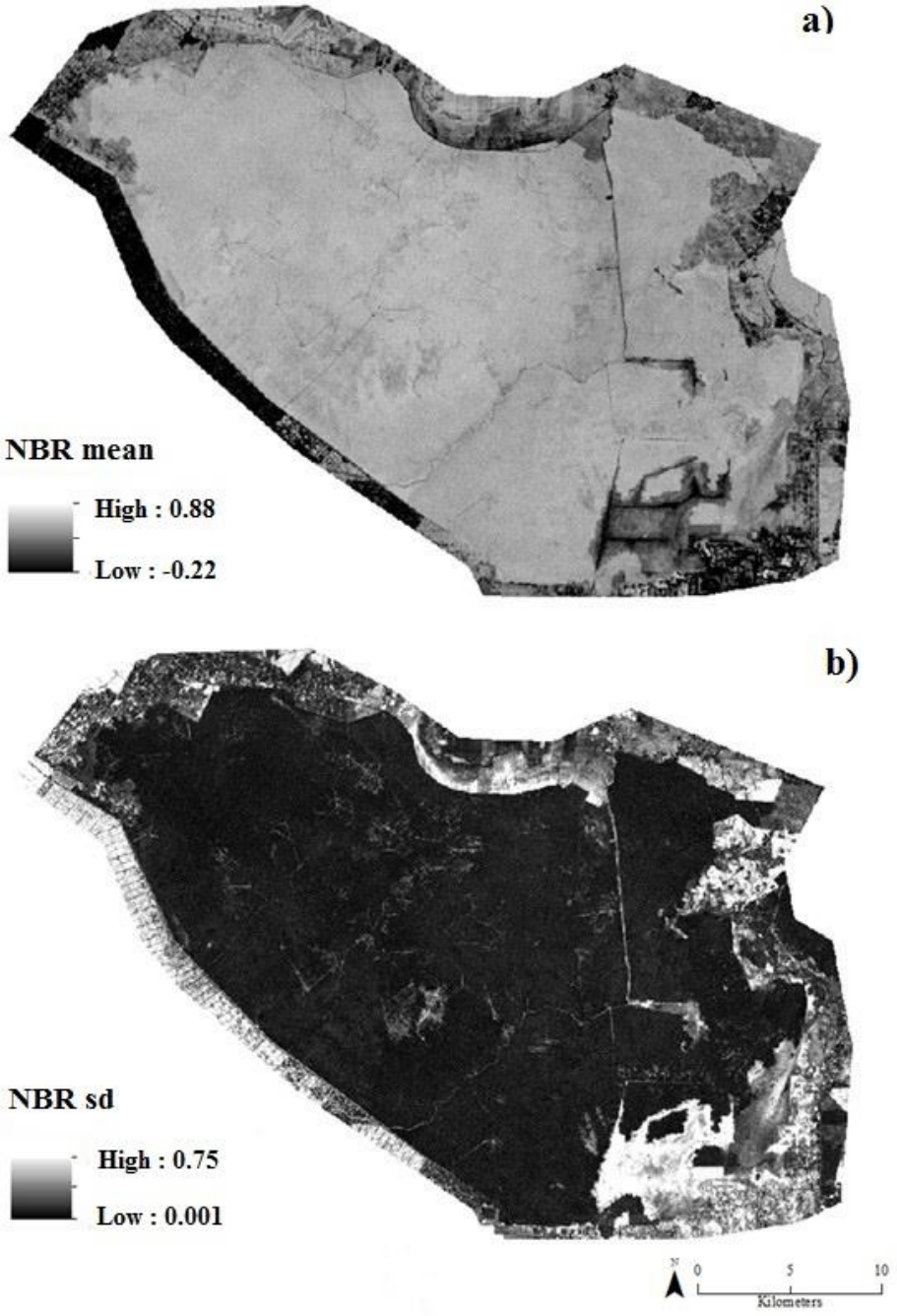


Figure 6-3 Remote sensing derived products: (a) Normalised Burn Ratio (NBR) mean; (b) Normalised Burn Ratio (NBR) standard deviation (sd).

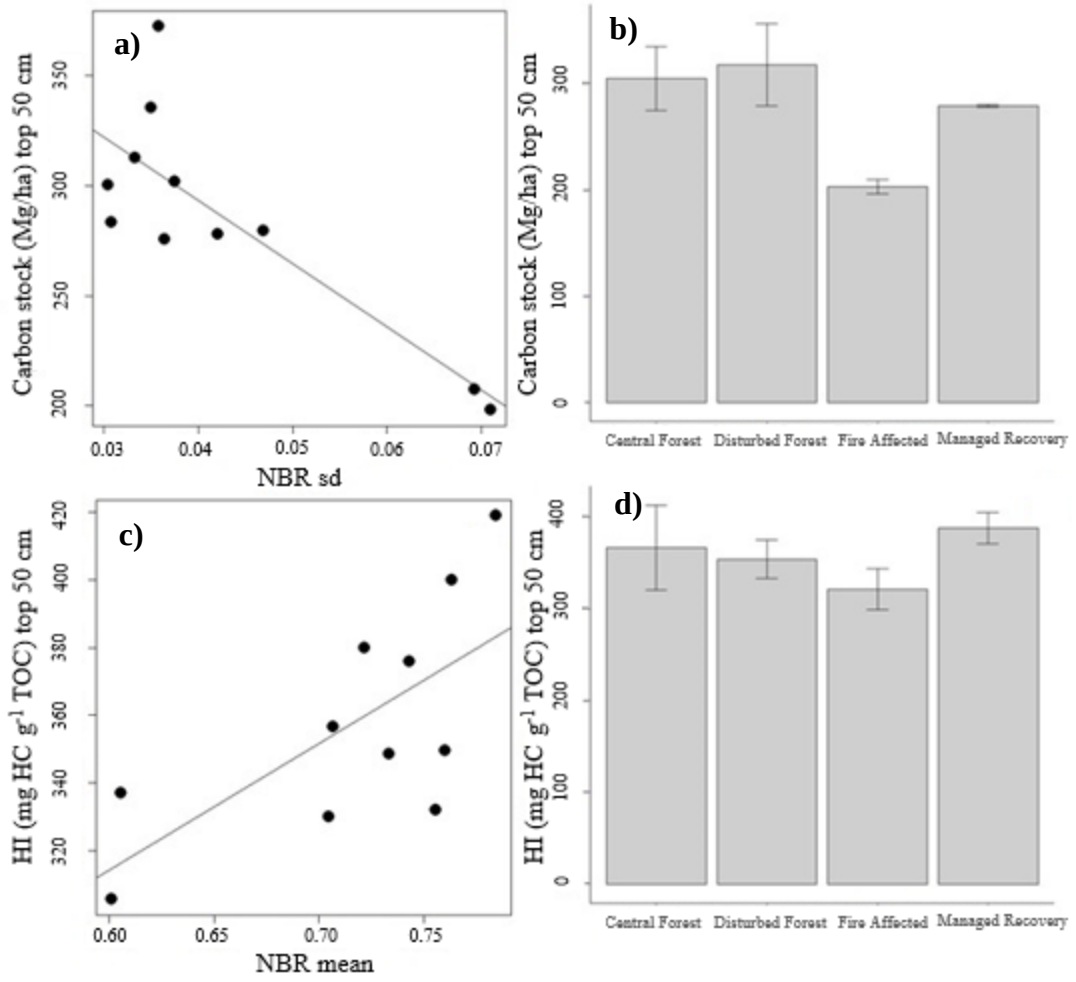


Figure 6-4 Significant relationships between remote sensing derived products and Rock-Eval analysis parameters: (a) correlation with Normalised Burn Ration Standard deviation (sd) and Carbon Stock held in the top 50 cm; (b) Carbon stock held in top 50 cm mean values and SEM for the four forest condition classes; (c) correlation with Normalised Burn Ration mean and HI for the top 50 cm; (d) HI for the top 50 cm mean values and SEM for the four forest condition classes.

6.3.3 Rock-Eval indices and parameters

Trends in peat decomposition can be followed on an I-index vs R-index diagram (I/R diagram). Peat core sub-samples and litter collected from Central Forest locations (Figure 6-5a) illustrate the expected (natural) decomposition trend found in a stable, relatively undisturbed tropical peat ecosystem. The I/R diagram presents a general decrease in the proportions of immature labile

carbons (average I-index range 0.18 to 0.8) and an increase in the proportion of refractory carbon (average R-index range 0.51 to 0.57) with depth, this trend is comparable with Rock-Eval analysis of peats from pristine wetlands of Bocas del Toro, Panama (Supplementary material). There is some overlap in the below water table and deeper peat layers with intervals both above and below the general downward trend. It should be noted that these peat cores do not cover the deepest layers of peat found in NSPSF (2-3 m depth) therefore samples labelled as below the water table and at deeper layers are relatively close together within these peat profiles.

Peat core sub-samples and litter collected from Fire Affected, Disturbed Forest, and Managed Recovery locations (i.e. disturbed sites) (Figure 6-6a) do not follow the same decomposition trend found in the Central Forest sites. The upper peat layer sections on average produce lower I-index values (average I-index range in upper section 0.15 to -0.06) and higher R -index (average R-index range in upper section 0.51 to 0.65) than the deeper sections of the peat profile (i.e more thermally stable).

Based on the Rock-Eval I- and R- indices the effects of peat core location and disturbance were assessed between the different depth layers in the peat profiles. For the upper 50cm section of the peat profile, R-index and I-index values were found to be significantly different between locations (R-index: Kruskal-Wallis chi-squared =11.196, d.f. = 3 , p-value = <0.05; I-index: Kruskal-Wallis chi-squared =10.693, d.f. = 3 , p-value = <0.05)(Table 6-3).

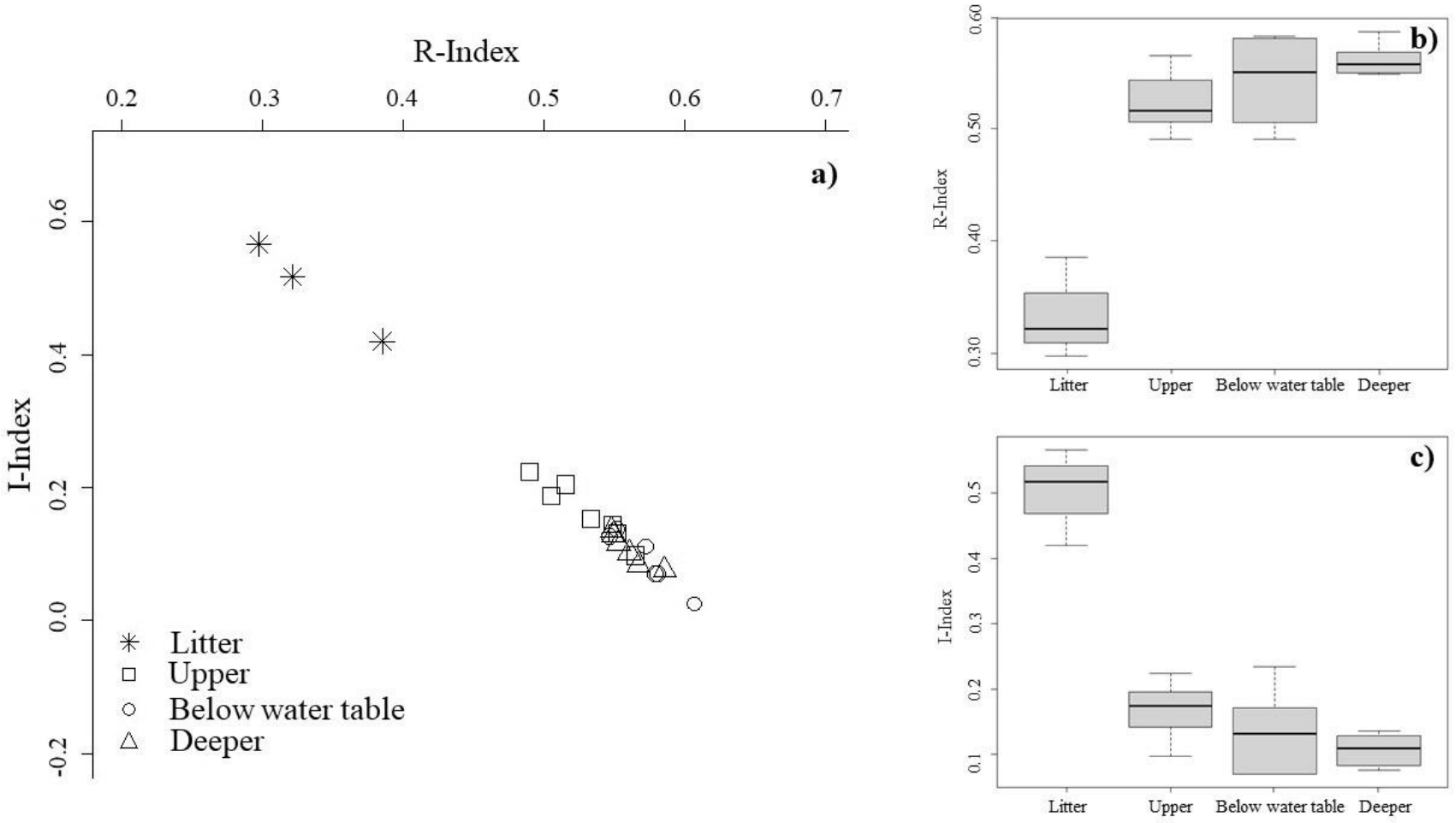


Figure 6-5 Rock-Eval indices for Central Forest sites: a) I/R diagram; b) boxplots of R-index values for peat profile layers; c) boxplots of I-index values for peat profile layers.

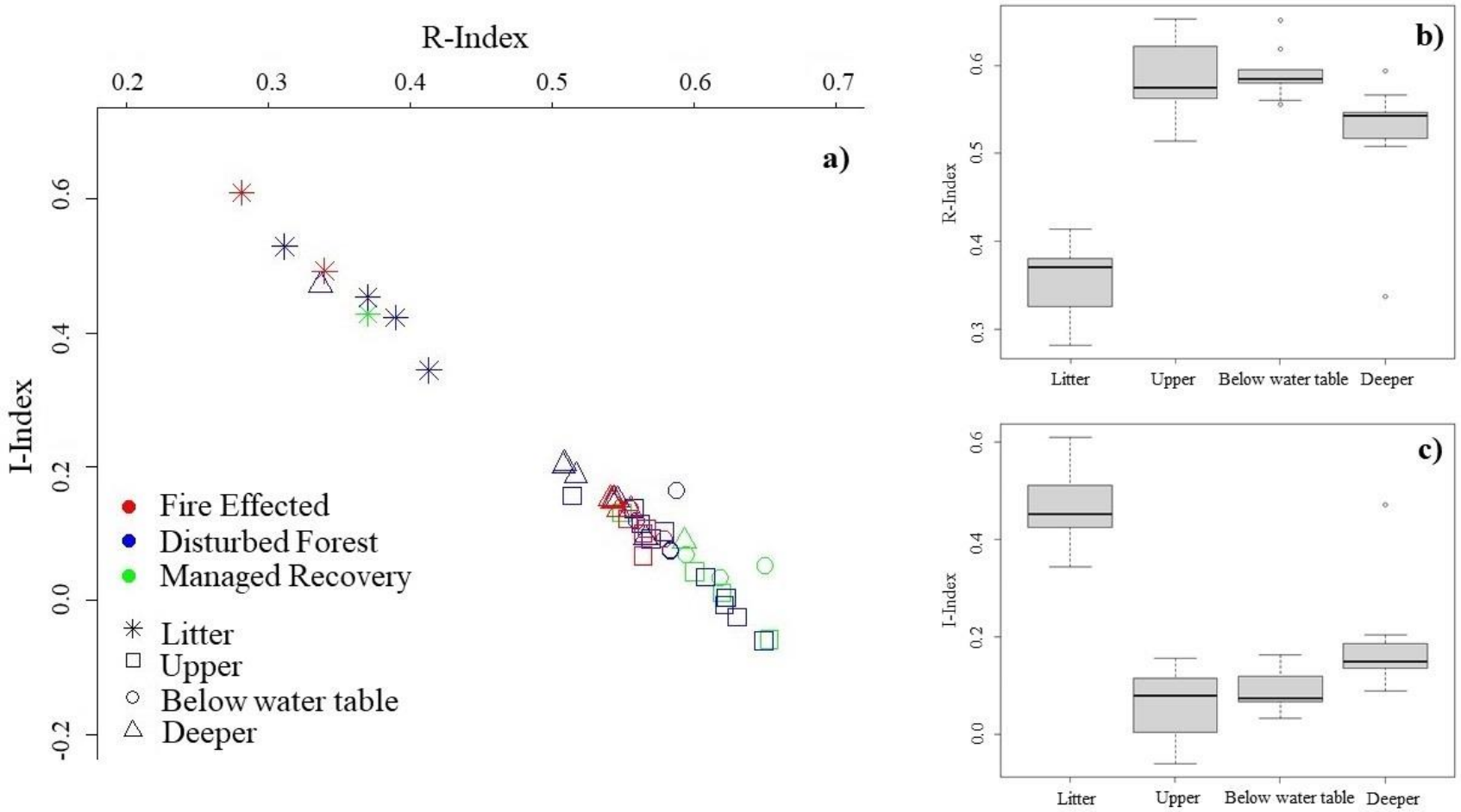


Figure 6-6 Rock-Eval indices for disturbed sites: a) I/R diagram; b) boxplots of R-index values for peat profile layers; c) boxplots of I-index values for peat profile layers.

A significant difference in R-index and I-index values were found between Central Forest locations and disturbed sites (R-index: W=11 , d.f. = 1 , p-value = <0.001; I-index: W=115 , d.f. = 1, p-value = <0.001)(Table 6-4).

Table 6- 3 R- and I- index median and interquartile range (IQR) for upper 50 cm section in the peat profile for the four forest condition classes. Significant pairwise Wilcoxon tests with Bonferroni adjustments share the same subscript letter.

Forest Condition Class	**N**	**R-index**		**I-index**	
		median	**IQR**	**median**	**IQR**
Central Forest	3	0.52[a]	0.04	0.17[b]	0.05
Disturbed Forest	4	0.59[a]	0.06	0.06[b]	0.12
Fire Affected	2	0.56	0.01	0.10	0.02
Managed Recovery	2	0.61	0.04	0.03	0.07

Table 6-4 R- and I- index median and interquartile range (IQR) for upper 50 cm section in the peat profile for Central Forest and disturbed sites.

	N	**R-index**		**I-index**	
		median	**IQR**	**median**	**IQR**
Central Forest	3	0.52	0.04	0.17	0.05
disturbed	8	0.57	0.06	0.08	0.11

For the combined below water table and deeper sections of the peat profile, R-index and I-index values were found to be significantly different between locations (R-index: Kruskal-Wallis chi-squared = 12.79, d.f. = 3 , p-value = <0.001; I-index: Kruskal-Wallis chi-squared =13.907, d.f. = 3 , p-value =<0.001)(Table 6-5). No significant difference in R-index and I-index values were found between Central Forest locations and disturbed sites.

Table 6-5 R- and I- index median and interquartile range (IQR) for combined below water table and deeper layers for the four forest condition classes. Significant pairwise Wilcoxon tests with Bonferroni adjustments share the same subscript letter.

Forest Condition Class	N	R-index		I-index	
		median	IQR	median	IQR
Central Forest	3	0.56[a]	0.03	0.11[d]	0.05
Disturbed Forest	4	0.55[b]	0.06	0.15[e]	0.09
Fire Affected	2	0.55[c]	0.01	0.14[df]	0.02
Managed Recovery	2	0.61[abc]	0.03	0.06[ef]	0.03

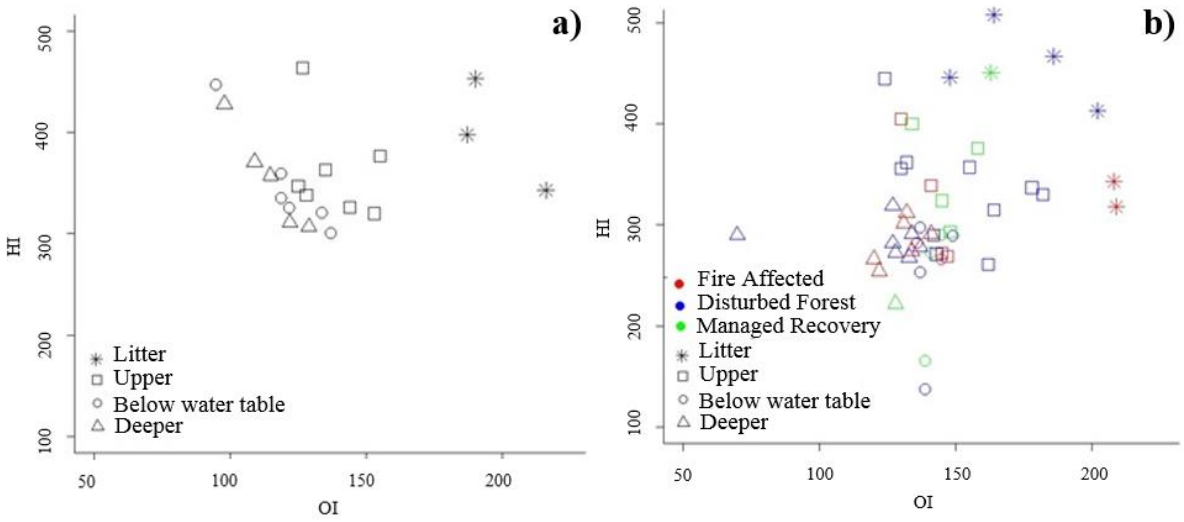


Figure 6-7 Van Krevelen pseudo diagrams. (a) Central Forest; (b) disturbed sites.

A HI vs OI diagram (Van Krevelen pseudo diagram) plotted for Central Forest sites showed HI values remained high through the peat profile (300 - 475 mg HC g^{-1}TOC), with OI values continuously decreasing from the leaf litter down the peat profile to the deeper peat layers (Figure 6-7a). The high HI values throughout the whole peat profile (≥300 HC g^{-1}TOC) indicating a high concentration of plant tissue and other material rich in polysaccharides with a high degree of hydrogenation and mineral transformation. For the disturbed

sites (Figure 6-7b), OI and HI decreased with depth from leaf litter down the peat profile to the deeper peat layers. This reflects the degradation of plant material and an increased humification of SOM, including greater aromaticity and dehydrogenation of organic compounds (loss of H).

6.4 Discussion

6.4.1 Carbon stocks

Tropical peat swamp forests combine the carbon storage potential in tropical forests with high biomass productivity and the capacity to create and store long-term carbon deposits in the underlying peat soil. However, there is a substantial difference between the magnitude of carbon stocks held by the vegetation and peat soil. Peat soil carbon stocks dwarf the carbon stored in the above ground vegetation in NSPSF (Table 6-2), which is an important feature in active, accumulative tropical peatlands (Dargie *et al.,* 2017; Kauffman *et al.,* 2016; Page *et al.,* 2011). This may seem an obvious result, however, it is important to quantify and report the carbon difference between above ground vegetation and peat soil as the majority of large-scale landscape monitoring activates in tropical peat swamp forests concentrate on above ground forest dynamics.

In this research, the sites holding the highest carbon stock in the peat soil were found to also have the highest AGB (Managed Recovery and Central Forest sites). A healthy, productive AGB layer protects and promotes the underlying peat soil, creating a continuous supply of litter and organic material deposits to incorporate into the waterlogged peat over prolonged periods (Yule *et al.,* 2009). Previous ecological studies have explored the positive

relationship between vegetation cover and peat soil; AGB, species richness and plant functional type have been found to relate to the degree of water-logging and peat mineralization (Jonsson and Wardle, 2009; Dorrepaal *et al.*, 2005). To secure a productive and functional peatland ecosystem, there is an urgent need to conserve and protect both the above ground and below ground carbon stores. Conservation and regeneration programs should aim to tackle both in order to promote ecosystem health and climate change mitigation.

6.4.2 Application of remote sensing in tropical peat soil degradation

Traditional field based measurement techniques are often limited in large-scale tropical peatlands in terms of cost, spatial coverage and accessibility to remote locations (Lawson *et al.*, 2015). Within a peatland environment, peat soil depth and properties can vary widely with location, and in particular for tropical peat swamps with a peat dome morphology (Kool *et al.*, 2006). Small spatial scale sampling programmes do not allow for easy upscaling due to the difficulty of averaging or interpolating results across such a varied landscape. Remote sensing and GIS present an opportunity to provide data over larger areas quickly and at low cost.

In this research, no significant correlation was found between remote sensing and GIS derived products with peat carbon stock and Rock-Eval parameters representative of the total peat profile. The spectral data and analysis methods adopted in this research (Figure 6-4) were ultimately limited by optical remote sensing data's inability to penetrate and record past the ground surface (Tokola, 2015). As has been previously discussed, a relationship exists between vegetation cover and the underlying peat soil (Page *et al.*, 1999),

however, it is not representative of the entire peat profile and cannot demonstrate destabilization of peat throughout the peat profile.

Importantly, a significant correlation was found between remote sensing derived data (NBR sd and carbon stock; NBR mean and HI (Figure 6-4)) in the top 50 cm section of the peat profile, suggesting that remote sensing products can predict carbon stocks and peat degradation parameters in the surface layers of tropical peat. The surface (0-30 cm) and sub-surface (30 cm-water table) layers represent a dynamic environment in the peat profile linked to fluctuations in the water table. These layers are the interface of a number of active chemical and biological processes in tropical peat (Mishra *et al.,* 2014; Lampela *et al.,* 2014). These processes are influenced by changes in the water table position (both seasonal and as a consequence of disturbance), which then determines the potential depth of oxygen availability in peat. In oxygen rich conditions, decomposition is enhanced and thus nutrient availability due to mineralization increases. Surface and subsurface peat has been recognized as significant contributors to greenhouse gas production in tropical peatlands (Hoyos-Santillan *et al.,* 2016; Wright *et al.,* 2011); land-use change induced deforestation, drainage and fire are all linked to accelerating degradation and the release of greenhouse gases (Cooper *et al.,* 2019; Couwenber *et al.,* 2010; Rein *et al.,* 2008). These land-use changes and disturbances can be mapped and monitored by remote sensing data (Saputra *et al.,* 2017; Konecny *et al.,* 2016; Miettinen *et al.,* 2016; Hoscilo *et al.,* 2011).

In view of the strengths and limitations of remote sensing, I suggest the application of remote sensing coupled with systematic field and laboratory measurements for the assessment of tropical peat soil carbon stock and

degradation. This complementary, targeted approach has the potential to provide detailed field-based information of peat profiles in key locations, while at the same time allowing for spatially explicit assessments of peat degradation patterns and its severity over time.

6.4.3 Tropical peat decomposition trends

Based on the I/R diagrams (Figure 6-5 and Figure 6-6), the dynamics of SOM can be assessed within the different peat profile depth layers (top 50 cm section, water table, and deeper) and leaf litter, or by comparing the peat profiles from the various forest condition classes and disturbance (i.e. Central Forest compared to disturbed sites). The R- and I-index have proven to be powerful indictors in the assessment of the thermal stability of SOM (Schomburg *et al.*, 2018; Sebag *et al.*, 2016). Peat profiles collected in Central Forest sites follow a general negative linear relationship between I- and R-index with depth. This reflects the relationship between decay processes and SOM stabilization, however disturbed sites (Fire Affected, Disturbed Forest, Managed Recovery) do not follow this uniform pattern. This difference in the I/R diagrams is most apparent in the top 50 cm section of the peat profiles. For disturbed sites, samples taken from the top 50 cm section of the profile have a high R-index (0.514 to 0.653) and low I-index (0.156 to -0.061) and typically mark the tail-end values on the I/R diagram, indicating that the peat surface and subsurface layers have experienced a rapid depletion of the most thermally labile compounds in this layer, leaving thermally stable compounds behind (Sebag *et al.*, 2016). Whereas the Central Forest sites have a relatively lower R-index (0.490 to 0.565) and higher I-index (0.235 to -0.097) vales, reflective of an environment characterised by a continuous supply of fresh

labile substrates (Jauhianen *et al.*, 2012) in anaerobic conditions. The relationship found between disturbed sites and greater thermal stability in the top 50 cm section has previously been explored by Cooper *et al.,* (2019) with forest conversion to mature oil palm.

In the deeper peat layers, Central Forest and disturbed sites generally hold similar positions in the I/R diagrams, suggesting that the deeper underlying peat in NSPSF has the same composition across all forest condition classes. In the disturbed sites (Figure 6-6), a number of deeper samples are plotted with very low R-index and high I-index values relative to their position in the peat profile, this is thought to be the result of marine clay banding in the peat samples. Clay particles have been reported to create organo-mineral complexes which protect the organic matter from microbial decomposition (Six *et al.,* 2002), hence the preservation of organic material in deeper layers.

6.4.4 Limitations of peat sampling strategy

Peat core depth in this research ranged from 0.5 – 3.5 m. These depths are below the average recorded peat depth of 3.6 m across the reserve (Parish *et al.,* 2014), this could be the impact of peat coring activities being restricted to forest edge (range of 0.5-1 km in) and river edge locations, or the result of different peat depth measurement techniques in past research. The assessment of the thermal stability of SOM in deep peat layers is restricted in this research by the relatively limited deep peat representation in the samples. Future research should aim to sample a wider range of peat depths, with particular focus on the deepest peat in NSPSF which has been previously recorded at 10.15 m in Sungai Karang Forest Reserve. Additionally, this research recognises that a larger sample size is advisable in future work, however this

sample size is consistent with past organic geochemistry research in tropical peatlands (Girkin *et al.,* 2019; Upton *et al.,* 2018). Future sampling design should incorporate knowledge from this research, in particular the use of spectral indices time-stack data, to guide and prioritise areas for sampling with the goal to capture a larger sample number, increased spatial coverage, and a wider range of sites that have experienced degradation and/or regeneration.

6.5 Conclusion

Active and targeted tropical peat swamp forest management is essential in order to restore the carbon sink function of degraded tropical peatlands. Restoration efforts should aim to both reduce the carbon losses from the peat and increase carbon sequestration potential in the AGB (Lawson *et al.*, 2015). Remote sensing derived products have proven to be a useful tool in ecosystem restoration programmes (Suding *et al.,* 2015; Aronson and Alexanger, 2013; Young *et al.*, 2005), however field based sampling and geochemical analyses remains an integral part in tropical peatland assessment.

The research found the following conclusions:

1. Based on the data, below ground peat soil held more carbon compared to the vegetation for the four forest condition classes.
2. Remote sensing derived products cannot predict peat soil carbon stocks and peat properties associated with degradation for the entire peat profile. However, remote sensing derived products do have a relationship with carbon stock and HI for the top 50 cm section of the peat profile demonstrating that remote sensing can be used to identify areas of potentially high carbon stock in the

surface peat layers to be targeted for conservation and areas of degradation that should be the focus for restoration activities.

3. The impact of disturbance can be detected in the top 50 cm section of the peat profile with Rock-Eval parameters and indices. At greater depths no clear marker of disturbance was identified clearly indicating the critical role of water table management in avoiding further peat degradation.

Landscape-scale assessments and mapping of tropical peat swamp forest degradation and peat soil health are critically needed to better understand the impacts of drainage, vegetation clearance and intense fire events on ecosystem function. This information is vital in guiding management strategies and restoration interventions.

6.6 Supplementary material

NSPSF has experienced multiple forms of anthropogenic disturbance, in order to better understand the decomposition trends afforded by Rock-Eval 6 pyrolysis a peat core sampled from a pristine peatland in Bocas del Toro, Panama (source data from Upton *et al.*, 2018) was processed as a control dataset. The same methodology as outlined in this chapter was applied to the Panama peat core in order to show the expected (natural) decomposition trend (Figure 6-8). Important to not here that the above ground vegetation was a mangrove forest not a tropical peat swamp forest. Inspection of the I/R diagram clearly shows a systematic decrease in the proportions of immature labile carbons (I-index 0.48 to 0.22) and increase in the proportion of refractory carbon (R-index 0.34 to 0.54) with depth. Although there is some overlap of the middle section of the core (92-320 cm).

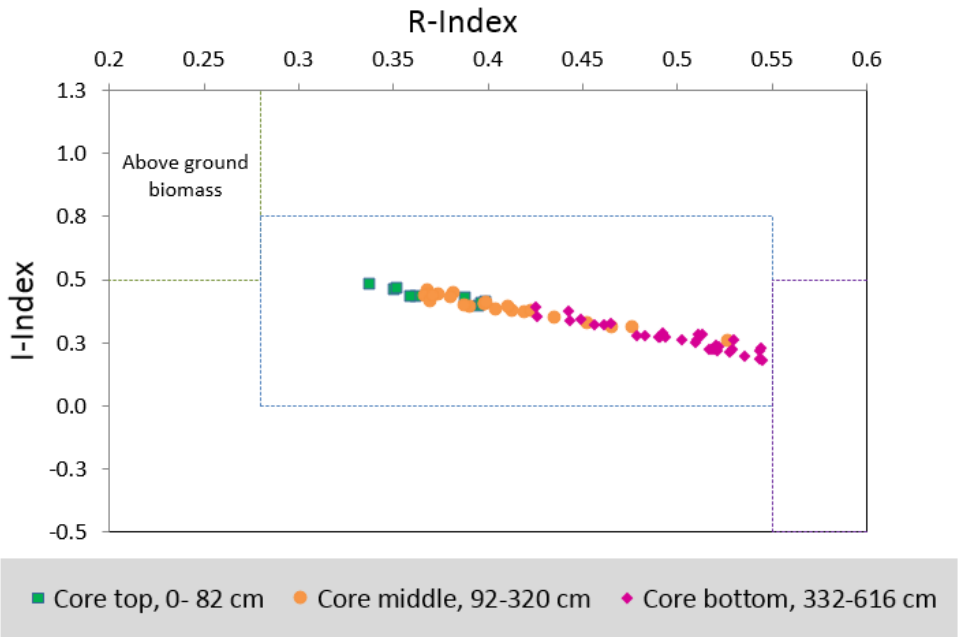


Figure 6-8 I/R diagram for mangrove peat core from Bocas Del Toro Panama (source data from (Upton *et al.*, 2018)).

Chapter 7: Synthesis

This thesis presents innovative research in the application of remote sensing for supporting the sustainable management and recovery of tropical peat swamp forests in South-East Asia. Past experience of degradation and the dynamic nature of tropical peat swamp forests under active recovery, made NSPSF the ideal study site to investigate cutting-edge remote sensing approaches and landscape-scale assessment, building on the growing body of work focused on tropical peat ecosystem function and their response to degradation and rehabilitation. As well as advancing the field of tropical peatland assessment, the methods and results reported in this thesis present the opportunity to support and guide on-going peatland restoration activities in NSPSF, encouraging the continued drive to restore and safeguard this important carbon-rich environment.

This chapter summarises the research undertaken in this thesis (**Chapters 4, 5 and 6**), and address the research objectives met. The impact of this thesis research is discussed in view of the methodological contributions and the environmental management and policy contributions. Limitations of the research, a future outlook and recommendation for future tropical peat swamp forest mapping and monitoring is also presented.

7.1 Research chapter summary

The methods and product development presented in the research chapters (**Chapters 4, 5 and 6**) were designed around meeting the four research objectives:

1. To investigate the optimal use of occupied airborne Light Detection and Ranging (lidar) technology to quantify tropical peat swamp forest AGB.
2. To quantify the AGB stored in NSPSF using space-borne optical data.
3. To assess the effectiveness of tropical peat restoration activities on AGB dynamics over a focused period of rehabilitation interventions (2015 - 2018) in NSPSF.
4. To examine the impact of tropical peatland degradation in NSPSF on the underlying peat soil deposits.

Chapter 4 examined the relationship between tropical peat swamp forest AGB and small-footprint airborne lidar DR and FW derived metrics, with a view to establishing the optimal use of this technology in this environment, which has different characteristics to other environments readily studied using lidar data (e.g., temperate/boreal forests). Plot-based multiple regression analysis was performed to establish the strongest predictive models of peat swamp forest AGB using DR metrics (only), FW metrics (only), and a combination of both DR and FW metrics. Overall, the results demonstrated that a combination-model, coupling the benefits derived from both DR and

FW metrics, had the best performance in modelling AGB for tropical peat swamp forest (R^2 = 0.77, RMSE = 36.4, rRMSE = 10.8%), meeting **research objective 1**. However, no statistical difference was found between the rRMSE of the combination-model and the best models using only one lidar system. The research concluded that the optimal approach for using airborne lidar in the estimation of peat swamp forest AGB was more dependent on the inclusion of lidar metrics that describe the mid-canopy structures than the type of lidar system.

Chapter 5 demonstrated the use of Sentinel-2 MSI satellite data in delivering accurate, high resolution AGB maps of NSPSF for the years 2015 and 2018. This research adopted the site specific AGB model built in **Chapter 4** as model training and testing data using a Random Forest machine learning approach. The results demonstrated that a Random Forest algorithm is a useful and robust method for estimating AGB with Sentinel-2 derived spectral and textural predictor variables; 2015 (R^2 = 0.80, RMSE = 55.2, rRMSE = 24.6%) and 2018 (R^2 = 0.92, RMSE = 23.4, rRMSE =8.73%). The wall-to-wall AGB maps generated were used to **meet research objective 2**. For the entire NSPSF reserve total AGB was estimated at 19.3 Tg for 2015 and 19.8 Tg for 2018. To meet **research objective 3**, an AGB change analysis map was generated from the 2015 and 2018 AGB maps. The change analysis map afforded the characterisation of AGB gain and loss across the entire NSPSF reserve at level of detail never previously seen. Reference datasets and expert knowledge of the site complied in this research revealed a number of key areas of change in NSPSF. Areas of AGB gain were found to be focused on central areas of the reserve were natural regeneration has been encouraged through

forest protection and drain blocking activities. Further AGB loss was found to be attributed to frequent fire events hampering recovery efforts or the negative impacts of poorly designed water management. The research concluded by recommending the continued tracking of AGB across NSPSF in order to build an archive of data which is representative of this on-going active period of conservation and regeneration. This data is key to increasing our understanding of the complex processes of a recovering peatland ecosystem and aid in the development of best practice for tropical peat management.

Chapter 6 investigated the use of remote sensing and organic geochemistry methods for assessing the impact of tropical peat swamp forest degradation on the underlying peat soil profile to meet **research objective 4**. The research demonstrated the utility of stacked Landsat archive data for landscape scale assessment of degradation in NSPSF over a 30 year time period (1989 - 2019). The Landsat time-series stack provided representation of the above ground dynamics of the reserve over an active period of change from pre- permanent reserve status in 1990, the halt in logging activates in 2007, up to the present-day phase of active peat swamp forest recovery. Peat cores collected from 4 different forest condition classes (Central Forest, Managed Recovery, Disturbed Forest, and Fire Affected) were processed using Rock-Eval 6 pyrolysis, to quantify the carbon stored in the peat and track soil organic matter thermal stability throughout the peat profiles. The research found carbon stocks to be significantly different between vegetation (derived from AGB values produced in **Chapter 5**) and peat soil ($W= 121$, d.f. = 1, p-value = <0.001), with 12.2 times more carbon stock held in peat than found in the above ground vegetation. Peat profiles collected in Central Forest sites

followed a general negative linear relationship between I- and R- index with depth. This reflects the relationship between decay processes and SOM stabilisation, however the research found that disturbed sites (Fire Affected, Disturbed Forest, and Managed Recovery) did not follow this uniform pattern. This difference in the I/R diagrams between disturbed and undisturbed tropical peat sites was found to be most apparent in the top 50 cm section of the peat profiles, with Central Forest sites reporting a relatively low R-index (0.490 - 0.565) and high I-index (0.235 - 0.097) and disturbed sites having a higher R-index (0.514 - 0.653) and lower I-index (0.156 - 0.061). This indicating that the peat surface and subsurface layers experience a more rapid depletion of the most thermally labile compounds as a result of degradation compared to deeper peat layers. The research concluded that remote sensing derived products cannot predict peat soil carbon stocks and peat properties associated with degradation for the entire peat profile. However, remote sensing derived products do have a relationship with carbon stock (Spearman's rho = -0.66, S = 366, p-value = 0.030) and the Hydrogen Index (Spearman's rho = 0.7, S = 66, p-value = 0.020) for the surface and sub-surface layers in the peat profiles. The research recommended the use of remote sensing as a tool for identify key areas of surface peat degradation, to focus regeneration and restoration activates.

7.2 Contribution of research

The key findings from this thesis will be discussed in terms of the methodological implications for future remote sensing research in tropical peat swamp forests and the implications of this research on sustainable tropical peatland management (local and international scales).

7.2.1 Methodological contribution

Use of DR and FW lidar in tropical peat swamp forest AGB estimation:

To the best of our knowledge, techniques on AGB estimation based on FW airborne lidar metrics, in particular with the fusion of DR airborne lidar data, has not been previously explored in tropical peat swamp forest environments. The research presented in **Chapter 4** contributes to the development of lidar technology in tropical peatlands. Previous research (not from tropical peat swamp forests), have documented the potential added value of FW lidar systems relative to DR systems in forest assessment (Nie *et al.*, 2017; Sumnall *et al.*, 2016; Cao *et al.*, 2014a). Results from past studies modelling AGB across a variety of forest environments (temperate and sub-tropical) have identified height metrics from both DR and FW to be the most important inputs in AGB modelling. The addition of echo-width metrics derived from FW lidar in these studies had variable success. The research in this thesis however, found for tropical peat swamp forests FW echo-width variables, such as HOME, produced some of the strongest positive relationships with AGB plot data. Tropical peat swamp forests do not have a uniform forest structure; in particular for disturbed tropical peatlands, selective logging operations, drainage and fire can severally impact the forest composition. The results from the thesis suggest a combined approach of DR and FW lidar to be the optimal method to estimate AGB in this complex environment. This is a key finding in the development of methods for lidar derived AGB, highlighting that there is not one universal approach (or model) for forest AGB estimation worldwide. Recommendations from the research in **Chapter 4** should be used to guide future lidar applications in tropical peat swamp forest assessment.

Use of remote sensing in peat soil analysis:

To the best of our knowledge, time-series stack remote sensing derived indictors of peatland degradation have not been linked with carbon stock and peat degradation parameters in the surface and sub-surface layers of tropical peat (depth 50 cm). The research in **Chapter 6** contributes to the growing body of work investigating the relationships between above ground cover and dynamics with the underlying peat soil (Rudiyanto *et al.,* 2018; Nguyen *et al.,* 2016; Wedeux and Coomes, 2015). Tropical peat swamp forests, especially those that are degraded, are not static systems. Temporal shifts in vegetation cover and productivity from stochastic disturbance and ecosystem recovery, and the associated impacts on peat soil, need to be understood to fully assess the current state of a tropical peat swamp environments and inform future management strategies. Time-series optical data acquired from the Landsat archive allowed the research in this thesis to represent a 30 year time period of tropical peatland change for NSPSF. The results found the relationship between above ground processes detected by remotely sensed optical data with peat carbon stock and degradation parameters to be restricted to the surface and near-surface layers (to a depth 50 cm); this is a key finding of the research and an important limitation to recognise in the application of optical data in peat soil assessment. As previously mentioned, tropical peat depth has been measured up to 20 m (Anderson, 1983). If this approach is purely restricted to the top 50 cm then a large proportion of carbon and degradation parameters are not being accounted for.

The approach developed in **Chapter 6** provides an initial step in tropical peat soil assessment. Given the importance of carbon stock and emission

accounting to support both national and international climate mitigation agreements this method could provide vital information to guide and inform future tropical peat research. The approach requires further work and testing using larger datasets of peat core samples from other locations. The research concluded by recommending the application of remote sensing optical data coupled with systematic field measurements for the assessment of tropical peat soil carbon stock and degradation. To this end, I propose the adoption of a 'top-down' approach to tropical peatland assessment, using knowledge of the spatial and temporal distribution of above ground change, determined by optical remote sensing time-series data to base field sampling design on. For example, future large-scale peat sampling campaigns in NSPSF could use Figure 6-3 to inform the selection of peat core sample locations to ensure that sample design incorporates the full range of vegetation cover and conditions found in NSPSF (Figure 6-3a), as well as identifying target areas of change in both peat swamp forest disturbance and recovery (Figure 6-3b). By prioritising sampling efforts (peat core removal) in key areas of change and stability, datasets that represent the varied levels of tropical peat degradation can be built to fully assess the impacts of present day actives on ancient peat stores.

7.2.2 Environmental management and policy contribution

International:

AGB is an important input to several environmental management and policy initiatives. Accurate and timely AGB estimates, such as those produced in **Chapter 5**, are vital in achieving international goals and national commitments related to forest conservation and restoration, climate change, and sustainable management. For example, the Paris Agreement on Climate

Change requires accurate reporting on national greenhouse gas emissions. AGB data is required for carbon and greenhouse gas emission accounting and to aid in the reporting and verification of forest restoration related activates. Accurate AGB measurements are also required to support the UN SDG 15. Specifically, indictors 15.2.1 Forest cover under sustainable forest management; 15.2.2 Net permanent forest loss; and 15.3.1 Percentage of land that is degraded over total land. Policy-makers and forest managers require AGB data to track the achievements and shortcoming of these indicates in meeting SDG 15. Data on AGB stock and dynamics are not only required for international information needs, local forest managers need AGB data to support national policy formation and mitigation activities. The AGB mapping approach set out in **Chapter 5** provides an example for the opportunities to track and assess AGB change in response to restoration activities and forest dynamics under varying degrees of degradation and regrowth.

NSPSF:

Knowledge of the health and function of NSPSF is required by local stakeholders to inform and guide resource management. This thesis is part of ongoing research in the tropical peatlands of Selangor, Malaysia as part of the research consortium Tropical Catchment Research Initiative (TROCARI), a collaboration between The University of Nottingham, Liverpool John Moores University, The University of Leicester, GEC and supported by the Selangor State Forestry Department. The research in **Chapters 4, 5 and 6** have produced practical map outputs, as well as establishing ground (forest inventory and peat sampling) datasets to build on and methods to replicate to produce long-standing tropical peatland data records for NSPSF. Findings and

products derived from this research have fed into the updated Integrated Management Plan for the reserve. For a tropical peat swamp forest reserve actively working towards restoration and sustainable resource management, updated resources are essential to guide interventions and conservation activities. Previous to this thesis research, management strategies were based on maps and datasets collected before any restoration activities had been put in place, for example, Figure 4-1 presents the forest management inventory undertaken in 2000. In a dynamic landscape such as the NSPSF, building current resource management strategies from information collected more than 10 years before the 2014 IMP was produced is unsuitable. Reserve maps and datasets presented in this research provides a more current representation of NSPSF.

The research in **Chapter 5** specifically investigated the restoration and regeneration efforts from local NGO's and Selangor State Forestry Department between the years 2015 and 2018, in the context of AGB dynamics at a landscape-scale. Results found canal blocking activities and water table management to be an effective restoration strategy, however it was evident that restoration efforts need to be monitored to insure the success of these strategies. The research concluded that a longer term AGB assessment (+5 years) should be conducted, recommending the continued tracking of AGB dynamics in view of reserve management and resource distribution. Additionally, the AGB maps presented in **Chapter 5** have been incorporated into research outside of this thesis. For example, AGB data for the reserve (**Chapter 5**) is currently being used in a UK Space Agency International Partnership Programme (IPP2) funded project called "Peatland Assessment In

SE Asia With Satellite (PASSES)”(https://www.gov.uk/government/news/uk-space-agency-to-run-22mil-project-in-malaysia-indonesia).

7.3 Limitations

There are a number of limitations highlighted in the aforementioned technologies and approaches used in this thesis. Discussion sections in **Chapters 4, 5 and 6** outline the limitations specific to each research area. Overall, data availability, both in accessing remote sensing and field data, was a major constraint for this thesis.

High cloud cover is a major obstacle in this research and in the use of optical wavelength remote sensing in tropical environments in general. In this thesis, the use of optical multispectral space-borne data (Landsat archive and Sentinel-2) and airborne lidar data (laser emitted at 1064 nm) was restricted by cloud cover and haze. Covering a total area of 81, 304 ha, the large extent of NSPSF reduces the chances of gaining a cloud free data scene for the entire area of the reserve. Sentinel-2’s high revisit frequency (5 days) has generated a large volume of data increasing the chance for obtaining usable data. In this research, Sentinel-2 cloud free data for the years of interest was easily obtained. However, the lower revisit frequency of Landsat data (16/18 days) severely impacted the data available. On average, a cloud free scene of the reserve was captured every 3.75 years. This is a particular limitation in specific surface change detection that requires data before and after a particular change or disturbance event. Lack of Landsat data restricted this research to a more general investigation on long-term patterns and trends in tropical peatland degradation (**Chapter 6**). The lidar data acquired in the

ARF's 2014 Malaysia Campaign was also impacted by low hanging cloud. In total 29 flightlines covering an area 69,000 ha was flown within and adjacent to the reserve, however only 9,457.08 ha (covering areas only within reserve) was used in this research (**Chapter 4**) due to the laser light's inability to penetrate through heavy cloud.

Temporal discrepancies between the field data campaigns, airborne lidar acquisition and space-borne datasets is a major challenge for AGB product validation (**Chapters 4 and 5**) in this research. Different areas of the reserve change at different rates in response to the resource management and peatland degradation in NSPSF. The rate of change therefore determines the importance of collecting validation data that temporally matches the remote sensing derived AGB products produced. For the research in **Chapter 4**, the forest plots (sampled 2017) used to create the 'lidar AGB model' were specifically positioned in secondary peat swamp forest where no obvious structural disturbances were observed since the lidar survey (sampled 2014). This was based on existing forest management plans and expert knowledge from NSPSF Rangers. Despite these efforts to limit the effect of temporal discrepancies', product validation is still restricted. Further analysis and interpretation of the results should keep this in mind.

Accessibility of the reserve was a major constraint for fieldwork and plot sampling design. As previously mentioned, NSPSF covers a large area, time restrictions and access by foot reduced the distance into the reserve where field plots could be established. Access to the reserve is additionally limited to key entrances due to a large canal running along the reserve boundary. The

difficult logistics of fieldwork posed by often waterlogged, swampy conditions, further hindered data collection.

Sample number, including both field plots and peat cores, proved to be a limiting factor in data analysis and modelling efforts. For example, the small sample size of forest inventory plots may have caused issues in the model-based prediction of AGB in **Chapter 4**, which in turn could introduce error into the following research chapter's incorporating the **Chapter 4** AGB prediction results. To reduce sample size error, field plots were positioned to ensure a representative sample cover across different forest structure types (height and density). Additionally, methods such as LOOCV (**Chapter 4**) and incorporating the 'AGB lidar model' as training and validation data (**Chapter 5**) were adopted in this research to reduce the uncertainties and errors introduced by a relatively small sample number. Fieldwork is inevitably restricted by the trade-off between sample size and cost; future research should utilise resources such as the products produced in this thesis to plan field campaigns in order to achieve the optimal configuration, for example, the 'top-down' strategy discussed in section 7.2.1.

Measurement error during field data collection should be acknowledged as a limitation in this thesis research. For example, the accuracy of field plot AGB estimates used for both calibration and validation of AGB models are based on the measurement of only a few variables (DBH, species and height). Low level inaccuracy (human error) in the measurement of these variables in fieldwork could impact plot estimates and the overall accuracy of the AGB prediction models. Additionally, spatial measurement error originating from field GPS may have introduced plot positional errors between field data and remote

sensing datasets. This could have a substantial impact on the bias and accuracy of model outputs. Future research could invest in a higher survey grade GPS/GLONASS receivers and incorporate a local base station to determine coordinates in the field. This may suppress the impact of co-registration error, however, the dense nature of the NSPSF will likely still cause issues with positional errors.

7.4 Recommendations for further research

Suggestions for future research that builds on the results of this thesis:

- A reference data archive of AGB for NSPSF, including both field inventory validation data and remote sensing derived AGB map products, should be established, building on the methods set out in **Chapters 4 and 5** for future AGB estimates. Furthering the work developed in this thesis will benefit local resource planning and future prioritisation of peatland restoration programs for NSPSF. In addition, this AGB data resource would allow the long-term trend analysis of tropical peat swamp AGB providing evidence of the most successful techniques and approaches to base tropical peatland restoration activities in other degraded peatlands in South-East Asia. To this end, advancing the field of tropical peatland restoration science, and aiding in enforcement and policy making to achieve global climate and land restoration goals. This is of particular importance in view of the increasing destruction associated with annual catastrophic fire events in South-East Asia

(Taufik *et al.*, 2019) and the continued expansion and conversion of the oil palm industry (Gatti *et al.,* 2019).

- A cost-sharing approach with multiple stakeholders (researchers (e.g. TROCARI and PASSES), NGO's (e.g. GEC and Sahabat Hutan Gambut Selangor Utara), Selangor State Forestry Department, Selangor State Government, etc.) is recommended as a pragmatic approach for funding remote sensing data, in particular future airborne lidar campaigns. Remote sensing data and products derived can assist in a number of tropical peatland applications (as discussed in **Chapter 2**). For example a digital terrain model derived from airborne lidar data could be used in terrain mapping, hydrological studies and fire scar burn detection, as well as providing essential data inputs for AGB application. As previously discussed, occupied airborne lidar data is associated with high cost, a collaborative cost-sharing approach would minimise costs for individual studies and increase the opportunity for repeated yearly/ seasonal data collection. This idea of collaborative cost-sharing for data acquisition should be extended out to a general encouragement of more collaboration between the different disciplines in the field of tropical peat swamp forests, in particular in view to recovery and rehabilitation.

- The field of remote sensing is entering a new era of data availability from innovation in platform and senor technology and an increase in the number of space-borne sensor missions planned. This thesis recommends the adoption of data acquired from UAV

or drone platforms (as discussed in **Chapter 4),** the application of microsat data (as discussed in **Chapter 5**), and the use of data from upcoming space-borne mission such as GEDI, BIOMASS, ICEsat-2, and NISAR (as discussed in **Chapter 5**) in future landscape-scale mapping and monitoring activites in tropical peat swamp forests. It is hoped that the increase in data availability will reduce this limitation.

- Further peat sampling and coring programs should be implemented in NSPSF to gain a fuller representation of peat depth, carbon stock, and measures of degradation and peat stability in the reserve. Sampling design should incorporate knowledge from the research presented in **Chapter 6**, in particular the use of spectral indices time-stack data, to guide and prioritise areas for sampling. Peat sampling and coring activates should aim to cover a wide range of sites that have experienced degradation and/or regeneration to varying degrees.

7.5 Concluding remarks

Degraded tropical peat swamp forests in South-East Asia urgently need to seek successful restoration measures and halt further human-induced destruction in order to secure carbon stores, reduce greenhouse gas emissions and sustain tropical peatland biodiversity. Given the large spatial coverage associated with tropical peatlands, successful restoration actions ultimately need to be employed and assessed at landscape-scales. The research presented in this thesis confirms that remote sensing is a valuable tool in the landscape-

scale assessment of tropical peat swamp forest environments. Remote sensing data, coupled with field-based measurements, combine the accuracy and detail of traditional ecological field assessment with the spatial and temporal coverage afforded by remote sensing.

The continued development of sensor technology and data analysis in tropical peatland environments is essential for improving tropical peat restoration and sustainable management practices, as well as supporting global environmental policy and climate mitigation efforts. It is hoped that the approaches and evidence of tropical peatland rehabilitation monitoring built in this thesis will defend degraded tropical peatlands against the idea of being wastelands, and champion their restoration in the face of present-day and future disturbance and land use pressures.

References

Abdulkarim, B., Yacob, M.R., Abdullahi, A.M. and Radam, A., 2017. Farmers' perceptions and attitudes toward forest watershed conservation of the North Selangor Peat Swamp Forest. *Journal of sustainable forestry*, *36*(4), pp.309-323.

Adam, E., Mutanga, O., Abdel-Rahman, E.M. and Ismail, R., 2014. Estimating standing biomass in papyrus (Cyperus papyrus L.) swamp: exploratory of in situ hyperspectral indices and random forest regression. *International journal of remote sensing*, *35*(2), pp.693-714.

Adila, N., Sasidhran, S., Kamarudin, N., Puan, C.L., Azhar, B. and Lindenmayer, D.B., 2017. Effects of peat swamp logging and agricultural expansion on species richness of native mammals in Peninsular Malaysia. *Basic and applied ecology*, *22*, pp.1-10.

Ahmed, O.S., Franklin, S.E., Wulder, M.A. and White, J.C., 2015. Characterizing stand-level forest canopy cover and height using landsat time series, samples of airborne LiDAR, and the random forest algorithm. *ISPRS Journal of Photogrammetry and Remote Sensing*, *101*, pp.89-101

Ahmad, N. Guardians of the North Selangor Peat Swamp Forest. 2014. Available online: https://peatlandsinternational.wordpress.com/2014/06/20/peatlands-international-2-2014/ (accessed on 20 June 2014).

Ainuddin, N.A. and Goh, K., 2010. Effect of forest fire on stand structure in Raja Musa peat swamp forest reserve, Selangor, Malaysia. *Journal of Environmental Science and Technology*, *3*(1), pp.56-62.

Alexander, C., Korstjens, A.H. and Hill, R.A., 2018. Influence of micro-topography and crown characteristics on tree height estimations in tropical forests based on LiDAR canopy height models. *International journal of applied earth observation and geoinformation*, *65*, pp.105-113.

Anderson, J.A.R., 1983. The tropical peat swamps of western Malesia. *Mires: swamp, bog, fen and moor: regional studies*.

Anderson, J.A.R., 1961. The ecology and forest types of the peat swamp forests of Sarawak and Brunei in relation to their silviculture. *Ph. D thesis, Edinburgh University*.

Anshari, G.Z., Afifudin, M., Nuriman, M., Gusmayanti, E., Arianie, L., Susana, R., Nusantara, R.W., Sugardjito, J. and Rafiastanto, A., 2010. Drainage and land use impacts on changes in selected peat properties and peat degradation in West Kalimantan Province, Indonesia. *Biogeosciences*, *7*(11), pp.3403-3419.

Aplin, P. 2005. Remote sensing: Ecology. *Progress. Physical*. *Geography*. 29, pp.104–113.

Appanah, S., Ismail, H., Samsudin, M. and Sadali, S., 1999. Flora survey of north Selangor peat swamp forest. *Sustainable Management of Peat Swamp Forest in Peninsular Malaysia: Resource and Environment*, *1*, pp.199-238.

ARF. 2011. ARSF Data Processing. Available online: http://arsf.nerc.ac.uk/data/ (accessed on 10 May 2016)

Aronson, J. and Alexander, S., 2013. Ecosystem restoration is now a global priority: time to roll up our sleeves. *Restoration Ecology*, *21*(3), pp.293-296.

ASEAN Secretariat and Global Environment Centre. 2011. Peatlands in Southeast Asia – A Profile. Rehabilitation and Sustainable Use of Peatland Forests in Southeast Asia, ASEAN Peatland Forests Project. ASEAN Secretariat, Jakarta, Indonesia.

Asner, G.P., Brodrick, P.G., Philipson, C., Vaughn, N.R., Martin, R.E., Knapp, D.E., Heckler, J., Evans, L.J., Jucker, T., Goossens, B. and Stark, D.J., 2018. Mapped aboveground carbon stocks to advance forest conservation and recovery in Malaysian Borneo. *Biological conservation*, *217*, pp.289-310.

Asner, G.P., Martin, R.E., Anderson, C.B. and Knapp, D.E., 2015. Quantifying forest canopy traits: Imaging spectroscopy versus field survey. *Remote Sensing of Environment*, *158*, pp.15-27.

Asner, G.P., Mascaro, J., Muller-Landau, H.C., Vieilledent, G., Vaudry, R., Rasamoelina, M., Hall, J.S. and Van Breugel, M., 2012. A universal airborne LiDAR approach for tropical forest carbon mapping. *Oecologia*, *168*(4), pp.1147-1160.

Asner, G.P., Powell, G.V., Mascaro, J., Knapp, D.E., Clark, J.K., Jacobson, J., Kennedy-Bowdoin, T., Balaji, A., Paez-Acosta, G., Victoria, E. and Secada, L., 2010. High-resolution forest carbon stocks and emissions in the Amazon. *Proceedings of the National Academy of Sciences*, *107*(38), pp.16738-16742.

Azamathulla, H.M., Ghani, A.A. and Fei, S.Y., 2012. ANFIS-based approach for predicting sediment transport in clean sewer. *Applied Soft Computing*, *12*(3), pp.1227-1230.

Azhar, B., Lindenmayer, D.B., Wood, J., Fischer, J., Manning, A., McElhinny, C. and Zakaria, M., 2011. The conservation value of oil palm plantation estates, smallholdings and logged peat swamp forest for birds. *Forest Ecology and Management*, *262*(12), pp.2306-2315.

Ballhorn, U., Jubanski, J. and Siegert, F., 2011. ICESat/GLAS data as a measurement tool for peatland topography and peat swamp forest biomass in Kalimantan, Indonesia. *Remote Sensing*, *3*(9), pp.1957-1982.

Ballhorn, U., Siegert, F., Mason, M. and Limin, S., 2009. Derivation of burn scar depths and estimation of carbon emissions with LIDAR in Indonesian peatlands. *Proceedings of the National Academy of Sciences*, *106*(50), pp.21213-21218.

Barton, K., 2009. MuMIn: multi-model inference, R package version 0.12. 0. Available online: *http://r-forge. r-project. org/projects/mumin/.*

Beamish, F.W.H., Beamish, R.B. and Lim, S.L.H., 2003. Fish assemblages and habitat in a Malaysian blackwater peat swamp. *Environmental Biology of Fishes*, *68*(1), pp.1-13.

Behar, F., Beaumont, V. and Penteado, H.D.B., 2001. Rock-Eval 6 technology: performances and developments. *Oil & Gas Science and Technology*, *56*(2), pp.111-134.

Belgiu, M. and Drăguţ, L., 2016. Random forest in remote sensing: A review of applications and future directions. *ISPRS Journal of Photogrammetry and Remote Sensing*, *114*, pp.24-31.

Berninger, A., Lohberger, S., Stängel, M. and Siegert, F., 2018. SAR-based estimation of above-ground biomass and its changes in tropical forests of Kalimantan using L-and C-Band. *Remote Sensing*, *10*(6), p.831.

Biester, H., Knorr, K.H., Schellekens, J., Basler, A. and Hermanns, Y.M., 2014. Comparison of different methods to determine the degree of peat decomposition in peat bogs. *Biogeosciences*, *11*(10), pp.2691-2707.

Blackham, G.V., Webb, E.L. and Corlett, R.T., 2014. Natural regeneration in a degraded tropical peatland, Central Kalimantan, Indonesia: Implications for forest restoration. *Forest Ecology and Management*, *324*, pp.8-15.

Blackham, G.V., Thomas, A., Webb, E.L. and Corlett, R.T., 2013. Seed rain into a degraded tropical peatland in Central Kalimantan, Indonesia. *Biological conservation*, *167*, pp.215-223.

Boehm, H.D.V., Liesenberg, V. and Limin, S.H., 2013. Multi-temporal airborne LiDAR-survey and field measurements of tropical peat swamp forest to monitor changes. *IEEE Journal of Selected Topics in Applied Earth Observations and Remote Sensing*, *6*(3), pp.1524-1530.

Böhm, H.D.V. and Siegert, F., 2001, August. Land use change and (il)-legal logging in Central Kalimantan, Indonesia. In *Peatlands for People Natural Resources Function and Sustainable Management, Proceedings of the International Peat Symposium, held Jakarta, Indonesia* (pp. 22-24).

Bolton, D.K., White, J.C., Wulder, M.A., Coops, N.C., Hermosilla, T. and Yuan, X., 2018. Updating stand-level forest inventories using airborne laser scanning and Landsat time series data. *International journal of applied earth observation and geoinformation*, *66*, pp.174-183.

Bonn, A., Allott, T., Evans, M., Joosten, H. and Stoneman, R. eds., 2016. *Peatland restoration and ecosystem services: science, policy and practice*. Cambridge University Press.

Boudreau, J., Nelson, R.F., Margolis, H.A., Beaudoin, A., Guindon, L. and Kimes, D.S., 2008. Regional aboveground forest biomass using airborne and spaceborne LiDAR in Québec. *Remote Sensing of Environment*, *112*(10), pp.3876-3890.

Brandtberg, T., Warner, T.A., Landenberger, R.E. and McGraw, J.B., 2003. Detection and analysis of individual leaf-off tree crowns in small footprint, high sampling density lidar data from the eastern deciduous forest in North America. *Remote sensing of Environment*, *85*(3), pp.290-303.

Breiman, L., 2001. Random forests. Machine learning, 45(1), pp.5-32.

Brovelli, M.A., Crespi, M., Fratarcangeli, F., Giannone, F. and Realini, E., 2008. Accuracy assessment of high resolution satellite imagery orientation by leave-one-out method. *ISPRS Journal of Photogrammetry and Remote Sensing*, 63(4), pp.427-440.

Brown, C., Boyd, D., Sjögersten, S., Clewley, D., Evers, S. and Aplin, P., 2018. Tropical peatland vegetation structure and biomass: optimal exploitation of airborne laser scanning. *Remote Sensing*, 10(5), p.671.

Brown, M.E., Lary, D.J., Vrieling, A., Stathakis, D. and Mussa, H., 2008. Neural networks as a tool for constructing continuous NDVI time series from AVHRR and MODIS. *International Journal of Remote Sensing*, *29*(24), pp.7141-7158.

Bruenig, E.F. and Droste, H.J., 1995. Structure, dynamics and management of rainforests on nutrient-deficient soils in Sarawak. *Ecology, conservation and management of Southeast Asian rainforests*, pp.41-53.

Bryan, J.E., Shearman, P.L., Asner, G.P., Knapp, D.E., Aoro, G. and Lokes, B., 2013. Extreme differences in forest degradation in Borneo: comparing practices in Sarawak, Sabah, and Brunei. *PloS one*, *8*(7), p.e69679.

Bunting, P., Armston, J., Clewley, D. and Lucas, R.M., 2013. Sorted pulse data (SPD) library—Part II: A processing framework for LiDAR data from pulsed laser systems in terrestrial environments. *Computers & geosciences*, *56*, pp.207-215.

Burnham, K.P.; Anderson, D.R., 2003. Model Selection and Multimodel Inference: A Practical Information-Theoretic Approach; Springer: Berlin, Germany.

Butler, D. 2014. “Many eyes on Earth: swarms of small satellites set to deliver close to real-time imagery of swathes of the planet.” Nature, Vol. 505: pp. 143–144.

Bye, I.J., North, P.R., Los, S.O., Kljun, N., Rosette, J.A.B., Hopkinson, C., Chasmer, L. and Mahoney, C., 2017. Estimating forest canopy parameters from satellite waveform LiDAR by inversion of the FLIGHT three-dimensional radiative transfer model. *Remote sensing of environment*, *188*, pp.177-189.

Campbell, J.B. and Wynne, R.H., 2011. *Introduction to remote sensing*. Guilford Press.

Cao, L., Coops, N., Hermosilla, T., Innes, J., Dai, J. and She, G., 2014a. Using small-footprint discrete and full-waveform airborne LiDAR metrics to estimate total biomass and biomass components in subtropical forests. *Remote Sensing*, *6*(8), pp.7110-7135.

Cao, L., Coops, N., Innes, J., Dai, J. and She, G., 2014b. Mapping above-and below-ground biomass components in subtropical forests using small-footprint LiDAR. *Forests*, *5*(6), pp.1356-1373.

Carroll, M.J., Heinemeyer, A., Pearce-Higgins, J.W., Dennis, P., West, C., Holden, J., Wallage, Z.E. and Thomas, C.D., 2015. Hydrologically driven ecosystem processes determine the distribution and persistence of ecosystem-specialist predators under climate change. *Nature communications*, *6*, p.7851.

Casson, A. and Obidzinski, K., 2002. From new order to regional autonomy: shifting dynamics of "illegal" logging in Kalimantan, Indonesia. *World development*, *30*(12), pp.2133-2151.

Cattau, M.E., Harrison, M.E., Shinyo, I., Tungau, S., Uriarte, M. and DeFries, R., 2016. Sources of anthropogenic fire ignitions on the peat-swamp landscape in Kalimantan, Indonesia. *Global Environmental Change*, *39*, pp.205-219.

Charters, L.J., Aplin, P., Marston, C.G., Padfield, R., Rengasamy, N., Bin Dahalan, M.P. and Evers, S., 2019. Peat swamp forest conservation withstands pervasive land conversion to oil palm plantation in North Selangor, Malaysia. *International Journal of Remote Sensing*, pp.1-30.

Chauve, A., Bretar, F., Durrieu, S., Pierrot-Deseilligny, M. and Puech, W., 2009, July. Fullanalyze: a research tool for handling, processing and analyzing full-waveform lidar data. In *2009 IEEE International Geoscience and Remote Sensing Symposium* (Vol. 4, pp. IV-841). IEEE.

Chave, J., Réjou-Méchain, M., Búrquez, A., Chidumayo, E., Colgan, M.S., Delitti, W.B., Duque, A., Eid, T., Fearnside, P.M., Goodman, R.C. and Henry, M., 2014. Improved allometric models to estimate the aboveground biomass of tropical trees. *Global change biology*, *20*(10), pp.3177-3190.

Chave, J., Coomes, D., Jansen, S., Lewis, S.L., Swenson, N.G. and Zanne, A.E., 2009. Towards a worldwide wood economics spectrum. *Ecology letters*, 12(4), pp.351-366.

Chave, J., Andalo, C., Brown, S., Cairns, M.A., Chambers, J.Q., Eamus, D., Fölster, H., Fromard, F., Higuchi, N., Kira, T. and Lescure, J.P., 2005. Tree allometry and improved estimation of carbon stocks and balance in tropical forests. *Oecologia*, *145*(1), pp.87-99.

Chen, K., Jacobson, C. and Blong, R., 2001, November. Using NDVI image texture analysis for bushfire-prone landscape assessment. In 22nd Asian Conference on Remote Sensing (pp. 5-9). Centre for Remote Imaging, Sensing and Processing, National University of Singapore.

Chimner, R.A. and Ewel, K.C., 2005. A tropical freshwater wetland: II. Production, decomposition, and peat formation. *Wetlands Ecology and Management*, *13*(6), pp.671-684.

Chokkalingam, U., Sabogal, C., Almeida, E., Carandang, A.P., Gumartini, T., de Jong, W., Brienza, S., Lopez, A.M., Nawir, A.A., Wibowo, L.R. and Toma, T., 2005. Local participation, livelihood needs, and institutional arrangements: three keys to sustainable rehabilitation of degraded tropical forest lands. In *Forest restoration in landscapes* (pp. 405-414). Springer, New York, NY.

Chrysafis, I., Mallinis, G., Siachalou, S. and Patias, P., 2017. Assessing the relationships between growing stock volume and Sentinel-2 imagery in a Mediterranean forest ecosystem. *Remote Sensing Letters*, *8*(6), pp.508-517.

Cigna, F. and Sowter, A., 2017. The relationship between intermittent coherence and precision of ISBAS InSAR ground motion velocities: ERS-1/2 case studies in the UK. *Remote sensing of environment*, *202*, pp.177-198.

Coomes, D.A., Dalponte, M., Jucker, T., Asner, G.P., Banin, L.F., Burslem, D.F., Lewis, S.L., Nilus, R., Phillips, O.L., Phua, M.H. and Qie, L., 2017. Area-based vs tree-centric approaches to mapping forest carbon in Southeast Asian forests from airborne laser scanning data. *Remote Sensing of Environment*, *194*, pp.77-88.

Cooper, H.V., Vane, C.H., Evers, S., Aplin, P., Girkin, N.T. and Sjögersten, S., 2019. From peat swamp forest to oil palm plantations: The stability of tropical peatland carbon. *Geoderma*, *342*, pp.109-117.

Corona, P., 2016. Consolidating new paradigms in large-scale monitoring and assessment of forest ecosystems. *Environmental research*, *144*, pp.8-14.

Couwenberg, J. and Hooijer, A., 2013. Towards robust subsidence-based soil carbon emission factors for peat soils in south-east Asia, with special reference to oil palm plantations. *Mires & Peat*, *12*.

Couwenberg, J., Dommain, R. and Joosten, H., 2010. Greenhouse gas fluxes from tropical peatlands in south-east Asia. *Global Change Biology*, *16*(6), pp.1715-1732.

Cracknell, M.J. and Reading, A.M., 2014. Geological mapping using remote sensing data: A comparison of five machine learning algorithms, their response to variations in the spatial distribution of training data and the use of explicit spatial information. Computers & Geosciences, 63, pp.22-33.

Cundill, S., van der Werff, H. and van der Meijde, M., 2015. Adjusting spectral indices for spectral response function differences of very high spatial resolution sensors simulated from field spectra. *Sensors*, *15*(3), pp.6221-6240.

Curran, P.J., 1986. The importance of measurement error for certain procedures in remote sensing at optical wavelengths, Photogramm. *Eng. Remote Sensing*, *52*, pp.229-241.

Dahalan, M. P., Manaf, M. B. A.., Rahman, B. H. A., Khalid, S. M. A. S., Sukri, A. M., Yusoff, D. M., Muda, M. et al., 2016. Implementation of Integrated Management Plan for North Selangor Peat Swamp Forest 2014–2023. Paper presented at 15th International Peat Congress, Sarawak, Malaysia, August 15–19.

Danielsen, F., Beukema, H., Burgess, N.D., Parish, F., Brühl, C.A., Donald, P.F., Murdiyarso, D., Phalan, B.E.N., Reijnders, L., Struebig, M. and Fitzherbert, E.B., 2009. Biofuel plantations on forested lands: double jeopardy for biodiversity and climate. *Conservation Biology*, *23*(2), pp.348-358.

D'Arcy, L.J. and Graham, L.L.B., 2008. The potential effects of naturally low rates of secondary seed dispersal, coupled with a reduction in densities of primary seed dispersers on forest tree species diversity in regenerating peat swamp forest. *Restoration of Tropical Peatlands*, p.45.

Dargie, G.C., Lewis, S.L., Lawson, I.T., Mitchard, E.T., Page, S.E., Bocko, Y.E. and Ifo, S.A., 2017. Age, extent and carbon storage of the central Congo Basin peatland complex. *Nature*, *542*(7639), p.86.

Davies, J. 2011. Training Module on Peatland Assessment and Management. ASEAN Peatland Forests Project. ASEAN Secretariat and Global Environment Centre, Kuala Lumpur, Malaysia.

Delarue, F., Disnar, J.R., Copard, Y., Gogo, S., Jacob, J. and Laggoun-Défarge, F., 2013. Can Rock-Eval pyrolysis assess the biogeochemical composition of organic matter during peatification?. *Organic geochemistry*, *61*, pp.66-72.

Disnar, J.R., Guillet, B., Kéravis, D., Di-Giovanni, C. and Sebag, D., 2003. Soil organic matter (SOM) characterization by Rock-Eval pyrolysis: scope and limitations. *Organic geochemistry*, *34*(3), pp.327-343.

Dohong, A., Aziz, A.A. and Dargusch, P., 2018. A review of techniques for effective tropical peatland restoration. *Wetlands*, *38*(2), pp.275-292.

Dohong, A., Aziz, A.A. and Dargusch, P., 2017. A review of the drivers of tropical peatland degradation in South-East Asia. *Land Use Policy*, 69, pp.349-360.

Dommain, R., Couwenberg, J. and Joosten, H., 2011. Development and carbon sequestration of tropical peat domes in south-east Asia: links to post-glacial sea-level changes and Holocene climate variability. *Quaternary Science Reviews*, *30*(7-8), pp.999-1010.

Dorrepaal, E., Cornelissen, J.H., Aerts, R., Wallen, B.O. and Van Logtestijn, R.S., 2005. Are growth forms consistent predictors of leaf litter quality and decomposability across peatlands along a latitudinal gradient?. *Journal of Ecology*, *93*(4), pp.817-828.

Drake, J.B., Knox, R.G., Dubayah, R.O., Clark, D.B., Condit, R., Blair, J.B. and Hofton, M., 2003. Above-ground biomass estimation in closed canopy neotropical forests using lidar remote sensing: Factors affecting the generality of relationships. *Global ecology and biogeography*, *12*(2), pp.147-159.

Drake, J.B., Dubayah, R.O., Clark, D.B., Knox, R.G., Blair, J.B., Hofton, M.A., Chazdon, R.L., Weishampel, J.F. and Prince, S., 2002. Estimation of tropical forest structural characteristics using large-footprint lidar. *Remote Sensing of Environment*, *79*(2-3), pp.305-319.

Drusch, M., Del Bello, U., Carlier, S., Colin, O., Fernandez, V., Gascon, F., Hoersch, B., Isola, C., Laberinti, P., Martimort, P. and Meygret, A., 2012. Sentinel-2: ESA's optical high-resolution mission for GMES operational services. Remote Sensing of Environment, 120, pp.25-36.

Dubayah, R.O., Sheldon, S.L., Clark, D.B., Hofton, M.A., Blair, J.B., Hurtt, G.C. and Chazdon, R.L., 2010. Estimation of tropical forest height and biomass dynamics using lidar remote sensing at La Selva, Costa Rica. *Journal of Geophysical Research: Biogeosciences*, *115*(G2).

Dubayah, R.O. and Drake, J.B., 2000. Lidar remote sensing for forestry. *Journal of Forestry*, *98*(6), pp.44-46.

Duncanson, L., Armston, J., Disney, M., Avitabile, V., Barbier, N., Calders, K., Carter, S., Chave, J., Herold, M., Crowther, T.W. and Falkowski, M., 2019. The importance of consistent global forest aboveground biomass product validation. *Surveys in Geophysics*, pp.1-21.

Duncanson, L.I., Dubayah, R.O., Cook, B.D., Rosette, J. and Parker, G., 2015. The importance of spatial detail: Assessing the utility of individual crown information and scaling approaches for lidar-based biomass density estimation. *Remote Sensing of Environment*, 168, pp.102-112.

Eckert, S., 2012. Improved forest biomass and carbon estimations using texture measures from WorldView-2 satellite data. *Remote sensing*, *4*(4), pp.810-829.

Efron, B., 1981. Nonparametric estimates of standard error: the jackknife, the bootstrap and other methods. *Biometrika*, *68*(3), pp.589-599.

Egberth, M., Nyberg, G., Næsset, E., Gobakken, T., Mauya, E., Malimbwi, R., Katani, J., Chamuya, N., Bulenga, G. and Olsson, H., 2017. Combining airborne laser scanning and Landsat data for statistical modeling of soil carbon and tree biomass in Tanzanian Miombo woodlands. *Carbon balance and management*, 12(1), p.8.

Elvidge, C.D., Zhizhin, M., Hsu, F.C., Baugh, K., Khomarudin, M.R., Vetrita, Y., Sofan, P. and Hilman, D., 2015. Long-wave infrared identification of smoldering peat fires in Indonesia with nighttime Landsat data. *Environmental Research Letters*, *10*(6), p.065002.

Englhart, S., Jubanski, J. and Siegert, F., 2013a. Quantifying dynamics in tropical peat swamp forest biomass with multi-temporal LiDAR datasets. *Remote Sensing*, *5*(5), pp.2368-2388.

Engelhart, S.E., Horton, B.P., Nelson, A.R., Hawkes, A.D., Witter, R.C., Wang, K., Wang, P.L. and Vane, C.H., 2013b. Testing the use of microfossils to reconstruct great earthquakes at Cascadia. *Geology*, *41*(10), pp.1067-1070.

Englhart, S., Keuck, V. and Siegert, F., 2011. Aboveground biomass retrieval in tropical forests—The potential of combined X-and L-band SAR data use. *Remote sensing of environment*, *115*(5), pp.1260-1271.

ESA. 2012. BIOMASS Report for mission selection May 2012. Report No.: SP-1324/1.

Evans, J.S. and Hudak, A.T., 2007. A multiscale curvature algorithm for classifying discrete return LiDAR in forested environments. *IEEE Transactions on Geoscience and Remote Sensing*, *45*(4), pp.1029-1038.

Even, M. and Schulz, K., 2018. InSAR deformation analysis with distributed scatterers: A review complemented by new advances. *Remote Sensing*, *10*(5), p.744.

Evers, S., Yule, C.M., Padfield, R., O'reilly, P. and Varkkey, H., 2017. Keep wetlands wet: the myth of sustainable development of tropical peatlands–implications for policies and management. *Global change biology*, *23*(2), pp.534-549.

Fassnacht, F.E., Hartig, F., Latifi, H., Berger, C., Hernández, J., Corvalán, P. and Koch, B., 2014. Importance of sample size, data type and prediction method for remote sensing-based estimations of aboveground forest biomass. *Remote Sensing of Environment*, *154*, pp.102-114.

Fekety, P.A., Falkowski, M.J. and Hudak, A.T., 2015. Temporal transferability of LiDAR-based imputation of forest inventory attributes. *Canadian journal of forest research*, *45*(4), pp.422-435.

Feldpausch, T.R., Lloyd, J., Lewis, S.L., Brienen, R.J., Gloor, M., Monteagudo Mendoza, A., Lopez-Gonzalez, G., Banin, L., Abu Salim, K., Affum-Baffoe, K. and Alexiades, M., 2012. Tree height integrated into pantropical forest biomass estimates. *Biogeosciences*, pp.3381-3403.

Fernández-Manso, A., Fernández-Manso, O. and Quintano, C., 2016. SENTINEL-2A red-edge spectral indices suitability for discriminating burn severity. *International journal of applied earth observation and geoinformation*, *50*, pp.170-175.

Ferraz, A., Bretar, F., Jacquemoud, S. and Gonçalves G., 2009. The Role of Lidar Systems in Fuel Mapping. Instituto de Engenharia de Sistemas e Computadores de Coimbra INESC - Coimbra Rua Antero de Quental, 199; 3000-033 Coimbra; Portugal. No 13.

Finer, M., Novoa, S., Weisse, M.J., Petersen, R., Mascaro, J., Souto, T., Stearns, F. and Martinez, R.G., 2018. Combating deforestation: From satellite to intervention. *Science*, 360(6395), pp.1303-1305.

Foody, G.M., Boyd, D.S. and Cutler, M.E., 2003. Predictive relations of tropical forest biomass from Landsat TM data and their transferability between regions. *Remote sensing of environment*, *85*(4), pp.463-474.

Fornacca, D., Ren, G. and Xiao, W., 2018. Evaluating the best spectral indices for the detection of burn scars at several post-fire dates in a mountainous region of Northwest Yunnan, China. *Remote Sensing*, 10(8), p.1196.

Frampton, W.J., Dash, J., Watmough, G. and Milton, E.J., 2013. Evaluating the capabilities of Sentinel-2 for quantitative estimation of biophysical variables in vegetation. *ISPRS journal of photogrammetry and remote sensing*, *82*, pp.83-92.

Franke, J., Navratil, P., Keuck, V., Peterson, K. and Siegert, F., 2012. Monitoring fire and selective logging activities in tropical peat swamp forests. *IEEE Journal of Selected Topics in Applied Earth Observations and Remote Sensing*, *5*(6), pp.1811-1820.

Frazer, G.W., Magnussen, S., Wulder, M.A. and Niemann, K.O., 2011. Simulated impact of sample plot size and co-registration error on the accuracy and uncertainty of LiDAR-derived estimates of forest stand biomass. *Remote Sensing of Environment*, 115(2), pp.636-649.

Frazier, R.J., Coops, N.C., Wulder, M.A. and Kennedy, R., 2014. Characterization of aboveground biomass in an unmanaged boreal forest using Landsat temporal segmentation metrics. *ISPRS journal of photogrammetry and remote sensing*, *92*, pp.137-146.

French, N.H., Kasischke, E.S., Hall, R.J., Murphy, K.A., Verbyla, D.L., Hoy, E.E. and Allen, J.L., 2008. Using Landsat data to assess fire and burn severity in the North American boreal forest region: an overview and summary of results. *International Journal of Wildland Fire*, *17*(4), pp.443-462.

Furukawa, Y., Inubushi, K., Ali, M., Itang, A.M. and Tsuruta, H., 2005. Effect of changing groundwater levels caused by land-use changes on greenhouse gas fluxes from tropical peat lands. *Nutrient Cycling in Agroecosystems*, *71*(1), pp.81-91.

Galidaki, G., Zianis, D., Gitas, I., Radoglou, K., Karathanassi, V., Tsakiri–Strati, M., Woodhouse, I. and Mallinis, G., 2017. Vegetation biomass estimation with remote sensing: focus on forest and other wooded land over the Mediterranean ecosystem. *International Journal of Remote Sensing*, *38*(7), pp.1940-1966.

Gao, J., Holden, J. and Kirkby, M., 2016. The impact of land-cover change on flood peaks in peatland basins. *Water Resources Research*, *52*(5), pp.3477-3492.

García, M., Saatchi, S., Ustin, S. and Balzter, H., 2018. Modelling forest canopy height by integrating airborne LiDAR samples with satellite Radar and multispectral imagery. *International journal of applied earth observation and geoinformation*, *66*, pp.159-173.

García, M.L. and Caselles, V., 1991. Mapping burns and natural reforestation using Thematic Mapper data. *Geocarto International*, *6*(1), pp.31-37.

García-Martín, A., de la Riva, J., Pérez-Cabello, F., Montorio, R. and Fatoyinbo, T., 2012. Using remote sensing to estimate a renewable resource: forest residual biomass. *Remote Sensing of Biomass-Principles and Applications*.

Gatti, R.C., Liang, J., Velichevskaya, A. and Zhou, M., 2019. Sustainable palm oil may not be so sustainable. *Science of The Total Environment*, *652*, pp.48-51.

Gaveau, D.L., Sloan, S., Molidena, E., Yaen, H., Sheil, D., Abram, N.K., Ancrenaz, M., Nasi, R., Quinones, M., Wielaard, N. and Meijaard, E., 2014a. Four decades of forest persistence, clearance and logging on Borneo. *PloS one*, *9*(7), p.e101654.

Gaveau, D.L., Salim, M.A., Hergoualc'h, K., Locatelli, B., Sloan, S., Wooster, M., Marlier, M.E., Molidena, E., Yaen, H., DeFries, R. and Verchot, L., 2014b. Major atmospheric emissions from peat fires in Southeast Asia during non-drought years: evidence from the 2013 Sumatran fires. *Scientific reports*, *4*, p.6112.

Gibbs, H.K., Brown, S., Niles, J.O. and Foley, J.A., 2007. Monitoring and estimating tropical forest carbon stocks: making REDD a reality. *Environmental Research Letters*, *2*(4), p.045023.

Gill, E., Sundaramoorthy, P., Bouwmeester, J., Zandbergen, B. and Reinhard, R., 2013. Formation flying within a constellation of nano-satellites: The QB50 mission. *Acta Astronautica*, *82*(1), pp.110-117.

Girkin, N.T., Vane, C.H., Cooper, H.V., Moss-Hayes, V., Craigon, J., Turner, B.L., Ostle, N. and Sjögersten, S., 2019. Spatial variability of organic matter properties determines methane fluxes in a tropical forested peatland. *Biogeochemistry*, *142*(2), pp.231-245.

Gleason, C.J. and Im, J., 2011. A review of remote sensing of forest biomass and biofuel: options for small-area applications. *GIScience & Remote Sensing*, *48*(2), pp.141-170.

Goetz, S.J., Baccini, A., Laporte, N.T., Johns, T., Walker, W., Kellndorfer, J., Houghton, R.A. and Sun, M., 2009. Mapping and monitoring carbon stocks with satellite observations: a comparison of methods. *Carbon balance and management*, *4*(1), p.2.

Gomez, C., White, J.C. and Wulder, M.A., 2016. Optical remotely sensed time series data for land cover classification: A review. *ISPRS Journal of Photogrammetry and Remote Sensing*, *116*, pp.55-72.

Gorham, E., Janssens, J.A. and Glaser, P.H., 2003. Rates of peat accumulation during the postglacial period in 32 sites from Alaska to Newfoundland, with special emphasis on northern Minnesota. *Canadian Journal of Botany*, *81*(5), pp.429-438.

Graham, L.L. and Page, S.E., 2014. 14.2. Forest restoration in degraded tropical peat swamp forests. *GENETIC CONSIDERATIONS IN ECOSYSTEM RESTORATION USING NATIVE TREE SPECIES*, *15*(3-4), p.200.

Graham, L.L., Turjaman, M. and Page, S.E., 2013. Shorea balangeran and Dyera polyphylla (syn. Dyera lowii) as tropical peat swamp forest restoration transplant species: effects of mycorrhizae and level of disturbance. *Wetlands ecology and management*, *21*(5), pp.307-321.

Gunawan, H., Kobayashi, S., Mizuno, K. and Kono, Y., 2012. Peat swamp forest types and their regeneration in Giam Siak Kecil-Bukit Batu Biosphere Reserve, Riau, East Sumatra, Indonesia. *Mires & Peat*, *10*.

Hahn-Schilling, B., 1994. *Struktur, sukzessionale Entwicklung und Bewirtschaftung selektiv genutzter Moorwälder in Malaysia*. Institut für Pflanzenbau und Tierhygiene in den Tropen und Subtropen, Georg-August-Universität Göttingen.

Ham, J., Chen, Y., Crawford, M.M. and Ghosh, J., 2005. Investigation of the random forest framework for classification of hyperspectral data. *IEEE Transactions on Geoscience and Remote Sensing*, *43*(3), pp.492-501.

Hancock, S., Armston, J., Li, Z., Gaulton, R., Lewis, P., Disney, M., Danson, F.M., Strahler, A., Schaaf, C., Anderson, K. and Gaston, K.J., 2015. Waveform lidar over vegetation: An evaluation of inversion methods for estimating return energy. *Remote Sensing of Environment*, *164*, pp.208-224.

Hand, E. 2015. “Startup liftoff.” *Science*, Vol. 348(No. 6231): pp. 172.

Hansen, M.C., Potapov, P.V., Goetz, S.J., Turubanova, S., Tyukavina, A., Krylov, A., Kommareddy, A. and Egorov, A., 2016a. Mapping tree height distributions in Sub-Saharan Africa using Landsat 7 and 8 data. *Remote Sensing of Environment*, *185*, pp.221-232.

Hansen, M.C., Krylov, A., Tyukavina, A., Potapov, P.V., Turubanova, S., Zutta, B., Ifo, S., Margono, B., Stolle, F. and Moore, R., 2016b. Humid tropical forest disturbance alerts using Landsat data. *Environmental Research Letters*, *11*(3), p.034008.

Haralick, R.M. and Shanmugam, K., 1973. Textural features for image classification. *IEEE Transactions on systems, man, and cybernetics*, (6), pp.610-621.

Hare, A.A., Kuzyk, Z.Z.A., Macdonald, R.W., Sanei, H., Barber, D., Stern, G.A. and Wang, F., 2014. Characterization of sedimentary organic matter in recent marine sediments from Hudson Bay, Canada, by Rock-Eval pyrolysis. *Organic geochemistry*, *68*, pp.52-60.

Hawkins, D.M., 2004. The problem of overfitting. *Journal of chemical information and computer sciences*, *44*(1), pp.1-12.

He, Q., Chen, E., An, R. and Li, Y., 2013. Above-ground biomass and biomass components estimation using LiDAR data in a coniferous forest. *Forests*, *4*(4), pp.984-1002.

Heil, A. and Goldammer, J., 2001. Smoke-haze pollution: a review of the 1997 episode in Southeast Asia. *Regional Environmental Change*, *2*(1), pp.24-37.

Herawati, H. and Santoso, H., 2011. Tropical forest susceptibility to and risk of fire under changing climate: A review of fire nature, policy and institutions in Indonesia. *Forest Policy and Economics*, *13*(4), pp.227-233.

Hergoualc'h, K. and Verchot, L.V., 2011. Stocks and fluxes of carbon associated with land use change in Southeast Asian tropical peatlands: A review. *Global Biogeochemical Cycles*, *25*(2).

Hermosilla, T., Ruiz, L.A., Kazakova, A.N., Coops, N.C. and Moskal, L.M., 2014. Estimation of forest structure and canopy fuel parameters from small-footprint full-waveform LiDAR data. *International journal of wildland fire*, *23*(2), pp.224-233.

Hernández-Stefanoni, J.L., Reyes-Palomeque, G., Castillo-Santiago, M.Á., George-Chacón, S.P., Huechacona-Ruiz, A.H., Tun-Dzul, F., Rondon-Rivera, D. and Dupuy, J.M., 2018. Effects of sample plot size and GPS location errors on aboveground biomass estimates from LiDAR in tropical dry forests. *Remote Sensing*, 10(10), p.1586.

Herold, M., Carter, S., Avitabile, V., Espejo, A.B., Jonckheere, I., Lucas, R., McRoberts, R.E., Næsset, E., Nightingale, J., Petersen, R. and Reiche, J., 2019. The role and need for space-based forest biomass-related measurements in environmental management and policy. *Surveys in Geophysics*, pp.1-22.

Hijmans, R.J., 2018. raster: Geographic Data Analysis and Modeling. R package version 2.8-4. Available online: https://CRAN.R-project.org/package=raster

Hiraishi, T. ed., 2014. *2013 Revised Supplementary Methods and Good Practice Guidance Arising from the Kyoto Protocol*. Intergovernmental Panel on Climate Change.

Hislop, S., Jones, S., Soto-Berelov, M., Skidmore, A., Haywood, A. and Nguyen, T.H., 2018. Using landsat spectral indices in time-series to assess wildfire disturbance and recovery. *Remote sensing*, 10(3), p.460.

Holden, J., Evans, M.G., Burt, T.P. and Horton, M., 2006. Impact of land drainage on peatland hydrology. *Journal of Environmental Quality*, *35*(5), pp.1764-1778.

Holden, J., 2005. Peatland hydrology and carbon release: why small-scale process matters. *Philosophical Transactions of the Royal Society A: Mathematical, Physical and Engineering Sciences*, *363*(1837), pp.2891-2913.

Hooijer, A., Page, S., Navratil, P., Vernimmen, R., van der Vat, M., Tansey, K., Konecny, K., Siegert, F., Ballhorn, U. and Mawdsley, N., 2014. Carbon emissions from drained and degraded peatland in Indonesia and emission factors for measurement, reporting and verification (MRV) of peatland greenhouse gas emissions–a summary of KFCP research results for practitioners. *IAFCP, Jakarta, Indonesia*.

Hooijer, A., Page, S., Jauhiainen, J., Lee, W.A., Lu, X.X., Idris, A. and Anshari, G., 2012. Subsidence and carbon loss in drained tropical peatlands. *Biogeosciences*, *9*(3), pp.1053-1071.

Hooijer, A., Page, S., Canadell, J.G., Silvius, M., Kwadijk, J., Wosten, H. and Jauhiainen, J., 2010. Current and future CO2 emissions from drained peatlands in Southeast Asia. *Biogeosciences*.

Hooijer, A., Silvius, M., Wösten, H., Page, S., Hooijer, A., Silvius, M., Wösten, H. and Page, S., 2006. PEAT-CO2. *Assessment of CO2 emissions from drained peatlands in SE Asia, Delft Hydraulics report Q*, *3943*.

Hopkinson, C., Chasmer, L.E., Sass, G., Creed, I.F., Sitar, M., Kalbfleisch, W. and Treitz, P., 2005. Vegetation class dependent errors in lidar ground elevation and canopy height estimates in a boreal wetland environment. *Canadian Journal of Remote Sensing*, *31*(2), pp.191-206.

Hoscilo, A., Page, S.E., Tansey, K.J. and Rieley, J.O., 2011. Effect of repeated fires on land-cover change on peatland in southern Central Kalimantan, Indonesia, from 1973 to 2005. *International Journal of Wildland Fire*, *20*(4), pp.578-588.

Hoyos-Santillan, J., Lomax, B.H., Large, D., Turner, B.L., Lopez, O.R., Boom, A., Sepulveda-Jauregui, A. and Sjögersten, S., 2019. Evaluation of vegetation communities, water table, and peat composition as drivers of greenhouse gas emissions in lowland tropical peatlands. *Science of The Total Environment*.

Hoyos-Santillan, J., Lomax, B.H., Large, D., Turner, B.L., Boom, A., Lopez, O.R. and Sjögersten, S., 2016. Quality not quantity: organic matter composition controls of CO2 and CH4 fluxes in neotropical peat profiles. *Soil Biology and Biochemistry*, *103*, pp.86-96.

Huang, S., Ramirez, C., McElhaney, M. and Evans, K., 2018. F3: Simulating spatiotemporal forest change from field inventory, remote sensing, growth modelling, and management actions. *Forest ecology and management*, 415, pp.26-37.

Hyyppä, J., Hyyppä, H., Leckie, D., Gougeon, F., Yu, X. and Maltamo, M., 2008. Review of methods of small-footprint airborne laser scanning for extracting forest inventory data in boreal forests. *International Journal of Remote Sensing*, *29*(5), pp.1339-1366.

Intergovernmental Panel on Climate Change (IPCC). Summary for Policymakers. In Climate Change 2007: The Physical Science Basis. Contribution of Working Group I to the Fourth Assessment; Solomon, S., Qin, D., Manning, M., Chen, Z., Marquis, M., Averyt, K.B., Tignor, M., Miller, H.L., Eds.; Report of the Intergovernmental Panel on Climate Change; Cambridge University Press: Cambridge, UK, 2007.

IPCC. Hiraishi, T., Krug, T., Tanabe, K., Srivastava, N., Baasansuren, J., Fukuda, M. and Troxler, T.G., 2014. 2013 supplement to the 2006 IPCC guidelines for national greenhouse gas inventories: Wetlands. *IPCC, Switzerland*.

Irvine, K., Vermette, S. and Mustafa, F.B., 2012, October. The “black waters” of Malaysia: tracking water quality from the peat swamp forest to the sea. In *2012 International Symposium on Geomatics for Integrated Water Resource Management* (pp. 1-6). IEEE.

Jackson, C.R., Liew, K.C. and Yule, C.M., 2009. Structural and functional changes with depth in microbial communities in a tropical Malaysian peat swamp forest. *Microbial ecology*, *57*(3), p.402.

Jaenicke, J., Wösten, H., Budiman, A. and Siegert, F., 2010. Planning hydrological restoration of peatlands in Indonesia to mitigate carbon dioxide emissions. *Mitigation and Adaptation Strategies for Global Change*, *15*(3), pp.223-239.

Jaenicke, J., Rieley, J.O., Mott, C., Kimman, P. and Siegert, F., 2008. Determination of the amount of carbon stored in Indonesian peatlands. *Geoderma*, *147*(3-4), pp.151-158.

Jauhiainen, J., Kerojoki, O., Silvennoinen, H., Limin, S. and Vasander, H., 2014. Heterotrophic respiration in drained tropical peat is greatly affected by temperature—a passive ecosystem cooling experiment. *Environmental Research Letters*, *9*(10), p.105013.

Jauhiainen, J., Hooijer, A. and Page, S.E., 2012. Carbon dioxide emissions from an Acacia plantation on peatland in Sumatra, Indonesia. *Biogeosciences*.

Jauhiainen, J., Limin, S., Silvennoinen, H. and Vasander, H., 2008. Carbon dioxide and methane fluxes in drained tropical peat before and after hydrological restoration. *Ecology*, *89*(12), pp.3503-3514.

Jauhiainen, J., Takahashi, H., Heikkinen, J.E., Martikainen, P.J. and Vasander, H., 2005. Carbon fluxes from a tropical peat swamp forest floor. *Global Change Biology*, *11*(10), pp.1788-1797.

Jin, S., Su, Y., Gao, S., Hu, T., Liu, J. and Guo, Q., 2018. The Transferability of Random Forest in Canopy Height Estimation from Multi-Source Remote Sensing Data. *Remote Sensing*, *10*(8), p.1183.

Jonsson, M. and Wardle, D.A., 2009. Structural equation modelling reveals plant-community drivers of carbon storage in boreal forest ecosystems. *Biology letters*, *6*(1), pp.116-119.

Jordan, C.F., 1969. Derivation of leaf-area index from quality of light on the forest floor. *Ecology*, *50*(4), pp.663-666.

Jubanski, J., Ballhorn, U., Kronseder, K., Franke, J. and Siegert, F., 2013. Detection of large above-ground biomass variability in lowland forest ecosystems by airborne LiDAR. *Biogeosciences*, *10*(6), pp.3917-3930.

Karlson, M., Ostwald, M., Reese, H., Sanou, J., Tankoano, B. and Mattsson, E., 2015. Mapping tree canopy cover and aboveground biomass in Sudano-Sahelian woodlands using Landsat 8 and random forest. *Remote Sensing*, *7*(8), pp.10017-10041.

Kauffman, J.B., Trejo, H.H., Garcia, M.D.C.J., Heider, C. and Contreras, W.M., 2016. Carbon stocks of mangroves and losses arising from their conversion to cattle pastures in the Pantanos de Centla, Mexico. *Wetlands Ecology and Management*, *24*(2), pp.203-216.

Kelsey, K.C. and Neff, J.C., 2014. Estimates of aboveground biomass from texture analysis of Landsat imagery. *Remote Sensing*, 6(7), pp.6407-6422.

Kemp, A.C., Horton, B.P., Nikitina, D., Vane, C.H., Potapova, M., Weber-Bruya, E., Culver, S.J., Repkina, T. and Hill, D.F., 2017. The distribution and utility of sea-level indicators in Eurasian sub-Arctic salt marshes (White Sea, Russia). *Boreas*, *46*(3), pp.562-584.

Kennedy, R.E., Andréfouët, S., Cohen, W.B., Gómez, C., Griffiths, P., Hais, M., Healey, S.P., Helmer, E.H., Hostert, P., Lyons, M.B. and Meigs, G.W., 2014. Bringing an ecological view of change to Landsat-based remote sensing. *Frontiers in Ecology and the Environment*, 12(6), pp.339-346.

Kennedy, R.E., Townsend, P.A., Gross, J.E., Cohen, W.B., Bolstad, P., Wang, Y.Q. and Adams, P., 2009. Remote sensing change detection tools for natural resource managers: Understanding concepts and tradeoffs in the design of landscape monitoring projects. *Remote sensing of environment*, 113(7), pp.1382-1396.

Kettridge, N., Comas, X., Baird, A., Slater, L., Strack, M., Thompson, D., Jol, H. and Binley, A., 2008. Ecohydrologically important subsurface structures in peatlands revealed by ground-penetrating radar and complex conductivity surveys. *Journal of Geophysical Research: Biogeosciences*, *113*(G4).

Kim, S., McGaughey, R.J., Andersen, H.E. and Schreuder, G., 2009. Tree species differentiation using intensity data derived from leaf-on and leaf-off airborne laser scanner data. *Remote Sensing of Environment*, *113*(8), pp.1575-1586.

Koh, L.P., Miettinen, J., Liew, S.C. and Ghazoul, J., 2011. Remotely sensed evidence of tropical peatland conversion to oil palm. *Proceedings of the National Academy of Sciences*, *108*(12), pp.5127-5132.

Kolka, R.K., Murdiyarso, D., Kauffman, J.B. and Birdsey, R.A., 2016. Tropical wetlands, climate, and land-use change: adaptation and mitigation opportunities. *Wetlands Ecology and Management*, *24*(2), pp.107-112.

Konecny, K., Ballhorn, U., Navratil, P., Jubanski, J., Page, S.E., Tansey, K., Hooijer, A., Vernimmen, R. and Siegert, F., 2016. Variable carbon losses from recurrent fires in drained tropical peatlands. *Global Change Biology*, *22*(4), pp.1469-1480.

Kool, D.M., Buurman, P. and Hoekman, D.H., 2006. Oxidation and compaction of a collapsed peat dome in Central Kalimantan. *Geoderma*, *137*(1-2), pp.217-225.

Korhonen, L., Packalen, P. and Rautiainen, M., 2017. Comparison of Sentinel-2 and Landsat 8 in the estimation of boreal forest canopy cover and leaf area index. *Remote sensing of environment*, 195, pp.259-274

Krankina, O.N., Pflugmacher, D., Friedl, M., Cohen, W.B., Nelson, P. and Baccini, A., 2008. Meeting the challenge of mapping peatlands with remotely sensed data. *Biogeosciences*, *5*(6), pp.1809-1820.

Kronseder, K., Ballhorn, U., Böhm, V. and Siegert, F., 2012. Above ground biomass estimation across forest types at different degradation levels in Central Kalimantan using LiDAR data. *International Journal of Applied Earth Observation and Geoinformation*, *18*, pp.37-48.

Lampela, M., Jauhiainen, J. and Vasander, H., 2014. Surface peat structure and chemistry in a tropical peat swamp forest. *Plant and soil*, *382*(1-2), pp.329-347.

Langner, A. and Siegert, F., 2009. Spatiotemporal fire occurrence in Borneo over a period of 10 years. *Global Change Biology*, *15*(1), pp.48-62.

Langner, A., Miettinen, J. and Siegert, F., 2007. Land cover change 2002–2005 in Borneo and the role of fire derived from MODIS imagery. *Global Change Biology*, *13*(11), pp.2329-2340.

Langton, S.D., Briggs, P.A. and Haysom, K.A., 2010. Daubenton's bat distribution along rivers–developing and testing a predictive model. *Aquatic Conservation: Marine and Freshwater Ecosystems*, *20*(S1), pp.S45-S54.

Lary, D.J., Alavi, A.H., Gandomi, A.H. and Walker, A.L., 2016. Machine learning in geosciences and remote sensing. *Geoscience Frontiers*, *7*(1), pp.3-10.

Lary, D.J., Remer, L.A., MacNeill, D., Roscoe, B. and Paradise, S., 2009. Machine learning and bias correction of MODIS aerosol optical depth. *IEEE Geoscience and Remote Sensing Letters*, *6*(4), pp.694-698.

LAStools, 2017. “Efficient LiDAR Processing Software” (Version 141017, Academic). Available online: http://rapidlasso.com/LAStools (accessed on 2 October 2017).

Laurin, G.V., Puletti, N., Hawthorne, W., Liesenberg, V., Corona, P., Papale, D., Chen, Q. and Valentini, R., 2016. Discrimination of tropical forest types, dominant species, and mapping of functional guilds by hyperspectral and simulated multispectral Sentinel-2 data. *Remote Sensing of Environment*, *176*, pp.163-176.

Lawrence, R.L., Wood, S.D. and Sheley, R.L., 2006. Mapping invasive plants using hyperspectral imagery and Breiman Cutler classifications (RandomForest). *Remote Sensing of Environment*, *100*(3), pp.356-362.

Lawson, I.T., Kelly, T.J., Aplin, P., Boom, A., Dargie, G., Draper, F.C.H., Hassan, P.N.Z.B.P., Hoyos-Santillan, J., Kaduk, J., Large, D. and Murphy, W., 2015. Improving estimates of tropical peatland area, carbon storage, and greenhouse gas fluxes. *Wetlands ecology and management*, *23*(3), pp.327-346.

Li, M., Im, J., Quackenbush, L.J. and Liu, T., 2014. Forest biomass and carbon stock quantification using airborne LiDAR data: A case study over Huntington Wildlife Forest in the Adirondack Park. *IEEE Journal of Selected Topics in Applied Earth Observations and Remote Sensing*, *7*(7), pp.3143-3156.

Lim, K., Treitz, P., Wulder, M., St-Onge, B. and Flood, M., 2003. LiDAR remote sensing of forest structure. *Progress in physical geography*, *27*(1), pp.88-106.

Lindberg, E., Olofsson, K., Holmgren, J. and Olsson, H., 2012. Estimation of 3D vegetation structure from waveform and discrete return airborne laser scanning data. *Remote Sensing of Environment*, *118*, pp.151-161.

Loveland, T.R. and Dwyer, J.L., 2012. Landsat: Building a strong future. *Remote Sensing of Environment*, *122*, pp.22-29.

Lu, M., Hamunyela, E., Verbesselt, J. and Pebesma, E., 2017. Dimension reduction of multi-spectral satellite image time series to improve deforestation monitoring. *Remote Sensing*, *9*(10), p.1025.

Lu, D., Chen, Q., Wang, G., Liu, L., Li, G. and Moran, E., 2016. A survey of remote sensing-based aboveground biomass estimation methods in forest ecosystems. *International Journal of Digital Earth*, 9(1), pp.63-105.

Lu, D., Chen, Q., Wang, G., Moran, E., Batistella, M., Zhang, M., Vaglio Laurin, G. and Saah, D., 2012. Aboveground forest biomass estimation with Landsat and LiDAR data and uncertainty analysis of the estimates. *International Journal of Forestry Research*, *2012*.

Lu, D., 2006. The potential and challenge of remote sensing-based biomass estimation. *International journal of remote sensing*, *27*(7), pp.1297-1328.

Lu, D., 2005. Aboveground biomass estimation using Landsat TM data in the Brazilian Amazon. *International Journal of Remote Sensing*, *26*(12), pp.2509-2525.

Madadi, M.R., Azamathulla, H.M. and Yakhkeshi, M., 2015. Application of Google earth to investigate the change of flood inundation area due to flood detention dam. *Earth Science Informatics*, *8*(3), pp.627-638.

Magruder, L.A., Neuenschwander, A.L., Marmillion, S.P. and Tweddale, S.A., 2010, April. Obstruction detection comparison of small-footprint full-waveform and discrete return lidar. In *Laser Radar Technology and Applications XV* (Vol. 7684, p. 768410). International Society for Optics and Photonics.

Main-Knorn, M., Moisen, G.G., Healey, S.P., Keeton, W.S., Freeman, E.A. and Hostert, P., 2011. Evaluating the remote sensing and inventory-based estimation of biomass in the Western Carpathians. *Remote Sensing*, *3*(7), pp.1427-1446.

Majasalmi, T. and Rautiainen, M., 2016. The potential of Sentinel-2 data for estimating biophysical variables in a boreal forest: a simulation study. *Remote Sensing Letters*, *7*(5), pp.427-436.

Mallet, C. and Bretar, F., 2009. Full-waveform topographic lidar: State-of-the-art. *ISPRS Journal of photogrammetry and remote sensing*, *64*(1), pp.1-16.

Maltamo, M., Eerikäinen, K., Packalén, P. and Hyyppä, J., 2006. Estimation of stem volume using laser scanning-based canopy height metrics. *Forestry*, 79(2), pp.217-229.

Manuri, S., Andersen, H.E., McGaughey, R.J. and Brack, C., 2017. Assessing the influence of return density on estimation of lidar-based aboveground biomass in tropical peat swamp forests of Kalimantan, Indonesia. *International journal of applied earth observation and geoinformation*, *56*, pp.24-35.

Manuri, S., Brack, C., Nugroho, N.P., Hergoualc'h, K., Novita, N., Dotzauer, H., Verchot, L., Putra, C.A.S. and Widyasari, E., 2014. Tree biomass equations for

tropical peat swamp forest ecosystems in Indonesia. *Forest Ecology and Management*, *334*, pp.241-253.

Margono, B.A., Potapov, P.V., Turubanova, S., Stolle, F. and Hansen, M.C., 2014a. Primary forest cover loss in Indonesia over 2000–2012. *Nature climate change*, *4*(8), p.730.

Margono, B.A., Bwangoy, J.R.B., Potapov, P.V. and Hansen, M.C., 2014b. Mapping wetlands in Indonesia using Landsat and PALSAR data-sets and derived topographical indices. *Geo-spatial Information Science*, *17*(1), pp.60-71.

Markham, B.L. and Helder, D.L., 2012. Forty-year calibrated record of earth-reflected radiance from Landsat: A review. *Remote Sensing of Environment*, *122*, pp.30-40.

Marshall, C., Large, D.J., Athab, A., Evers, S.L., Sowter, A., Marsh, S. and Sjögersten, S., 2018. Monitoring tropical peat related settlement using ISBAS InSAR, Kuala Lumpur International Airport (KLIA). *Engineering Geology*, *244*, pp.57-65.

Martin, A.R. and Thomas, S.C., 2011. A reassessment of carbon content in tropical trees. *PloS one*, *6*(8), p.e23533.

Masek, J.G., Vermote, E.F., Saleous, N.E., Wolfe, R., Hall, F.G., Huemmrich, K.F., Gao, F., Kutler, J. and Lim, T.K., 2006. A Landsat surface reflectance dataset for North America, 1990-2000. *IEEE Geoscience and Remote Sensing Letters*, *3*(1), pp.68-72.

Mather, P.M. and Koch, M., 2011. *Computer processing of remotely-sensed images: an introduction*. John Wiley & Sons.

Mauya, E.W., Hansen, E.H., Gobakken, T., Bollandsås, O.M., Malimbwi, R.E. and Næsset, E., 2015. Effects of field plot size on prediction accuracy of aboveground biomass in airborne laser scanning-assisted inventories in tropical rain forests of Tanzania. *Carbon balance and management*, 10(1), p.10.

Maxwell, A.E., Warner, T.A. and Fang, F., 2018. Implementation of machine-learning classification in remote sensing: An applied review. *International Journal of Remote Sensing*, *39*(9), pp.2784-2817.

Miettinen, J., Shi, C. and Liew, S.C., 2016. Land cover distribution in the peatlands of Peninsular Malaysia, Sumatra and Borneo in 2015 with changes since 1990. *Global Ecology and Conservation*, *6*, pp.67-78.

Miettinen, J., Shi, C. and Liew, S.C., 2012a. Two decades of destruction in Southeast Asia's peat swamp forests. *Frontiers in Ecology and the Environment*, *10*(3), pp.124-128.

Miettinen, J., Hooijer, A., Tollenaar, D., Page, S., Malins, C., Vernimmen, R., Shi, C. and Liew, S.C., 2012b. Historical analysis and projection of oil palm plantation expansion on peatland in Southeast Asia. *ICCT White Paper*, *17*.

Miettinen, J., Hooijer, A., Shi, C., Tollenaar, D., Vernimmen, R., Liew, S.C., Malins, C. and Page, S.E., 2012c. Extent of industrial plantations on Southeast Asian peatlands in 2010 with analysis of historical expansion and future projections. *Gcb Bioenergy*, *4*(6), pp.908-918.

Miettinen, J., Shi, C. and Liew, S.C., 2011. Deforestation rates in insular Southeast Asia between 2000 and 2010. *Global Change Biology*, *17*(7), pp.2261-2270.

Miettinen, J. and Liew, S.C., 2010. Degradation and development of peatlands in Peninsular Malaysia and in the islands of Sumatra and Borneo since 1990. *Land degradation & development*, *21*(3), pp.285-296.

Mika, M. and Siejka, M., 2016. The Use of Handheld Navigation Receivers GARMIN GPSmap62st for the Unambiguous Identifi cation of the Cadastral Plots in the Field. *Geomatics and Environmental Engineering*, 10.

Minasny, B., Berglund, Ö., Connolly, J., Hedley, C., de Vries, F., Gimona, A., Kempen, B., Kidd, D., Lilja, H., Malone, B. and McBratney, A., 2019. Digital mapping of peatlands–A critical review. *Earth-Science Reviews*.

Minasny, B., Setiawan, B.I., Saptomo, S.K. and McBratney, A.B., 2018. Open digital mapping as a cost-effective method for mapping peat thickness and assessing the carbon stock of tropical peatlands. *Geoderma*, *313*, pp.25-40.

Mishra, S., Lee, W.A., Hooijer, A., Reuben, S., Sudiana, I.M., Idris, A. and Swarup, S., 2014. Microbial and metabolic profiling reveal strong influence of water table and land-use patterns on classification of degraded tropical peatlands. *Biogeosciences*, *11*(7), pp.1727-1741.

Mitchard, E.T., Saatchi, S.S., White, L., Abernethy, K., Jeffery, K.J., Lewis, S.L., Collins, M., Lefsky, M.A., Leal, M.E., Woodhouse, I.H. and Meir, P., 2012. Mapping tropical forest biomass with radar and spaceborne LiDAR in Lopé National Park,

Gabon: overcoming problems of high biomass and persistent cloud. *Biogeosciences*, *9*(1), pp.179-191.

Moffiet, T., Mengersen, K., Witte, C., King, R. and Denham, R., 2005. Airborne laser scanning: Exploratory data analysis indicates potential variables for classification of individual trees or forest stands according to species. *ISPRS Journal of Photogrammetry and Remote Sensing*, *59*(5), pp.289-309.

Mora, B., Wulder, M.A., Hobart, G.W., White, J.C., Bater, C.W., Gougeon, F.A., Varhola, A. and Coops, N.C., 2013. Forest inventory stand height estimates from very high spatial resolution satellite imagery calibrated with lidar plots. *International journal of remote sensing*, *34*(12), pp.4406-4424.

Murdiyarso, D., Lilleskov, E. and Kolka, R., 2019. Tropical peatlands under siege: the need for evidence-based policies and strategies. *Mitigation and adaptation strategies for global change*, *24*(4), pp.493-505.

Murdiyarso, D., Hergoualc'h, K. and Verchot, L.V., 2010. Opportunities for reducing greenhouse gas emissions in tropical peatlands. *Proceedings of the National Academy of Sciences*, *107*(46), pp.19655-19660.

Mutanga, O., Adam, E. and Cho, M.A., 2012. High density biomass estimation for wetland vegetation using WorldView-2 imagery and random forest regression algorithm. *International Journal of Applied Earth Observation and Geoinformation*, *18*, pp.399-406.

Næsset, E., Ørka, H.O., Solberg, S., Bollandsås, O.M., Hansen, E.H., Mauya, E., Zahabu, E., Malimbwi, R., Chamuya, N., Olsson, H. and Gobakken, T., 2016. Mapping and estimating forest area and aboveground biomass in miombo woodlands in Tanzania using data from airborne laser scanning, TanDEM-X, RapidEye, and global forest maps: A comparison of estimated precision. *Remote Sensing of Environment*, 175, pp.282-300.

Næsset, E. and Gobakken, T., 2008. Estimation of above-and below-ground biomass across regions of the boreal forest zone using airborne laser. *Remote Sensing of Environment*, *112*(6), pp.3079-3090.

Næsset, E., 2004. Practical large-scale forest stand inventory using a small-footprint airborne scanning laser. *Scandinavian Journal of Forest Research*, *19*(2), pp.164-179.

Nagendra, H., Lucas, R., Honrado, J.P., Jongman, R.H., Tarantino, C., Adamo, M. and Mairota, P., 2013. Remote sensing for conservation monitoring: Assessing

protected areas, habitat extent, habitat condition, species diversity, and threats. *Ecological Indicators*, 33, pp.45-59.

Neuenschwander, A.L., Magruder, L.A. and Tyler, M., 2009. Landcover classification of small-footprint, full-waveform lidar data. *Journal of applied remote sensing*, *3*(1), p.033544.

Newell, A.J., Vane, C.H., Sorensen, J.P., Moss-Hayes, V. and Gooddy, D.C., 2016. Long-term Holocene groundwater fluctuations in a chalk catchment: evidence from Rock-Eval pyrolysis of riparian peats. *Hydrological processes*, *30*(24), pp.4556-4567.

Ng, P.K., Tay, J.B. and Lim, K.K., 1994. Diversity and conservation of blackwater fishes in Peninsular Malaysia, particularly in the North Selangor peat swamp forest. *Hydrobiologia*, *285*(1-3), pp.203-218.

Nguyen, H.T., Hutyra, L.R., Hardiman, B.S. and Raciti, S.M., 2016. Characterizing forest structure variations across an intact tropical peat dome using field samplings and airborne Li DAR. *Ecological applications*, *26*(2), pp.587-601.

Nichol, J.E. and Sarker, M.L.R., 2010. Improved biomass estimation using the texture parameters of two high-resolution optical sensors. *IEEE Transactions on Geoscience and Remote Sensing*, *49*(3), pp.930-948.

Nie, S., Wang, C., Zeng, H., Xi, X. and Li, G., 2017. Above-ground biomass estimation using airborne discrete-return and full-waveform LiDAR data in a coniferous forest. *Ecological Indicators*, *78*, pp.221-228.

Ni-Meister, W. and Lee, S., 2016, December. Allometric Relationship between Full Waveform LiDAR measurements and Above-ground Biomass. In *AGU Fall Meeting Abstracts*.

Ni-Meister, W., Lee, S., Strahler, A.H., Woodcock, C.E., Schaaf, C., Yao, T., Ranson, K.J., Sun, G. and Blair, J.B., 2010. Assessing general relationships between aboveground biomass and vegetation structure parameters for improved carbon estimate from lidar remote sensing. *Journal of Geophysical Research: Biogeosciences*, *115*(G2).

Ning, H.A.N., Jing, W.U., Tahmassebi, A.R.S., XU, H.W. and Ke, W.A.N.G., 2011. NDVI-based lacunarity texture for improving identification of torreya using object-oriented method. *Agricultural Sciences in China*, 10(9), pp.1431-1444.

O'Shea, T., 2019. Developing The World's First Indicator Of Forest Carbon Stocks & Emissions – Update: IT'S WORKING!. Available online: https://www.planet.com/pulse/developing-the-worlds-first-indicator-of-forest-carbon-stocks-emissions/ (accessed on 3 July 2019)

Padfield, R., Waldron, S., Drew, S., Papargyropoulou, E., Kumaran, S., Page, S., Gilvear, D., Armstrong, A., Evers, S., Williams, P. and Zakaria, Z., 2014. Research agendas for the sustainable management of tropical peatland in Malaysia. *Environmental Conservation*, *42*(1), pp.73-83.

Page, S.E. and Hooijer, A., 2016. In the line of fire: the peatlands of Southeast Asia. Philosophical Transactions of the Royal Society B: *Biological Sciences*, 371(1696).

Page, S.E., Rieley, J.O. and Banks, C.J., 2011. Global and regional importance of the tropical peatland carbon pool. *Global Change Biology*, *17*(2), pp.798-818.

Page, S., Hoscilo, A., Langner, A., Tansey, K., Siegert, F., Limin, S. and Rieley, J., 2009a. Tropical peatland fires in Southeast Asia. In *Tropical fire ecology* (pp. 263-287). Springer, Berlin, Heidelberg.

Page, S., Hosciło, A., Wösten, H., Jauhiainen, J., Silvius, M., Rieley, J., Ritzema, H., Tansey, K., Graham, L., Vasander, H. and Limin, S., 2009b. Restoration ecology of lowland tropical peatlands in Southeast Asia: current knowledge and future research directions. *Ecosystems*, *12*(6), pp.888-905.

Page, S.E., Banks, C.J. and Rieley, J.O., 2007. Tropical peatlands: distribution, extent and carbon storage-uncertainties and knowledge gaps. *Peatlands International*, *2*(2), pp.26-27.

Page, S.E., Wűst, R.A.J., Weiss, D., Rieley, J.O., Shotyk, W. and Limin, S.H., 2004. A record of Late Pleistocene and Holocene carbon accumulation and climate change from an equatorial peat bog (Kalimantan, Indonesia): implications for past, present and future carbon dynamics. *Journal of Quaternary Science*, *19*(7), pp.625-635.

Page, S.E., Siegert, F., Rieley, J.O., Boehm, H.D.V., Jaya, A. and Limin, S., 2002. The amount of carbon released from peat and forest fires in Indonesia during 1997. *Nature*, *420*(6911), p.61.

Page, S.E., Rieley, J.O., Shotyk, Ø.W. and Weiss, D., 1999. Interdependence of peat and vegetation in a tropical peat swamp forest. In *Changes And Disturbance In Tropical Rainforest In South-East Asia* (pp. 161-173).

Palace, Michael W., Franklin B. Sullivan, Mark J. Ducey, Robert N. Treuhaft, Christina Herrick, Julia Z. Shimbo, and Jonas Mota-E-Silva. "Estimating forest structure in a tropical forest using field measurements, a synthetic model and discrete return lidar data." *Remote Sensing of Environment* 161 (2015): 1-11.

Pan, Y., Birdsey, R.A., Fang, J., Houghton, R., Kauppi, P.E., Kurz, W.A., Phillips, O.L., Shvidenko, A., Lewis, S.L., Canadell, J.G. and Ciais, P., 2011. A large and persistent carbon sink in the world's forests. *Science*, *333*(6045), pp.988-993.

Pandit, S., Tsuyuki, S. and Dube, T., 2018. Estimating above-ground biomass in sub-tropical buffer zone community forests, Nepal, using Sentinel 2 data. *Remote Sensing*, *10*(4), p.601.

Pang, Y., Li, Z., Ju, H., Lu, H., Jia, W., Si, L., Guo, Y., Liu, Q., Li, S., Liu, L. and Xie, B., 2016. LiCHy: The CAF's LiDAR, CCD and hyperspectral integrated airborne observation system. *Remote Sensing*, *8*(5), p.398.

Panta, M., Kim, K. and Joshi, C., 2008. Temporal mapping of deforestation and forest degradation in Nepal: applications to forest conservation. *Forest Ecology and Management*, 256(9), pp.1587-1595.

Parish, F., Dahalan, M., and Rahim, H,.2014. Integrated Management Plan for North Selangor Peat Swamp Forest 2014-2023 for Selangor State Forestry Department. Draft (30 June 2014) Revision 2.4. Prepared by Global Environment Centre.

Peduzzi, A., Wynne, R.H., Fox, T.R., Nelson, R.F. and Thomas, V.A., 2012. Estimating leaf area index in intensively managed pine plantations using airborne laser scanner data. *Forest Ecology and Management*, *270*, pp.54-65.

Pettorelli, N., Schulte to Buehne, H., Shapiro, A. and Glover-Kapfer, P., 2018. Conservation Technology Series Issue 4: SATELLITE REMOTE SENSING FOR CONSERVATION. WWF United Kingdom.

Pettorelli, N., Laurance, W.F., O'Brien, T.G., Wegmann, M., Nagendra, H. and Turner, W., 2014. Satellite remote sensing for applied ecologists: opportunities and challenges. *Journal of Applied Ecology*, 51(4), pp.839-848.

Pflugmacher, D., Cohen, W.B., Kennedy, R.E. and Yang, Z., 2014. Using Landsat-derived disturbance and recovery history and lidar to map forest biomass dynamics. *Remote Sensing of Environment*, *151*, pp.124-137.

Pflugmacher, D., Cohen, W.B. and Kennedy, R.E., 2012. Using Landsat-derived disturbance history (1972–2010) to predict current forest structure. *Remote Sensing of Environment, 122,* pp.146-165.

Pirotti, F., Laurin, G., Vettore, A., Masiero, A. and Valentini, R., 2014. Small footprint full-waveform metrics contribution to the prediction of biomass in tropical forests. *Remote Sensing, 6*(10), pp.9576-9599.

Popescu, S.C., Zhao, K., Neuenschwander, A. and Lin, C., 2011. Satellite lidar vs. small footprint airborne lidar: Comparing the accuracy of aboveground biomass estimates and forest structure metrics at footprint level. *Remote Sensing of Environment, 115*(11), pp.2786-2797.

Posa, M.R.C., Wijedasa, L.S. and Corlett, R.T., 2011. Biodiversity and conservation of tropical peat swamp forests. BioScience, 61(1), pp.49-57.

Prentice, R.C., 2011. The Peatland Biodiversity Management Toolbox: A Handbook for the Conservation and Management of Peatland Biodiversity in Southeast Asia. *A Compilation. ASEAN Peatland Forests Project–Rehabilitation and Sustainable Use of Peatland Forests in Southeast Asia. ASEAN Secretariat and the Global Environment Centre*.

Prentice, C. and Aikanathan, S., 1989. A preliminary faunal assessment of the North Selangor Peat swamp Forest. *Asian Wetland Bureau, Kuala Lumpur*.

Reddy, A.D., Hawbaker, T.J., Wurster, F., Zhu, Z., Ward, S., Newcomb, D. and Murray, R., 2015. Quantifying soil carbon loss and uncertainty from a peatland wildfire using multi-temporal LiDAR. *Remote Sensing of Environment, 170,* pp.306-316.

Reed, M.S., Bonn, A., Evans, C., Glenk, K. and Hansjurgens, B., 2014. Assessing and valuing peatland ecosystem services for sustainable management. *Ecosystem Services, 9,* pp.1-4

Regional Centre for Forest Management (RCFM) and Ecosystem Management Services (EMS). 2000. Report on The Management Inventory of the North Selangor Peat Swamp Forest; Malaysian-DANCED Project on Sustainable Managment of Peat Swamp Forest; Project Document Number 25; Malaysia Office: Petaling Jaya, Malaysia.

Rein, G., Cleaver, N., Ashton, C., Pironi, P. and Torero, J.L., 2008. The severity of smouldering peat fires and damage to the forest soil. *Catena*, *74*(3), pp.304-309.

Rengasamy, N., Parish, F., Lew, S.Y., and Azura, N., 2016. Peatland Rehabilitation Efforts in North Selangor Peat Swamp Forests. Paper presented at 15th International Peat Congress, Sarawak, Malaysia, August 15–19.

Regional Centre for Forest Management (RCFM) and Ecosystem Management Services (EMS). Report on The Management Inventory of the North Selangor Peat Swamp Forest; Malaysian-DANCED Project on Sustainable Managment of Peat Swamp Forest; Project Document Number 25;Malaysia Office: Petaling Jaya,Malaysia, 2000.

Reijnders, L. and Huijbregts, M.A.J., 2008. Palm oil and the emission of carbon-based greenhouse gases. *Journal of cleaner production*, *16*(4), pp.477-482.

Reitberger, J., Schnörr, C., Krzystek, P. and Stilla, U., 2009. 3D segmentation of single trees exploiting full waveform LIDAR data. *ISPRS Journal of Photogrammetry and Remote Sensing*, *64*(6), pp.561-574.

Reitberger, J., Krzystek, P. and Stilla, U., 2008. Analysis of full waveform LIDAR data for the classification of deciduous and coniferous trees. *International journal of remote sensing*, *29*(5), pp.1407-1431.

Réjou-Méchain, M., Tanguy, A., Piponiot, C., Chave, J. and Hérault, B., 2017. biomass: an r package for estimating above-ground biomass and its uncertainty in tropical forests. *Methods in Ecology and Evolution*, *8*(9), pp.1163-1167.

Richardson, J.J. and Moskal, L.M., 2011. Strengths and limitations of assessing forest density and spatial configuration with aerial LiDAR. *Remote Sensing of Environment*, *115*(10), pp.2640-2651.

Rieley, J. and Page, S., 2016. Tropical peatland of the world. In *Tropical Peatland Ecosystems* (pp. 3-32). Springer, Tokyo.

Rieley, J. and Page, S., 2008. The science of tropical peatlands and the Central Kalimantan peatland development area. *Technical Review*, (1).

Ritzema, H., Limin, S., Kusin, K., Jauhiainen, J. and Wösten, H., 2014. Canal blocking strategies for hydrological restoration of degraded tropical peatlands in Central Kalimantan, Indonesia. *Catena*, *114*, pp.11-20.

Rodríguez-Veiga, P., Wheeler, J., Louis, V., Tansey, K. and Balzter, H., 2017. Quantifying forest biomass carbon stocks from space. Current Forestry Reports, 3(1), pp.1-18.

Rudiyano, B. Minasny, B., Setiawan, B.I., Saptomo, S.K. and McBratney, A.B., 2018. Open digital mapping as a cost-effective method for mapping peat thickness and assessing the carbon stock of tropical peatlands. *Geoderma*, *313*, pp.25-40.

Rudiyano, B. Minasny, B., Setiawan, B.I., Arif, C., Saptomo, S.K. and Chadirin, Y., 2016. Digital mapping for cost-effective and accurate prediction of the depth and carbon stocks in Indonesian peatlands. *Geoderma*, *272*, pp.20-31.

Ruiz, L.A., Hermosilla, T., Mauro, F. and Godino, M., 2014. Analysis of the influence of plot size and LiDAR density on forest structure attribute estimates. *Forests*, 5(5), pp.936-951.

Saatchi, S.S., Harris, N.L., Brown, S., Lefsky, M., Mitchard, E.T., Salas, W., Zutta, B.R., Buermann, W., Lewis, S.L., Hagen, S. and Petrova, S., 2011. Benchmark map of forest carbon stocks in tropical regions across three continents. *Proceedings of the national academy of sciences*, *108*(24), pp.9899-9904.

Saenger, A., Cécillon, L., Sebag, D. and Brun, J.J., 2013. Soil organic carbon quantity, chemistry and thermal stability in a mountainous landscape: a Rock–Eval pyrolysis survey. *Organic Geochemistry*, *54*, pp.101-114.

Safyan, M., 2019. First Up For 2019: PSLV Launch Of 20 Next-Generation Doves., Accessed online: https://www.planet.com/pulse/first-up-for-2019-pslv-launch-of-20-next-generation-doves/ (accessed data 28 June 2019)

Sakamoto, Y., Ishiguro, M. and Kitagawa, G., 1986. Akaike information criterion statistics. *Dordrecht, The Netherlands: D. Reidel*, *81*.

Sandau, R., Brieß, K. and D'Errico, M., 2010. Small satellites for global coverage: Potential and limits. *ISPRS Journal of photogrammetry and Remote Sensing*, *65*(6), pp.492-504.

Saputra, A.D., Setiabudidaya, D., Setyawan, D., Khakim, M.Y.N. and Iskandar, I., 2017, July. Burnscar analysis using normalized burning ratio (NBR) index during 2015 forest fire at Merang-Kepahyang peat forest, South Sumatra, Indonesia. In *AIP Conference Proceedings* (Vol. 1857, No. 1, p. 100001). AIP Publishing.

Sarker, L.R. and Nichol, J.E., 2011. Improved forest biomass estimates using ALOS AVNIR-2 texture indices. *Remote Sensing of Environment*, 115(4), pp.968-977.

Sasidhran, S., Adila, N., Hamdan, M.S., Samantha, L.D., Aziz, N., Kamarudin, N., Puan, C.L., Turner, E. and Azhar, B., 2016. Habitat occupancy patterns and activity rate of native mammals in tropical fragmented peat swamp reserves in Peninsular Malaysia. *Forest Ecology and Management*, *363*, pp.140-148.

Satrio, A.E., Gandaseca, S., Ahmed, O.H. and Majid, N.M., 2009. Effect of logging operation on soil carbon storage of a tropical peat swamp forest. *American Journal of Environmental Sciences*, *5*(6), pp.748-752.

Scharlemann, J.P., Tanner, E.V., Hiederer, R. and Kapos, V., 2014. Global soil carbon: understanding and managing the largest terrestrial carbon pool. *Carbon Management*, *5*(1), pp.81-91.

Schomburg, A., Verrecchia, E.P., Guenat, C., Brunner, P., Sebag, D. and Le Bayon, R.C., 2018. Rock-Eval pyrolysis discriminates soil macro-aggregates formed by plants and earthworms. *Soil Biology and Biochemistry*, *117*, pp.117-124.

Schrier-Uijl, A.P., Silvius, M., Parish, F., Lim, K.H., Rosediana, S. and Anshari, G., 2013. Environmental and social impacts of oil palm cultivation on tropical peat: a scientific review. *Roundtable of Sustainable Palm Oil, Kuala Lumpur, Malaysia*, pp.131-168.

Science Beta, NASA, National Academy of Sciences and NASA's Science Mission Directorate 2016. Available online: https://science.nasa.gov/missions/gedi (accessed on 13 February 2018).

SDG Knowledge platform, 2018. Accessed online: https://sustainabledevelopment.un.org/sdg15 (accessed on 22 January 2018.)

Sebag, D., Verrecchia, E.P., Cécillon, L., Adatte, T., Albrecht, R., Aubert, M., Bureau, F., Cailleau, G., Copard, Y., Decaens, T. and Disnar, J.R., 2016. Dynamics of soil organic matter based on new Rock-Eval indices. *Geoderma*, *284*, pp.185-203.

See, S.W., Balasubramanian, R., Rianawati, E., Karthikeyan, S. and Streets, D.G., 2007. Characterization and source apportionment of particulate matter≤ 2.5 μm in Sumatra, Indonesia, during a recent peat fire episode. *Environmental science & technology*, *41*(10), pp.3488-3494.

Segah, H., Tani, H. and Hirano, T., 2010. Detection of fire impact and vegetation recovery over tropical peat swamp forest by satellite data and ground-based NDVI instrument. *International Journal of Remote Sensing*, *31*(20), pp.5297-5314.

Shang, X. and Chazette, P., 2014. Interest of a full-waveform flown UV lidar to derive forest vertical structures and aboveground carbon. *Forests*, *5*(6), pp.1454-1480.

Shao, Z., Zhang, L. and Wang, L., 2017. Stacked sparse autoencoder modeling using the synergy of airborne LiDAR and satellite optical and SAR data to map forest above-ground biomass. *IEEE Journal of Selected Topics in Applied Earth Observations and Remote Sensing*, *10*(12), pp.5569-5582.

Sharif, M., Stein, A. and Schetselaar, E.M., 2004. Integrated approach to predict confidence of GPS measurement.

Shepherd, P.A., 1997. The relationship between forest structure and peat characteristics in the upper catchment of Sungai Sebangau, Central Kalimantan. *Biodiversity and sustainability of tropical peatlands*.

Shimamura, T. and Momose, K., 2005. Organic matter dynamics control plant species coexistence in a tropical peat swamp forest. *Proceedings of the Royal Society B: Biological Sciences*, *272*(1571), pp.1503-1510.

Siegert, F., Ruecker, G., Hinrichs, A. and Hoffmann, A.A., 2001. Increased damage from fires in logged forests during droughts caused by El Nino. *Nature*, *414*(6862), p.437.

Simpson, J., Wooster, M., Smith, T., Trivedi, M., Vernimmen, R., Dedi, R., Shakti, M. and Dinata, Y., 2016. Tropical peatland burn depth and combustion heterogeneity assessed using UAV photogrammetry and airborne LiDAR. *Remote Sensing*, *8*(12), p.1000.

Six, J., Conant, R.T., Paul, E.A. and Paustian, K., 2002. Stabilization mechanisms of soil organic matter: implications for C-saturation of soils. *Plant and soil*, *241*(2), pp.155-176.

Sjögersten, S., Black, C.R., Evers, S., Hoyos-Santillan, J., Wright, E.L. and Turner, B.L., 2014. Tropical wetlands: A missing link in the global carbon cycle?. *Global biogeochemical cycles*, *28*(12), pp.1371-1386.

Smith, J., Obidzinski, K., Subarudi, S. and Suramenggala, I., 2012. Illegal logging, collusive corruption and fragmented governments in Kalimantan, Indonesia. In *Illegal Logging* (pp. 107-125). Routledge.

Sowter, A., Athab, A., Novellino, A., Grebby, S. and Gee, D., 2018. Supporting energy regulation by monitoring land motion on a regional and national scale: A case study of Scotland. *Proceedings of the Institution of Mechanical Engineers, Part A: Journal of Power and Energy*, *232*(1), pp.85-99.

Sowter, A., Amat, M.B.C., Cigna, F., Marsh, S., Athab, A. and Alshammari, L., 2016. Mexico City land subsidence in 2014–2015 with Sentinel-1 IW TOPS: Results using the Intermittent SBAS (ISBAS) technique. *International journal of applied earth observation and geoinformation*, *52*, pp.230-242.

Sowter, A., Bateson, L., Strange, P., Ambrose, K. and Syafiudin, M.F., 2013. DInSAR estimation of land motion using intermittent coherence with application to the South Derbyshire and Leicestershire coalfields. *Remote Sensing Letters*, *4*(10), pp.979-987.

Suding, K., Higgs, E., Palmer, M., Callicott, J.B., Anderson, C.B., Baker, M., Gutrich, J.J., Hondula, K.L., LaFevor, M.C., Larson, B.M. and Randall, A., 2015. Committing to ecological restoration. *Science*, *348*(6235), pp.638-640.

Sullivan, M.J., Lewis, S.L., Hubau, W., Qie, L., Baker, T.R., Banin, L.F., Chave, J., Cuni‐Sanchez, A., Feldpausch, T.R., Lopez‐Gonzalez, G. and Arets, E., 2018. Field methods for sampling tree height for tropical forest biomass estimation. *Methods in ecology and evolution*, 9(5), pp.1179-1189.

Sullivan, M.J., Talbot, J., Lewis, S.L., Phillips, O.L., Qie, L., Begne, S.K., Chave, J., Cuni-Sanchez, A., Hubau, W., Lopez-Gonzalez, G. and Miles, L., 2017a. Diversity and carbon storage across the tropical forest biome. *Scientific Reports*, *7*, p.39102.

Sullivan, F.B., Ducey, M.J., Orwig, D.A., Cook, B. and Palace, M.W., 2017b. Comparison of lidar-and allometry-derived canopy height models in an eastern deciduous forest. *Forest ecology and management*, *406*, pp.83-94.

Sumnall, M., Fox, T.R., Wynne, R.H. and Thomas, V.A., 2017. Mapping the height and spatial cover of features beneath the forest canopy at small-scales using airborne scanning discrete return Lidar. *ISPRS Journal of Photogrammetry and Remote Sensing*, *133*, pp.186-200.

Sumnall, M.J., Hill, R.A. and Hinsley, S.A., 2016. Comparison of small-footprint discrete return and full waveform airborne LiDAR data for estimating multiple forest variables. *Remote Sensing of Environment*, *173*, pp.214-223.

Sunarto, S., Kelly, M.J., Parakkasi, K., Klenzendorf, S., Septayuda, E. and Kurniawan, H., 2012. Tigers need cover: multi-scale occupancy study of the big cat in Sumatran forest and plantation landscapes. *Plos one*, *7*(1), p.e30859.

Suryadiputra, I.N.N., 2005. guide to the blocking of canals and ditches in conjunction with the community.

Talocchi, 2014. 10 Reasons to Save the Indonesian Peat (Wait, Peat? What's That?), Accessed online: https://www.greenpeace.org/usa/9-reasons-save-peat-wait-whats/. (accessed on 15 December 2018)

Tansey, K., Beston, J., Hoscilo, A., Page, S.E. and Paredes Hernández, C.U., 2008. Relationship between MODIS fire hot spot count and burned area in a degraded tropical peat swamp forest in Central Kalimantan, Indonesia. *Journal of Geophysical Research: Atmospheres*, *113*(D23).

Taufik, M., Setiawan, B.I. and Van Lanen, H.A., 2019. Increased fire hazard in human-modified wetlands in Southeast Asia. *Ambio*, *48*(4), pp.363-373.

Thanh Noi, P. and Kappas, M., 2018. Comparison of random forest, k-nearest neighbor, and support vector machine classifiers for land cover classification using Sentinel-2 imagery. *Sensors*, *18*(1), p.18.

Thapa, R.B., Watanabe, M., Motohka, T., Shiraishi, T. and Shimada, M., 2014. Calibration of aboveground forest carbon stock models for major tropical forests in central Sumatra using airborne LiDAR and field measurement data. *IEEE Journal of Selected Topics in Applied Earth Observations and Remote Sensing*, *8*(2), pp.661-673.

Timothy, D., Onisimo, M. and Riyad, I., 2016. Quantifying aboveground biomass in African environments: A review of the trade-offs between sensor estimation accuracy and costs. *Tropical Ecology*, 57(3), pp.393-405.

Tokola, T., 2015. Remote sensing concepts and their applicability in REDD+ monitoring. *Current forestry reports*, *1*(4), pp.252-260.

Tonks, A.J., Aplin, P., Beriro, D.J., Cooper, H., Evers, S., Vane, C.H. and Sjögersten, S., 2017. Impacts of conversion of tropical peat swamp forest to oil palm plantation

on peat organic chemistry, physical properties and carbon stocks. *Geoderma*, *289*, pp.36-45.

Torbick, N., Ledoux, L., Salas, W. and Zhao, M., 2016. Regional mapping of plantation extent using multisensor imagery. *Remote Sensing*, *8*(3), p.236.

Tsui, O.W., Coops, N.C., Wulder, M.A. and Marshall, P.L., 2013. Integrating airborne LiDAR and space-borne radar via multivariate kriging to estimate above-ground biomass. *Remote Sensing of Environment*, *139*, pp.340-352.

UNFCCC, 2009. Methodological giudance for activities relating to reducing emissions from deforestation and forest degradation and the role of conservation, sustainable management of forests and enhancement of forest carbon stocks in developing countries CU.N.F.C. o. C. Change (Ed.), Decision 4/CP.15, UNFCCC, Copenhagen, Denmark.

Unger, D.R., Hung, I.K., Brooks, R. and Williams, H., 2014. Estimating number of trees, tree height and crown width using Lidar data. *GIScience & remote sensing*, *51*(3), pp.227-238.

Upton, A., Vane, C.H., Girkin, N., Turner, B.L. and Sjögersten, S., 2018. Does litter input determine carbon storage and peat organic chemistry in tropical peatlands?. *Geoderma*, *326*, pp.76-87.

Urbazaev, M., Thiel, C., Cremer, F. and Schmullius, C., 2018, July. Assessment of the Mapping of Aboveground Biomass and its Uncertainties Using Field Measurements, Airborne Lidar and Satellite Data in Mexico. In *IGARSS 2018-2018 IEEE International Geoscience and Remote Sensing Symposium* (pp. 8793-8796). IEEE.

Ussyshkin, V. and Theriault, L., 2011. Airborne lidar: advances in discrete return technology for 3D vegetation mapping. *Remote sensing*, *3*(3), pp.416-434.

van der Werf, G.R., Dempewolf, J., Trigg, S.N., Randerson, J.T., Kasibhatla, P.S., Giglio, L., Murdiyarso, D., Peters, W., Morton, D.C., Collatz, G.J. and Dolman, A.J., 2008. Climate regulation of fire emissions and deforestation in equatorial Asia. *Proceedings of the National Academy of Sciences*, *105*(51), pp.20350-20355.

Verkerk, P.J., Mavsar, R., Giergiczny, M., Lindner, M., Edwards, D. and Schelhaas, M.J., 2014. Assessing impacts of intensified biomass production and biodiversity

protection on ecosystem services provided by European forests. *Ecosystem Services*, *9*, pp.155-165.

Vermote, E., Justice, C., Claverie, M. and Franch, B., 2016. Preliminary analysis of the performance of the Landsat 8/OLI land surface reflectance product. *Remote Sensing of Environment*, *185*, pp.46-56.

Voglmayr, H. and Yule, C.M., 2006. Polyancora globosa gen. sp. nov., an aeroaquatic fungus from Malaysian peat swamp forests. *mycological research*, *110*(10), pp.1242-1252.

Wagner, W., Hollaus, M., Briese, C. and Ducic, V., 2008. 3D vegetation mapping using small-footprint full-waveform airborne laser scanners. *International Journal of Remote Sensing*, *29*(5), pp.1433-1452.

Wagner, W., Ullrich, A., Melzer, T., Briese, C. and Kraus, K., 2004. *From single-pulse to full-waveform airborne laser scanners: potential and practical challenges*. Available online: http://www.isprs.org/proceedings/XXXV/congress/comm3/papers/267.pdf (accessed on 10 October 2017).

Wallace, L., Lucieer, A. and Watson, C.S., 2014. Evaluating tree detection and segmentation routines on very high resolution UAV LiDAR data. *IEEE Transactions on Geoscience and Remote Sensing*, *52*(12), pp.7619-7628.

Wang, C., Menenti, M., Stoll, M.P., Feola, A., Belluco, E. and Marani, M., 2009. Separation of ground and low vegetation signatures in LiDAR measurements of salt-marsh environments. *IEEE Transactions on Geoscience and Remote Sensing*, *47*(7), pp.2014-2023.

Wan-Mohd-Jaafar, W.S., Woodhouse, I.H., Silva, C.A., Omar, H. and Hudak, A.T., 2017. Modelling individual tree aboveground biomass using discrete return lidar in lowland dipterocarp forest of Malaysia. *Journal of Tropical Forest Science*, pp.465-484.

Wedeux, B.M.M. and Coomes, D.A., 2015. Landscape-scale changes in forest canopy structure across a partially logged tropical peat swamp.

White, J.C., Coops, N.C., Wulder, M.A., Vastaranta, M., Hilker, T. and Tompalski, P., 2016. Remote sensing technologies for enhancing forest inventories: A review. *Canadian Journal of Remote Sensing*, *42*(5), pp.619-641.

Wijaya, A., Reddy Marpu, P. and Gloaguen, R., 2010. Discrimination of peatlands in tropical swamp forests using dual-polarimetric SAR and Landsat ETM data. *International Journal of Image and Data Fusion*, *1*(3), pp.257-270.

Wijedasa, L.S., Jauhiainen, J., Könönen, M., Lampela, M., Vasander, H., Leblanc, M.C., Evers, S., Smith, T.E., Yule, C.M., Varkkey, H. and Lupascu, M., 2017. Denial of long-term issues with agriculture on tropical peatlands will have devastating consequences. *Global change biology*, *23*(3), pp.977-982.

Wijedasa, L.S., Posa, M.R.C. and Clements, G.R., 2015. Peat fires: consumers to help beat them out. *Nature*, *527*(7578), p.305.

Wijedasa, L.S., Sloan, S., Michelakis, D.G. and Clements, G.R., 2012. Overcoming limitations with Landsat I magery for mapping of peat swamp forests in Sundaland. *Remote Sensing*, *4*(9), pp.2595-2618.

Willis, K.S., 2015. Remote sensing change detection for ecological monitoring in United States protected areas. *Biological Conservation*, 182, pp.233-242.

Wilkes, P., Jones, S., Suarez, L., Mellor, A., Woodgate, W., Soto-Berelov, M., Haywood, A. and Skidmore, A., 2015. Mapping forest canopy height across large areas by upscaling ALS estimates with freely available satellite data. *Remote sensing*, *7*(9), pp.12563-12587.

Wong, T.T., 2015. Performance evaluation of classification algorithms by k-fold and leave-one-out cross validation. *Pattern Recognition*, *48*(9), pp.2839-2846.

Wood, E.M., Pidgeon, A.M., Radeloff, V.C. and Keuler, N.S., 2012. Image texture as a remotely sensed measure of vegetation structure. *Remote Sensing of Environment*, 121, pp.516-526.

Wösten, J.H.M., Rieley, J.O. and Page, S.E. 2008. Restoration of tropical peatlands. Alterra - Wageningen University and Research Centre, and the EU INCO – RESTORPEAT Partnership. 252 pp. ISBN**:** 978-90-327-0361-5.

Wösten, J.H.M., Van Den Berg, J., Van Eijk, P., Gevers, G.J.M., Giesen, W.B.J.T., Hooijer, A., Idris, A., Leenman, P.H., Rais, D.S., Siderius, C. and Silvius, M.J., 2006. Interrelationships between hydrology and ecology in fire degraded tropical peat swamp forests. *Water Resources Development*, *22*(1), pp.157-174.

Wright, M.N. and Ziegler, A., 2015. ranger: A fast implementation of random forests for high dimensional data in C++ and R. *arXiv preprint arXiv:1508.04409*.

Wright, E.L., Black, C.R., Turner, B.L. and Sjögersten, S., 2013. Environmental controls of temporal and spatial variability in CO2 and CH4 fluxes in a neotropical peatland. *Global change biology*, *19*(12), pp.3775-3789.

Wright, E.L., Black, C.R., Cheesman, A.W., Drage, T., Large, D., Turner, B.L. and Sjoegersten, S., 2011. Contribution of subsurface peat to CO2 and CH4 fluxes in a neotropical peatland. *Global Change Biology*, *17*(9), pp.2867-2881.

Wu, J., Van Aardt, J.A.N., Asner, G.P., Kennedy-Bowdoin, T., Knapp, D., Erasmus, B.F.N., Mathieu, R., Wessels, K. and Smit, I.P.J., 2009. Lidar waveform-based woody and foliar biomass estimation in savanna environments. *Rochester Institute of Technology*.

Wulder, M.A., White, J.C., Nelson, R.F., Næsset, E., Ørka, H.O., Coops, N.C., Hilker, T., Bater, C.W. and Gobakken, T., 2012a. Lidar sampling for large-area forest characterization: A review. *Remote Sensing of Environment*, *121*, pp.196-209.

Wulder, M.A., White, J.C., Bater, C.W., Coops, N.C., Hopkinson, C. and Chen, G., 2012b. Lidar plots—A new large-area data collection option: Context, concepts, and case study. *Canadian Journal of Remote Sensing*, *38*(5), pp.600-618.

Wulder, M.A., White, J.C., Masek, J.G., Dwyer, J. and Roy, D.P., 2011. Continuity of Landsat observations: Short term considerations. *Remote Sensing of Environment*, *115*(2), pp.747-751.

Wulder, M.A., White, J.C., Alvarez, F., Han, T., Rogan, J. and Hawkes, B., 2009. Characterizing boreal forest wildfire with multi-temporal Landsat and LIDAR data. *Remote Sensing of Environment*, *113*(7), pp.1540-1555.

Xu, J., Morris, P.J., Liu, J. and Holden, J., 2018. PEATMAP: Refining estimates of global peatland distribution based on a meta-analysis. *Catena*, *160*, pp.134-140.

Young, T.P., Petersen, D.A. and Clary, J.J., 2005. The ecology of restoration: historical links, emerging issues and unexplored realms. *Ecology letters*, *8*(6), pp.662-673.

Yu, L., Liang, L., Wang, J., Zhao, Y., Cheng, Q., Hu, L., Liu, S., Yu, L., Wang, X., Zhu, P. and Li, X., 2014. Meta-discoveries from a synthesis of satellite-based land-cover mapping research. *International Journal of Remote Sensing*, *35*(13), pp.4573-4588.

Yu, Z.C., 2012. Northern peatland carbon stocks and dynamics: a review. *Biogeosciences*, *9*(10), pp.4071-4085.

Yuen, J.Q., Fung, T. and Ziegler, A.D., 2016. Review of allometric equations for major land covers in SE Asia: uncertainty and implications for above-and below-ground carbon estimates. *Forest Ecology and Management*, *360*, pp.323-340.

Yule, C.M., 2010. Loss of biodiversity and ecosystem functioning in Indo-Malayan peat swamp forests. *Biodiversity and Conservation*, *19*(2), pp.393-409.

Yule, C.M. and Gomez, L.N., 2009. Leaf litter decomposition in a tropical peat swamp forest in Peninsular Malaysia. *Wetlands Ecology and Management*, *17*(3), pp.231-241.

Zald, H.S., Wulder, M.A., White, J.C., Hilker, T., Hermosilla, T., Hobart, G.W. and Coops, N.C., 2016. Integrating Landsat pixel composites and change metrics with lidar plots to predictively map forest structure and aboveground biomass in Saskatchewan, Canada. *Remote Sensing of Environment*, *176*, pp.188-201.

Zanne, A.E., Lopez-Gonzalez, G., Coomes, D.A., Ilic, J., Jansen, S., Lewis, S.L., Miller, R.B., Swenson, N.G., Wiemann, M.C. and Chave, J., 2009. Global wood density database.

Zhang, K., Chen, S.C., Whitman, D., Shyu, M.L., Yan, J. and Zhang, C., 2003. A progressive morphological filter for removing nonground measurements from airborne LIDAR data. *IEEE transactions on geoscience and remote sensing*, *41*(4), pp.872-882.

Zhao, K., Popescu, S. and Nelson, R., 2009. Lidar remote sensing of forest biomass: A scale-invariant estimation approach using airborne lasers. *Remote Sensing of Environment*, *113*(1), pp.182-196.

Zhu, X.X., Tuia, D., Mou, L., Xia, G.S., Zhang, L., Xu, F. and Fraundorfer, F., 2017. Deep learning in remote sensing: A comprehensive review and list of resources. *IEEE Geoscience and Remote Sensing Magazine*, *5*(4), pp.8-36.

Zhu, Z., Wang, S. and Woodcock, C.E., 2015. Improvement and expansion of the Fmask algorithm: Cloud, cloud shadow, and snow detection for Landsats 4–7, 8, and Sentinel 2 images. *Remote Sensing of Environment*, *159*, pp.269-277.

Zvoleff, A., 2016. glcm: Calculate Textures from Grey-Level Co-Occurrence Matrices (GLCMs). R package version 1.6.1. Accessed online: https://CRAN.R-project.org/package=glcm

Appendix 1: Tropical peatland vegetation structure and biomass: optimal exploitation of airborne laser scanning

remote sensing

MDPI

Article

Tropical Peatland Vegetation Structure and Biomass: Optimal Exploitation of Airborne Laser Scanning

Chloe Brown [1,*], Doreen S. Boyd [1], Sofie Sjögersten [2], Daniel Clewley [3], Stephanie L. Evers [4,5,6] and Paul Aplin [7]

1 School of Geography, University of Nottingham, Nottingham NG7 2RD, UK; doreen.boyd@nottingham.ac.uk
2 School of Biosciences, University of Nottingham, Nottingham NG7 2RD, UK; Sofie.Sjogersten@nottingham.ac.uk
3 Plymouth Marine Laboratory, Plymouth PL1 3DH, UK; dac@pml.ac.uk
4 School of Natural Sciences and Psychology, Liverpool John Moores University, Liverpool L3 3AF, UK; S.L.Evers@ljmu.ac.uk
5 School of Environmental and Geographical Sciences, University of Nottingham Malaysia Campus, Semenyih 43500, Selangor, Malaysia
6 Tropical Catchment Research Initiative (TROCARI), Semenyih 43500, Selangor, Malaysia
7 School of Geography, Edge Hill University, Ormskirk L39 4QP, UK; paul.aplin@edgehill.ac.uk
* Correspondence: chloe.brown@nottingham.ac.uk; Tel.: +44-115-846-7052

Received: 19 March 2018; Accepted: 24 April 2018; Published: 25 April 2018



Abstract: Accurate estimation of above ground biomass (AGB) is required to better understand the variability and dynamics of tropical peat swamp forest (PSF) ecosystem function and resilience to disturbance events. The objective of this work is to examine the relationship between tropical PSF AGB and small-footprint airborne Light Detection and Ranging (LiDAR) discrete return (DR) and full waveform (FW) derived metrics, with a view to establishing the optimal use of this technology in this environment. The study was undertaken in North Selangor peat swamp forest (NSPSF) reserve, Peninsular Malaysia. Plot-based multiple regression analysis was performed to established the strongest predictive models of PSF AGB using DR metrics (only), FW metrics (only), and a combination of DR and FW metrics. Overall, the results demonstrate that a Combination-model, coupling the benefits derived from both DR and FW metrics, had the best performance in modelling AGB for tropical PSF (R^2 = 0.77, RMSE = 36.4, rRMSE = 10.8%); however, no statistical difference was found between the rRMSE of this model and the best models using only DR and FW metrics. We conclude that the optimal approach to using airborne LiDAR for the estimation of PSF AGB is to use LiDAR metrics that relate to the description of the mid-canopy. This should inform the use of remote sensing in this ecosystem and how innovation in LiDAR-based technology could be usefully deployed.

Keywords: tropical peat swamp; LiDAR; discrete return LiDAR; full waveform LiDAR; above ground biomass

1. Introduction

Tropical Peat Swamp Forests (PSF) are unique ecosystems; their health and functionality are dependent on the interactions between forest, peat and hydrology. Any unbalance in this sensitive environment from change in one can amplify across the ecosystem and impact the multitude of services they provide, creating positive feedback loops [1,2]. Tropical PSF are thus particularly vulnerable to human disturbances (as well as natural change). This is especially the case in South East Asia where there has been a long history of tropical PSF degradation [3,4]. At an estimated 88.6 Gt, tropical

PSF are one of the largest pools of terrestrial carbon [5,6], however, high volumes of deforestation and land conversion rates have transformed South East Asian PSF into one of the largest emitters of carbon globally [7–9]. Forest clearance and conversion not only decreases carbon stores directly due to reduction in above ground biomass (AGB), but also indirectly increases carbon emissions as a result of peat exposure [10,11]. Fire susceptibility in the landscape also increases [12–14], further compounding carbon losses. This, coupled with the need to understand the variability and dynamics of tropical ecosystems in general with respect to their role in the global carbon cycle [5,15], means there is an urgent need to track change in PSF via estimation of AGB over space and time. Not only will this afford understanding of carbon losses, this will also help guide tropical PSF restoration and sustainable management activities [16,17].

The structurally complex nature of tropical PSF, supporting high (50–70 m) to low (15–25 m) dense canopy forest vegetation, typically with buttresses and thick root mat floors [18], presents a challenging landscape for monitoring purposes. This is further complicated by degraded (and/or recovering) PSF generating even greater variation in forest structure, in response to disturbance events and changes in peat characteristics. Traditionally, forest AGB estimates have been based on field plot inventories, where plot measurements are used to infer AGB estimates through allometric equations [19]. This manual approach provides the most accurate AGB estimates [20], however it is labour intensive, time consuming and expensive [21]. Additionally, the extent and inaccessibility of PSF, coupled with the difficult logistics of field work posed by often waterlogged, swampy conditions, has restricted forest inventory data collection.

Development in remote sensing technology over the last two decades, specifically in Light Detection and Ranging (LiDAR) [22,23], has revolutionised the retrieval and accuracy of forest structural attributes, including AGB, across landscapes scales [24]. LiDAR data has been widely adopted in forest structural applications, both at the stand and individual tree level [25], due to its ability to characterise both vertical and horizontal structures. A common theme for many studies is the development of LiDAR-derived metrics related to height distribution, density, and intensity of returns [26–28]. Typically, in LiDAR AGB studies, models are developed from the relationships between field plot estimated AGB, calculated from tree allometry, and LiDAR-derived metrics [29–31]. Establishing these relationships between metrics and forest attributes are complex, in particular for dense, multi-layered forest canopies associated with the tropics. The majority of work conducted in this area has employed discrete return (DR) derived metrics [32], with focus on the utility of DR data for carbon accounting and environmental modelling [33,34]. Asner et al. [35] examined the effectiveness of DR LiDAR derived mean canopy height to estimate AGB in four tropical regions (Panama, Peru, Madagascar, and Hawaii). The results highlighted the value of DR LiDAR in generating high-resolution carbon maps across the tropics. However, the application of DR LiDAR is restricted by the number of returns which can penetrate through dense canopies down to the forest floor, and by the limited point measurements from the canopy and the understory vertical structure [36,37].

Full Waveform (FW) LiDAR data has the potential to provide a more detailed and comprehensive 3D view of forest canopy structure in comparison to DR sensors [38,39]. Consequently, a growing body of research has focused on developing FW metrics for forest assessment. Drake et al. [40,41] are early examples of the development of FW metrics, using large-footprint FW data (laser vegetation imaging sensor) to generate a list of metrics for AGB estimations. Height of medium energy (HOME) was demonstrated to correlate strongly with mean stem diameter, basal area and AGB. For small-footprint FW LiDAR, Wu et al. [38] explored the potential of a list of structural and statistics-based AGB predictor metrics. The results produced a high correlation between FW-derived metrics with individual tree height, foliar and biomass for a savanna environment. Pirotti et al. [42] also explored the potential for estimating AGB from small-footprint FW data, finding the median height of echo count (HOMTC) performed best at estimating AGB at plot level for a complex tropical forest.

Recently, several studies have evaluated the fusion of DR and FW metrics in forest AGB estimation [43–46]. Cao et al. [47,48] assessed the potential of DR and FW metrics, individually and in

combination, as predictors of total living biomass and its components (AGB, root, foliage, branch and trunk) for sub-tropical forests. The study found metrics related to canopy height to be the strongest predictors for AGB; additionally, the combination of DR and FW metrics, by multivariate linear regression, improved AGB estimation.

The benefits of LiDAR data for monitoring tropical environments has been well established, however with the structural complexity and unique interactions between forest and peat swamp, general tropical forest models may not be transferable. Limited research has been published on the application of LiDAR in tropical PSF [49,50]. Jubanski et al. [51] and Kronseder et al. [52] examined the use of LiDAR point cloud data in AGB estimation for varied levels of degraded lowland dipterocarp PSF in Central Kalimantan, Indonesia. Both studies concluded that AGB could be estimated successfully, though with varying levels of accuracy.

According to our knowledge, no previous study has examined the use of both DR and FW metrics or the fusion of DR and FW metrics in AGB estimation for tropical PSF. This paper will examine the relationship between the AGB of a tropical PSF in North Selangor, Peninsular Malaysia, and small-footprint airborne LiDAR (DR and FW) derived metrics. This forest is of particular importance since it is one of the few large areas of PSF remaining in peninsular Malaysia [53]. Three LiDAR-based approaches are investigated for modelling AGB: (1) DR-derived metrics (only); (2) FW-derived metrics (only); (3) and a combination of DR- and FW-derived metrics. The accuracy of the models is evaluated by comparing LiDAR-based AGB estimates with field (in situ plots) measured AGB, with a view to establishing the optimal model for estimating AGB of the North Selangor PSF.

2. Materials and Methods

2.1. Study Site

The North Selangor Peat Swamp Forest (NSPSF) is located on the flat coastal plains of northwest Selangor, Peninsular Malaysia (Figure 1). With a combined total of 81,304 hectares, NSPSF is one of the largest remaining PSF in the region; however, over 30 years of intensive timber harvesting has left the once pristine NSPSF degraded and vulnerable to further environmental threat [18,54]. Repeated cycles of logging activities have created a complex, multi-layered canopy structure, indicated by mixed stand density and height (Figure 1). Additionally, the extraction of timber from the forest has led to the formation of a 500 km network of canals [55], scarring the forest and accelerating the drainage and erosion of valuable peat soil stores (and the carbon they hold) [53].

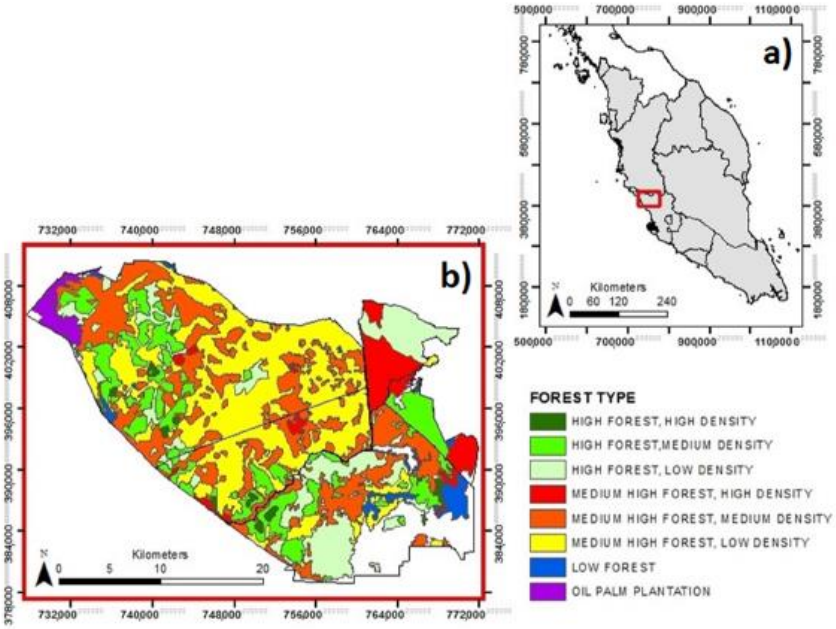


Figure 1. (**a**) The location of the North Selangor Peat Swamp Forest in Peninsular Malaysia; (**b**) Magnified study area map at bottom left corner shows forest type (forest height (high, medium, low) and forest density (high, medium, low)) results from a forest management inventory undertaken in 2000 [56].

In response to the damaging impact of past logging activities on tropical PSF ecosystem health and the services they provide, the Selangor State Government agreed on a 25-year moratorium on timber harvesting for the State of Selangor, with all logging activities ceased in 2007 [55]. Despite this halt in logging activities, the reserve remains exposed to disturbance from the surrounding land uses, in particular accelerated drainage from Tanjong Karang Irrigation Scheme and land conversion to oil palm agriculture [57].

2.2. Field Data

To obtain field estimates of AGB, thirty circular field plots with a radius of 15 m were established within the reserve during 2017. This relatively small sample size, albeit statistically relevant, was determined by the challenging logistics of tropical PSF fieldwork, as previously mentioned. The forests plots were established to be representative of a secondary PSF ecosystem, where no obvious structural disturbances were observed since the LiDAR survey (2014)—for example major tree fall, logging activities or fire events—based on an existing forestry management plan [55], multispectral imagery and expert knowledge and experience from NSPSF Rangers. The location of the central tree, and thus the centre point of the plot, was recorded by a field GPS (Garmin GPSMAP 64), with an average horizontal error of <5 m when measurements were averaged over ten minutes. The positions of all further trees within the plot were noted relative to the centre (distance and angle) (Figure 2). For each plot, all live trees with a diameter at breast height (DBH) of >5 cm were measured and tree species recorded. Additionally, dependent on the top of tree visibility, selected trees of varying height classes were measured by a laser height meter.

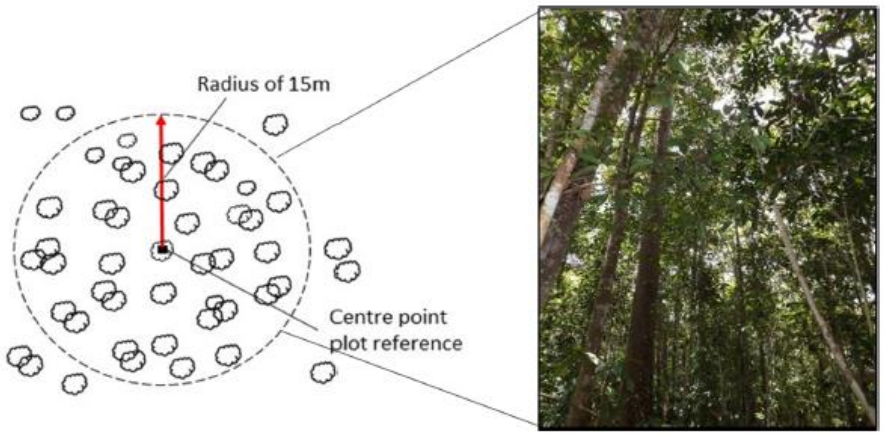


Figure 2. Example field inventory plot design.

An allometric equation developed by Chave et al. [19] was used to calculate AGB from field measured DBH, species (to estimate wood density), and additionally tree height when available (missing height was inferred from pantropical model). The AGB allometric equation used was:

$$AGB = 0.0673 \times (\varrho D2H)^{0.976}$$

where ϱ = wood density (g/cm^3), D = DBH (cm) and H = height (m).

The 'BIOMASS' package in R software (version 2.10.0) [58] was used to run AGB estimation. AGB values were calculated for individual trees within each 15 m radius field plot, and then summed to obtain a total AGB value for each plot.

2.3. LiDAR Data Acquisition

Airborne LiDAR data was flown by the UK's Natural Environment Research Council (NERC) Airborne Research Facility (ARF) as part of its 2014 Malaysia Campaign. It is important to note the three-year time delay between the airborne LiDAR data collection (2014) and field plot inventory collection (2017). This may introduce error into the AGB models, however as previously mentioned, all field plots were established to be free from logging and fire, with no obvious disturbance within the three-year period. The data was captured in November 2014 from a Leica ALS50-II LiDAR system, a small footprint LiDAR sensor with the capacity to record both DR and FW LiDAR simultaneously. The Leica ALS50-II LiDAR system was on board a Dornier 228-201, flying at 132–136 knots at an altitude of 2145–2181 m. The sensor emits the laser beam at 1064 nm, additionally providing an intensity digital image from the return signal intensity data. The accuracy report that accompanied the LiDAR data estimated the vertical accuracy to be 0.023 m RMSE, where LiDAR elevation was assessed against ground control points. In total 29 flightlines were flown, surveying an area covering 690 km^2 of the reserve and surrounding area. However, given the constraints of fieldwork and to ensure representation, a subset of the LiDAR flightlines (161.73 km^2), focused on the north-west of the NSPSF reserve (Figure 3), was extracted for optimal LiDAR-derived AGB model development and assessment. The dataset has an average point density of 2.03 m^2 and a point spacing of 0.70 m. The LiDAR data, DR and FW, was pre-processed by NERC's Data Analysis Node and delivered in LAS 1.3 format.

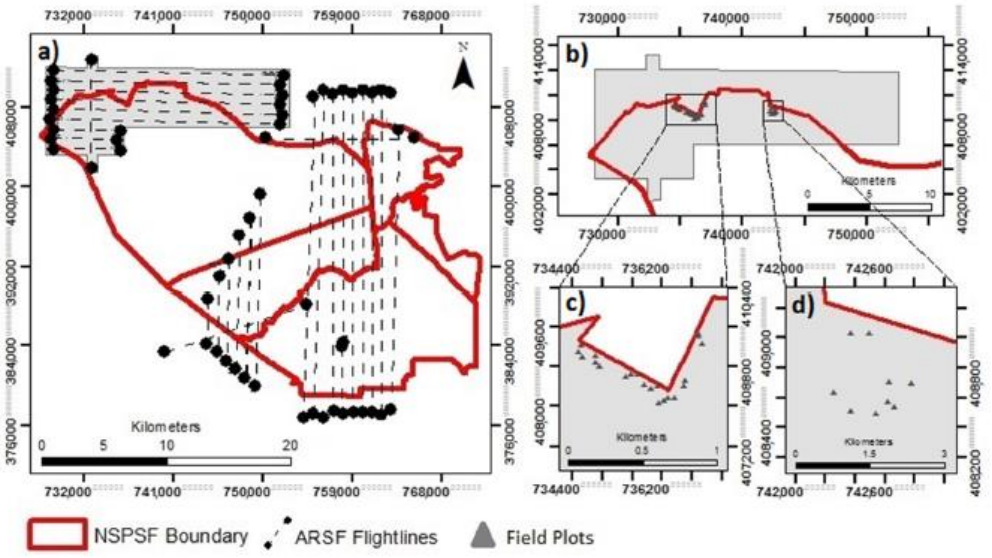


Figure 3. (**a**) ARSF LiDAR flightlines; (**b**) LiDAR flightline subset; (**c**,**d**) field plot locations.

2.4. DR-Derived Metrics

A number of descriptive structural plot-level metrics were calculated from a DR height normalised point cloud. All data processing was carried out in LAStools software [59]—a complimentary full academic LAStools licence was generously supplied through the LASmoons programme. Outliers, or noisy data, were first eliminated from the DR LAS. files supplied, and the data was then filtered to identify laser ground and non-ground (unclassified) hits. The normalised above ground heights were calculated by subtracting the ground points, interpolated into a surface using the adaptive triangulated irregular network (TIN) filtering algorithm, from the non-ground (unclassified) points. Above ground height DR metrics were then calculated. DR plot metrics included: minimum height (min), maximum height (max), average height (avg), standard deviation (std), skewness (skw), kurtosis (kur), average square height (qav), height percentile (p01, p05, p10, p25, p50, p75, p90, P9, P99), height bincentiles (b10, b20, b30, b40, b50, b60, b70, b80, b90).

2.5. FW-Derived Metrics

Informed from the success in previous studies-based in the sub-tropics [47,48], three plot-level FW metrics were derived from the recorded waveform. All data processing was carried out in the Sorted Pulse Software Library (SPDlib) [60], benefiting from the recent additions made to the metric library. Gaussian decomposition [61] was applied to each waveform to derive point information (x, y, z). Points were classified into ground or non-ground using a combination of progressive morphology filtering [62] and maximum curvature classification (MCC) [63] algorithms to produce a Digital Terrain Model (DTM), to which heights were normalised. The FW plot metrics included: height of median energy (HOME), waveform distance (WD) and roughness of the outermost canopy (ROUGH) (Figure 4). FW metrics were summarized as the mean and standard deviation for each plot.

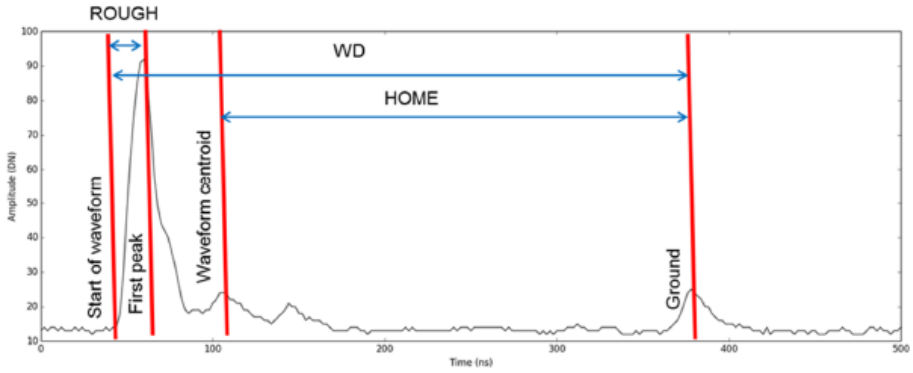


Figure 4. Illustration of FW metrics location on an example pseudo-vertical waveform from the NSPSF FW dataset. Plotted Amplitude (DN)/Time (ns).

2.6. Statistical Modelling and Analyses

Simple linear regression analysis on field measured plot AGB values against LiDAR derived DR and FW metrics was conducted. Multiple linear regression models were developed independently from the DR metrics, FW metrics and DR and FW metrics in combination for estimating AGB. To ensure model variables were not highly correlated, a 'data mining' approach, outlined by Langton et al. [64], was first adopted to identify the key predictor variables for multiple regression analyses. This stage was required to avoid model over-fitting given the relatively small sample size (n = 30) and potential high collinearity of a number of LiDAR metrics with one another. The 'MuMIn' package for R software (version 1.9.5) [65] was used to run a modified Akaike Information Criterion (AIC), termed AICc [66], this comparing the quality of predictive multiple regression model inputs. An automated stepwise AICc was performed to select input variables for the final models. The delta-AIC value was assessed for each candidate model, a threshold value for delta-AIC was set to <2, models which met this requirement were determined to be within range of plausible models that best fit the observed values [66]. The top ranked AICc regression models were assessed based on a number of diagnostics tests (ANOVA, students t-test and variance inflation factor ($\leq$1)) to produce final predictive models for DR metrics (only), FW metrics (only), and a combination of DR and FW metrics. The final predictive modes—DR-model, FW-model, and Combination-model—were fitted and assessed based on a combination of: R-square (R2), adjusted R-square (Adj-R2), Root Mean Square Error (RMSE), and the relative Root Mean Square Error (rRMSE).

To judge the reliability of the models, leave-one-out-cross validation (LOOCV) was performed. The LOOCV method for model evaluation was selected due to its proven effectiveness for models with a small sample size [67]. The Root Mean Square Error from the cross-validation analysis (RMSEcv) and bias (BIAScv) was calculated and presented as indicators of the three models' predictive power. Finally, to investigate the significance of the addition of FW metrics in PSF AGB estimation, the Kruskal-Wallis H test (or one-way ANOVA on ranks) was used to determine if there were statistically significant differences between the three final models' AGB plot predictions.

3. Results

Plot-based AGB values were calculated from field measured DBH, species and height data (when available). For the 30 plots, AGB ranged from 126.96 Mg/ha to 443.27 Mg/ha, with a mean value of 319.52 Mg/ha, with a standard deviation of 76.34 Mg/ha (Table 1).

Table 1. Plot measured forest parameters.

Plot Measurements	Values: Mean (Std Dev) Min/Max
Tree number	89.33 (21.09) 39/128
DBH (cm)	46.39 (37.16) 17/375
AGB (Mg/ha)	319.52 (76.34) 126.96/443.27

The results from simple linear regression analysis between field-based AGB estimates and 31 LiDAR derived DR and FW metrics are presented in Tables 2 and 3. For DR metrics, the 50th height percentile ('p50') showed the highest correlation with field-based AGB (R^2 = 0.68, RMSE = 42.1), followed by average height ('avg') (R^2 = 0.64, RMSE = 45.2). Both minimum height ('min') and standard deviation ('std') displayed no significant relationship or sensitivity to field-based AGB. For FW metrics, the mean HOME ('H_mean') provided the highest correlation with field-based AGB (R^2 = 0.72, RMSE = 39.4) (Figure 5). The mean input variables calculated for all FW metrics displayed a moderate correlation and significant relationship with field-based AGB, however, the standard deviation input variables calculated for all FW metrics showed very low correlation, with standard deviation HOME ('H_sd') and standard deviation ROUGH ('R_sd') presenting no significant relationship to field-based AGB estimates. It is evident from the linear regression results that metrics representing mid-canopy levels, for example 'p50' and 'H_mean', are important predictors for AGB estimation in PSF. The variation in mid-canopy structure captured by these metrics can be seen in Figure 6. Where a waveform has been extracted from the centre point (1 m buffer) for each of the 30 field plots

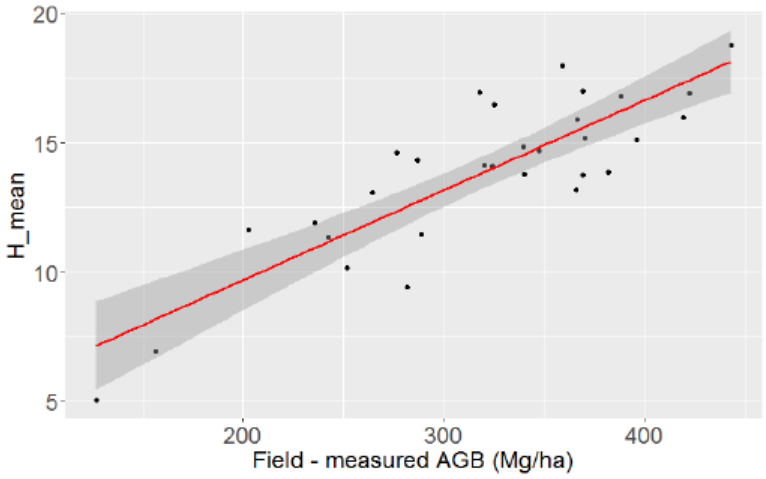


Figure 5. Field measured AGB modelled by the mean value from the FW mean HOME metric (H_mean). Bands represent the 95% confidence envelope.

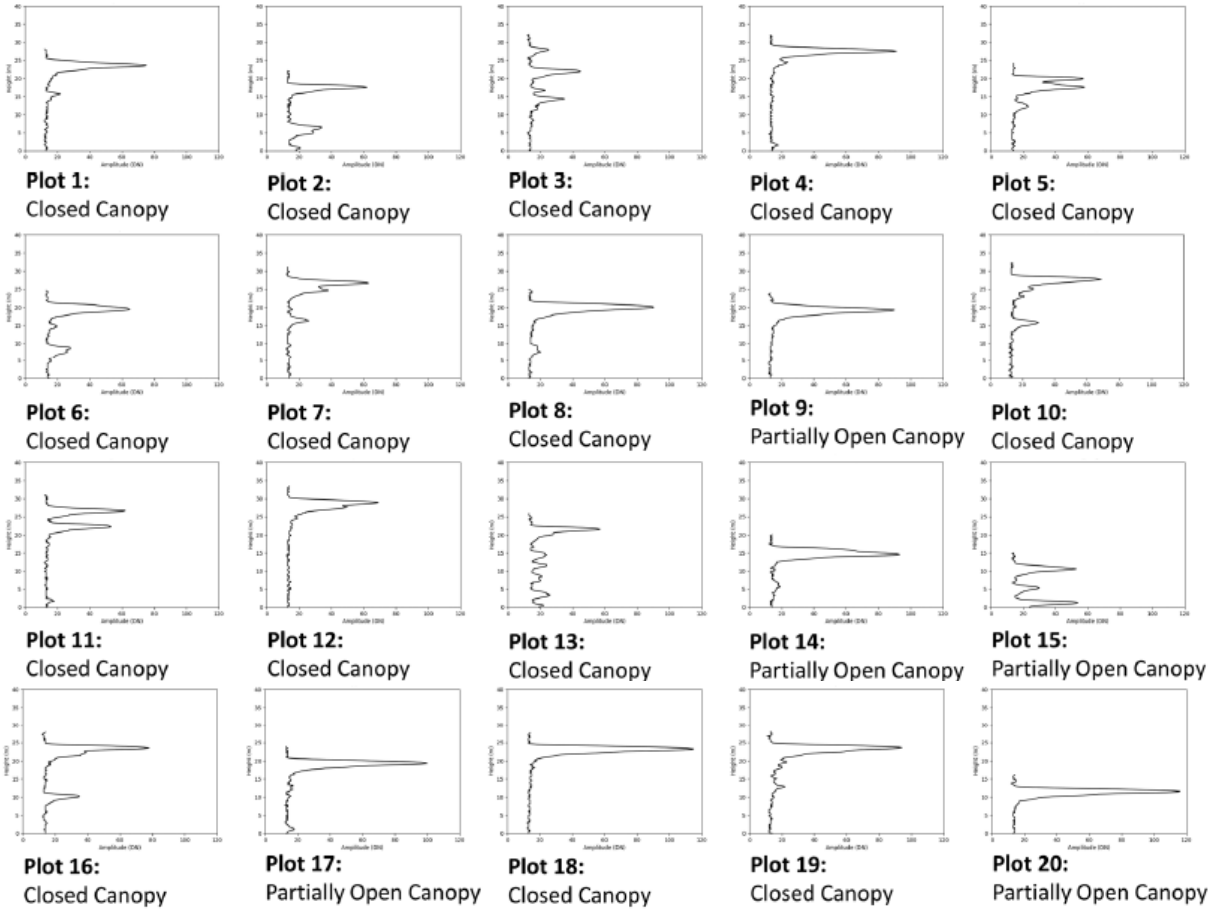


Figure 6. *Cont.*

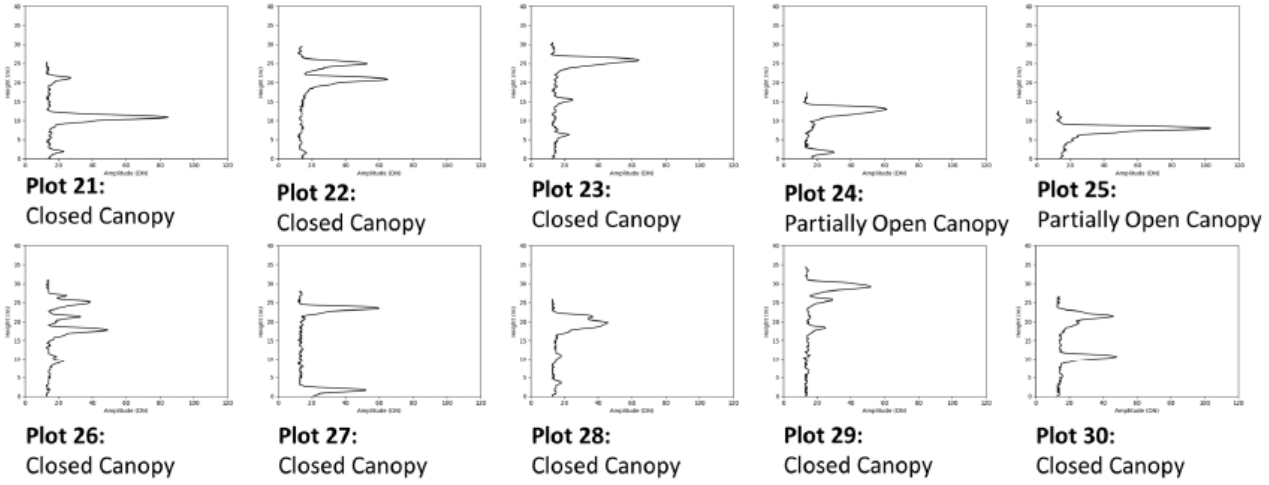


Figure 6. Centre point (1 m buffer) plot vegetation profiles, each waveform height has been subtracted from LiDAR derived DTM; graphs are fitted Height (m)/Amplitude (DN). Height scale (y-axis) ranges from 0 to 40 m, and the amplitude (x-axis) from 0 to 120 DN. Graphs are accompanied with forest canopy structure description.

Table 2. Results from simple linear regression using DR metrics. Values underlined represent metrics of non-significance $p > 0.05$.

DR Metric	R^2	Adj-R^2	RMSE (Mg/ha)	rRMSE (%)
Min	0.04	0.01	73.4	23
Max	0.21	0.18	66.6	20.8
Avg	0.64	0.62	45.2	14.2
Qav	0.59	0.58	48	15
Std	0.1	0.07	71.2	22.3
Ske	0.61	0.6	46.7	14.6
Kur	0.23	0.21	65.7	20.6
P01	0.29	0.26	63.4	19.8
P05	0.29	0.26	63.4	19.8
P10	0.30	0.28	62.7	19.6
P25	0.58	0.57	48.5	15.2
P50	0.68	0.67	42.1	13.2
P75	0.58	0.56	48.9	15.3
P90	0.39	0.36	58.8	18.4
P95	0.30	0.28	62.7	19.6
P99	0.25	0.22	65	20.3
B10	0.25	0.22	65	20.3
B20	0.35	0.33	60.6	19
B30	0.49	0.48	53.4	16.7
B40	0.59	0.57	48.1	15.1
B50	0.62	0.61	46.3	14.5
B60	0.52	0.51	51.8	16.2
B70	0.39	0.37	58.6	18.4
B80	0.25	0.23	64.9	20.3
B90	0.16	0.13	68.9	21.5

Table 3. Results from simple linear regression using FW metrics. Values underlined represent metrics of non-significance $p > 0.05$.

FW Metric	R^2	Adj-R^2	RMSE (Mg/ha)	rRMSE (%)
H_mean	0.72	0.71	39.4	12.3
H_sd	0.00	−0.03	75	23.5
W_mean	0.57	0.55	49.3	15.4
W_sd	0.17	0.14	68.5	21.4
R_mean	0.61	0.59	47.1	14.7
R_sd	0.00	−0.04	75.1	23.5

The results of the best models for predicting PSF AGB (DR, FW and Combination) (Table 4 are summarised in Table 5 and visualized in Figure 7. The Combination-model, H_mean/B50, displayed the best agreement with field-based AGB values (R^2 = 0.77; RMSE = 36.4; rRMSE = 10.8%). Figure 8 displays an example of AGB (Mg/ha) estimates calculated from the Combination-model for a subset of the LiDAR flightlines in the northwest of the NSPSF reserve at a 5 m (0.0025 ha) spatial resolution.

Table 4. Model equations.

	Model Equations
DR	$=81.786 + 8.940 \times P75 - 78.063 \times Ske$
FW	$=101.457 + 19.579 \times H_mean - 12.555 \times W_sd$
Combination	$=171.3731 + 14.7802 \times H_mean - 1.5752 \times B50$

Table 5. Results from the best preforming models for predicting AGB.

	Model Variables	R^2	Adj-R^2	RMSE (Mg/ha)	$RMSE_{cv}$ (Mg/ha)	$BIAS_{cv}$ (Mg/ha)	rRMSE (%)
DR	P75 Ske	0.73	0.71	39.2	42.9	−0.83	12.3
FW	H_mean W_sd	0.76	0.74	36.9	40.9	−0.17	11.6
Combination	H_mean B50	0.77	0.75	36.4	39.8	0.38	10.8

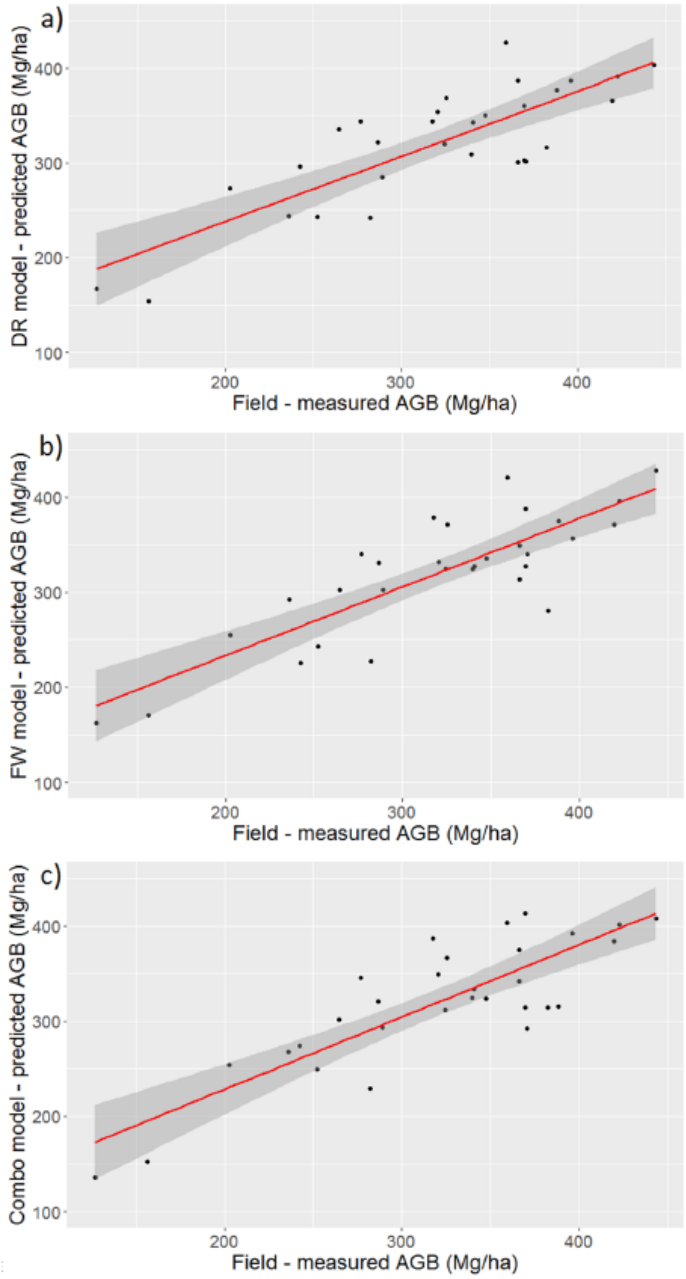


Figure 7. Predicted vs field measured AGB from the best performing models: (**a**) DR-model; (**b**) FW-model; (**c**) Combination-model. Bands represent the 95% confidence envelope.

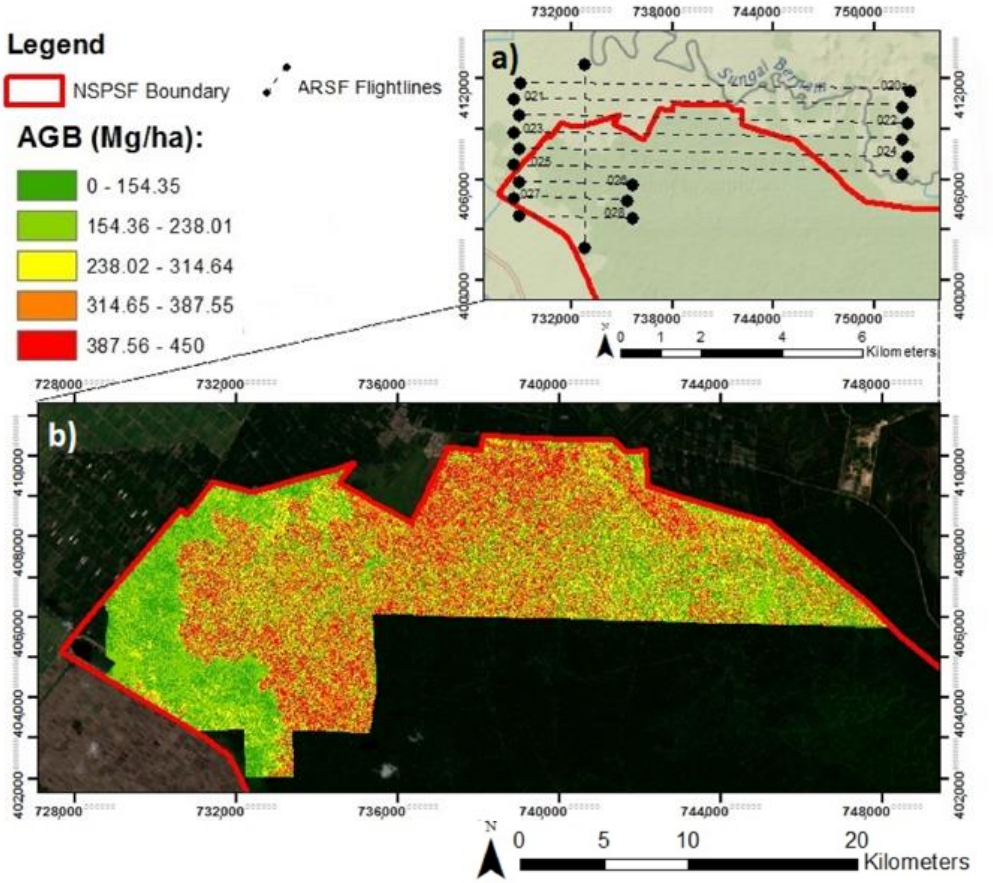


Figure 8. (**a**) LiDAR flightline subset; (**b**) estimation of AGB (Mg/ha) within the NSPSF boundary calculated from the Combination-model, at a 5 m (0.0025 ha) spatial resolution, overlaid on Sentinel-2 multispectral image.

However, all three predictive models displayed a strong positive correlation and a significant relationship to field-based AGB estimates (DR-model—R^2 = 0.73; RMSE = 39.2; rRMSE = 12.3%) and (FW-model—R^2 =0.76; RMSE = 36.9; rRMSE = 11.6%). Figure 9 displays the frequency distribution for model generated AGB (Mg/ha) values for the 30 plots, presented with model AGB (Mg/ha) summary statistics. The Kruskal-Wallis test showed that there was no statistically significant difference between the three models for PSF AGB prediction (H(2) = 0.0038095; p = 0.99). In summary, the synergistic use of DR- and FW-derived metrics displayed a stronger correlation with field-based AGB estimates in comparison to individual and multiple DR- and FW-models, however, there was no significant difference in tropical PSF AGB prediction between the three best multiple regression models (DR, FW and Combination).

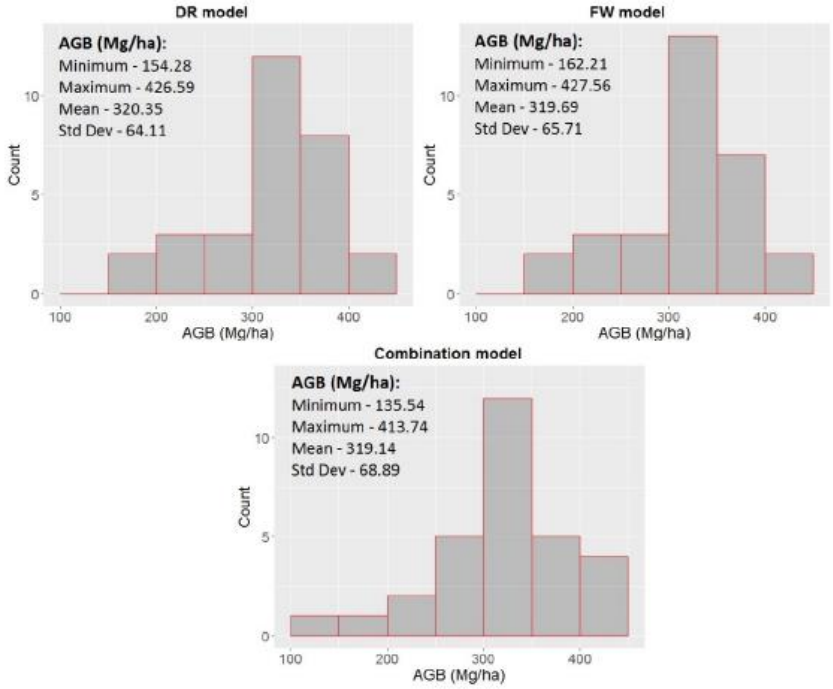


Figure 9. Frequency distribution for DR-, FW- and Combination-model generated AGB (Mg/ha) across the 30 field plots, presented with model generated plot minimum, maximum, mean and standard deviation AGB (Mg/ha).

4. Discussion

Quantification of tropical PSF AGB cover is required to better understand and safeguard tropical peatlands' ecosystem function and resilience to disturbance, both natural and anthropogenic [68]. AGB products provide accurate baseline estimates to support international climate change policies and programs such as the UN REDD+ (United Nations Reducing Emissions from Deforestation and Forest Degradation), as well as the development of sustainable management strategies for local stakeholders. Additionally, knowledge gained from the precise assessment of PSF AGB distribution will assist in Malaysia's work towards meeting their Sustainable Development Goals (SDGs), specifically relating to SDG-13 'Climate action'. Using a remote sensing approach to acquiring AGB estimates is attractive in that large spatial extents are covered and monitoring can be frequent, particularly once a calibrated model has been established between forest inventory and remotely sensed data. In this case, the LiDAR campaign covered 53% of the NSPSF reserve. This is the first time such data had been captured for NSPSF and used in this way. The study demonstrates the utility of both DR and FW LiDAR data for tropical PSF AGB estimation and thus illustrates the real potential for a monitoring approach underpinned by laser scanning technologies.

The AGB range presented in the in-situ plots was 126.96–443.27 Mg/ha. AGB plot values are consistent with PSF estimates from the literature [52] and therefore considered reliable and reflective of a secondary tropical PSF, with a diverse structure and density (Figure 1). The investigation is limited by the relatively small sample size (n = 30) used for model development and validation [69]. However, the training plots were identified as being representative of the PSF conditions found in NSPSF; all field plots had good correspondence with LiDAR data providing detailed information on both forest canopy and ground (mean ground-classified hits = 8.3% per plot) relative to a densely closed and partially open canopy structure (Figure 6). The study recognises that a larger sample size is

advisable in future work for model validation. Nevertheless, the plots sampled in this study cover a wide range of forest types found across NSPSF, with plots positioned in high, medium, and low forest height stands with varying densities (Figure 1).

From the numerous DR and FW LiDAR metrics tested against this range in AGB measured in the in situ plots, three AGB prediction models were determined to have a high accuracy with an rRMSE <15%: one model using discrete return data only (DR-model = 12.3%), one model using full waveform data only (FW-model = 11.6%) and one model using a combination of DR and FW data (Combination-model = 10.8%). Overall, the Combination-model was best for explaining AGB, with an R^2 of 0.77 (RMSE = 36.4, rRMSE = 10.8%). There was no statistically significant difference between these three best models for PSF AGB prediction.

Simple linear regression revealed LiDAR-derived metrics relating to mid-story canopy levels—for example average height, 50th height percentile, 50th height bincentile and HOME—to be the strongest predictors of AGB in tropical PSF. In this study, models which included FW metrics were dominated by the strong predictive capabilities of the mean HOME metric. Waveform derived HOME is the distance from the waveform centroid to the 'ground' (i.e., the ground position of the pseudo-waveform), HOME has previously been found to be sensitive to canopy openness (including tree density) and the vertical arrangement of a forest stand [40,41]. This suggests that for complex tropical PSF the often unobserved structural and compositional diversity in the lower portions of the forest canopy is crucial for accurate AGB model prediction. This observation is crucial for understanding how LiDAR technologies should be employed for optimal AGB estimation in these environments.

Focusing on the FW LiDAR data it can be seen that the mean values of all FW metrics displayed moderate to high correlations and significant relationships with in situ plot AGB values. These findings are consistent with past research in the use of FW LiDAR in forestry applications [70,71]. Reitberger et al. [72] found FW metrics to improve the detection of under and mid-story trees compared to first/last DR LiDAR by 10–15%, though the study was unable to detect 65% of mid-story trees, and 74% of understory trees in leaf on conditions. Indeed, FW LiDAR is still limited by the lack of significant transmission through dense forest leaves and stems, however its potential to improve our knowledge and understanding of multi-layered forest structures has been widely recognised by the remote sensing community [73]. Although in this study we found no statically significant enhancement (at 95% level of confidence) with the addition of FW metrics in the predictive models for AGB estimation, the full waveforms per plot do show discernible differences. Our focus here was on the use of FW LiDAR metrics common in related literature [41,42,47]. There may exist alternative FW metrics not tested here which could be implemented in future research. This could improve the already strong predictive AGB models, and also describe other structural variables in the forest. These include crown bulk density, canopy fuel weight and for larger dominant trees, crown width [74,75]. Thus, the continued development and application of FW LiDAR in future tropical PSF AGB research is recommended, with a focus on capturing and describing FW. Recent initiatives, such as the Global Ecosystems Dynamics Investigation (GEDI) LiDAR due to be deployed on the International Space Station, respond to the recognised need for vertical structure measurements of the Earth's surface, as put forward by the host country's (USA) National Academy of Sciences and NASA's Science Mission Directorate [76]. The GEDI is just one example of the progress and development in LiDAR systems and platforms that should encourage the continued application of LiDAR data in future PSF applications. Other examples include advancements in small-scale sensor technology which has permitted the use of Unmanned Aerial Vehicles (UAVs) as a LiDAR sensor platform [77,78] thus profiting from potentially higher resolution data capture at a considerably lower surveying cost at local scales. Integration with hyperspectral systems could also be advantageous [79].

Of those alternative metrics which should be implemented in future tropical PSF AGB research, those relating to LiDAR intensity [80–82] are worth considering. Small-footprint LiDAR intensity data (amount of energy reflected back to the sensor) has been increasingly adopted in forestry applications [80,83]. Top of canopy intensity metrics, in combination with LiDAR derived height

values, have been proven to contribute significantly to improved forest AGB estimations [84] and have been linked with tree species number at mid-story canopy level [85]. For this particular investigation, LiDAR intensity metrics were not included in AGB forest estimation because of uneven atmospheric conditions during the flight, therefore the resulting intensity data could not be reliably corrected for or compared between flightlines. This represents a challenge to be tackled in the future.

The results in this study demonstrate the advantage of using both DR and FW LiDAR data in tropical PSF AGB inventory programmes, which in turn provide a more detailed and accurate account of PSF structural cover and above ground carbon allocation across landscape scales. Apart from discerning the role for LiDAR in estimating AGB of these PSFs, this study has also provided in situ plot AGB data for the NSPSF, providing new PSF AGB plot data for an ecosystem underrepresented by global forest inventory databases [86,87]. This is important for subsequent research on how these forests function. As stated earlier the airborne LiDAR data does not fully cover the whole of the NSPSF reserve, in such cases satellite data (i.e., Sentinel-2 or very high-resolution systems) may be used to scale up AGB estimates across larger landscape scales [88,89]. Indeed, given how well the LiDAR estimates AGB in this environment, forward monitoring could be based on the passive satellite systems with LiDAR technologies used in a sampling capacity to provide calibration and validation data [24].

5. Conclusions

This study examined the relationship between tropical PSF AGB and small-footprint airborne LiDAR DR- and FW-derived metrics with a view to establishing the optimal use of this technology in this environment. Plot-based multiple regression analysis was performed to establish the best predictive models of PSF AGB using DR metrics (only), FW metrics (only), and a combination of DR and FW metrics. All three final models presented a high correlation with AGB estimates, with an $R^2 \geq 0.73$ and no statistical difference between the rRMSE of these models.

Overall, the results demonstrate that a Combination-model, coupling the benefits derived from both DR and FW metrics, had the best performance in modelling AGB for tropical PSF ($R^2 = 0.77$, RMSE = 36.4, rRMSE = 10.8%). The study found that perhaps of greater importance is metric selection, as opposed to LiDAR data type (DR, FW, Combination) for assessing AGB prediction. In particular, the top ranked metrics in the best performing models related to mid-canopy order height metrics, this indicating the importance of suppressed tree crowns and forest structural diversity in the mid-level portions of PSF for reliable AGB assessment.

Overall, the utility of LiDAR for tropical PSF AGB mapping and monitoring is enormous. The ever-increasing role of LiDAR in supporting forestry applications is encouraged by the recent development and expansion in sensor technology and platforms, with LiDAR data more accessible and at a lower cost than ever before. Published studies on tropical PSF AGB are few, in particular for Peninsular Malaysia, thus as a result this study contributes significantly to tropical PSF ecology. The study underpins AGB estimation across the NSPSF reserve going forward and has direct applications for sustainable tropical PSF management, supporting decision and policy makers in the preservation and protection of South East Asia's vulnerable tropical peatlands.

Author Contributions: C.B. is a PhD student and under the supervision of D.S.B. and S.S. conceived and executed the research. C.B. was assisted in the field by S.L.E. and with data processing by D.C. C.B. undertook analyses and C.B. and D.S.B. wrote the manuscripts with input from S.S. and P.A.

Acknowledgments: We would like to thank the Airborne Research Facility of the UK's Natural Environment Research Council for providing the airborne LiDAR datasets (to PA and DB). This work was supported by the Natural Environment Research Council [NE/L002604/1], under the Envision DTP (to PA, SS, and DB). Additional support from the University of Nottingham. We are very grateful to Martin Isenburg for generously granting the project with a complimentary full academic LAStools licence, under the LASmoons programme. We would like to thank Lahirus S. Wijedasa for his assistance and guidance with fieldwork at the pilot stage of the project. Special thanks go to the Selangor State Forestry Department for granting reserve access and providing field ranger support for data collection, and sharing their expert knowledge and experiences working in the reserve.

Conflicts of Interest: The authors declare no conflict of interest.

References

1. Page, S.E.; Rieley, J.O.; Shotyk, Ø.W.; Weiss, D. Interdependence of peat and vegetation in a tropical peat swamp forest. In *Changes and Disturbance in Tropical Rainforest in South-East Asia*; Royal Society: London, UK, 1999; pp. 161–173.
2. Wijedasa, L.S.; Jauhiainen, J.; Könönen, M.; Lampela, M.; Vasander, H.; Leblanc, M.C.; Evers, S.; Smith, T.E.; Yule, C.M.; Varkkey, H.; et al. Denial of long-term issues with agriculture on tropical peatlands will have devastating consequences. *Glob. Chang. Biol.* **2017**, *23*, 977–982. [CrossRef] [PubMed]
3. Miettinen, J.; Shi, C.; Liew, S.C. Land cover distribution in the peatlands of Peninsular Malaysia, Sumatra and Borneo in 2015 with changes since 1990. *Glob. Ecol. Conserv.* **2016**, *6*, 67–78. [CrossRef]
4. Miettinen, J.; Shi, C.; Liew, S.C. Two decades of destruction in Southeast Asia's peat swamp forests. *Front. Ecol. Environ.* **2012**, *10*, 124–128. [CrossRef]
5. Page, S.E.; Rieley, J.O.; Banks, C.J. Global and regional importance of the tropical peatland carbon pool. *Glob. Chang. Biol.* **2011**, *17*, 798–818. [CrossRef]
6. Intergovernmental Panel on Climate Change (IPCC). Summary for Policymakers. In *Climate Change 2007: The Physical Science Basis. Contribution of Working Group I to the Fourth Assessment*; Solomon, S., Qin, D., Manning, M., Chen, Z., Marquis, M., Averyt, K.B., Tignor, M., Miller, H.L., Eds.; Report of the Intergovernmental Panel on Climate Change; Cambridge University Press: Cambridge, UK, 2007.
7. Ballhorn, U.; Siegert, F.; Mason, M.; Limin, S. Derivation of burn scar depths and estimation of carbon emissions with LIDAR in Indonesian peatlands. *Proc. Natl. Acad. Sci. USA* **2009**, *106*, 21213–21218. [CrossRef] [PubMed]
8. Hooijer, A.; Page, S.; Canadell, J.G.; Silvius, M.; Kwadijk, J.; Wösten, H.; Jauhiainen, J. Current and future CO_2 emissions from drained peatlands in Southeast Asia. *Biogeosciences* **2010**, *7*, 1505–1514. [CrossRef]
9. Page, S.E.; Siegert, F.; Rieley, J.O.; Boehm, H.D.; Jaya, A.; Limin, S. The amount of carbon released from peat and forest fires in Indonesia during 1997. *Nature* **2002**, *420*, 61–65. [CrossRef] [PubMed]
10. Page, S.E.; Banks, C.J.; Rieley, J.O. Tropical peatlands: Distribution, extent and carbon storage-uncertainties and knowledge gaps. *Peatl. Int.* **2007**, *2*, 26–27.
11. Jauhiainen, J.; Takahashi, H.; Heikkinen, J.E.; Martikainen, P.J.; Vasander, H. Carbon fluxes from a tropical peat swamp forest floor. *Glob. Chang. Biol.* **2005**, *11*, 1788–1797. [CrossRef]
12. Langner, A.; Miettinen, J.; Siegert, F. Land cover change 2002–2005 in Borneo and the role of fire derived from MODIS imagery. *Glob. Chang. Biol.* **2007**, *13*, 2329–2340. [CrossRef]
13. Gaveau, D.L.; Salim, M.A.; Hergoualc'h, K.; Locatelli, B.; Sloan, S.; Wooster, M.; Marlier, M.E.; Molidena, E.; Yaen, H.; DeFries, R.; et al. Major atmospheric emissions from peat fires in Southeast Asia during non-drought years: Evidence from the 2013 Sumatran fires. *Sci. Rep.* **2014**, *4*, 6112. [CrossRef] [PubMed]
14. Van der Werf, G.R.; Dempewolf, J.; Trigg, S.N.; Randerson, J.T.; Kasibhatla, P.S.; Giglio, L.; Murdiyarso, D.; Peters, W.; Morton, D.C.; Collatz, G.J.; et al. Climate regulation of fire emissions and deforestation in equatorial Asia. *Proc. Natl. Acad. Sci. USA* **2008**, *105*, 20350–20355. [CrossRef] [PubMed]
15. Murdiyarso, D.; Hergoualc'h, K.; Verchot, L.V. Opportunities for reducing greenhouse gas emissions in tropical peatlands. *Proc. Natl. Acad. Sci. USA* **2010**, *107*, 19655–19660. [CrossRef] [PubMed]
16. Asner, G.P.; Brodrick, P.G.; Philipson, C.; Vaughn, N.R.; Martin, R.E.; Knapp, D.E.; Heckler, J.; Evans, L.J.; Jucker, T.; Goossens, B.; et al. Mapped aboveground carbon stocks to advance forest conservation and recovery in Malaysian Borneo. *Biol. Conserv.* **2018**, *217*, 289–310. [CrossRef]
17. Sullivan, M.J.; Talbot, J.; Lewis, S.L.; Phillips, O.L.; Qie, L.; Begne, S.K.; Chave, J.; Cuni-Sanchez, A.; Hubau, W.; Lopez-Gonzalez, G.; et al. Diversity and carbon storage across the tropical forest biome. *Sci. Rep.* **2017**, *7*, 39102. [CrossRef] [PubMed]
18. Yule, C.M.; Gomez, L.N. Leaf litter decomposition in a tropical peat swamp forest in Peninsular Malaysia. *Wetl. Ecol. Manag.* **2009**, *17*, 231–241. [CrossRef]
19. Chave, J.; Réjou-Méchain, M.; Búrquez, A.; Chidumayo, E.; Colgan, M.S.; Delitti, W.B.; Duque, A.; Eid, T.; Fearnside, P.M.; Goodman, R.C.; et al. Improved allometric models to estimate the aboveground biomass of tropical trees. *Glob. Chang. Biol.* **2014**, *20*, 3177–3190. [CrossRef] [PubMed]
20. Asner, G.P.; Martin, R.E.; Anderson, C.B.; Knapp, D.E. Quantifying forest canopy traits: Imaging spectroscopy versus field survey. *Remote Sens. Environ.* **2015**, *158*, 15–27. [CrossRef]
21. Aplin, P. Remote sensing: Ecology. *Prog. Phys. Geogr.* **2005**, *29*, 104–113. [CrossRef]

22. Dubayah, R.O.; Drake, J.B. Lidar remote sensing for forestry. *J. For.* **2000**, *98*, 44–46.
23. Lim, K.; Treitz, P.; Wulder, M.; St-Onge, B.; Flood, M. LiDAR remote sensing of forest structure. *Prog. Phys. Geogr.* **2003**, *27*, 88–106. [CrossRef]
24. Wulder, M.A.; White, J.C.; Bater, C.W.; Coops, N.C.; Hopkinson, C.; Chen, G. Lidar plots—A new large-area data collection option: Context, concepts, and case study. *Can. J. Remote Sens.* **2012**, *38*, 600–618. [CrossRef]
25. Coomes, D.A.; Dalponte, M.; Jucker, T.; Asner, G.P.; Banin, L.F.; Burslem, D.F.; Lewis, S.L.; Nilus, R.; Phillips, O.L.; Phua, M.H.; et al. Area-based vs. tree-centric approaches to mapping forest carbon in Southeast Asian forests from airborne laser scanning data. *Remote Sens. Environ.* **2017**, *194*, 77–88. [CrossRef]
26. Ni-Meister, W.; Lee, S.; Strahler, A.H.; Woodcock, C.E.; Schaaf, C.; Yao, T.; Ranson, K.J.; Sun, G.; Blair, J.B. Assessing general relationships between aboveground biomass and vegetation structure parameters for improved carbon estimate from lidar remote sensing. *J. Geophys. Res. Biogeosci.* **2010**, *115*. [CrossRef]
27. Thapa, R.B.; Watanabe, M.; Motohka, T.; Shiraishi, T.; Shimada, M. Calibration of aboveground forest carbon stock models for major tropical forests in central Sumatra using airborne LiDAR and field measurement data. *IEEE J. Sel. Top. Appl. Earth Obs. Remote Sens.* **2015**, *8*, 661–673. [CrossRef]
28. Dubayah, R.O.; Sheldon, S.L.; Clark, D.B.; Hofton, M.A.; Blair, J.B.; Hurtt, G.C.; Chazdon, R.L. Estimation of tropical forest height and biomass dynamics using lidar remote sensing at La Selva, Costa Rica. *J. Geophys. Res. Biogeosci.* **2010**, *115*. [CrossRef]
29. He, Q.; Chen, E.; An, R.; Li, Y. Above-ground biomass and biomass components estimation using LiDAR data in a coniferous forest. *Forests* **2013**, *4*, 984–1002. [CrossRef]
30. Ni-Meister, W.; Lee, S. Allometric Relationship between Full Waveform LiDAR measurements and Above-ground Biomass. In Proceedings of the AGU Fall Meeting Abstracts, New Orleans, LA, USA, 21–26 February 2016.
31. Sullivan, F.B.; Ducey, M.J.; Orwig, D.A.; Cook, B.; Palace, M.W. Comparison of lidar-and allometry-derived canopy height models in an eastern deciduous forest. *For. Ecol. Manag.* **2017**, *406*, 83–94. [CrossRef]
32. Palace, M.W.; Sullivan, F.B.; Ducey, M.J.; Treuhaft, R.N.; Herrick, C.; Shimbo, J.Z.; Mota-E-Silva, J. Estimating forest structure in a tropical forest using field measurements, a synthetic model and discrete return lidar data. *Remote Sens. Environ.* **2015**, *161*, 1–11. [CrossRef]
33. Saatchi, S.S.; Harris, N.L.; Brown, S.; Lefsky, M.; Mitchard, E.T.; Salas, W.; Zutta, B.R.; Buermann, W.; Lewis, S.L.; Hagen, S.; et al. Benchmark map of forest carbon stocks in tropical regions across three continents. *Proc. Natl. Acad. Sci. USA* **2011**, *108*, 9899–9904. [CrossRef] [PubMed]
34. Asner, G.P.; Powell, G.V.; Mascaro, J.; Knapp, D.E.; Clark, J.K.; Jacobson, J.; Kennedy-Bowdoin, T.; Balaji, A.; Paez-Acosta, G.; Victoria, E.; et al. High-resolution forest carbon stocks and emissions in the Amazon. *Proc. Natl. Acad. Sci. USA* **2010**, *107*, 16738–16742. [CrossRef] [PubMed]
35. Asner, G.P.; Mascaro, J.; Muller-Landau, H.C.; Vieilledent, G.; Vaudry, R.; Rasamoelina, M.; Hall, J.S.; Van Breugel, M. A universal airborne LiDAR approach for tropical forest carbon mapping. *Oecologia* **2012**, *168*, 1147–1160. [CrossRef] [PubMed]
36. Wang, C.; Menenti, M.; Stoll, M.P.; Feola, A.; Belluco, E.; Marani, M. Separation of ground and low vegetation signatures in LiDAR measurements of salt-marsh environments. *IEEE Trans. Geosci. Remote Sens.* **2009**, *47*, 2014–2023. [CrossRef]
37. Hopkinson, C.; Chasmer, L.E.; Sass, G.; Creed, I.F.; Sitar, M.; Kalbfleisch, W.; Treitz, P. Vegetation class dependent errors in lidar ground elevation and canopy height estimates in a boreal wetland environment. *Can. J. Remote Sens.* **2005**, *31*, 191–206. [CrossRef]
38. Wu, J.; Van Aardt, J.A.; Asner, G.P.; Kennedy-Bowdoin, T.; Knapp, D.; Erasmus, B.F.; Mathieu, R.; Wessels, K.; Smit, I.P. *Lidar Waveform-Based Woody and Foliar Biomass Estimation in Savanna Environments*; Rochester Institute of Technology: Rochester, NY, USA, 2009. Available online: https://www.researchgate.net/profile/Jan_Van_Aardt/publication/216859169_LiDAR_Waveform-based_Woody_and_Foliar_Biomass_Estimation_in_Savanna_Environments/links/00b7d515c456a3afb9000000.pdfb (accessed on 4 December 2017).
39. Hancock, S.; Armston, J.; Li, Z.; Gaulton, R.; Lewis, P.; Disney, M.; Danson, F.M.; Strahler, A.; Schaaf, C.; Anderson, K.; et al. Waveform lidar over vegetation: An evaluation of inversion methods for estimating return energy. *Remote Sens. Environ.* **2015**, *164*, 208–224. [CrossRef]

40. Drake, J.B.; Knox, R.G.; Dubayah, R.O.; Clark, D.B.; Condit, R.; Blair, J.B.; Hofton, M. Above-ground biomass estimation in closed canopy neotropical forests using lidar remote sensing: Factors affecting the generality of relationships. *Glob. Ecol. Biogeogr.* **2003**, *12*, 147–159. [CrossRef]
41. Drake, J.B.; Dubayah, R.O.; Clark, D.B.; Knox, R.G.; Blair, J.B.; Hofton, M.A.; Chazdon, R.L.; Weishampel, J.F.; Prince, S. Estimation of tropical forest structural characteristics using large-footprint lidar. *Remote Sens. Environ.* **2002**, *79*, 305–319. [CrossRef]
42. Pirotti, F.; Laurin, G.V.; Vettore, A.; Masiero, A.; Valentini, R. Small footprint full-waveform metrics contribution to the prediction of biomass in tropical forests. *Remote Sens.* **2014**, *6*, 9576–9599. [CrossRef]
43. Nie, S.; Wang, C.; Zeng, H.; Xi, X.; Li, G. Above-ground biomass estimation using airborne discrete-return and full-waveform LiDAR data in a coniferous forest. *Ecol. Indic.* **2017**, *78*, 221–228. [CrossRef]
44. Sumnall, M.J.; Hill, R.A.; Hinsley, S.A. Comparison of small-footprint discrete return and full waveform airborne LiDAR data for estimating multiple forest variables. *Remote Sens. Environ.* **2016**, *173*, 214–223. [CrossRef]
45. Lindberg, E.; Olofsson, K.; Holmgren, J.; Olsson, H. Estimation of 3D vegetation structure from waveform and discrete return airborne laser scanning data. *Remote Sens. Environ.* **2012**, *118*, 151–161. [CrossRef]
46. Neuenschwander, A.L.; Magruder, L.A.; Tyler, M. Landcover classification of small-footprint, full-waveform lidar data. *J. Appl. Remote Sens.* **2009**, *3*, 033544. [CrossRef]
47. Cao, L.; Coops, N.C.; Hermosilla, T.; Innes, J.; Dai, J.; She, G. Using small-footprint discrete and full-waveform airborne LiDAR metrics to estimate total biomass and biomass components in subtropical forests. *Remote Sens.* **2014**, *6*, 7110–7135. [CrossRef]
48. Cao, L.; Coops, N.C.; Innes, J.; Dai, J.; She, G. Mapping above-and below-ground biomass components in subtropical forests using small-footprint LiDAR. *Forests* **2014**, *5*, 1356–1373. [CrossRef]
49. Wan-Mohd-Jaafar, W.S.; Woodhouse, I.H.; Silva, C.A.; Omar, H.; Hudak, A.T. Modelling individual tree aboveground biomass using discrete return lidar in lowland dipterocarp forest of Malaysia. *J. Trop. For. Sci.* **2017**, *29*, 465–484.
50. Manuri, S.; Andersen, H.E.; McGaughey, R.J.; Brack, C. Assessing the influence of return density on estimation of lidar-based aboveground biomass in tropical peat swamp forests of Kalimantan, Indonesia. International. *J. Appl. Earth Obs. Geoinf.* **2017**, *56*, 24–35. [CrossRef]
51. Jubanski, J.; Ballhorn, U.; Kronseder, K.; Franke, J.; Siegert, F. Detection of large above-ground biomass variability in lowland forest ecosystems by airborne LiDAR. *Biogeosciences* **2013**, *10*, 3917–3930. [CrossRef]
52. Kronseder, K.; Ballhorn, U.; Böhm, V.; Siegert, F. Above ground biomass estimation across forest types at different degradation levels in Central Kalimantan using LiDAR data. *Int. J. Appl. Earth Obs. Geoinf.* **2012**, *18*, 37–48. [CrossRef]
53. Ahmad, N. Guardians of the North Selangor Peat Swamp Forest. 2014. Available online: https://peatlandsinternational.wordpress.com/2014/06/20/peatlands-international-2-2014/ (accessed on 20 June 2014).
54. Prentice, C.; Aikanathan, S. *A Preliminary Faunal Survey of the North Selangor Peat Swamp Forest*; World Wildlife Fund Malaysia: Petaling Jaya, Malaysia, 1989.
55. Parish, F.; Dahalan, M.; Rahim, H. *Integrated Management Plan for North Selangor Peat Swamp Forest 2014–2023 for Selangor State Forestry Department*; Draft (30 June 2014) Revision 2.4; Global Environment Centre: Petaling Jaya, Malaysia, 2014.
56. Regional Centre for Forest Management (RCFM) and Ecosystem Management Services (EMS). *Report on The Management Inventory of the North Selangor Peat Swamp Forest*; Malaysian-DANCED Project on Sustainable Managment of Peat Swamp Forest; Project Document Number 25; Malaysia Office: Petaling Jaya, Malaysia, 2000.
57. Tonks, A.J.; Aplin, P.; Beriro, D.J.; Cooper, H.; Evers, S.; Vane, C.H.; Sjögersten, S. Impacts of conversion of tropical peat swamp forest to oil palm plantation on peat organic chemistry, physical properties and carbon stocks. *Geoderma* **2017**, *289*, 36–45. [CrossRef]
58. Rejou-Mechain, M.; Tanguy, A.; Piponiot, C.; Chave, J.; Herault, B. BIOMASS: Estimating Aboveground Biomass and Its Uncertainty in Tropical Forests. 2017. R Package Version 1.1. Available online: https://CRAN.R-project.org/package=BIOMASS (accessed on 2 October 2017).
59. LAStools, "Efficient LiDAR Processing Software" (Version 141017, Academic). Available online: http://rapidlasso.com/LAStools (accessed on 2 October 2017).

60. Bunting, P.; Armston, J.; Clewley, D.; Lucas, R.M. Sorted pulse data (SPD) library—Part II: A processing framework for LiDAR data from pulsed laser systems in terrestrial environments. *Comput. Geosci.* **2013**, *56*, 207–215. [CrossRef]
61. Wagner, W.; Ullrich, A.; Melzer, T.; Briese, C.; Kraus, K. From Single-Pulse to Full-Waveform Airborne Laser Scanners: Potential and Practical Challenges. 2 July 2004. Available online: http://www.isprs.org/proceedings/XXXV/congress/comm3/papers/267.pdf (accessed on 10 October 2017).
62. Zhang, K.; Chen, S.C.; Whitman, D.; Shyu, M.L.; Yan, J.; Zhang, C. A progressive morphological filter for removing nonground measurements from airborne LIDAR data. *IEEE Trans. Geosci. Remote Sens.* **2003**, *41*, 872–882. [CrossRef]
63. Evans, J.S.; Hudak, A.T. A multiscale curvature algorithm for classifying discrete return LiDAR in forested environments. *IEEE Trans. Geosci. Remote Sens.* **2007**, *45*, 1029–1038. [CrossRef]
64. Langton, S.D.; Briggs, P.A.; Haysom, K.A. Daubenton's bat distribution along rivers–developing and testing a predictive model. *Aquat. Conserv. Mar. Freshw. Ecosyst.* **2010**, *20*. [CrossRef]
65. Barton, K. MuMIn: Multi-Model Inference. 2017. R Package Version 1.40.0. Available online: https://CRAN.R-project.org/package=MuMIn (accessed on 20 November 2017).
66. Burnham, K.P.; Anderson, D.R. *Model Selection and Multimodel Inference: A Practical Information-Theoretic Approach*; Springer: Berlin, Germany, 2003.
67. Peduzzi, A.; Wynne, R.H.; Fox, T.R.; Nelson, R.F.; Thomas, V.A. Estimating leaf area index in intensively managed pine plantations using airborne laser scanner data. *For. Ecol. Manag.* **2012**, *270*, 54–65. [CrossRef]
68. Lawson, I.T.; Kelly, T.J.; Aplin, P.; Boom, A.; Dargie, G.; Draper, F.C.; Hassan, P.N.; Hoyos-Santillan, J.; Kaduk, J.; Large, D.; et al. Improving estimates of tropical peatland area, carbon storage, and greenhouse gas fluxes. *Wetl. Ecol. Manag.* **2015**, *23*, 327–346. [CrossRef]
69. Zhao, K.; Popescu, S.; Nelson, R. Lidar remote sensing of forest biomass: A scale-invariant estimation approach using airborne lasers. *Remote Sens. Environ.* **2009**, *113*, 182–196. [CrossRef]
70. Hermosilla, T.; Ruiz, L.A.; Kazakova, A.N.; Coops, N.C.; Moskal, L.M. Estimation of forest structure and canopy fuel parameters from small-footprint full-waveform LiDAR data. *Int. J. Wildl. Fire* **2014**, *23*, 224–233. [CrossRef]
71. Richardson, J.J.; Moskal, L.M. Strengths and limitations of assessing forest density and spatial configuration with aerial LiDAR. *Remote Sens. Environ.* **2011**, *115*, 2640–2651. [CrossRef]
72. Reitberger, J.; Schnörr, C.; Krzystek, P.; Stilla, U. 3D segmentation of single trees exploiting full waveform LIDAR data. *ISPRS J. Photogramm. Remote Sens.* **2009**, *64*, 561–574. [CrossRef]
73. Bye, I.J.; North, P.R.; Los, S.O.; Kljun, N.; Rosette, J.A.; Hopkinson, C.; Chasmer, L.; Mahoney, C. Estimating forest canopy parameters from satellite waveform LiDAR by inversion of the FLIGHT three-dimensional radiative transfer model. *Remote Sens. Environ.* **2017**, *188*, 177–189. [CrossRef]
74. Unger, D.R.; Hung, I.K.; Brooks, R.; Williams, H. Estimating number of trees, tree height and crown width using Lidar data. *GISci. Remote Sens.* **2014**, *51*, 227–238. [CrossRef]
75. Alexander, C.; Korstjens, A.H.; Hill, R.A. Influence of micro-topography and crown characteristics on tree height estimations in tropical forests based on LiDAR canopy height models. *Int. J. Appl. Earth Obs. Geoinf.* **2018**, *65*, 105–113. [CrossRef]
76. Science Beta, NASA, National Academy of Sciences and NASA's Science Mission Directorate 2016. Available online: https://science.nasa.gov/missions/gedi (accessed on 13 February 2018).
77. Wallace, L.; Lucieer, A.; Watson, C.S. Evaluating tree detection and segmentation routines on very high resolution UAV LiDAR data. *IEEE Trans. Geosci. Remote Sens.* **2014**, *52*, 7619–7628. [CrossRef]
78. Shang, X.; Chazette, P. Interest of a full-waveform flown UV lidar to derive forest vertical structures and aboveground carbon. *Forests* **2014**, *5*, 1454–1480. [CrossRef]
79. Pang, Y.; Li, Z.; Ju, H.; Lu, H.; Jia, W.; Si, L.; Guo, Y.; Liu, Q.; Li, S.; Liu, L.; et al. LiCHy: The CAF's LiDAR, CCD and hyperspectral integrated airborne observation system. *Remote Sens.* **2016**, *8*, 398. [CrossRef]
80. Kim, S.; McGaughey, R.J.; Andersen, H.E.; Schreuder, G. Tree species differentiation using intensity data derived from leaf-on and leaf-off airborne laser scanner data. *Remote Sens. Environ.* **2009**, *113*, 1575–1586. [CrossRef]
81. Moffiet, T.; Mengersen, K.; Witte, C.; King, R.; Denham, R. Airborne laser scanning: Exploratory data analysis indicates potential variables for classification of individual trees or forest stands according to species. *ISPRS J. Photogramm. Remote Sens.* **2005**, *59*, 289–309. [CrossRef]

82. Reitberger, J.; Krzystek, P.; Stilla, U. Analysis of full waveform LIDAR data for the classification of deciduous and coniferous trees. *Int. J. Remote Sens.* **2008**, *29*, 1407–1431. [CrossRef]
83. Sumnall, M.; Fox, T.R.; Wynne, R.H.; Thomas, V.A. Mapping the height and spatial cover of features beneath the forest canopy at small-scales using airborne scanning discrete return Lidar. *ISPRS J. Photogramm. Remote Sens.* **2017**, *133*, 186–200. [CrossRef]
84. Li, M.; Im, J.; Quackenbush, L.J.; Liu, T. Forest biomass and carbon stock quantification using airborne LiDAR data: A case study over Huntington wildlife forest in the Adirondack Park. *IEEE J. Sel. Top. Appl. Earth Obs. Remote Sens.* **2014**, *7*, 3143–3156. [CrossRef]
85. Brandtberg, T.; Warner, T.A.; Landenberger, R.E.; McGraw, J.B. Detection and analysis of individual leaf-off tree crowns in small footprint, high sampling density lidar data from the eastern deciduous forest in North America. *Remote Sens. Environ.* **2003**, *85*, 290–303. [CrossRef]
86. Yuen, J.Q.; Fung, T.; Ziegler, A.D. Review of allometric equations for major land covers in SE Asia: Uncertainty and implications for above-and below-ground carbon estimates. *For. Ecol. Manag.* **2016**, *360*, 323–340. [CrossRef]
87. Manuri, S.; Brack, C.; Nugroho, N.P.; Hergoualc'h, K.; Novita, N.; Dotzauer, H.; Verchot, L.; Putra, C.A.; Widyasari, E. Tree biomass equations for tropical peat swamp forest ecosystems in Indonesia. *For. Ecol. Manag.* **2014**, *334*, 241–253. [CrossRef]
88. Mora, B.; Wulder, M.A.; Hobart, G.W.; White, J.C.; Bater, C.W.; Gougeon, F.A.; Varhola, A.; Coops, N.C. Forest inventory stand height estimates from very high spatial resolution satellite imagery calibrated with lidar plots. *Int. J. Remote Sens.* **2013**, *34*, 4406–4424. [CrossRef]
89. Wilkes, P.; Jones, S.D.; Suarez, L.; Mellor, A.; Woodgate, W.; Soto-Berelov, M.; Haywood, A.; Skidmore, A.K. Mapping forest canopy height across large areas by upscaling ALS estimates with freely available satellite data. *Remote Sens.* **2015**, *7*, 12563–12587. [CrossRef]



© 2018 by the authors. Licensee MDPI, Basel, Switzerland. This article is an open access article distributed under the terms and conditions of the Creative Commons Attribution (CC BY) license (http://creativecommons.org/licenses/by/4.0/).

Appendix 2: Denial of long-term issues with agriculture on tropical peatlands will have devastating consequences

Global Change Biology

Global Change Biology (2017) 23, 977–982, doi: 10.1111/gcb.13516

LETTER TO THE EDITOR

Denial of long-term issues with agriculture on tropical peatlands will have devastating consequences

LAHIRU S. WIJEDASA[1,2,3,*], JYRKI JAUHIAINEN[4], MARI KÖNÖNEN[4], MAIJA LAMPELA[4], HARRI VASANDER[4], MARIE-CLAIRE LEBLANC[5], STEPHANIE EVERS[6,7,8], THOMAS E. L. SMITH[9], CATHERINE M. YULE[7,10], HELENA VARKKEY[7,11], MASSIMO LUPASCU[12], FAIZAL PARISH[13], IAN SINGLETON[14], GOPALASAMY R. CLEMENTS[3,6,10,15,16], SHEEMA ABDUL AZIZ[3,6,16], MARK E. HARRISON[17,18], SUSAN CHEYNE[17], GUSTI Z. ANSHARI[19], ERIK MEIJAARD[20,21], JENNY E. GOLDSTEIN[22], SUSAN WALDRON[23], KRISTELL HERGOUALC'H[24], RENE DOMMAIN[25], STEVE FROLKING[26], CHRISTOPHER D. EVANS[27], MARY ROSE C. POSA[1], PAUL H. GLASER[28], NYOMAN SURYADIPUTRA[29], REZA LUBIS[29], TRULY SANTIKA[21], RORY PADFIELD[7,30,31], SOFYAN KURNIANTO[24,32], PANUT HADISISWOYO[33], TECK WYN LIM[34], SUSAN E. PAGE[18], VINCENT GAUCI[35], PETER J. VAN DER MEER[36], HELEN BUCKLAND[37], FABIEN GARNIER[37], MARSHALL K. SAMUEL[6,7,38,39], LIZA NURIATI LIM KIM CHOO[38], PATRICK O'REILLY[7,40,41], MATTHEW WARREN[42], SURIN SUKSUWAN[43], ELHAM SUMARGA[44], ANUJ JAIN[2,45], WILLIAM F. LAURANCE[46], JOHN COUWENBERG[47], HANS JOOSTEN[47], RONALD VERNIMMEN[48], ALJOSJA HOOIJER[48], CHRIS MALINS[49], MARK A. COCHRANE[50], BALU PERUMAL[51], FLORIAN SIEGERT[52,53], KELVIN S.-H. PEH[54,55], LOUIS-PIERRE COMEAU[56], LOUIS VERCHOT[57], CHARLES F. HARVEY[58,59], ALEX COBB[59], ZEEHAN JAAFAR[1,60], HENK WÖSTEN[61], SOLICHIN MANURI[62], MORITZ MÜLLER[63], WIM GIESEN[64], JACOB PHELPS[65], DING LI YONG[6,3,66], MARCEL SILVIUS[67], BÉATRICE M. M. WEDEUX[68], ALISON HOYT[58,59], MITSURU OSAKI[69], TAKASHI HIRANO[69], HIDENORI TAKAHASHI[70], TAKASHI S. KOHYAMA[69], AKIRA HARAGUCHI[71], NUNUNG P. NUGROHO[72], DAVID A. COOMES[68], LE PHAT QUOI[73], ALUE DOHONG[74], HARIS GUNAWAN[74], DAVID L. A. GAVEAU[24], ANDREAS LANGNER[75], FELIX K. S. LIM[76], DAVID P. EDWARDS[76], XINGLI GIAM[77], GUIDO VAN DER WERF[78], RACHEL CARMENTA[24], CASPAR C. VERWER[79], LUKE GIBSON[80], LAURE GANDOIS[81], LAURA LINDA BOZENA GRAHAM[82], JHANSON REGALINO[82], SERGE A. WICH[8,83], JACK RIELEY[84], NICHOLAS KETTRIDGE[85], CHLOE BROWN[84], ROMAIN PIRARD[24], SAM MOORE[86], B. RIPOLL CAPILLA[17], UWE BALLHORN[53], HUA CHEW HO[87], AGATA HOSCILO[88], SANDRA LOHBERGER[53], THEODORE A. EVANS[89], NINA YULIANTI[90], GRACE BLACKHAM[91], ONRIZAL[92], SIMON HUSSON[17], DANIEL MURDIYARSO[24,93], SUNITA PANGALA[35], LYDIA E. S. COLE[94], LUCA TACCONI[95], HENDRIK SEGAH[91], PRAYOTO TONOTO[96], JANICE S. H. LEE[97], GERALD SCHMILEWSKI[98], STEPHAN WULFFRAAT[99], ERIANTO INDRA PUTRA[2,5,100], MEGAN E. CATTAU[101], R. S. CLYMO[102], ROSS MORRISON[103], AAZANI MUJAHID[104], JUKKA MIETTINEN[105], SOO CHIN LIEW[105], SAMU VALPOLA[106], DAVID WILSON[107], LAURA D'ARCY[17], MICHIEL GERDING[98], SITI SUNDARI[108], SARA A. THORNTON[17,18], BARBARA KALISZ[109], STEPHEN J. CHAPMAN[110], AHMAD SUHAIZI MAT SU[111], IMAM BASUKI[24,32], MASAYUKI ITOH[112], CARL TRAEHOLT[113], SEAN SLOAN[46], ALEXANDER K. SAYOK[114] and ROXANE ANDERSEN[115,*]

[1]*Department of Biological Sciences, National University of Singapore, 14 Science Drive 4, 117543, Singapore,* [2]*ConservationLinks, 433 Clementi Avenue 3, #01-258, 120433, Singapore,* [3]*Rimba, Malaysia, Jalan 1/9D, Bandar Baru Bangi, Selangor, MY 43650, Malaysia,* [4]*University of Helsinki, P.O. Box 3 (Fabianinkatu 33), 00014 Helsinki, Finland,* [5]*Faculté des Sciences de l'Agriculture et de l'Alimentation, 2425, Rue de l'agriculture, Pavillon Paul-Comtois, Bureau 1122, Ville de Québec, QC G1V 0A6, Canada,* [6]*School of Biosciences, University of Nottingham Malaysia Campus, Jalan Broga, 43500 Semenyih, Selangor Darhul Ehsan, Malaysia,* [7]*Tropical Catchment Research Initiative (TROCARI), Kuala Lumpur, Malaysia,* [8]*School of Natural Sciences &*

Correspondence: Lahiru Wijedasa & Roxane Andersen, tel. +65-90667160, fax +65-67792486, e-mails: lahirux@gmail.com, Roxane.Andersen@uhi.ac.uk

© 2017 The Authors Global Change Biology Published by John Wiley & Sons Ltd.
This is an open access article under the terms of the Creative Commons Attribution-NonCommercial-NoDerivs License, which permits use and distribution in any medium, provided the original work is properly cited, the use is non-commercial and no modifications or adaptations are made.

Psychology, Liverpool John Moores University, Byrom Street, Liverpool L33AF, UK, [9]*School of Geography, King's College London, London WC2R 2NA, UK,* [10]*Monash University Malaysia, Jalan Lagoon Selatan, Bandar Sunway, 47500 Subang Jaya, Selangor, Malaysia,* [11]*Department of International & Strategic Studies and Asia-Europe Institute, University of Malaya, 50603 Kuala Lumpur, Malaysia,* [12]*Department of Geography, National University of Singapore, AS2, #03-01, 1 Arts Link, Kent Ridge, 117570, Singapore,* [13]*Global Environment Centre, 2nd Floor, Wisma Hing, 78, Jalan SS2/72, Petaling Jaya, Selangor 47300, Malaysia,* [14]*Sumatran Orangutan Conservation Programme, Jl. Wahid Hasyim No. 51/74 Medan, 20154 Sumatera Utara – Indonesia, ,* [15]*Kenyir Research Institute, Universiti MalaysiaTerengganu, T145, 21300 Kuala Terengganu, Malaysia,* [16]*Departement d'Écologie et Gestion de la Biodiversité, Muséum National d'Histoire Naturelle, UMR 7179/CNRS-MNHN, 1 Avenue du Petit Chateau, 91800 Brunoy, France,* [17]*Borneo Nature Foundation, Jalan Bukit Raya No. 82 Bukit Raya Palangka Raya, 73112 Central Kalimantan, Indonesia,* [18]*University of Leicester, University Rd, Leicester LE1 7RH, UK,* [19]*Centre for Wetlands, People and Biodiverstiy, Tanjungpura University, Pontianak Tenggara, Barat, 78124 Western Kalimantan, Indonesia,* [20]*Borneo Futures, Country Woods 306, Jalan WR Supratman, Pondok Ranji-Rengas, Ciputat, 15412 Tangerang, Indonesia,* [21]*School of Biological Sciences, University of Queensland, Brisbane, QLD 4072, Australia,* [22]*Cornell University, Ithaca, NY 14850, USA,* [23]*School of Geographical and Earth Sciences, University of Glasgow, R517B Level 5 GES, East Quadrangle, Main Building, Glasgow G12 8QQ, UK,* [24]*Center for International Forestry Research (CIFOR), P.O. Box 0113 BOCBD, Bogor 16000, Indonesia,* [25]*Human Origins Program, National Museum of Natural History, Smithsonian Institution, 10th St. & Constitution Ave. NW, Washington, D.C. 20560, USA,* [26]*Institute for the Study of Earth, Oceans and Space, University of New Hampshire, Durham, NH 03824, USA,* [27]*Centre for Ecology and Hydrology, Environment Centre, Deiniol Rd, Bangor LL57, UK,* [28]*Department of Earth Sciences, University of Minnesota, 310 Pillsbury Drive SE, Minneapolis, MN 55455-0231, USA,* [29]*Wetlands International Indonesia Programme, Jl. Bango No. 11, Bogor 16161, Indonesia,* [30]*Malaysia-Japan International Institute of Technology, Universiti Teknologi Malaysia, Jalan Sultan Yahya Petra, 54100 Kuala Lumpur, Wilayah Persekutuan Kuala Lumpur, Malaysia,* [31]*Department of Social Sciences, Oxford Brookes University, Headington Campus, Oxford OX3 0BP, UK,* [32]*Department of Fisheries and Wildlife, Oregon State University, Nash Hall, 2820 SW Campus Way, Corvallis, OR 97331, USA,* [33]*Orangutan Information Centre, Jl. Sembada XVI, Jl. Bunga Sedap Malam XVIII C No. 10 20131. Kecamatan Medan Selayang Medan, Sumatera Utara 20131, Indonesia,* [34]*Resource Stewardship Consultants Sdn Bhd, Jalan Othman, Petaling Jaya, Malaysia,* [35]*School of Environment, Earth and Ecosystem Sciences, The Open University, Walton Hall Milton Keynes MK7 6AA, UK,* [36]*Van Hall Larenstein, University of Applied Sciences, Agora 1, PO Box 1528, 8901 BV Leeuwarden, The Netherlands,* [37]*Sumatran Orangutan Society, London, 7 Stert Street, Abingdon, Oxfordshire OX14 3JF, UK,* [38]*Climate Change Programme, Malaysian Agricultural Research and Development Institute (MARDI), P.O. Box 59, Roban, 95300 Saratok, Sarawak, Malaysia,* [39]*Global Research Alliance (GRA), USDA-FAS, Washington State University, 1400 Independence Avenue, SW Mail Stop 1001, Washington, D.C. 20250, USA,* [40]*Crops for the Future, Jalan Broga, 43500 Semenyih, Selangor Darul Ehsan, Malaysia,* [41]*School of Politics, History and International Relations, University of Nottingham Malaysia Campus, Jalan Broga, 43500 Semenyih, Selangor Darul Ehsan, Malaysia,* [42]*USDA Forest Service, Northern Research Station, 410 MacInnes Drive, Houghton, MI 49931-1199, USA,* [43]*Proforest, Suite #303, MBE Desa Sri Hartamas No. 30G, Jalan 25/70 A, 50480, Kuala Lumpur, Malaysia,* [44]*School of Life Sciences and Technology, Institut Teknologi Bandung, Jl. Ganesa 10, Coblong, Kota Bandung, Jawa Barat 40132, Indonesia,* [45]*BirdLife International, The David Attenborough Building, 1st Floor, Pembroke Street, Cambridge CB2 3QZ, UK,* [46]*Centre for Tropical Environmental and Sustainability Science (TESS) & College of Science and Engineering, James Cook University, PO Box 6811, Cairns, Queensland 4870, Australia,* [47]*Partner in the Greifswald Mire Centre, Ernst Moritz Arndt University of Greifswald, c/o Michael Succow Stiftung, Ellernholzstr. 1/3, 17489 Greifswald, Germany,* [48]*Deltares, Boussinesqweg 1, 2629 HV Delft, Netherlands,* [49]*Cerulogy, The International Council on Clean Transportation, 11 Belgrave Road, London SW1V 1RB, UK,* [50]*Geospatial Sciences Center of Excellence, South Dakota State University, 1021 Medary Ave, Wecota Hall 115 Box 506B, Brookings, SD 57007, USA,* [51]*Malaysian Nature Society, JKR 641 Jalan Kelantan, Bukit Persekutuan, Kuala Lumpur 50480, Malaysia,* [52]*GeoBio Center, Ludwig-Maximilians-University, Richard-Wagner-Str. 10, 80333 Mü*nchen, Germany, [53]*RSS Remote Sensing Solutions GmbH, Isarstraß*e 3, 82065 Baierbrunn, Germany, [54]*Centre for Biological Sciences, University of Southampton, University Road, Southampton SO17 1BJ, UK,* [55]*Conservation Science Group, Department of Zoology, University of Cambridge, Downing St, Cambridge CB2 3EJ, UK,* [56]*Department of Geography and Resource Management, The Chinese University of Hong Kong, 2nd Floor, Wong Foo Yuan Building, Shatin, N.T., Hong Kong,* [57]*International Centre for Tropical Agriculture (CIAT), Km 17 Recta Cali-Palmira, Apartado Aé*reo 6713, 763537 Cali, Colombia, [58]*Singapore-MIT Alliance for Research and Technology, 1 CREATE Way, #10-01 CREATE Tower, 138602, Singapore,* [59]*Parsons Laboratory, Massachusetts Institute of Technology, Cambridge, 77 Massachusetts Ave 48, Cambridge, MA 02139, USA,* [60]*Department of Vertebrate Zoology, National Museum of Natural History, Smithsonian Institution, PO Box 37012 SI Building, Room 153, MRC 010, Washington, D.C. 20013-7012, USA,* [61]*Wageningen University and Research, 6708 PB Wageningen, The Netherlands,* [62]*Fenner School of Environment and Society, Australian National University, Linnaeus Way, Acton, ACT 2601, Australia,* [63]*Swinburne University of Technology Sarawak Campus, Jalan Simpang Tiga, 93300 Kuching, Sarawak, Malaysia,* [64]*Euroconsult Mott MacDonald,*

© 2017 The Authors Global Change Biology Published by John Wiley & Sons Ltd.,

Amsterdamseweg 15, 6814 CM Arnhem, The Netherlands, [65]*Lancaster Environment Centre, Library Avenue, Lancaster University, Lancaster LA1 4YQ, UK,* [66]*Southeast Asian Biodiversity Society, Raffles Museum of Biodiversity Research, Faculty of Science, The National University of Singapore, Block S6, Level 3, Science Drive 2, 117600, Singapore,* [67]*Wetlands International, P.O. Box 471, 6700 AL Wageningen, The Netherlands,* [68]*Department of Plant Sciences, University of Cambridge, Downing St, Cambridge CB2 3EA, UK,* [69]*Hokkaido University, 5 Chome Kita 8 Jonishi, Kita Ward, Sapporo, Hokkaido Prefecture 060-0808, Japan,* [70]*NPO Hokkaido Institute of Hydro-Climate, Frontier 14, N 14 W 3, Kita-ku, Sapporo 001-0014, Japan,* [71]*Kyushu Institute of Technology, 1-1 Sensui-cho, Tobata-ku, Kitakyushu-shi, Fukuoka 804-8550, Japan,* [72]*Research and Development Institute on Watershed Management Technology, Research, Development and Innovation Agency, Ministry of Environment and Forestry, Wanabakti Block I 2nd Floor Jalan Jenderal Gatot Subroto Jakarta Pusat, 10270 Jakarta, Indonesia,* [73]*Institute for Environment and Natural Resources, National University at HCM City, 6 Quarter, Linh Trung Ward, Thu Duc District, Ho Chi Minh City, Vietnam,* [74]*Peatland Restoration Agency (BRG), UNPAR, Jakarta LP3LH, Indonesia,* [75]*Joint Research Centre of the European Commission, Directorate D* – Sustainable Resources – Bio-Economy Unit, Via E. Fermi, 2749, I-21027 Ispra (VA), Italy, [76]*Department of Animal and Plant Sciences, University of Sheffield, Western Bank, Sheffield S10 2TN, UK,* [77]*School of Aquatic and Fishery Sciences, University of Washington, 1122 NE Boat St, Seattle, WA 98105, USA,* [78]*Faculty of Earth and Life Sciences, University Amsterdam, De Boelelaan 1085-1087, 1081 HV Amsterdam, The Netherlands,* [79]*International Union for Conservation of Nature (IUCN), National Committee of The Netherlands, Plantage Middenlaan 2K, 1018 DD Amsterdam, The Netherlands,* [80]*School of Biological Sciences, Kadoorie Biological Sciences Building, The University of Hong Kong, Pok Fu Lam Road, Hong Kong SAR, China,* [81]*Laboratoire Ecologie Fonctionnelle et Environnement, Universite de Toulouse, CNRS, INPT, UPS, 18, Route de Narbonne Bât.* 4R1, 31062 Toulouse Cedex 9, France, [82]*Borneo Orangutan Survival Foundation (BOSF), Jalan Papandayan No. 10, Bogor 16151, Indonesia,* [83]*Institute for Biodiversity and Ecosystem Dynamics, University of Amsterdam, P.O. Box 94248, 1090 GE Amsterdam, The Netherlands,* [84]*School of Geography, University of Nottingham, University Park, Notingham NG7 2RD, UK,* [85]*School of Geography, Earth and Environmental Science, University of Birmingham, Edgbaston, Birmingham B15 2TT, UK,* [86]*Environmental Change Institute, School of Geography and the Environment, University of Oxford, South Parks Road, Oxford OX1 3QY, UK,* [87]*Nature Society (Singapore), 510 Geylang Road, #02-05, The Sunflower, 389466, Singapore,* [88]*Remote Sensing Centre, Institute of Geodesy and Cartography, ul. Modzelewskiego 27, 02-679 Warsaw, Poland,* [89]*School of Animal Biology, University of Western Australia, 35 Stirling Highway, Crawley, Perth, WA 6009, Australia,* [90]*University of Palangka Raya, Palangkaraya, 73112 Central Kalimantan, Indonesia,* [91]*Wildfowl and Wetlands Trust, Queen Elizabeth's* Walk, London SW13 9WT, UK, [92]*Tropical Forest Ecology and Conservation Division, Faculty of Forestry, Universitas Sumatera Utara, Jl. Dr. Mansur No. 9B, Kampus USU, Padang Bulan, Kota Medan, Sumatera Utara 20155, Indonesia,* [93]*Department of Geophysics and Meteorology, Bogor Agricultural University, Jln. Meranti, Kampus IPB Darmaga, Bogor 16680, Indonesia,* [94]*Department of Global Change Biology Zoology, Oxford Long-term Ecology Laboratory, University of Oxford, The Tinbergen Building, South Parks Road, Oxford OX1 3PS, UK,* [95]*Crawford School of Public Policy, The Australian National University, Acton, Canberra, ACT 2601, Australia,* [96]*Graduate School for International Development and Cooperation, Hiroshima University, 1-5-1 Kagamiyama, Higashi-Hiroshima 739-8529, Japan,* [97]*Asian School of the Environment, Nanyang Technological University, Nanyang Avenue, Singapore,* [98]*International Peatland Society, Nisulankatu 78, 40720 Jyväskylä,* Finland, [99]*World Wide Fund for Nature, Simatupang Tower 2 Unit C 7 Floor Jl. Letjen TB. Simatupang Kav. 38, Jakarta Selatan 12540, Indonesia,* [100]*Faculty of Forestry, Bogor Agricultural University, Jl. Lingkar Akademik Kampus IPB, Dramaga, Bogor, Jawa Barat 16680, Indonesia,* [101]*Grand Challenge Earth Lab, University of Colorado, 4001 Discover Drive Suite S348, Boulder, CO 80303, USA,* [102]*Queen Mary University of London, Mile End Rd, London E1 4NS, UK,* [103]*Land Surface Flux Measurements Group, Centre for Ecology and Hydrology, Maclean Building, Benson Lane, Crowmarsh Gifford, Wallingford, Oxfordshire OX10 8BB, UK,* [104]*Department of Aquatic Science, Faculty of Resource Science and Technology, Universiti Malaysia Sarawak, 94300 Kota Samarahan, Sarawak, Malaysia,* [105]*Centre for Remote Imaging, Sensing and Processing, National University of Singapore, 10 Lower Kent Ridge Road, Blk S17, Level 2, 119076, Singapore,* [106]*Geological Survey of Finland, P.O. Box 97 (Vaasantie 6), FI 67101 Kokkola, Finland,* [107]*Earthy Matters Environmental Consultants, Glenvar, Letterkenny, Co., Donegal, Ireland,* [108]*Research Centre for Biology, Indonesian Institute of Sciences (LIPI), JL. Raya Jakarta* – Bogor Km. 46 Cibinong, 16911 Bogor, Indonesia, [109]*Department of Soil Science and Land Reclamation, Faculty of Environment and Agriculture, University of Warmia and Mazury, Michała Oczapowskiego 2, Olsztyn, Poland,* [110]*Ecological Sciences Group, The James Hutton Institute, Craigiebuckler, Aberdeen, AB158QH Scotland, UK,* [111]*Department of Agriculture Technology, Faculty of Agriculture, Universiti Putra Malaysia, 43400 Serdang, Malaysia,* [112]*Centre for Southeast Asian Studies, Kyoto University, 46 Shimoadachi-cho, Yoshida Sakyo-ku, Kyoto 606-8501, Japan,* [113]*Southeast Asia Program, Research and Conservation Division, Copenhagen Zoo, Roskildevej 32, 2000 Frederiksberg, Denmark,* [114]*Institute of Biodiversity and Environmental Conservation, Faculty of Resource Science and Technology, Universiti Malaysia Sarawak, 94300 Kota Samarahan, Sarawak, Malaysia,* [115]*Environmental Research Institute, University of Highlands and Islands, Castle St., Thurso KW147JD, UK*

© 2017 The Authors Global Change Biology Published by John Wiley & Sons Ltd., **23**, 977–982

The first International Peat Congress (IPC) held in the tropics – in Kuching (Malaysia) – brought together over 1000 international peatland scientists and industrial partners from across the world ('International Peat Congress with over 1000 participants!', 2016). The congress covered all aspects of peatland ecosystems and their management, with a strong focus on the environmental, societal and economic challenges associated with contemporary large-scale agricultural conversion of tropical peat.

However, recent encouraging developments towards better management of tropical peatlands have been undermined by misleading newspaper headlines and statements first published during the conference. Articles in leading regional newspapers ('Oil palm planting on peat soil handled well, says Uggah, 2016b; Cheng & Sibon, 2016; Nurbianto, 2016a,b; Wong, 2016) widely read across the region portrayed a general consensus, in summary of the conference, that current agricultural practices in peatland areas, such as oil palm plantations, do not have a negative impact on the environment. This view is not shared by many scientists or supported by the weight of evidence that business-as-usual management is not sustainable for tropical peatland agriculture.

Peer-reviewed scientific studies published over the last 19 years, as reflected in the Intergovernmental Panel on Climate Change (IPCC) Wetland Supplement on greenhouse gas inventories, affirm that drained tropical peatlands lose considerable amounts of carbon at high rates (Drösler *et al.*, 2014). Tropical peat swamp forests have sequestered carbon for millennia, storing a globally significant reservoir below ground in the peat (Page *et al.*, 2011; Dommain *et al.*, 2014). However, contemporary agriculture techniques on peatlands heavily impact this system through land clearance, drainage and fertilization, a process that too often involves fire. Along with biodiversity losses driven by deforestation (Koh *et al.*, 2011; Posa *et al.*, 2011; Giam *et al.*, 2012), the carbon stored in drained peatlands is rapidly lost through oxidation, dissolution and fire (Couwenberg *et al.*, 2009; Hirano *et al.*, 2012; Ramdani & Hino, 2013; Schrier-Uijl *et al.*, 2013; Carlson *et al.*, 2015; Warren *et al.*, 2016). Tropical peat fires are a major contributor to global greenhouse gas emissions and produce transboundary haze causing significant impacts on human health, regional economies and ecosystems (Page *et al.*, 2002; Marlier *et al.*, 2012; Jaafar & Loh, 2014; Chisholm *et al.*, 2016; Huijnen *et al.*, 2016; Stockwell *et al.*, 2016). With future El-Niño events predicted to increase in frequency and severity (Cai *et al.*, 2014) and with fire prevalence now decoupled from drought years (Gaveau *et al.*, 2014), future large-scale fire and haze events are imminent given the extensive areas of now-drained fire-prone drained peatlands (Kettridge *et al.*, 2015; Turetsky *et al.*, 2015; Page & Hooijer, 2016).

In reality, just how much of the estimated 69 gigatonnes of carbon (Page *et al.*, 2011) stored in South-East Asian tropical peatlands is being lost due to agricultural operations under the current management regime is still uncertain. Of great concern is that none of the agricultural management methods applied to date have been shown to prevent the loss of peat and the associated subsidence of the peatland surface following drainage (Wösten *et al.*, 1997; Melling *et al.*, 2008; Hooijer *et al.*, 2012; Evers *et al.*, 2016). Recent projections suggest that large areas of currently drained coastal peatlands will become undrainable and progressively be subjected to longer periods of inundation by river and ultimately sea water (Hooijer *et al.*, 2015a,b; Sumarga *et al.*, 2016). With growing risk of saltwater intrusion, agriculture in these coastal lands will become increasingly untenable, calling into question the very notion of 'long-term sustainability of tropical peatland agriculture'.

A more accurate view of drained peatland agriculture is that of an extractive industry, in which a finite resource (the peat) is 'mined' to produce food, fibre and fuel, driven by global demand. In developing countries with growing populations, there are strong socio-economic arguments for exploiting this resource to support local livelihoods and broader economic development (Mizuno *et al.*, 2016). However, we must accept that ongoing peat loss is inevitable under this scenario. Science-based measures towards improved management, including limitations on the extent of plantation development, can be used to minimize the rate of this peat loss (President of Indonesia, 2011). Such an evidence-based position, supported with data and necessary legal instruments, is needed for sustainable futures. The scientifically unfounded belief that drained peatland agriculture can be made 'sustainable', and peat loss can be halted, via unproven methods such as peat compaction debilitates the effort to find sustainable possibilities. To a large extent, the issues surrounding unsustainable peatland management have now been recognized by sections of industry (Wilmar, 2013; APP, 2014; Cargill Inc., 2014; Mondelēz International, 2014; Sime Darby Plantation, 2014; APRIL, 2015; Olam International, 2015), government (President of Indonesia, 2014, 2016, Mongabay, 2015; Mongabay Haze Beat, 2015; Hermansyah, 2016) and consumers (Wijedasa *et al.*, 2015). In recognition of the constraints and risks of peatland development, many large and experienced oil palm and pulpwood companies have halted further development on peat and introduced rigorous management requirements for existing peatland plantations (Lim *et al.*, 2012). However, the denial of the empirical basis calling for improved peatland management

remains persistent in influential policy spaces, as illustrated by the articles reporting on the conference ('Oil palm planting on peat soil handled well, says Uggah, 2016b; Cheng & Sibon, 2016; Nurbianto, 2016a,b).

The search for more responsible tropical peatland agriculture techniques includes promising recent initiatives to develop methods to cultivate crops on peat under wet conditions (Giesen, 2015; Dommain *et al.*, 2016; Mizuno *et al.*, 2016). While a truly sustainable peatland agriculture method does not yet exist, the scientific community and industry are collaborating in the search for solutions (International Peat Society, 2016), and for interim measures to mitigate ongoing rates of peat loss under existing plantations. Failing to recognize the devastating consequences of the current land use practices on peat soils and failing to work together to address them could mean that the next generation will have to deal with an irreversibly altered, dysfunctional landscape where neither environment nor society, globally or locally, will be winners.

Acknowledgements

Open access facilitated by Greifswald Mire Centre and Department of Forestry Sciences, University of Helsinki.

References

APP (2014) APP Forest Conservation Policy Update 2014.

APRIL (2015) APRIL Group's Sustainable Forest Management Policy 2.0. 1–4.

Cai W, Borlace S, Lengaigne M *et al.* (2014) Increasing frequency of extreme El Niño events due to greenhouse warming. *Nature Climate Change*, **5**, 1–6.

Cargill Inc. (2014) Cargill Policy on Sustainable Palm Oil.

Carlson KM, Goodman LK, May-Tobin CC (2015) Modeling relationships between water table depth and peat soil carbon loss in Southeast Asian plantations. *Environmental Research Letters*, **10**, 74006.

Cheng L, Sibon P (2016) Sarawak opening up coastal lowland areas for agriculture, plantation devt — Adenan. *BorneoPost*, Available at: http://www.theborneopost.com/2016/08/17/sarawak-opening-up-coastal-lowland-areas-for-agriculture-plantation-devt-adenan/ (accessed 17 August 206).

Chisholm RA, Wijedasa LS, Swinfield T (2016) The need for long-term remedies for Indonesia's forest fires. *Conservation Biology*, **30**, 5–6.

Couwenberg J, Dommain R, Joosten H (2009) Greenhouse gas fluxes from tropical peatlands in south-east Asia. *Global Change Biology*, **16**, 1715–1732.

Dommain R, Couwenberg J, Glaser PH, Joosten H, Suryadiputra I, Nyoman N (2014) Carbon storage and release in Indonesian peatlands since the last deglaciation. *Quaternary Science Reviews*, **97**, 1–32.

Dommain R, Dittrich I, Giesen W, Joosten H, Rais DS, Silvius M, Wibisono ITC (2016) Ecosystem services, degradation and restoration of peat swamps in the Southeast Asian tropics. In: *Peatland Restoration and Ecosystem Services: Science, Policy and Practice* (eds Bonn A, Allott T, Evans M, Stoneman R, Joosten H). Cambridge University Press, Cambridge.

Drösler M, Verchot LV, Freibauer A *et al.* (2014) Chapter 2: Drained inland organic soils. In: *2013 Supplement to the 2006 IPCC Guidelines for National Greenhouse Gas Inventories: Wetlands* (eds Hiraishi T, Krug T, Tanabe K, Srivastava N, Jamsranjav B, Fukuda M, Troxler T), pp. 1–79. IPCC, Switzerland.

Evers S, Yule C, Padfield R, O'Reilly P, Varkkey H (2016) Keep Wetlands Wet: The Myth of Sustainable Development of Tropical Peatlands - Implications for Policies and Management. *Global Change Biology*, 1–16, doi: 10.1111/gcb.13422/abstract

Gaveau DLA, Salim M, Hergoualc'h K *et al.* (2014) Major atmospheric emissions from peat fires in Southeast Asia during non-drought years: evidence from the 2013 Sumatran fires. *Scientific reports*, **4**, 1–7.

Giam X, Koh LP, Tan HH, Miettinen J, Tan HTW, Ng PKL (2012) Global extinctions of freshwater fishes follow peatland conversion in Sundaland. *Frontiers in Ecology and the Environment*, **10**, 465–470.

Giesen W (2015) Utilising non-timber forest products to conserve Indonesia's peat swamp forests and reduce carbon emissions. *Journal of Indonesian Natural History*, **3**, 10–19.

Hermansyah A (2016) Soil compaction puts peatland at risk, agency says. *The Jakarta Post*, Available at: http://www.thejakartapost.com/news/2016/03/08/soil-compaction-puts-peatland-risk-agency-says.html (accessed 8 March 2016).

Hirano T, Segah H, Kusin K, Limin S, Takahashi H, Osaki M (2012) Effects of disturbances on the carbon balance of tropical peat swamp forests. *Global Change Biology*, **18**, 3410–3422.

Hooijer A, Page S, Jauhiainen J, Lee WA, Lu XX, Idris A, Anshari G (2012) Subsidence and carbon loss in drained tropical peatlands. *Biogeosciences*, **9**, 1053–1071.

Hooijer A, Vernimmen R, Visser M, Mawdsley N (2015a) Flooding projections from elevation and subsidence models for oil palm plantations in the Rajang Delta peatlands, Sarawak, Malaysia. Deltares report 1207384, 76 pp.

Hooijer A, Vernimmen R, Mawdsley N, Page S, Mulyadi D, Visser M (2015b) *Assessment of Impacts of Plantation Drainage on the Kampar Peninsula Peatland*. Deltares Report, Riau.. 1207384.

Huijnen V, Wooster MJ, Kaiser JW *et al.* (2016) Fire carbon emissions over maritime southeast Asia in 2015 largest since 1997. *Scientific Reports*, **6**, 26886.

International Peat Congress with over 1000 participants! (2016a) PeatNews.

International Peat Society (2016) Statement regarding the Jakarta Post article of 18th August.

Jaafar Z, Loh TL (2014) Linking land, air and sea: Potential impacts of biomass burning and the resultant haze on marine ecosystems of Southeast Asia. *Global Change Biology*, **20**, 2701–2707.

Kettridge N, Turetsky MR, Sherwood JH *et al.* (2015) Moderate drop in water table increases peatland vulnerability to post-fire regime shift. *Scientific Reports*, **5**, 8063.

Koh LP, Miettinen J, Liew SC, Ghazoul J (2011) Remotely sensed evidence of tropical peatland conversion to oil palm. *Proceedings of the National Academy of Sciences of the United States of America*, **108**, 5127–5132.

Lim KH, Lim SS, Parish F, Suharto R (2012) *RSPO Manual on Best Management Practices (BMPs) for Existing Oil Palm Cultivation on Peat*. RSPO, Kuala Lumpur, Malaysia. 214 pp.

Marlier ME, DeFries RS, Voulgarakis A *et al.* (2012) El Niño and health risks from landscape fire emissions in southeast Asia. *Nature Climate Change*, **3**, 131–136.

Melling L, Goh KJ, Beauvais C, Hatano R (2008) Carbon Flow and Budget in Young Mature Oil Palm Agroecosystem on Deep Tropical Peat. *Planter*, **84**, 21.

Mizuno K, Fujita MS, Kawai S (2016) *Catastrophe & Regeneration in Indonesia's Peatlands: Ecology, Economy & Society* (eds Mizuno K, Fujita MS, Kawai S). NUS Press, Singapore, 466 pp.

Mondelēz International (2014) Mondelēz International Palm Oil Action Plan.

Mongabay (2015) Jokowi to oversee Indonesia peat restoration agency but details thin on the ground. Mongabay.

Mongabay Haze Beat (2015) Jokowi pledges Indonesia peatland "revitalization" to stop the burning. Mongabay.

Nurbianto B (2016a) Congress may change views on cultivation of peatland: IPS. *The Jakarta Post*, Available at: http://www.thejakartapost.com/news/2016/08/18/congress-may-change-views-on-cultivation-of-peatland-ips.html (accessed 18 August 2016).

Nurbianto B (2016b) Malaysia challenges the world over palm oil on peatland. *The Jakarta Post*, Available at: http://www.thejakartapost.com/news/2016/08/24/malaysia-challenges-the-world-over-palm-oil-on-peatland.html (accessed 24 August 2016).

Oil palm planting on peat soil handled well, says Uggah (2016b) BorneoPost. Available at: http://www.theborneopost.com/2016/08/19/oil-palm-planting-on-peat-soil-handled-well-says-uggah/ (accessed 19 August 2016).

Page SE, Hooijer A (2016) In the line of fire: the peatlands of Southeast Asia. *Philosophical transactions of the Royal Society of London. Series B, Biological sciences*, **371**, 20150176.

Page SE, Siegert F, Rieley JO, Boehm HV (2002) The amount of carbon released from peat and forest fires in Indonesia during 1997. *Nature*, **1999**, 61–65.

Page SE, Rieley JO, Banks CJ (2011) Global and regional importance of the tropical peatland carbon pool. *Global Change Biology*, **17**, 798–818.

Posa MRC, Wijedasa LS, Corlett RT (2011) Biodiversity and conservation of tropical peat swamp forests. *BioScience*, **61**, 49–57.

President of Indonesia (2011) Instruction of the President of the Republic of Indonesia number 10 of 2011 about suspension of granting of new licenses and improvement of governance of natural primary forest and peatland.

© 2017 The Authors Global Change Biology Published by John Wiley & Sons Ltd.,

President of Indonesia (2014) Government Regulation Number 71 of year 2014 about Protection and Management of Peat Ecosystems.
President of Indonesia (2016) Presidential Regulation Number 1 of year 2016 About Peat Restoration Agency.
Ramdani F, Hino M (2013) Land Use Changes and GHG Emissions from Tropical Forest Conversion by Oil Palm Plantations in Riau Province, Indonesia. *PLoS ONE*, **8**, 1–6.
Schrier-Uijl AP, Silvius M, Parish F, Lim KHH, Rosediana S, Anshari G (2013) *Environmental and Social Impacts of Oil Palm Cultivation on Tropical Peat: a Scientific Review*, pp. 131–168. Roundtable of Sustainable Palm Oil, Kuala Lumpur, Malaysia.
Sime Darby Plantation (2014) Sustainability: Peatland planting policy.
Stockwell CE, Jayarathne T, Cochrane MA *et al.* (2016) Field measurements of trace gases and aerosols emitted by peat fires in Central Kalimantan, Indonesia during the 2015 El Niño. *Atmospheric Chemistry and Physics Discussions*, **53**, 1–37.
Sumarga E, Hein L, Hooijer A, Vernimmen R (2016) Hydrological and economic effects of oil palm cultivation in Indonesian peatlands. *Ecology and Society*, **21**, 52.
Turetsky MR, Benscoter B, Page S, Rein G, Van Der Werf GR, Watts A (2015) Global vulnerability of peatlands to fire and carbon loss. *Nature Geoscience*, **8**, 11–14.
Warren M, Frolking S, Dai Z, Kurnianto S (2016) Impacts of land use, restoration, and climate change on tropical peat carbon stocks in the twenty-first century: implications for climate mitigation. *Mitigation and Adaptation Strategies for Global Change*, doi:10.1007/s11027-016-9712-1.
Wijedasa LS, Posa MRC, Clements GR (2015) Peat fires: consumers to help beat them out. *Nature*, **527**, 305.
Wilmar International (2013) *No Deforestation*, pp. 1–9. No Peat, No Exploitation Policy.
Wong J (2016) Yield of oil palm on peatland can be doubled. The Star.
Wösten JHM, Ismail AB, Van Wijk ALM (1997) Peat subsidence and its practical implications: A case study in Malaysia. *Geoderma*, **78**, 25–36.

© 2017 The Authors Global Change Biology Published by John Wiley & Sons Ltd.,